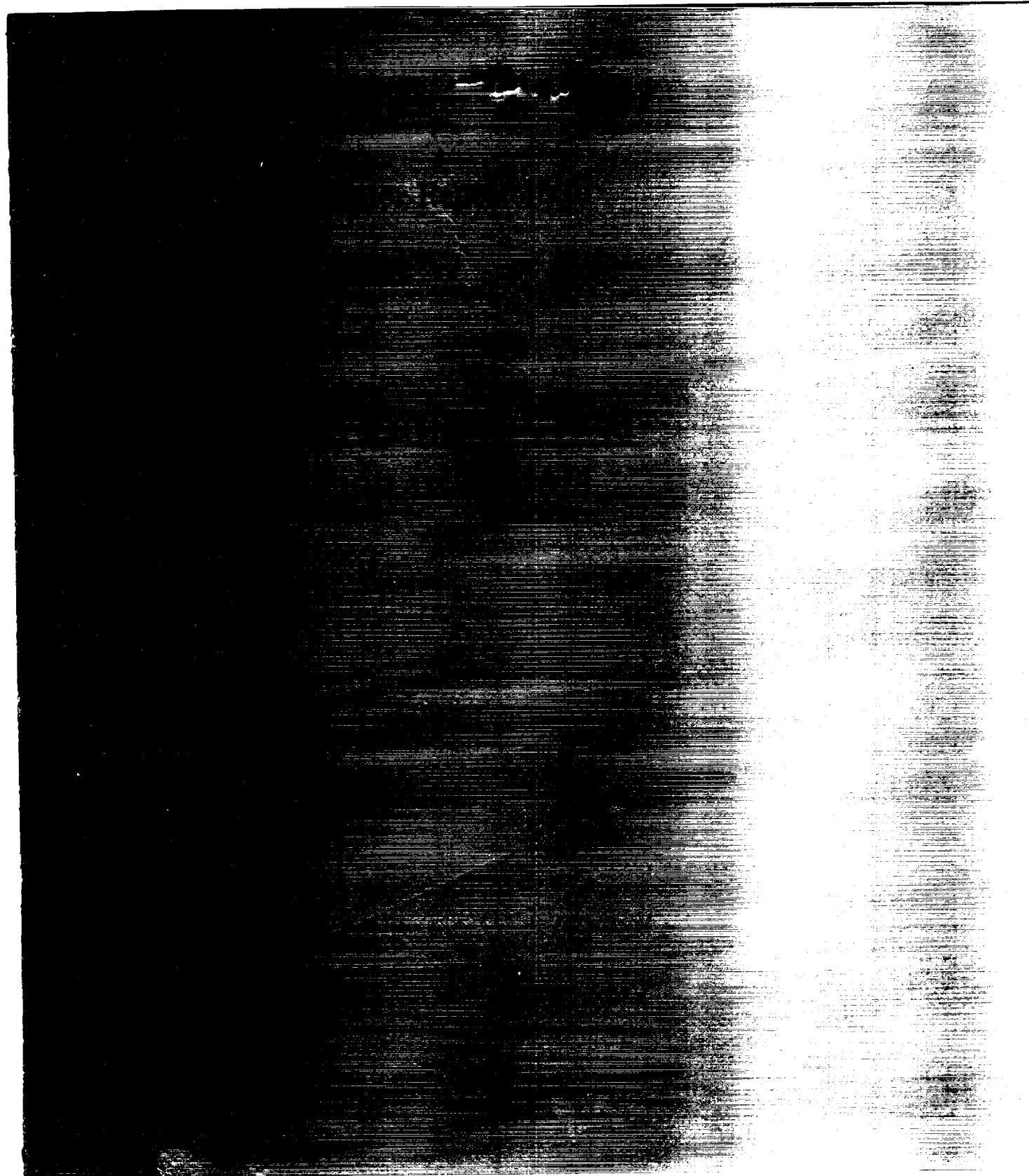

(NASA-CR-[illegible]) [illegible]

PROPAGATION IN METAL [illegible]

(Virginia Univ.) [illegible] CSCL 11F

unclas

H1/24 0238226

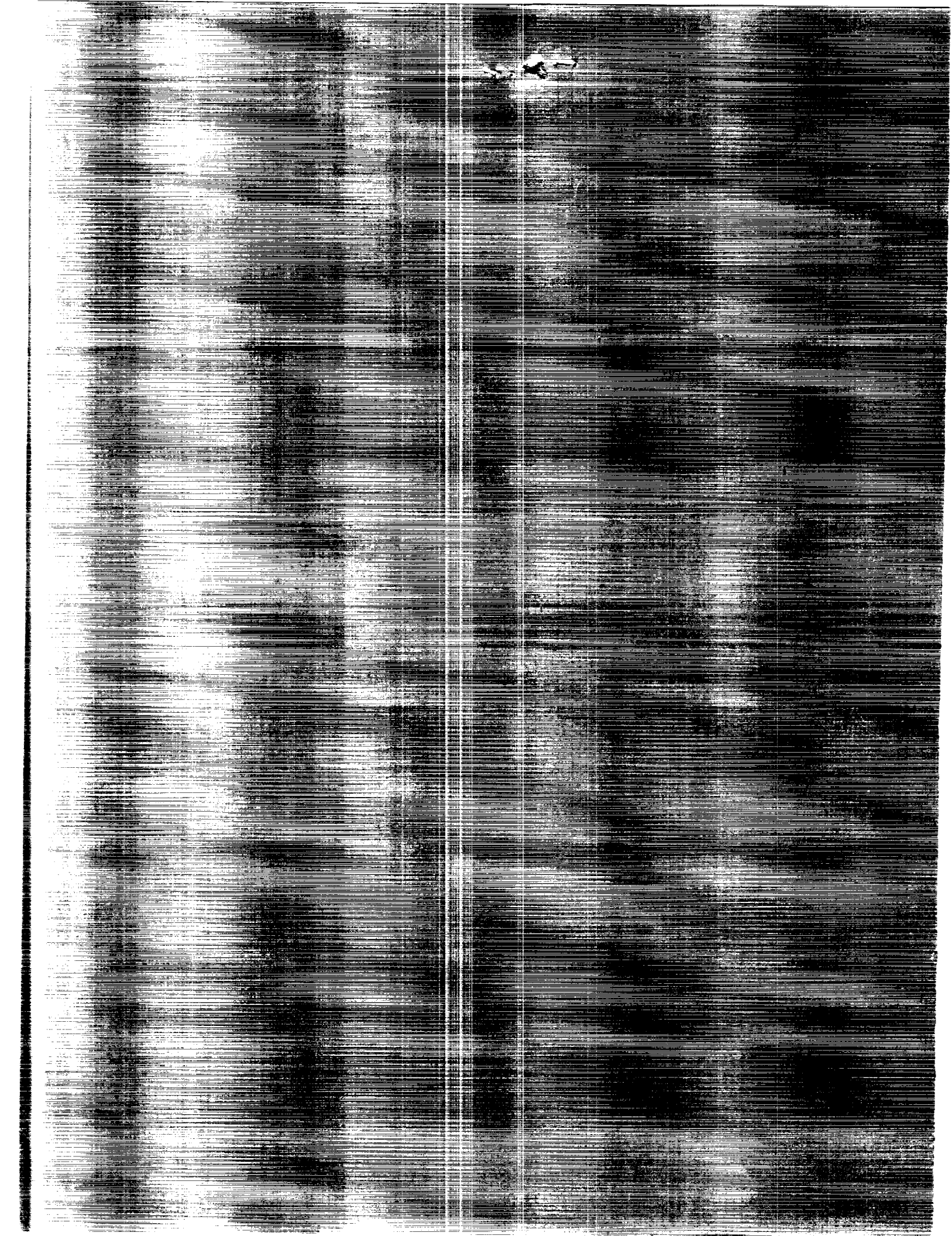

NASA Contractor Report 4301

Corrosion Fatigue Crack Propagation in Metals

Richard P. Gangloff
University of Virginia
Charlottesville, Virginia

Prepared for
Langley Research Center
under Grant NAG1-745

National Aeronautics and
Space Administration
Office of Management
Scientific and Technical
Information Division

1990

TABLE OF CONTENTS

I. ABSTRACT: CONCLUSIONS OF THE REVIEW

The objective of this paper is to critically compile and evaluate experimental results and mechanistic models for corrosion fatigue crack propagation in structural alloys exposed to ambient temperature gases and electrolytes. Data and models are based on continuum fracture mechanics descriptions of crack tip stress and strain fields, coupled with continuum modeling of occluded crack mass transport and chemical reactions. The aim is to inform the person seeking to broadly understand environmental effects on fatigue, to provide an experimental basis for life prediction analyses and evaluations of mechanistic models relevant to specialists, and to define current uncertainties and worthwhile directions for corrosion fatigue research.

Section II provides an introduction to corrosion fatigue crack propagation. The state-of-the-art which emanated from the Storrs and Firminy conferences is summarized. Qualitative mechanisms for cracking are presented.

Section III assesses the fracture mechanics approach to corrosion fatigue, while Section IV considers experimental methods. The following conclusions are established:

1. Fracture mechanics descriptions of corrosion fatigue crack propagation; viz, growth rate as a function of stress intensity factor; provide an established and physically meaningful basis which couples alloy performance, damage mechanisms and life prediction studies through the concept of growth rate similitude. Extensive data bases have been developed for structural alloys over the past three decades. (Section III)

2. Experimental methods are developed for determinations of average crack growth rate as a function of continuum fracture mechanics crack tip parameters, particularly ΔK. Non-steady state crack growth, unique to corrosion fatigue, and crack closure are not understood. Future procedures will incorporate precision crack length measurement and computer control of stress intensity to develop quantitative and novel corrosion fatigue crack growth rate data, particularly near threshold. Advances have been recorded in measurements of small crack growth kinetics, however, such approaches are not easily adapted to controlled environments. The fundamental experimental problem is the

lack of methods to probe mechanical and chemical damage processes local to the corrosion fatigue crack tip. (Section IV)

Section V illustrates important variables that affect corrosion fatigue crack growth. It is concluded that:

3. A plethora of interactive variables influences the corrosion fatigue crack growth rate-stress intensity relationship. The effects of chemical, metallurgical and mechanical variables are well characterized and reasonably explained by qualitative arguments. Growth rates are affected by environment chemistry variables (viz: temperature; gas pressure and impurity content; electrolyte pH, potential, conductivity, and halogen or sulfide ion content); by mechanical variables such as ΔK, mean stress, frequency, waveform and overloads; and by metallurgical variables including impurity composition, microstructure and cyclic deformation mode. Time, or loading frequency, is critical; complicating long-life component performance predictions based on shorter term laboratory data. Limited studies show that yield strength is not a critical variable in cycle-time dependent corrosion fatigue. Fractographic analyses of microscopic crack paths provide a basis for failure analyses and input to mechanistic studies. (Section V)

Section VI develops the mechanical crack tip field and chemical mass transport and reaction components which are central to quantitative models of corrosion fatigue crack growth rates. Current predictions of crack growth rate, from both the hydrogen embrittlement and dissolution/film rupture perspectives, are discussed.

4. Micromechanical-chemical models of crack tip driving forces and process zone corrosion fatigue damage provide a sensible means to predict and extrapolate the effects of variables, and to modify the fracture mechanics approach to account for compromises in similitude. Models have been formulated based on hydrogen embrittlement and film rupture/transient dissolution/repassivation. Fatigue damage due to crack surface films has not been considered quantitatively. Models successfully predict the time (frequency) dependence of corrosion fatigue and the effects of electrode potential, solution composition and gas activity. All are, however, hindered by uncertainties associated with crack tip processes and the fundamental mechanisms of environmental

embrittlement. A process zone model has not been developed for corrosion fatigue; as such, stress intensity, yield strength and microstructure effects are not predictable. Furthermore, absolute rates of hydrogen assisted crack growth are not predictable and the film rupture formulation is being debated. Successes to date indicate that a new level of mechanistic understanding is achievable. (Section VI)

Section VII reviews processes which compromise the fracture mechanics approach to corrosion fatigue.

5. Fracture mechanics descriptions of corrosion fatigue and the similitude concept are complicated by the inability of stress intensity to describe the controlling crack tip mechanical and chemical driving forces. The so-called "closure", "small crack" and "high strain" problems in mechanical fatigue are relevant to corrosion fatigue. Data and analyses demonstrate that the unique relationship between da/dN and ΔK is compromised by mechanisms including (1) premature crack wake surface contact, (2) deflected, branched and multiple cracking, and (3) time and geometry dependent occluded crack chemistry. Stress intensity descriptions of elastic-plastic stresses, strains and strain rates in the crack tip plastic zone are uncertain within about 5 μm of the crack tip, within single grains which are not well described by the constitutive behavior of the polycrystal and when deformation is time or environment sensitive. These limitations do not preclude the only quantitative approach developed to date to characterize subcritical crack propagation. Rather, they indicate the need for crack tip modeling. (Section VII)

Section VIII suggests necessary directions for future research in corrosion fatigue.

6. Opportunities exist for research on corrosion fatigue to: (a) broaden phenomenological understanding, particularly near threshold, (b) develop integrated and quantitative microchemical-mechanics models, (c) develop experimental methods to probe crack tip damage, and to measure near threshold time-cycle dependent crack growth, (d) characterize the behavior of advanced monolithic and composite alloys, and (e) develop damage tolerant life prediction methods and <u>in situ</u> sensors for environment chemistry and crack growth. (Section VIII)

II. INTRODUCTION

Corrosion fatigue is defined as the deleterious effect of an external chemical environment on one or more of the progressive stages of damage accumulation which constitute fatigue failure of metals and compared to behavior in inert surroundings. Damage results from the synergistic interaction of cyclic plastic deformation and local chemical or electrochemical reactions.

The cumulative damage processes for environmentally assisted fatigue are subdivided into four sequential categories: (1) cyclic plastic deformation, (2) microcrack initiation, (3) small crack growth to linkup and coalescence into a single short crack and (4) macrocrack propagation. The mechanisms for these processes are in part common.

A goal of fatigue research is the development of an integrated mechanistic description of whole life. A sensible means to this end is to isolate and quantitatively characterize each of the four regimes of fatigue damage. This approach is advocated because the experimental and analytical methods necessary to study each regime are different, variables may affect each regime uniquely, and many applications are dominated by one of the fatigue regimes; for example, the behavior of crack-like defected components in large structures. Environmental effects on cyclic deformation and microcrack initiation are considered separately in this volume by Duquette [1]. This paper reviews corrosion fatigue crack propagation; regimes 3 and 4 in the above hierarchy.

The development of an integrated and basic understanding of corrosion fatigue is hindered by several factors which are recurrent throughout studies of initiation and propagation. Corrosion fatigue is influenced by a wide variety of mechanical, chemical and microstructural variables which interact. It is necessary to investigate very slow rate deformation and cracking phenomena in a finite and realistic time. Model system studies on deformation and crack initiation have been conducted on relatively pure materials, often monocrystalline, while crack propagation studies are typically performed on complex structural

materials including steels and precipitation hardened aluminum or nickel based alloys. Corrosion fatigue damage is highly localized at slip substructure and near the crack tip; direct experimental observations are not available and behavioral interpretations must be based on indirect, averaged measurements. As the case for stress corrosion, corrosion fatigue is likely controlled by hydrogen based, cleavage and dissolution/ passivation mechanisms; the atomistics of which are not known.

II.1. Scope of the Review

The objective of this Review is to critically summarize the phenomenology and mechanistic models of corrosion fatigue crack propagation, and to identify current understanding and uncertainties which are principal to control of this failure mode in structural alloys. Results are emphasized which satisfy technological needs, including: (1) quantitative mechanism-based predictions of long term component life, derived from short term laboratory data and describing the effects of interactive variables, (2) high performance corrosion fatigue resistant monolithic and composited alloys, and chemically inhibited environments and (3) a basis for nondestructive inspection procedures and sensors of environment chemistry and corrosion fatigue cracking damage.

In scope this review emphasizes cycle-time-dependent corrosion fatigue crack propagation. Understanding of time-dependent fatigue above the threshold stress intensity (K_{ISCC}) for monotonic load stress corrosion cracking (SCC) follows from work summarized by Parkins [2]. Structural materials are discussed, including low carbon HSLA and heat treated alloy steels, austenitic stainless steels, and precipitation hardened aluminum alloys in various embrittling gaseous and electrolytic environments for temperatures near 300 K. Spahn discusses corrosion fatigue in ferritic and martensitic stainless steels, while Pineau reviews elevated temperature fatigue and creep-fatigue interactions elsewhere in this volume [3,4]. There are similarities between low temperature electrolytes and elevated temperature gas environments [5].

Despite important and controversial uncertainties, the fracture mechanics approach provides the foundation for this review of corrosion fatigue crack propagation data and predictive models. The issue considered here is the extent to which crack tip modeling can extend the applied stress intensity and bulk environment based approach to corrosion fatigue.

II.2. State-of-the-Art: Storrs and Firminy Conferences

Corrosion fatigue crack propagation has been the focal point for many international conferences [6-24] and major review papers [5,25-39]. Fatigue is described in a massive literature, with important symposia including discussions on environmental effects [40-48]. A foundation for the current review is provided by the proceedings of the seminal conferences held at Storrs, Connecticut in 1971 and in Firminy, France in 1973 [6,7]. Several points emerged from these meetings.

II.2.a. **Fracture Mechanics Characterization.** The fracture mechanics description of corrosion fatigue crack propagation, presented as average crack propagation rate (da/dN) as a function of applied stress intensity range (ΔK), was embraced by many researchers. The schematics in Fig. 1 indicate a variety of crack growth responses for embrittling environments, in sharp contrast to the power-law (Paris regime) relation between da/dN and ΔK coupled with a single crack growth threshold (ΔK_{th}) observed for alloys in vacuum and moist air [25].[1] The magnitude and pattern of corrosion fatigue cracking depend on stress corrosion cracking above K_{ISCC} and a synergistic fatigue-corrosion interaction at lower stress intensities. The proportions of these events depend upon material and environment.

II.2.b. **Classes of Corrosion Fatigue Crack Growth.** Purely time-dependent corrosion fatigue crack propagation is observed for materials and environments where monotonic loading SCC occurs over a portion of

[1] The older representation in Fig. 1, based on K_{max}, is equivalent to current growth rate data based on ΔK for fixed mean stress intensity. Two of these three parameters are independent variables in corrosion fatigue.

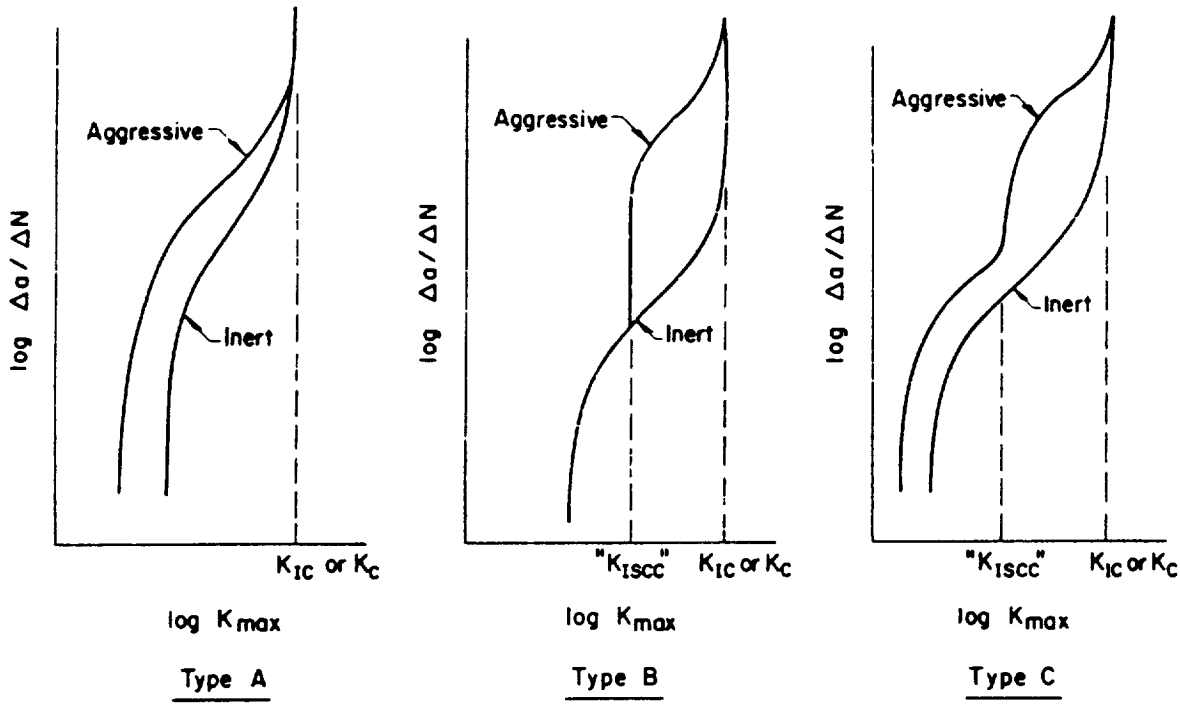

Fig. 1 Schematic representations of corrosion fatigue crack propagation rate behavior; after McEvily and Wei [25].

the cyclic stress intensity loading wave; Type B in Fig. 1. The cyclic character of loading and local plastic straining are not important. The fracture mechanics approach was launched by studies of subcritical fatigue crack propagation in high strength materials exposed to environments which readily induce stress corrosion crack growth. Type B behavior is prevalent for these systems, as illustrated by data for high strength 4340 steel in water vapor and argon, Fig. 2 [49].

The solid line in Fig. 2 demonstrates that time-dependent corrosion fatigue crack growth rates are accurately predicted by linear superposition of stress corrosion crack growth rates (da/dt) integrated over the load-time function for fatigue [50]. Equivalent corrosion fatigue behavior is predicted and observed for sinusoidal, square and asymmetric triangular load-time functions. Linear superposition modeling also predicts the effect of stress ratio.

A second class of corrosion fatigue behavior is based on synergistic interaction between cyclic plastic deformation and environment which produces cycle and time-dependent crack growth rates, Type A in Fig. 1. Here, the environment accelerates fatigue crack growth below K_{ISCC}, a common scenario for low to moderate strength alloys which are either immune to stress corrosion cracking, or exhibit high K_{ISCC} and low da/dt. This class of behavior was discussed by Barsom, based on data in Fig. 3 for a maraging steel exposed to 3% NaCl [51,52]. Note the substantial corrosion fatigue effect below the static load threshold, but only for those loading waveforms which include a slow deformation rate to maximum stress intensity.

At the time of the Storrs and Firminy conferences, there were only limited data which showed an environmentally induced reduction in ΔK_{th}; threshold measurements and concepts were in an infant state. Cycle-time-dependent corrosion fatigue below K_{ISCC} was further categorized based on observed frequency dependencies.

II.2.c. **Frequency Effects.** Wei, Barsom and Speidel independently emphasized the principal importance of loading frequency (f) for each class of corrosion fatigue, as typified by Fig. 4 for

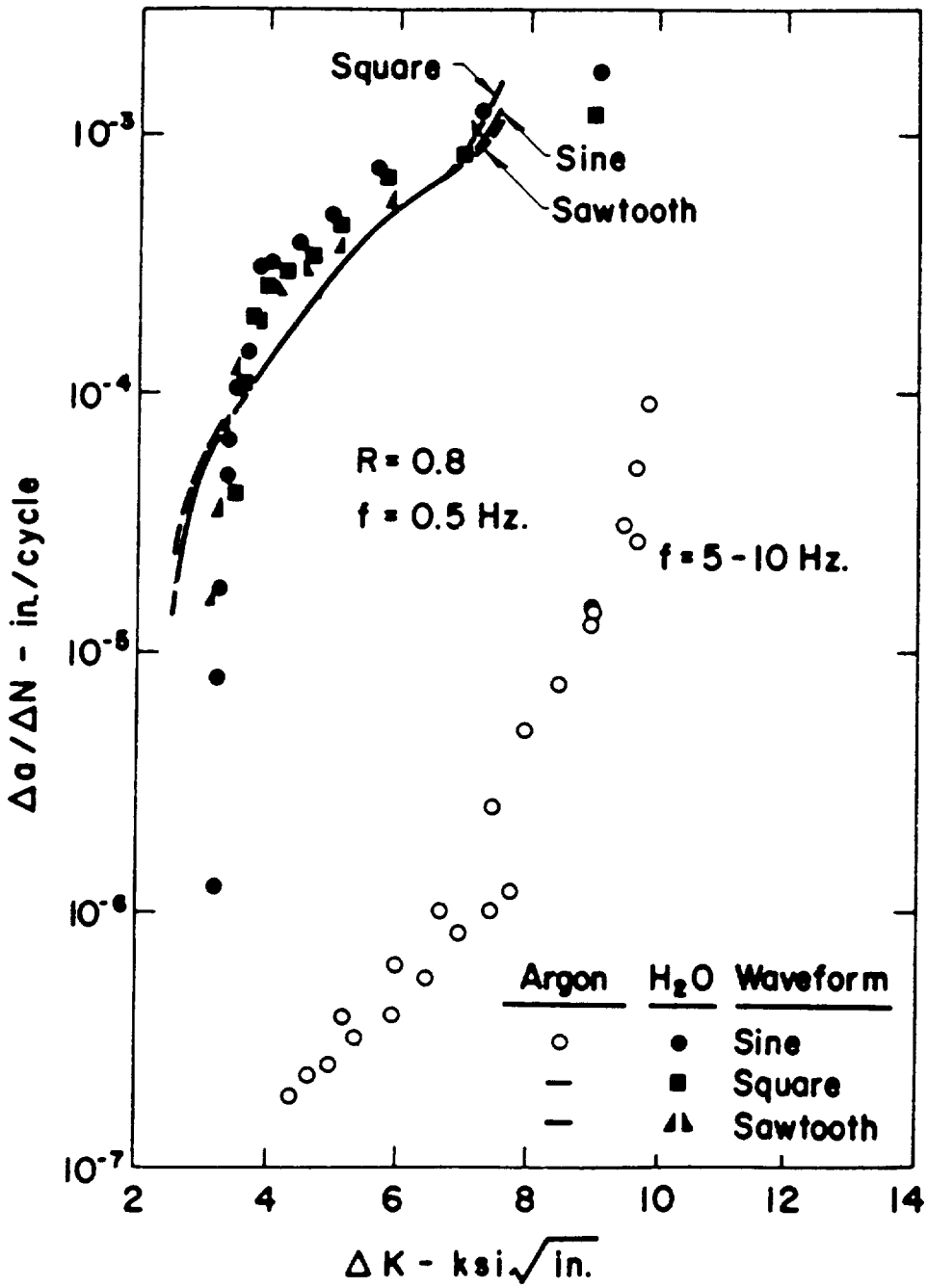

Fig. 2 Time-dependent corrosion fatigue above K_{ISCC} for high strength 4340 steel in water vapor, modeled by linear superposition; after Wei et al. [49,50]. (1 in/cycle = 25.4 mm/cycle; 1 ksi$\sqrt{\text{in}}$ = 1.098 MPa$\sqrt{\text{m}}$)

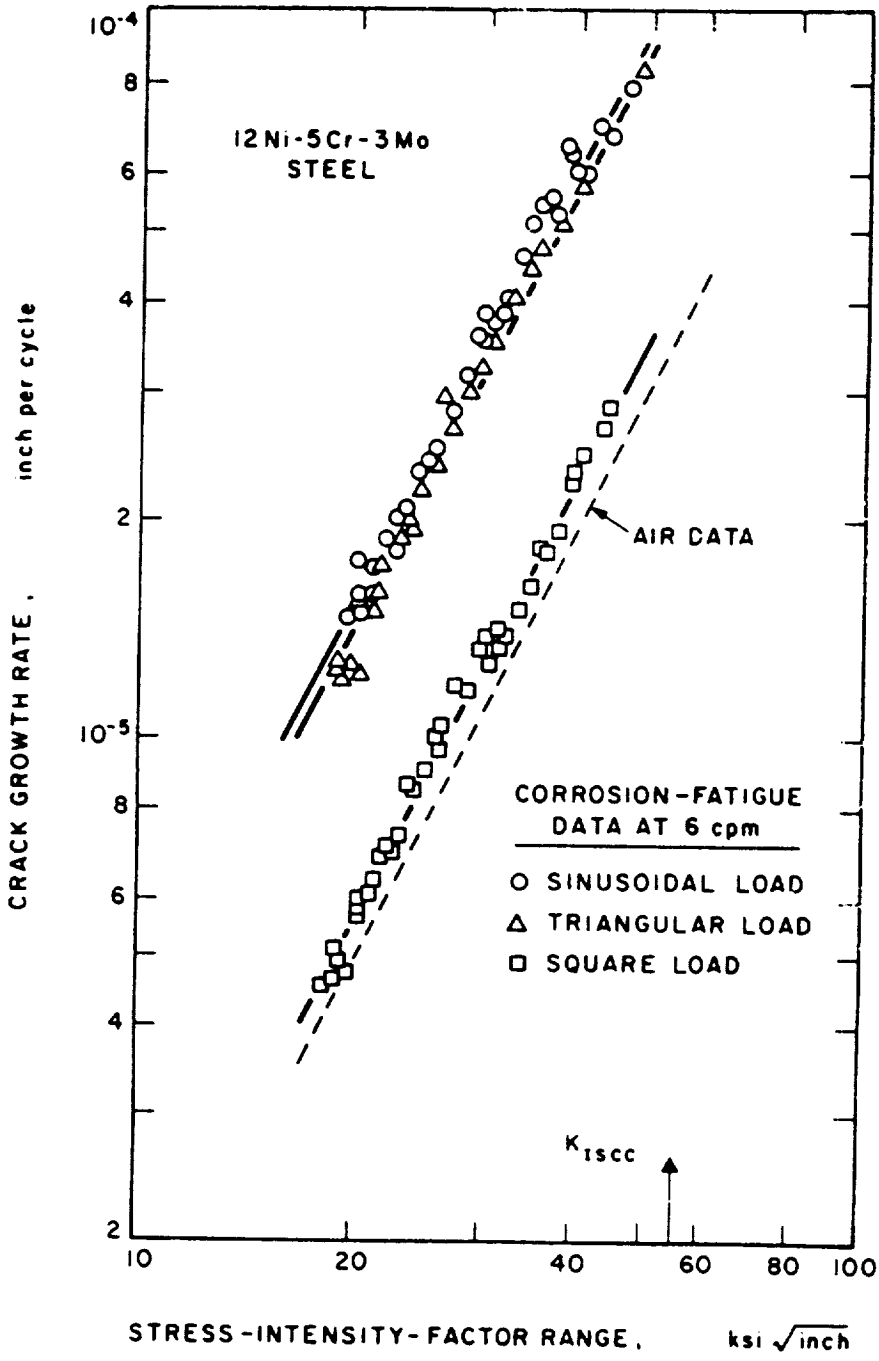

Fig. 3 Time-cycle-dependent corrosion fatigue crack propagation below K_{ISCC} for 12Ni maraging steel in aqueous 3% NaCl; after Barsom [51,52]. (1 in/cycle = 25.4 mm/cycle, 1 ksi $\sqrt{in}$ = 1.098 MPa $\sqrt{m}$)

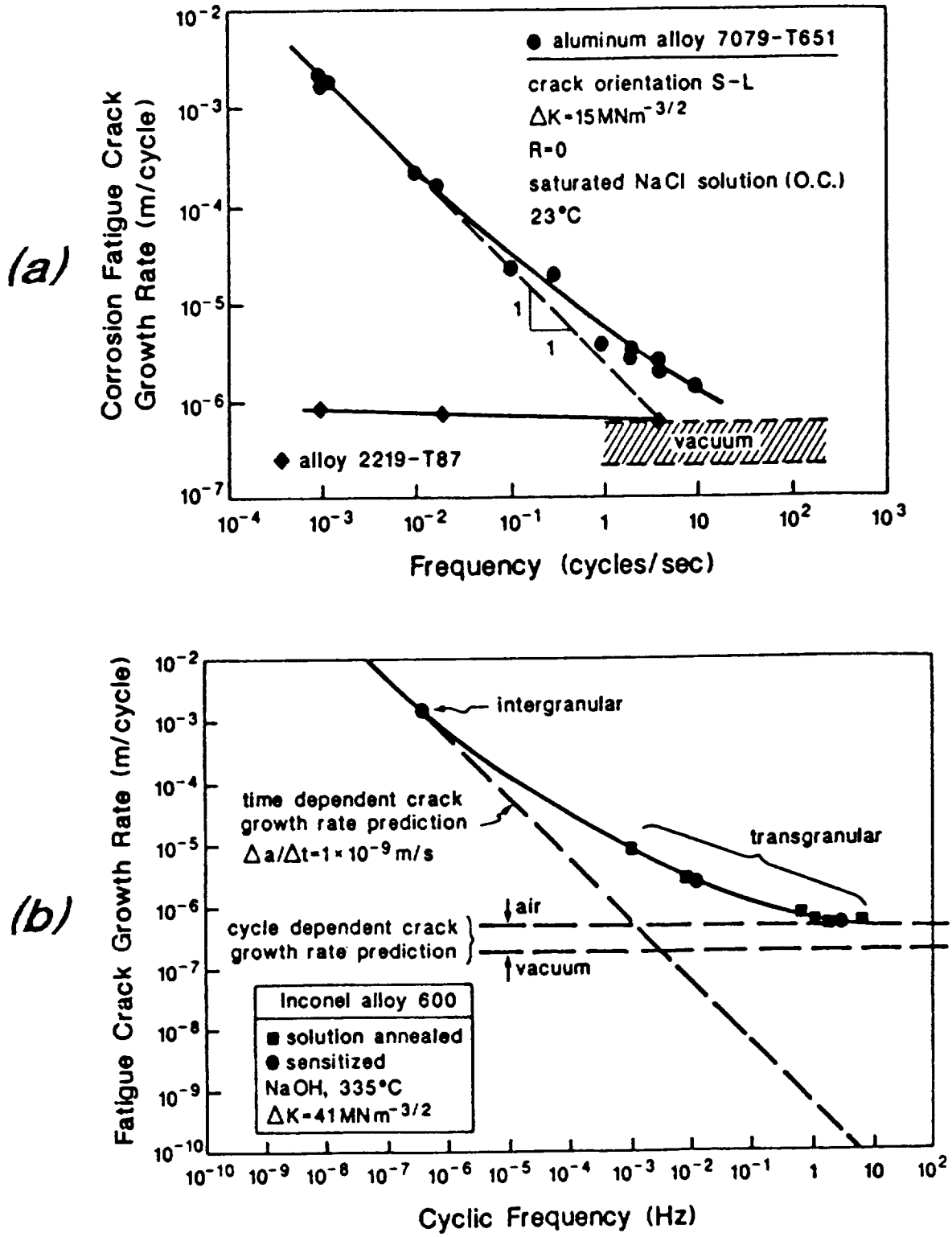

Fig. 4 Frequency dependence of corrosion fatigue crack propagation, illustrating time-dependent, cycle-dependent and time-cycle-dependent behavior for: (a) Aluminum alloys in NaCl and (b) Inconel 600 in hot NaOH; after Speidel [26,53].

aluminum alloy 7079 in aqueous sodium chloride and Inconel 600 in hot sodium hydroxide solutions [25,26,49-53]. For time-dependent corrosion fatigue, da/dN due to environment is inversely proportional to f if the stress corrosion growth rate is constant with K, and based on the assumptions that da/dN = (da/dt)·(1/f) and crack growth occurs throughout the loading and unloading portions of the fatigue cycle. This behavior is illustrated by the inclined dashed lines on the logarithmic plots in Fig. 4. Superposition modeling (Fig. 2 and Ref. 50) predicts the effect of cyclic load period on time dependent corrosion fatigue.

The frequency dependence of cycle-time-dependent corrosion fatigue is more complex. At low stress intensities, Speidel reported corrosion fatigue accelerations of da/dN for steels and nickel based alloys which were independent of frequency [5,26]. This behavior was defined as "true" or cycle-dependent corrosion fatigue, and is illustrated by horizontal lines in Fig.4 for air or the environments. A second behavior, that where sub-K_{ISCC} corrosion fatigue growth rates increase with decreasing frequency, reflects the more general case of synergistic mechanical-corrosion fatigue. This result is shown as the connecting region between time and cycle-dependent da/dN in Fig. 4 for those instances when da/dN calculated from da/dt and the vacuum rate sum to a value less than that measured for the environment. Speidel and others suggest that this behavior is best described as "cyclic SCC", where cyclic deformation lowers the susceptibility of the material to environmental cracking or "SCC". For the current review all forms of corrosion fatigue below K_{ISCC} are viewed as cycle-time-dependent behavior.

From this discussion, the most general form of corrosion fatigue, Type C in Fig. 1, involves cycle-time-dependent accelerations in da/dN below K_{ISCC}, combined with time-dependent cracking (SCC) above the threshold. ΔK_{th} may or may not be environment sensitive.

II.2.d. **Principal Variables.** Extensive crack growth rate data presented at Storrs and Firminy demonstrate that mechanical, chemical and metallurgical variables affect corrosion fatigue.

The effects of ΔK, loading waveform, and loading frequency are illustrated in Figs. 1 to 4. These conferences further established the important effects of environment chemistry, viz: temperature, gas pressure, electrolyte pH, electrode potential, dissolved oxygen, and environment composition. The effect of applied electrode potential on corrosion fatigue of a high strength aluminum alloy in an aqueous halogen solution is shown in Fig. 5 [5]. The deleterious effect of low pressure gaseous hydrogen and the associated beneficial poisoning effect of small O_2 additions on sub-K_{ISCC} corrosion fatigue in 4340 steel (σ_{ys} = 1240 MPa) are shown in Fig. 6 [54]. Note the mild frequency effect for pure hydrogen, consistent with cracking below K_{ISCC} and cycle-time-dependent embrittlement.

II.3. Mechanisms for Corrosion Fatigue Crack Propagation

Qualitative descriptions of the mechanisms for corrosion fatigue crack propagation provide a second foundation for this review. These mechanisms are the basis for understanding the corrosion fatigue crack propagation data presented in Section III, the necessary measurement methods discussed in Section IV, the effects of critical variables in Section V and quantitative models of corrosion fatigue cracking kinetics in Section VI.

While debate continues on the microscopic and atomistic details of corrosion fatigue, and while mechanisms are often specific to each material-environment system, several common concepts have been developed over the past 25 years. Corrosion fatigue involves the synergistic interaction of cyclically reversed plastic deformation and local chemical or electrochemical reactions. Models differ based on the chemical damage mechanism.

II.3.a. Hydrogen Environment Embrittlement. Since hydrogen embrittles many alloys under static and dynamic monotonic loading [55,56], this mechanism is invoked to explain corrosion fatigue crack propagation in a variety of alloy-gaseous or aqueous environment systems. Apart from occurring for many structural alloys in hydrogen gas, hydrogen embrittlement is proposed as the dominant

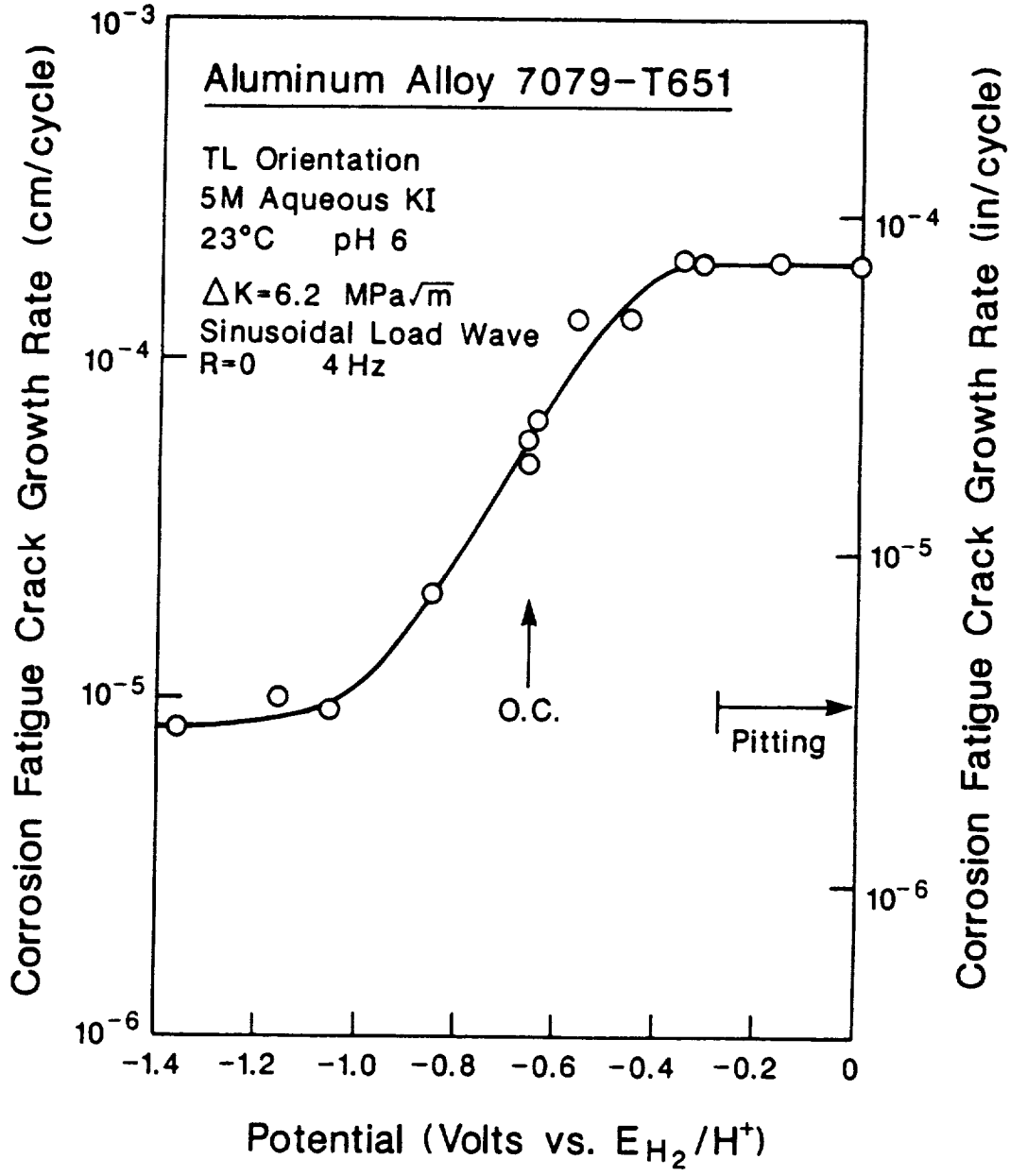

Fig. 5 Effect of applied electrode potential on corrosion fatigue crack propagation in an aluminum alloy in aqueous potassium iodide; after Speidel et al. [5].

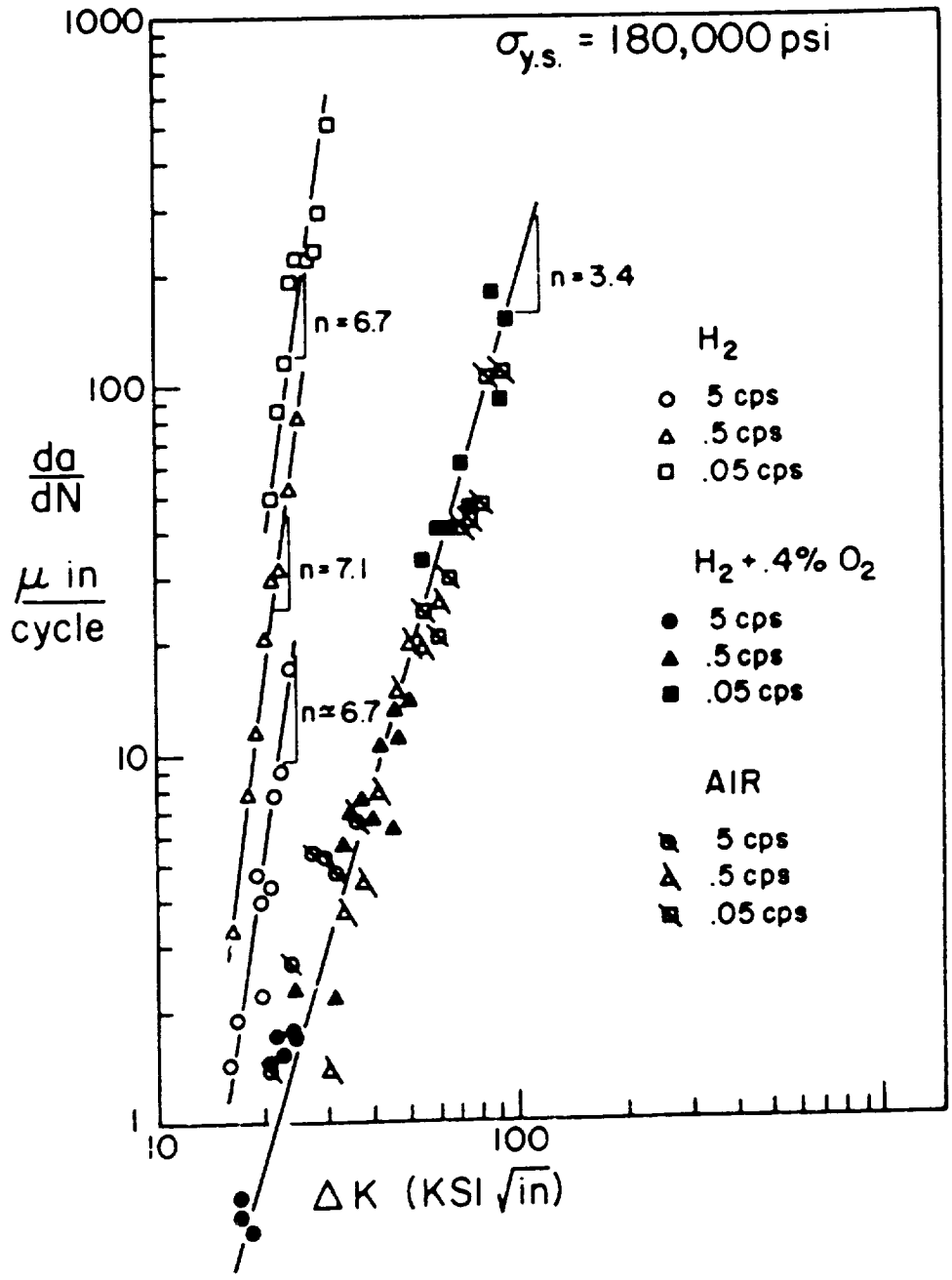

Fig. 6 Effect of gaseous hydrogen and H_2+O_2 mixtures on corrosion fatigue crack propagation in 4340 steel (σ_{ys} = 1240 MPa); after Johnson [54]. (1 μin/cycle = 0.0254 μm/cycle, 1 ksi $\sqrt{in}$ = 1.098 MPa $\sqrt{m}$)

mechanism for corrosion fatigue crack propagation of: C-Mn and alloy steels in various electrolytes [30,33,34,37,49,51,57-59]; aluminum alloys in water vapor [37,49,60-63]; and titanium alloys in aqueous chloride [37,64]. While controversial, corrosion fatigue of aluminum alloys in aqueous chloride solutions has been ascribed to hydrogen embrittlement [5,62,63,65,66].

In this view atomic hydrogen chemically adsorbs on clean crack tip surfaces as the result of dissociative gaseous H_2-metal reactions, of gas molecule (eg. H_2O or H_2S) surface chemical reactions, or of electrochemical cathodic reduction reactions involving hydrogen ions or water. These reactions are catalyzed by clean metal surfaces and proceed to near completion in short times near room temperature. At higher temperatures, recombination of H to evolving H_2 greatly reduces hydrogen embrittlement.

Hydrogen production on crack surfaces follows environment mass transport within the crack, and precedes hydrogen diffusion in the crack tip plastic zone to the points of fatigue damage. Hydrogen atoms are often segregated or "trapped" at grain boundaries, precipitate interfaces and dislocation cores. Trapping is detrimental if cracking occurs at such sites, but is beneficial if broadly distributed trapping reduces hydrogen transport kinetics and accumulation at fracture sites. Crack growth rates are likely to depend on the amount of adsorbed hydrogen produced per loading cycle by an environment. Crack growth will be rate limited by one or more of the slow steps in the crack environment mass transport, crack surface reaction and plastic zone hydrogen diffusion sequence.

Major uncertainties exist. The location of hydrogen enhanced crack tip fatigue damage is not known. The atomistic processes by which hydrogen embrittles the metal, including bond decohesion and hydrogen enhanced localized plasticity, are debated as discussed in this volume by Oriani and Birnbaum, and elsewhere by Lynch [67-69]. The occurrence of hydrogen embrittlement for a given corrosion fatigue system is inferred based on circumstantial evidence, as discussed in Section VI.6.a.

Quantitative hydrogen embrittlement models are discussed in Section VI.6.

II.3.b. **Film Rupture and Anodic Dissolution.** Chemical damage based on film rupture, transient electrochemical anodic dissolution and film reformation is invoked for several important corrosion fatigue problems, including carbon and stainless steels exposed to high temperature water environments [34,39,70,71]. This mechanism was originally developed for stress corrosion cracking and was extended to corrosion fatigue based on the common role of crack tip strain rate [70]. While controversial, film rupture models have been applied to the aluminum-aqueous chloride system [62,72].

In this view localized plastic straining ruptures otherwise protective films at the crack tip. Crack advance occurs during transient anodic dissolution of metal at the breached film and while the surface repassivates. The amount of corrosion fatigue crack growth per fatigue cycle depends Faradaically on the amount of anodic current which flows, and therefore on the kinetics of clean surface reaction (charge transfer) and on the time between film ruptures given by the crack tip strain rate and film ductility. The balance between sharp crack extension, and crack broadening or blunting by general corrosion is important. Quantitative film rupture models are discussed in Section VI.7.

II.3.c. **Surface Films.** Early studies of corrosion fatigue, predominantly smooth specimen whole life and crack initiation in gases, focused on the effects of environmentally produced thin surface films on slip based damage processes. This work was reviewed by Duquette [29,73], Marcus et al. [74], and Sudarshan and Louthan [38]. Over the past 20 years these concepts have been advanced for corrosion fatigue crack initiation in electrolytes [1,36]. Film based mechanisms have not been developed for crack propagation, however, recent advances in this regard were reviewed by Grinberg for moist air compared to vacuum [75].

Films may affect crack extension by one or more processes, viz: (1) interference with reversible slip, (2) localization of the distribution and morphology of persistent slip bands and resultant crack damage, (3) reduction of near surface plasticity

and thus either reduced or enhanced fatigue crack growth rates, depending on the cracking mechanism, and (4) localization of near surface dislocation debris and voids, and thus enhanced fatigue crack growth [1,29,36,38,73-76]. These mechanisms have not been developed quantitatively and tested experimentally.

Film effects on corrosion fatigue crack propagation are often speculatively considered. For example, Stoltz and Pelloux argue that crack tip surface films minimize plasticity for aluminum alloys in aqueous NaCl, and thereby trigger local cleavage at high resulting stresses [77]. Others argue that crack tip surface films reduce slip reversibility and thus increase damage and fatigue crack growth rates, at least for planar slip alloys [78,79]. A classic system here is aluminum alloys in vacuum compared to moist air. Faster crack growth in the latter occurs (hypothetically) by irreversible slip and crack blunting which produces striations. Flat striation free surfaces are observed for slowed crack propagation in vacuum, leading to the inference that slip is reversible due to the lack of an oxide film [75,80,81]. Others argue that crack tip surface films minimize slip localization by preventing the emergence of slip bands, and thus homogenizing plastic deformation and decreasing da/dN relative to film free environments such as vacuum [61]. Still others argue that crack tip slip is homogenized, plastic zone size at constant ΔK is increased and fatigue damage is least in vacuum compared to air [75].

Sieradzki and coworkers recently proposed that tens of angstroms thick, environmentally produced, crack tip films fracture to promote cleavage in the adjacent alloy substrate, over a distance considerably larger than the film thickness [82]. The implications of this model to corrosion fatigue are important, but have not been systematically considered.

The wide variety of film based explanations for corrosion fatigue is possible because of a lack of direct observations of crack tip damage processes and quantitative formulations of film effects. Controlled experiments in helium and film forming gaseous environments such as O_2 are lacking; effects of films are rather argued for complex electrochemical systems, or for moist

air where several damage processes may be operative. This view is amplified in Section VI.8.

II.3.d. **Adsorbed Atoms.** Adsorbed atoms may affect fatigue deformation and fracture by mechanisms similar to those of surface films, as reviewed by Marcus et al. [74] and Duquette [29,73]. A variety of processes are possible, however, none are modeled in detail for corrosion fatigue. For example, oxygen from the gas phase or a reduced cation from an electrolyte could adsorb on persistent slip sites at the crack tip, bind with dislocations and reduce slip reversibility. Alternately, such species could form on slip plane material to prevent rewelding on unloading. Presumably, these processes could lead to enhanced fatigue damage.

Reductions in surface energy by adsorption of an atom from the gas or liquid have long been proposed to reduce the associated work of fracture. For hydrogen embrittlement in gases or electrolytes, this mechanism is not viewed to be sufficient [67]. For fatigue of aluminum alloys in O_2, this mechanism has been proposed, but not proven convincingly [74]. Alternately, the chloride ion, oxidized from solution onto clean metal surfaces above a critical electrode potential, is held to embrittle austenitic stainless steels during stress corrosion cracking [83]. This concept has not been developed for corrosion fatigue.

II.3.e. **Anodic Dissolution and Plasticity.** Corrosion fatigue crack propagation by localized anodic dissolution, the electrochemical knife, is generally not proposed. Rather, Uhlig and coworkers [84-86] and more recently Jones [87] argue that anodic corrosion eliminates work hardened material and stimulates localized plastic deformation to produce corrosion fatigue damage. This model is based on the observation that smooth specimen corrosion fatigue life is only degraded for electrode potentials which are noble to a critical value [84]. The idea is that corrosion fatigue crack initiation requires a critical anodic current to progress.

Anodic dissolution-plastic deformation processes have not been modeled quantitatively, particularly for corrosion fatigue crack propagation.

III. THE FRACTURE MECHANICS APPROACH

III.1. Conclusion

Fracture mechanics descriptions of corrosion fatigue crack propagation; viz, growth rate as a function of stress intensity factor; provide an established and physically meaningful basis which couples alloy performance, damage mechanisms and life prediction studies through the concept of growth rate similitude. Extensive data bases have been developed for structural alloys over the past three decades.

III.2. Stress Intensity Similitude: Inert Environments

The fracture mechanics description of fatigue crack propagation illustrated in Fig. 7 is traceable to the seminal work of Paris and coworkers for the case of moist air environments [88]. This evolution is chronicled by Hertzberg [89].

Subcritical fatigue crack propagation is measured in precracked laboratory specimens according to standardized methods. Cyclic crack length data are analyzed to yield a material property: averaged fatigue crack growth rate (da/dN) as a function of the applied stress intensity range (ΔK). ΔK is the difference between maximum and minimum stress intensity values during any load cycle.

Paris experimentally demonstrated the principle of similitude; that is, equal fatigue crack growth rates are produced for equal applied stress intensity factors, independent of load, crack size and component or specimen geometry. This da/dN-ΔK behavior is explained based on the fact that ΔK uniquely describes the magnitude and distribution of: (a) elastic stresses, (b) elastic-plastic stresses, (c) plastic strains and (d) plastic zone and fracture process zone size; all local to the crack tip; Section VI.4. The similitude principle enables an

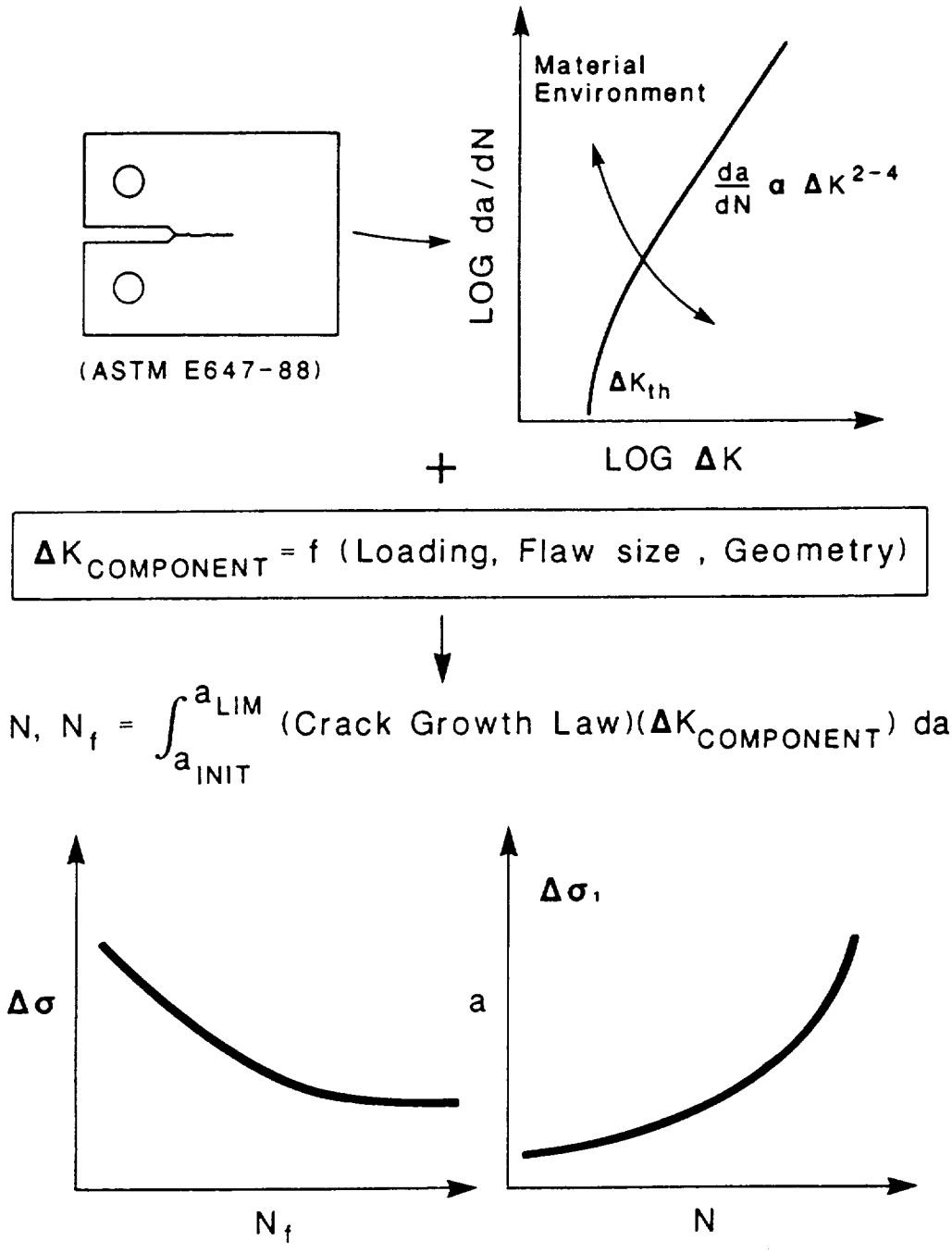

Fig. 7 Fracture mechanics approach to corrosion fatigue crack propagation characterization and component life prediction.

integration of laboratory da/dN-ΔK data to predict component fatigue behavior, in terms of either applied stress range-total life or crack length-load cycles, for any initial defect size.

Fatigue crack propagation rates for inert environments are reasonably approximated by a single function of applied stress intensity range, normalized by the modulus of elasticity, for a variety of engineering alloys and microstructures tested in vacuum, Fig. 8 [26]. This result provides a basis for comparisons of environmental effects. Caution is, however, required. Crack propagation rates in vacuum may be influenced by surface welding during unloading; a more meaningful reference may be provided by ultrahigh purity helium or argon gas, where physically adsorbed molecules minimize surface welding [74]. Secondly, data in Fig. 8 were obtained for near-zero stress intensity ratio ($R = K_{min}/K_{max}$) where extrinsic crack closure can complicate the interpretation of mechanical cracking as discussed in Section VII.2.a. Data in Fig. 8 are a useful guide, however, inert environment experimentation is a requirement for specific corrosion fatigue studies.

III.3. Stress Intensity Similitude: Reactive Environments

The application of fracture mechanics to subcritical stress corrosion and corrosion fatigue crack propagation progressed dramatically and in several periods over the past 25 years, as reviewed by Wei and Gangloff [37].

III.3.a. **The Beginning: 1965-1971.** Extension of the fracture mechanics method to stress corrosion and corrosion fatigue crack propagation was pioneered by Brown and by Wei [90,91], and was exploited by early experimentalists [92-94]. A highlight of this effort was the demonstration, following from the work of Paris on "K-increasing" remotely loaded and "K-decreasing" crack surface loaded specimens, that similitude is obeyed for corrosion fatigue crack growth. As shown in Fig. 9a, equal rates of corrosion fatigue crack growth are produced for equal ΔK, but for both increasing and decreasing net section stress specimens; demonstrating stress intensity control [95].

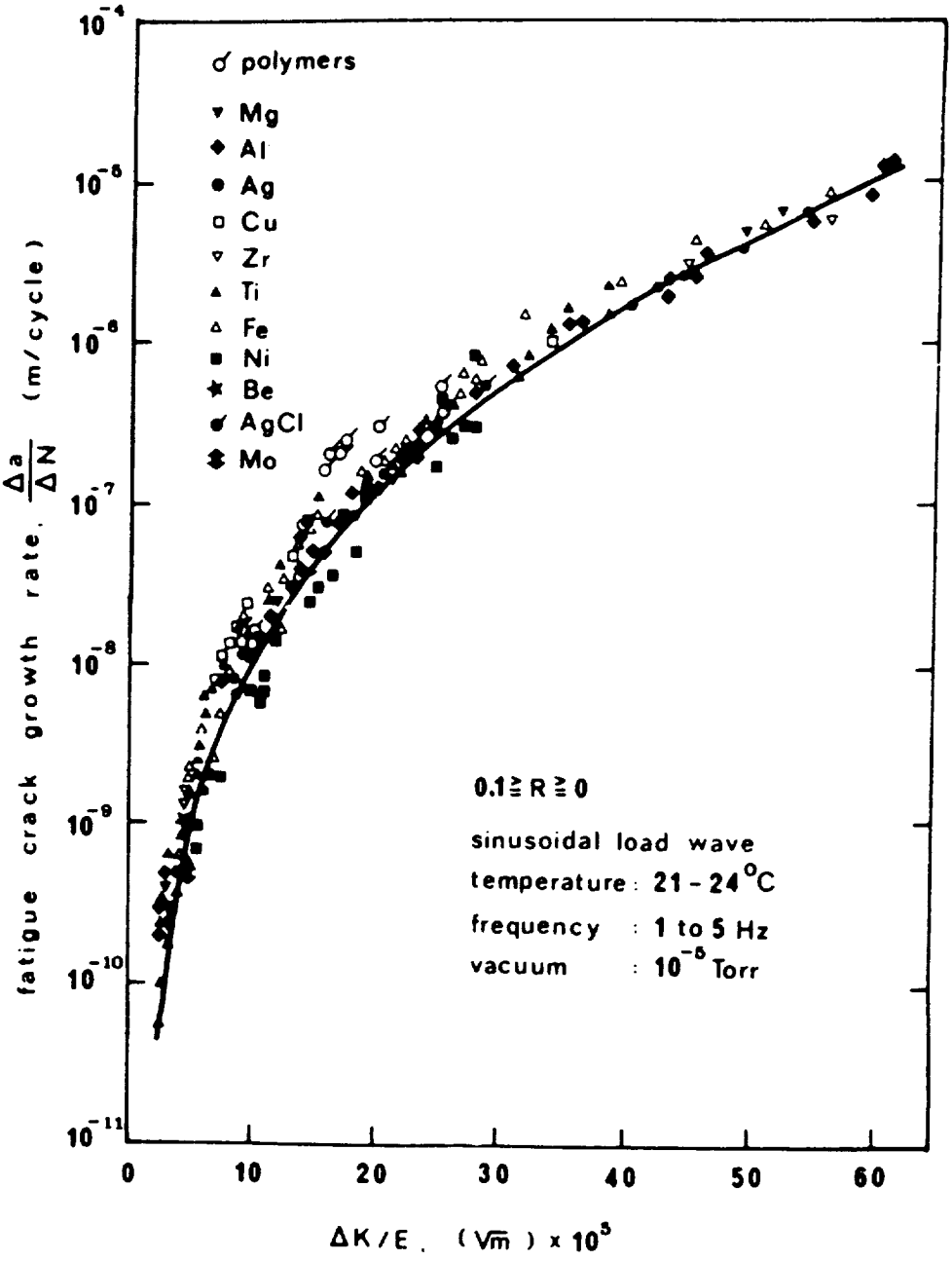

Fig. 8 Inert environment fatigue crack propagation rate as a function of modulus normalized stress intensity range for a variety of engineering alloys; after Speidel [26].

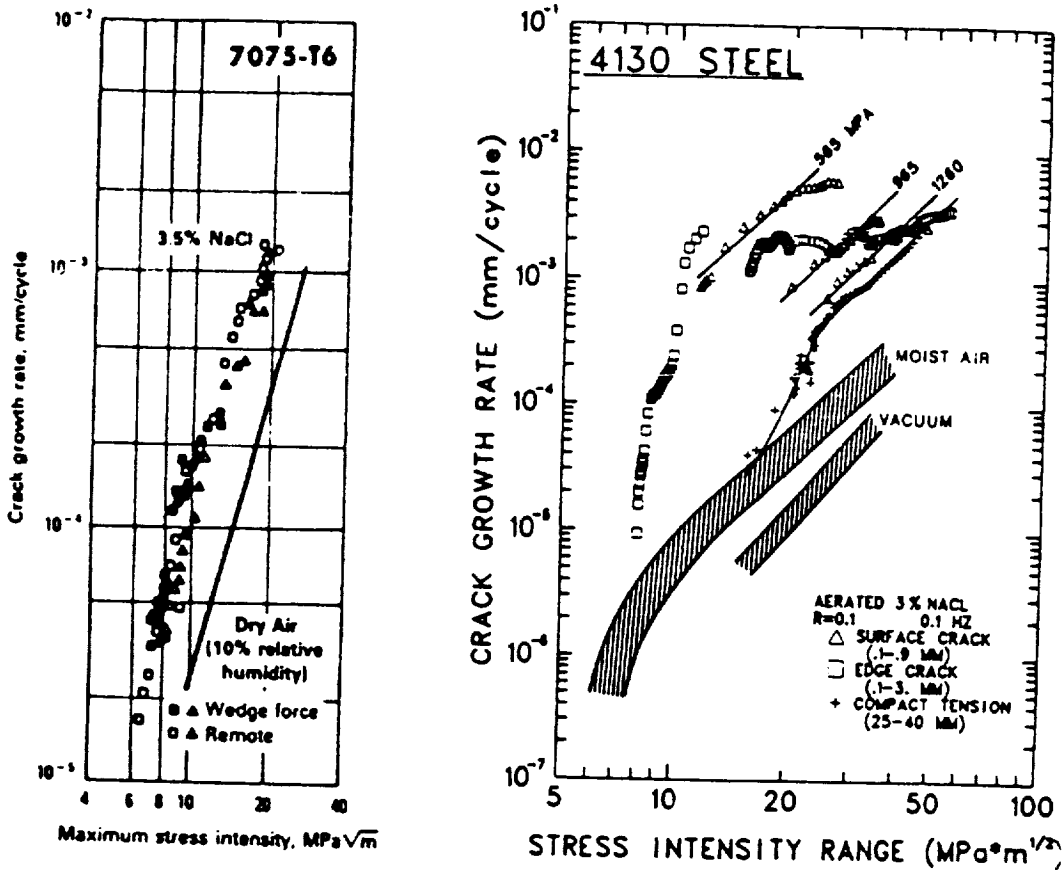

(a) (b)

Fig. 9 Effect of specimen geometry on corrosion fatigue crack growth; demonstrating (a) similitude for remote and crack surface loading; after Feeney, McMillan and Wei [95], and (b) a breakdown in similitude for short edge and surface cracks in aqueous 3% NaCl; after Gangloff [96,97].

III.3.b. **Phenomenological Characterizations: 1970-1984.** The fracture mechanics approach was broadly applied following these initial successes. High strength materials were investigated in the early stages of work, 1970-1976, while more recently (1976-1984) low strength stress corrosion resistant alloys were characterized.

During this later period, concepts of premature crack surface closure were developed, significant understanding of near-threshold fatigue crack propagation emerged, and the small crack problem was intensively investigated; largely for benign environments [41-47]. Work on the implications of these problems to corrosion fatigue indicated cases where the similitude concept was compromised. Data in Fig. 9b show a wide range of corrosion fatigue crack growth rates for any constant ΔK for high strength 4130 steel in aqueous 3% NaCl [96,97]. Here da/dN depends on varying short crack size and applied stress for the aqueous environment, but is uniquely ΔK controlled for benign moist air and vacuum. The origin of this effect is crack size dependent crack tip electrochemistry, as detailed in Section VII.3.

III.3.c. **Scientific Studies: 1973-1987.** Work during this period demonstrated that crack growth kinetics provide a basis for formulation and evaluation of corrosion fatigue crack propagation models [30,33,34,36,39,49,98]. Concepts of mass transport, chemical reaction rate and diffusion control of da/dN were developed for gaseous and aqueous environments. Work in this period emphasized the complex cycle-time-dependent class of corrosion fatigue problems, for the moderate ΔK regime, but with limited studies on near-threshold phenomena. These models are discussed in Section VI.

III.4. Applications to Corrosion Fatigue Life Prediction

III.4.a. **Synthesis of Life Prediction Methods: 1983-1987.** The fracture mechanics life prediction method illustrated in Fig. 7 has been developed for complex structural applications in the energy, petrochemical and transportation sectors as reviewed by Andresen and coworkers [95], Tompkins and Scott [100,101], and Novak and

Barsom [102]. Vosikovsky and Cooke provide an example analysis for corrosion fatigue crack propagation in a welded carbon steel pipeline carrying H_2S contaminated oil [103].

As a further example, the damage tolerant approach has been extensively investigated for welded carbon steel tubular components of oil and gas platforms operating in aggressive marine environments [104-107]. Here, classical design rules, based on smooth specimen fatigue data and modified to account for complex time-dependent corrosion fatigue [108], are being challenged by damage tolerant crack growth procedures [99-101,109-111].

An example of the fracture mechanics framework and component life predictions are shown in Fig. 10. An integrated approach includes fracture mechanics laboratory data, mechanism-based models to extrapolate the data base, and stress/stress intensity analyses of the component to predict cyclic life as a function of applied stress [57,99]. Such a prediction is represented by the band in Fig. 10 [111]. Additionally, full scale component tests are needed to verify the fracture mechanics analysis; the data points in Fig. 10 resulted from extensive (and expensive) fatigue experiments with 0.5 m diameter, 1.6 cm wall thickness welded carbon steel tubulars. Agreement is excellent. Note that the comparison in Fig. 10 is for moist air. Predictions and tests are in progress for tubulars fatigued in actual sea environments with applied cathodic polarization [104-107]. The state of this development is, however, less that than that represented for air.

Active sensors of environment chemistry and corrosion fatigue crack growth are important aspects of a life prediction approach. Such devices have been successfully employed in commercial nuclear power plants, piping systems and offshore structures [99,112-114].

III.5. Corrosion Fatigue Crack Propagation Data Bases

Extensive fracture mechanics-based corrosion fatigue crack propagation data bases were developed over the past two decades. Examples are presented in Figs. 11 through 15.

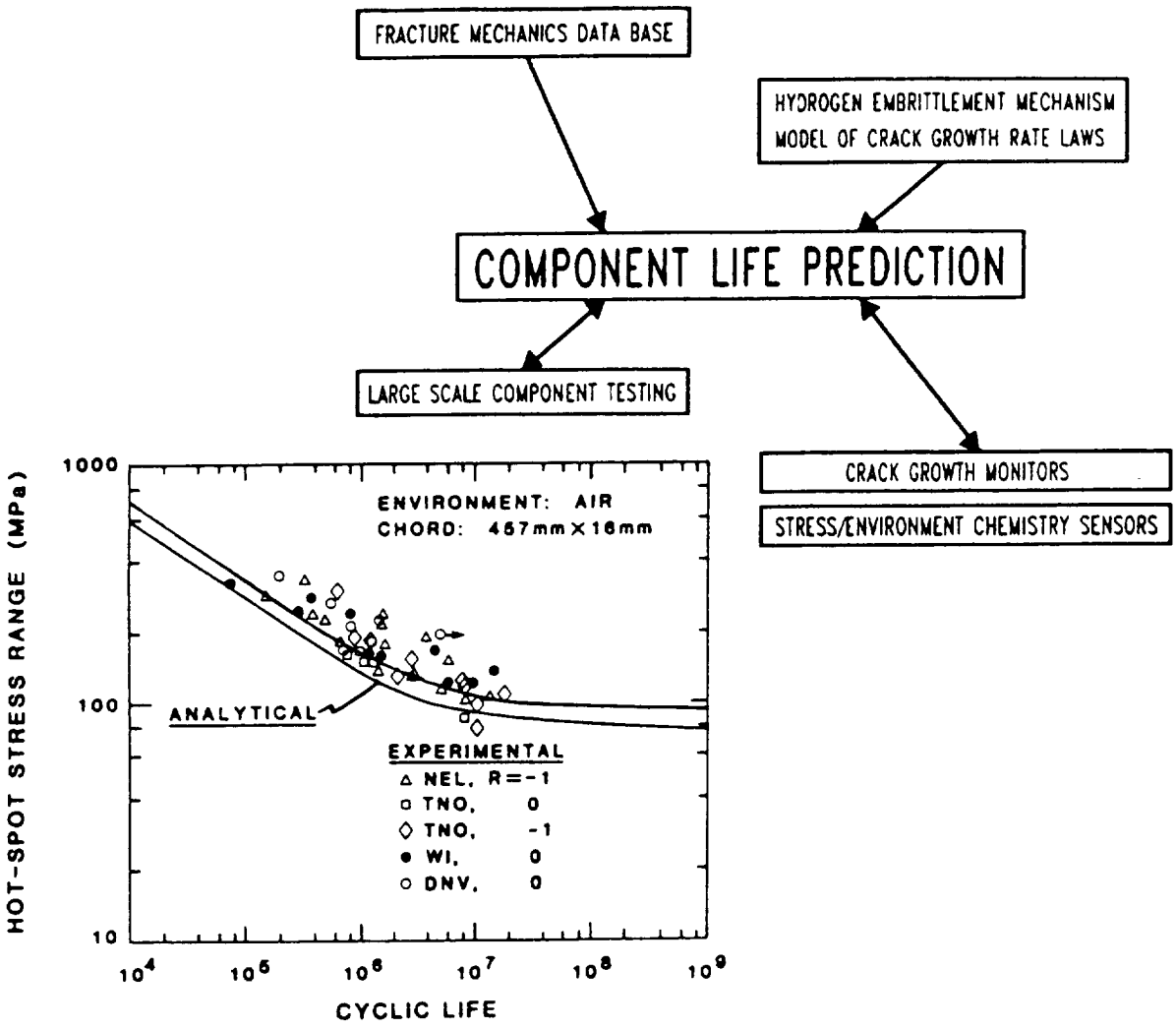

Fig. 10 Integrated fracture mechanics method for fatigue life prediction; after Andresen et al. [99], with a comparison between predicted and measured cyclic life for welded carbon steel tubular joints fatigued in moist air; after Hudak, Burnside and Chan [111].

III.5.a. **Carbon Steels in Hydrogen Producing Environments.** Corrosion fatigue is significant for low strength carbon-manganese steels, of normalized ferrite-pearlite microstructures, stressed in a variety of gaseous and aqueous marine environments. Extensive data are represented in Fig. 11 [115]. Here, K_{ISCC} is well above 100 MPa$\sqrt{m}$; corrosion fatigue is cycle-time-dependent.

Hydrogen embrittlement is implicated for these systems, as demonstrated by the two to three order of magnitude increase in da/dN for X42 steel in high pressure, purified hydrogen gas (curve 2) [117]. Nelson reported similar results for gaseous hydrogen embrittlement of low strength 1020 steel [118]. Considering aqueous environments, seawater produces enhanced fatigue crack growth relative to vacuum and moist air, with the magnitude of the effect increasing from free corrosion (curve 4) to cathodic polarization (curve 3) to H_2S additions at free corrosion (curve 1). The strong effect of H_2S is further evidence for hydrogen embrittlement, and is important to marine applications where biological reactions produce ionic sulfur bearing products [116,122].

The power-law regime of fatigue cracking observed for moist air and vacuum is altered by aqueous environments. A two-slope behavior is shown in Figure 11, where a strong ΔK dependence of rate at lower stress intensities transforms to a milder dependence at higher ΔK. For cathodic polarization, da/dN values within the latter regime are nearly independent of increasing ΔK; a plateau is sometimes observed. Environmental effects on near-threshold crack growth are less well characterized. For free corrosion, ΔK_{th} is reduced by seawater exposure, with the effect of stress ratio paralleling that reported for crack growth in benign environments. For cathodic polarization, high R thresholds are probably similar to those reported for free corrosion, but notably, very high ΔK_{th} values are reported for low R loading, curve 5. Cathodic polarization produces calcium and magnesium hydroxide precipitates within the fatigue crack, causing corrosion product induced crack surface closure contact and increased ΔK_{th}; Section VII.2.a.(2).

The carbon steel-hydrogen environment system was reviewed in

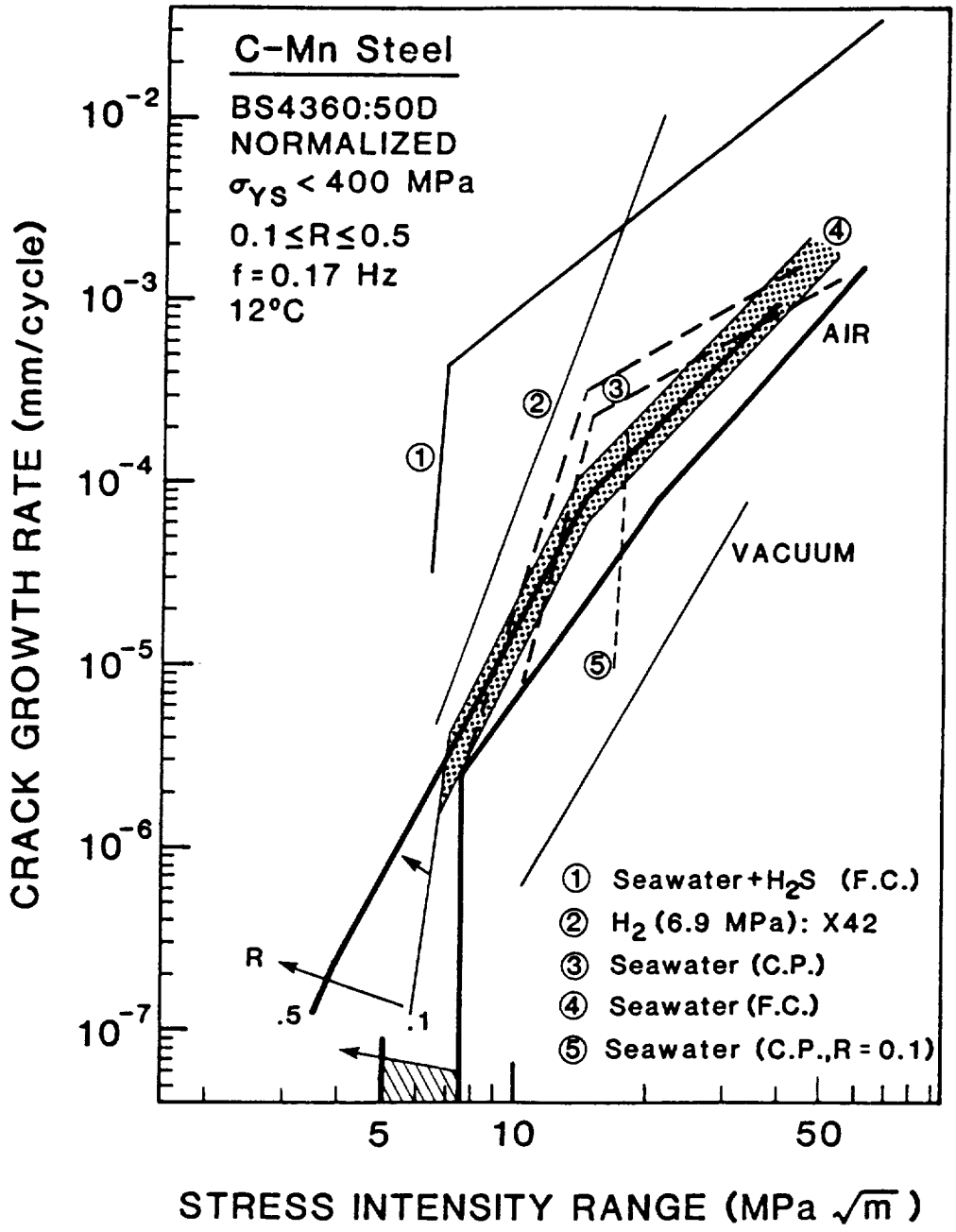

Fig. 11 Corrosion fatigue crack propagation in low strength, normalized carbon-manganese steels in hydrogen-producing environments: 1) Seawater contaminated by H_2S [116], 2) High pressure H_2 [117], 3) Seawater with cathodic polarization [119-122], 4) Seawater at free corrosion [119-123] and 5) Seawater with cathodic polarization at low R [121]; Moist air and vacuum [58,115,124].

detail by Gangloff and Krishnamurthy [115] and by Jaske et al. [32].

III.5.b. **Precipitation Hardened Aluminum Alloys in Aqueous Chloride and Water Vapor Environments.** Extensive corrosion fatigue data have been produced for high strength 2000 and 7000 series aluminum alloys in aqueous chloride and purified water vapor environments. Several conclusions are drawn from a tabulation of typical results, Fig. 12 [5,60,61,65,79,95,125-131].

Both gaseous and aqueous environments produce significant corrosion fatigue crack propagation in aluminum alloys, and relative to helium or vacuum for a wide range of stress intensities. Hydrogen production and embrittlement are implicated for these systems, however, the concurrent actions of anodic dissolution, passive film formation and hydrogen production obscure the dominant mechanism.

For 3% NaCl, the large amount of data at moderate ΔK and low R generally describes corrosion fatigue below K_{ISCC}. Here, aqueous chloride at typical free corrosion potentials (about -800 mV, SCE) increases da/dN by between 4 and 100-fold relative to helium. Distilled water also induces corrosion fatigue; Cl^- exacerbates, but is not a requisite for cracking. Moist air is an embrittling environment compared to helium, particularly for the 7000 series alloys. Wei and colleagues conducted extensive studies of the deleterious effect of pure water vapor on 7000 and 2000 series alloys at moderate stress intensity levels [61,129]. The range of rates varies between an upper bound provided by moist air and a lower bound for inert gas. 7000 series aluminum alloys containing Zn, Mg and Cu are more susceptible to corrosion fatigue compared to 2000 series alloys in the Mg+Cu and Li+Cu classes.

Only limited data have been obtained to describe near-threshold corrosion fatigue crack propagation in aluminum alloys [60,125,126,132]. Here, only high stress ratio results are reasonably interpreted because the complicating extrinsic effects of crack closure are minimal, Section VII.2.a. As shown in Fig. 12, water vapor, moist air and aqueous chloride (either free corrosion or cathodically polarized) are embrittling relative to

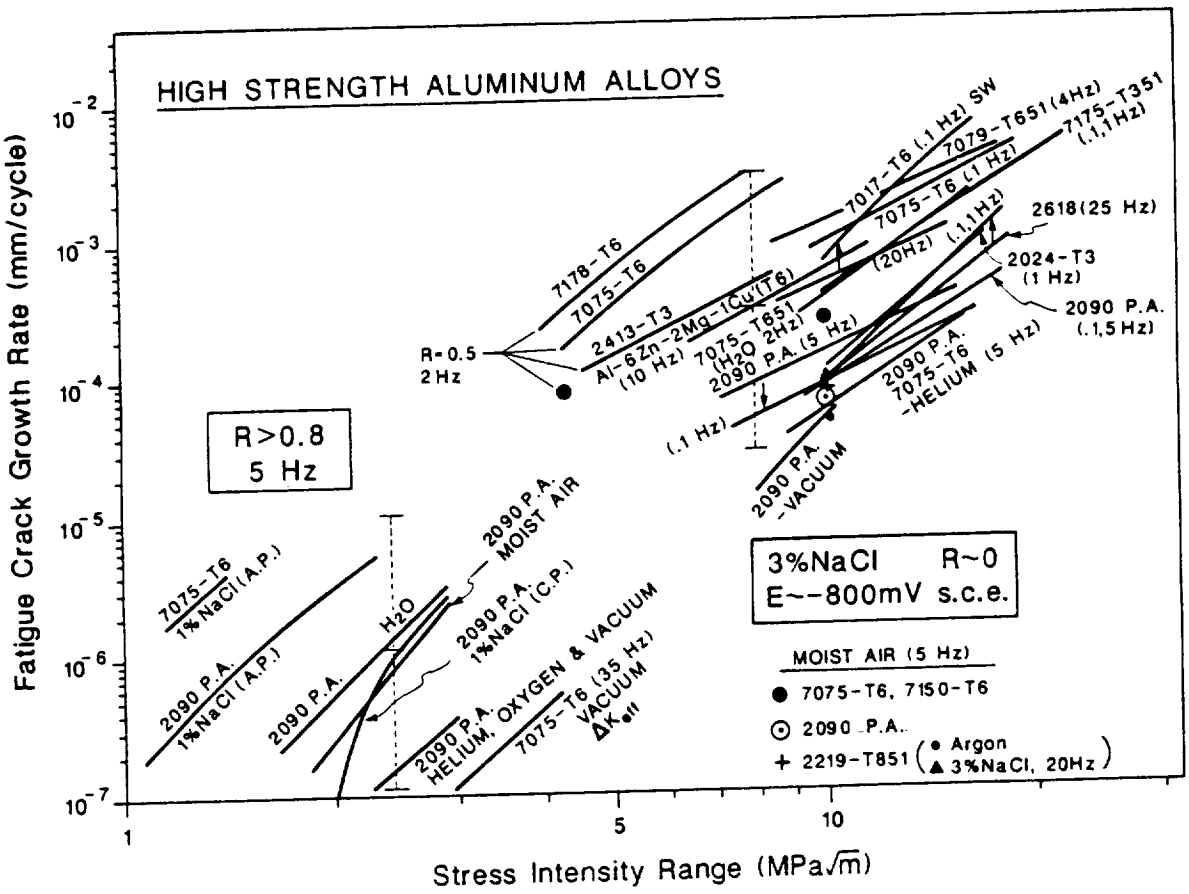

Fig. 12 Corrosion fatigue crack propagation in high strength 2000 and 7000 aluminum alloys for (1) Case A: High ΔK, low R; aqueous 3% NaCl near free corrosion [21,95,61,64,79,125-130] and (2) Case B: Near-threshold at high mean stress with aqueous chloride and gaseous environments [60,125,126].

helium. The mechanism for this effect is speculative, with both hydrogen embrittlement and film rupture/dissolution processes possible. Notably, similar da/dN are reported for helium and oxygen, suggesting a minimal effect of surface oxide films. The 7000 alloy is more prone to corrosion fatigue compared to 2090, an advanced Al-Li-Cu alloy.

The transgranular corrosion fatigue sensitivity of 7000 series alloys, Fig. 12, parallels the well known differences in intergranular SCC resistance for these alloy classes [133]; the fundamental mechanism for the effect of alloy composition is, however, unclear. That a similar ranking is observed for aqueous chloride, moist air and water vapor suggests that hydrogen embrittlement is central to the explanation. The systems represented in Fig. 12 were reviewed by Speidel and Duquette [5,62].

III.5.c. C-Mn and Austenitic Stainless Steels in High Temperature Water Environments.

An extensive data base describes the stress corrosion and corrosion fatigue crack propagation kinetics for austenitic stainless and C-Mn pressure vessel steels in elevated temperature, pressurized water environments [134,135]. Such data resulted from work over the past two decades, aimed at guaranteeing the structural integrity of light water nuclear reactor plant materials, and organized under the auspices of the International Cyclic Crack Growth Rate Group. These fracture mechanics data, the hypothesized film rupture mechanism, component life prediction procedures, and new environment chemistry and crack growth damage sensors were reviewed by Ford, Andresen and coworkers [39,70,71,99,136-138], and by Scott and Tompkins [34,100,101].

Corrosion fatigue crack propagation in nuclear reactor materials and environments is complex, owing to the interactive effects of many variables [39]. Typical data are presented in Figs. 13 and 14. Da/dN versus ΔK data for normalized C-Mn steel in 288^{o}C, low oxygen water (Fig. 13) show a strong environmental effect relative to inert environment behavior [39,136]. Note the low loading frequency (0.017 Hz) and high mean stress (R = 0.7)

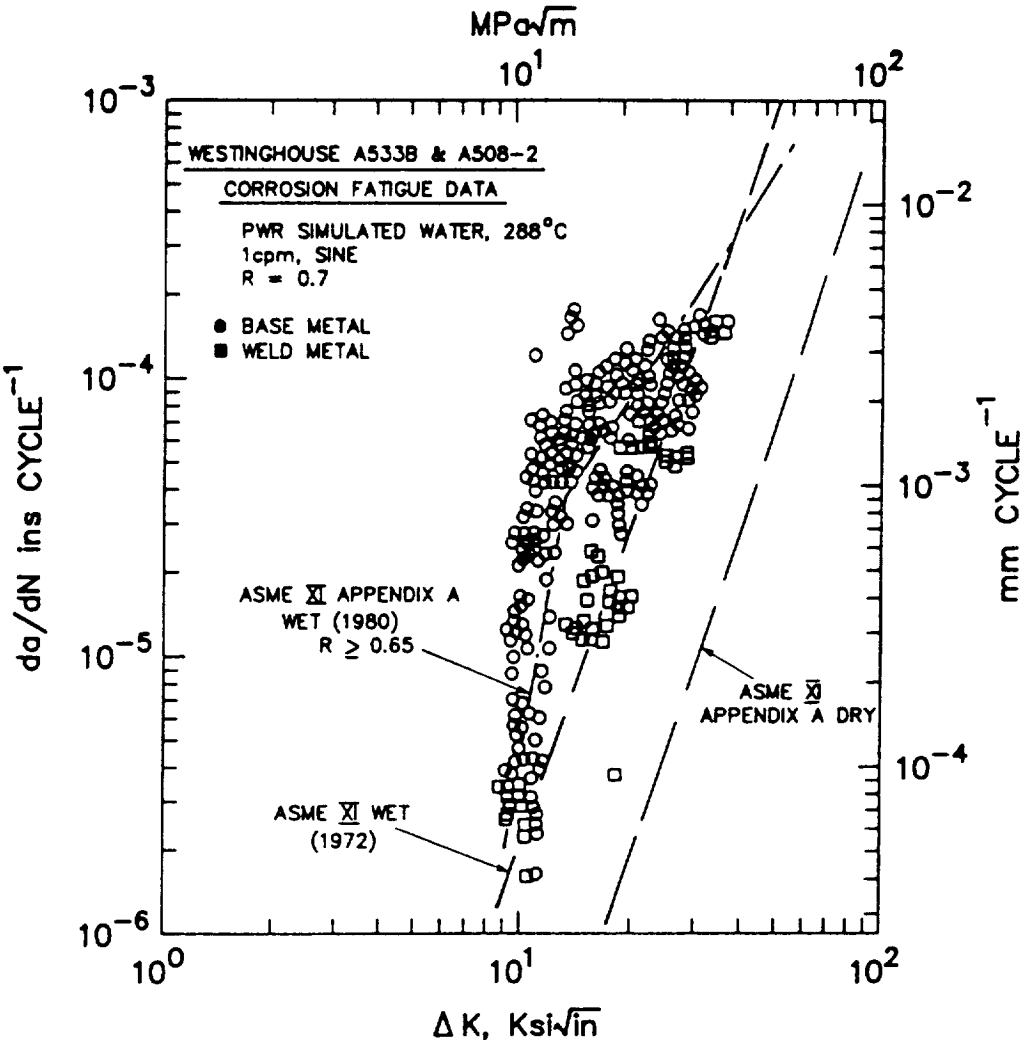

Fig. 13 Corrosion fatigue crack propagation data for normalized C-Mn steel in elevated temperature (288°C) pressurized water at low cyclic frequency and high R. After Jones [39,136].

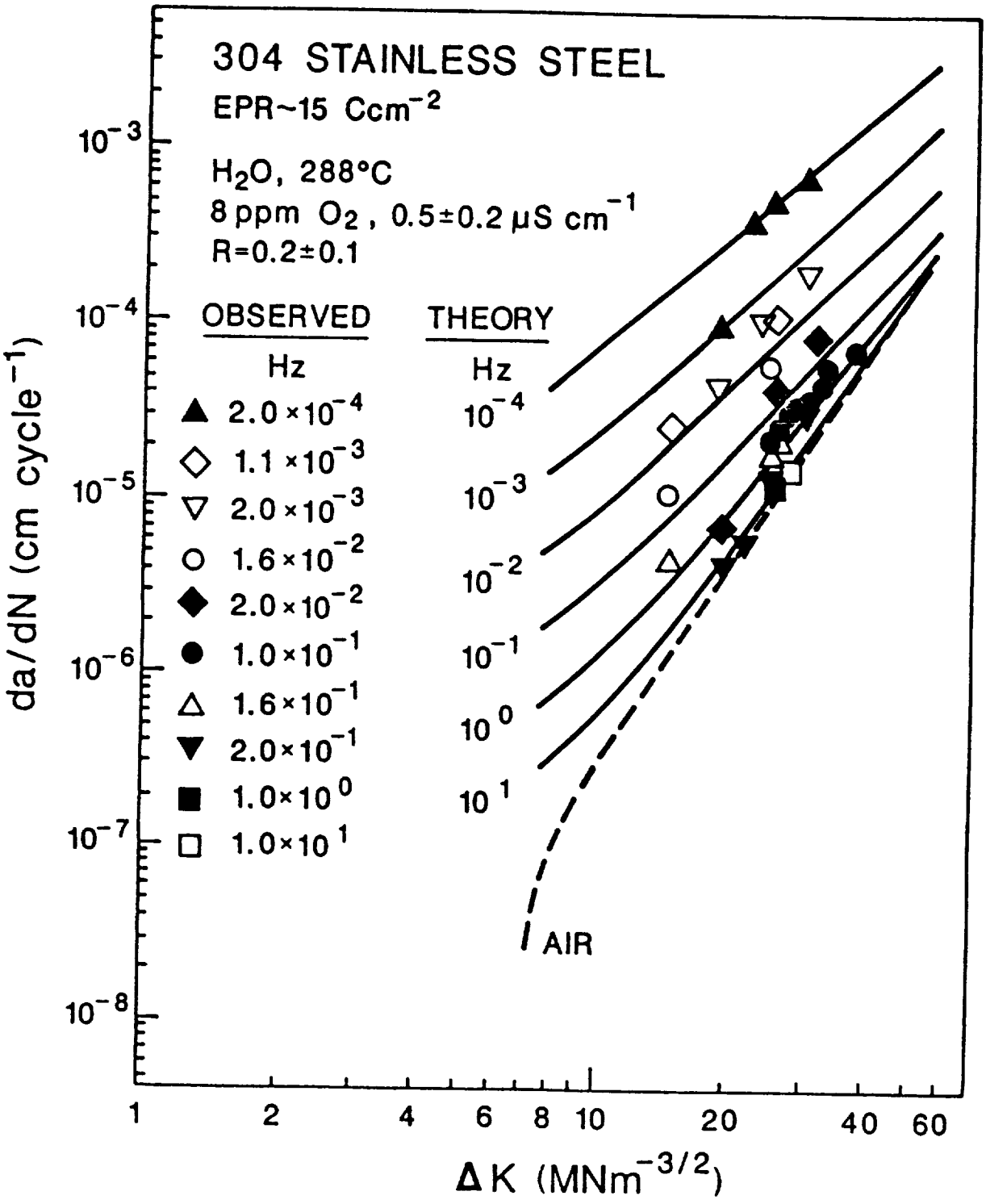

Fig. 14 Corrosion fatigue crack propagation data for sensitized stainless steel in oxygenated, high temperature water showing the deleterious effect of slow cyclic loading frequency; after Ford et al. [137].

conditions. Environmental cracking can exceed ASME Section XI criteria; such empirical guidelines have been increased as new results and heightened concerns on corrosion fatigue emerged from laboratory experimentation [100,136].

The significant variability shown in Fig. 13, and further emphasized if a larger population of results are considered [139], is traceable to a complex interaction between the MnS inclusions in the steel, the flow conditions of solution surrounding the fracture mechanics specimen in the autoclave and the electrode potential of the specimen, largely established by the dissolved oxygen content of the solution [39,139].

The strong effect of cyclic loading frequency is illustrated in Fig. 14 by da/dN-ΔK data for sensitized AISI 304 stainless steel in oxygenated, high temperature, pressurized water [137]. As typically observed, corrosion fatigue crack propagation rates increase with declining frequency; certainly for moderate levels of ΔK, with the near-threshold response unclear. Film rupture models, including detailed treatments of crack electrochemistry, explain the distributed results shown in Fig. 13 and predict the effects of a broad range of variables including frequency [39,71,99,136,138]. Comparison between measured and predicted da/dN, Fig. 14, provides an example of this predictive power.

III.5.d. **Titanium Alloys in Aqueous Electrolytes.** Since the pioneering stress corrosion cracking work of Brown, which showed the sensitivity of precracked titanium alloys to aqueous chloride solutions [140], many studies have investigated the corrosion fatigue behavior of this structural material [5]. Typical data are presented in Fig. 15. Here corrosion fatigue crack growth rates are enhanced up to 10-fold by cyclic loading in several halogen-bearing solutions at the free corrosion potential. A wide range of da/dN is likely, depending on solution electrochemistry, ΔK, frequency, and titanium alloy microstructure [65,141,142].

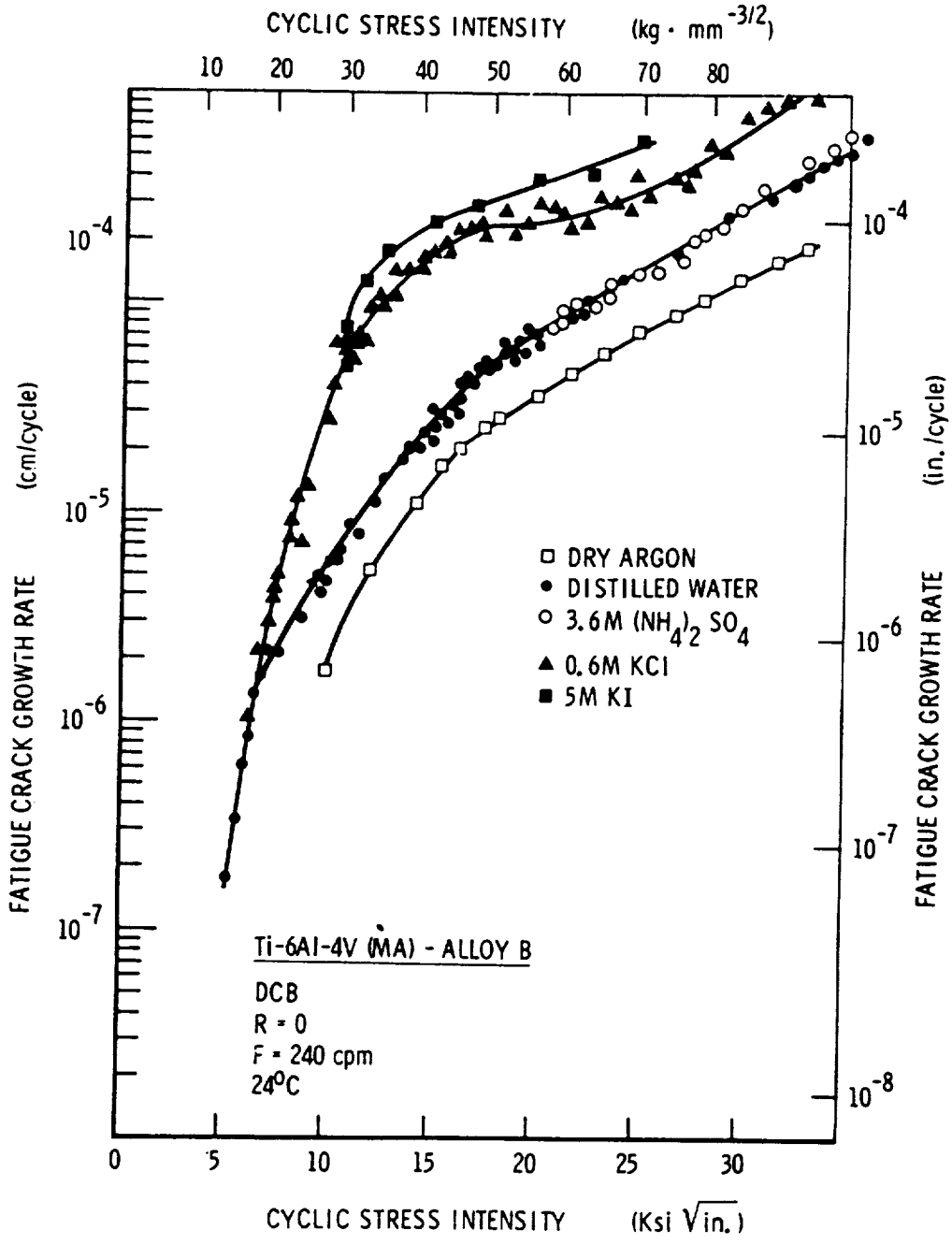

Fig. 15 Corrosion fatigue crack propagation data for a high strength titanium alloy in aqueous halide solutions; after Speidel et al. [5]. (1 ksi $\sqrt{in}$ = 1.098 MPa $\sqrt{m}$)

IV. EXPERIMENTAL PROCEDURES

IV.1. Conclusion

Experimental methods are developed for determinations of average crack growth rate as a function of continuum fracture mechanics crack tip parameters, particularly ΔK. Non-steady state crack growth, unique to corrosion fatigue, and crack closure are not understood. Future procedures will incorporate precision crack length measurement and computer control of stress intensity to develop quantitative and novel corrosion fatigue crack growth rate data, particularly near threshold. Advances have been recorded in measurements of small crack growth kinetics, however, such approaches are not easily adapted to controlled environments. The fundamental experimental problem is the lack of methods to probe mechanical and chemical damage processes local to the corrosion fatigue crack tip.

IV.2. Fracture Mechanics Methods

Following from Fig. 7, the procedure for laboratory measurement of fatigue crack growth rate as a function of ΔK is standardized by ASTM Committee E24 on Fracture Mechanics [143]. Additional details, specific to moist air, are provided by a summary chapter in the Metals Handbook and by user experiences [144-145]. Two aspects, environment control and crack length measurement, are uniquely important to corrosion fatigue, as indicated by an annex to the ASTM standard and a U.S. Navy procedure for seawater [143,146].

Control and characterization of the gaseous or aqueous environment which surrounds the specimen is of paramount importance to corrosion fatigue experiments. Particular emphasis must be placed on control and measurement of variables such as electrode potential, environment ionic and dissolved oxygen compositions, purity, flow rate and temperature. Successful approaches have been reported for most environments, as reviewed by Gangloff et al. [147]. Detailed procedures are often complex, as illustrated by work on fatigue in high temperature, pressurized water environments. Owing to the importance of slow

loading frequency in exacerbating corrosion fatigue, experiments must often be maintained for weeks or months.

A wide range of crack length monitoring methods are employed in fracture mechanics studies of fatigue, as illustrated in Fig. 16 after Marsh and Smith [148]. The indirect or remote methods are required for corrosion fatigue because the fracture mechanics specimen is immersed in an environmental chamber. Periodic interruption of loading or chemical exposure may introduce transient cracking. To date, successful applications have been reported for the compliance and electrical potential difference methods. Procedures for each approach are reviewed in two volumes edited by Beevers [149,150].

The electrical potential method has been widely applied to studies of corrosion fatigue (for example, References 50,61,97,121,151) because of the simplicity of employing simple wire probes in aggressive environments, and because the approach is applicable to through-thickness and surface crack geometries. Typical data are presented in Fig. 17, where computer acquisition and high gain stable amplification produced hundreds of measured data points which merge into a continuous line. Here, crack growth occurred at constant ΔK with a single rate observed for air but not the aqueous chloride environment. The averaged resolution of the potential difference approach varies between 2 and 30 μm, depending on circuity and specimen geometry.

In all cases reported, the application of high (1 to 50 amperes) direct or alternating current has no effect on corrosion fatigue for gases or electrolytes. Presumably, the conductivity of the specimen is orders of magnitude higher than that of electrolytes, including conductive chloride; current leakage into solution at the crack tip is not significant. Possible drawbacks of the potential difference method include specimen heating, crack surface electrical contact (or shorting) when the crack surfaces are maintained clean and conductive, and a lack of information on crack surface contact and mechanical load transfer.

Compliance measurements yield accurate determinations of crack length and provide an approximate indication of the extent

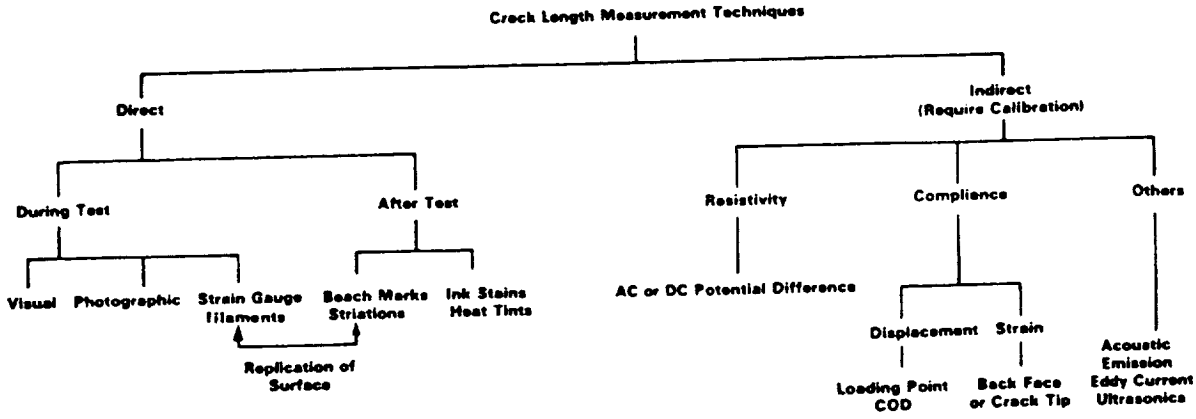

Fig. 16 Methods for measurement of fatigue crack length; after Marsh and Smith [148].

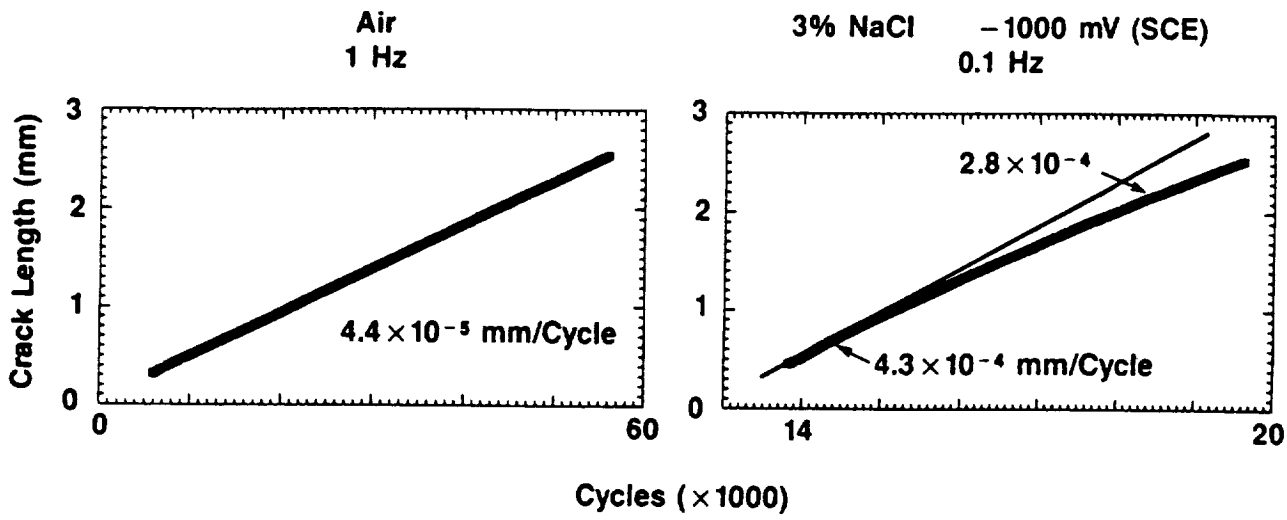

Fig. 17 Cyclic crack length data from automated dc electrical potential measurements of cracks in API-2H steel in moist air or aqueous NaCl with cathodic polarization and at constant ΔK; after Gangloff [158].

of crack closure (Section VII.2.a). Crack length resolution is on the order of 25 μm for typical long (25 mm) crack specimens. While the use of crack mouth or back face displacement gages in gases and liquids is complex, the problems are not insurmountable as indicated by specific applications [60,123,130,136,139,142, 152,153]. The main issue associated with the compliance approach is the arbitrary character of the determination of an "effective" stress intensity to describe growth rates independent of crack closure. In this regard, the usefulness of crack mouth-opening and back face compliance measurements is currently debated.

It is critical to experimentally differentiate transient and steady state corrosion fatigue crack growth rates, with the former dependent on time or equivalently loading cycles at constant applied stress intensity as discussed by Hudak and Wei [154]. Crack geometries, programmed loading histories and test interruptions; which are allowable under the standard and do not influence benign environment fatigue; can significantly influence corrosion fatigue crack propagation. This complicating phenomena is attributed to time dependent chemical contributions to fatigue damage, Section VII.3.

IV.3. New Procedures

The data presented in Figs. 11 through 15 were obtained by constant load, increasing ΔK, or by programmed continuously decreasing ΔK methods [155]. That such rates represent steady state conditions governed solely by ΔK is, however, generally not proven and the effects of loading history and crack size are not understood.

The coupling of recent advances in remote crack length measurement with the computer controlled servohydraulic test machine enables meaningful characterizations of corrosion fatigue crack propagation rates. A useful procedure to supplement constant load or continuously decreasing ΔK cracking is represented in Fig. 18 for the case of ferritic steel in aqueous chloride. Here, ΔK is maintained constant at selected levels labeled 1 through 7, and by either compliance or electrical potential measurements of crack length and computer controlled

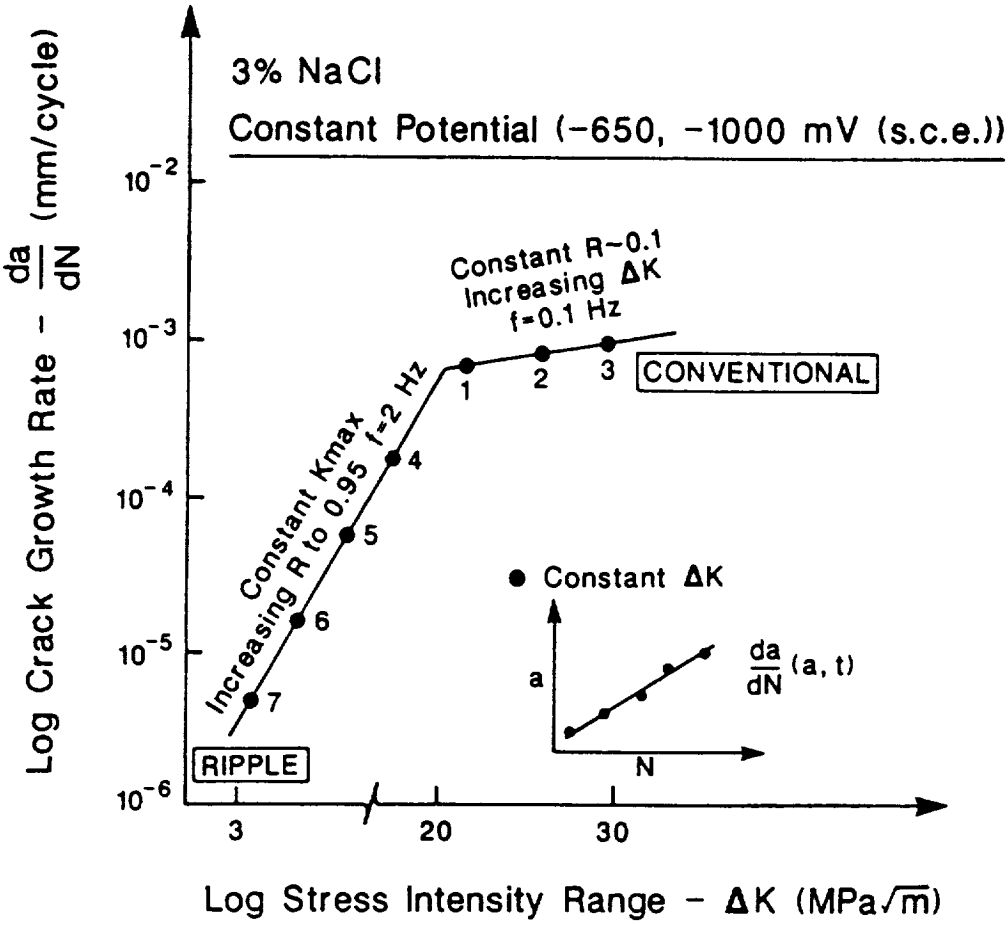

Fig. 18 Programmed stress intensity characterization of corrosion fatigue crack propagation for steel in chloride, based on constant ΔK segments at constant K_{max} and varying R.

load reductions. Steady state crack growth and transient behavior will be indicated by the character of the crack length versus loading cycles data; viz, linear for the former and nonlinear for the transient case.

As a second sophistication, two regimes of crack growth can be probed by a procedure recently discussed by Hertzberg and coworkers [156]. For high ΔK and low R (points 1 to 3) stress ratio is maintained constant as increasing levels of constant ΔK are programmed. Subsequent tests are conducted at constant K_{max} and several levels of constant ΔK selected to decrease, with increasing R. In this way near-threshold corrosion fatigue crack propagation is characterized without the complicating effects of delay retardation or crack closure. The possibility of closure effects at any combination of ΔK and R can be assessed by the linearity of cyclic crack length data, and by compliance measurements coupled with variations in K_{min} below the indicated crack opening load.

The approach in Fig. 18 has several advantages in addition to demonstrably steady state kinetics. With constant ΔK and precision measurements of crack length, low values of da/dN can be obtained for low frequency loading over a reasonable test time because the crack growth increment for a meaningful rate determination is small. Secondly, environmental and loading frequency variable effects are readily determined to within about $\pm$ 20% uncertainty, based on changing cyclic crack growth rate response at constant ΔK and R. Finally, the procedure in Fig. 18 probes two important regimes of fatigue crack propagation, including conventional high ΔK low R and high R near-threshold or "ripple" loading. This approach was successfully applied in an investigation of corrosion fatigue crack propagation in an aluminum-lithium alloy [125,126].

The methods discussed above are based on small scale yielding throughout the precracked specimen. Dowling extended this linear elastic approach to describe fatigue crack propagation during large scale yielding based on the J-integral characterization of the crack tip stress and strain field [157]. While established for moist air, this approach has not been

applied to corrosion fatigue.

IV.4. Novel Measurements of Corrosion Fatigue Cracking

The fracture mechanics approach is based on measurements of average crack growth rate and applied stress intensity for specimens containing single, large (> 25 mm) cracks. A second level of measurement probes mechanical and chemical damage processes local to the crack tip. Only limited successes have been recorded.

Electrical potential measurements can be employed to continuously monitor the growth of single, defect nucleated fatigue cracks sized above about 50 μm [158]. This method is applicable to aqueous (for example, Fig. 17) and high purity gaseous environments, and has been successfully used to monitor the growth of corrosion fatigue cracks in single, albeit large, grains of steels, nickel-based and aluminum alloys [97,125,126,159]. Despite these successes, this method does not directly probe crack tip damage processes.

Plastic tape replication measurements are employed to monitor the surface growth of small fatigue cracks in moist air [157]. This method requires periodic loading interruptions which may affect corrosion fatigue, it does not directly probe crack tip damage and it does not provide information on the crack perimeter. The only benefit over electrical potential monitoring is that replication methods characterize fatigue crack nucleation at natural microstructural features and defects such as inclusions.

Papers within this volume do not discuss experimental characterizations of crack tip chemical and mechanical damage. This omission is traceable to the complexity of such endeavors. Gerberich, Davidson and Lankford reviewed various microscopic techniques directed at crack tip fracture observations [160,161]. The following methods yielded insights on fatigue crack propagation for vacuum and moist air:

Insitu Scanning Electron Microscopy of a Cyclically Loaded

Specimen; Stereoimaging Analysis

Electron Channeling Pattern Techniques

High Voltage Transmission Electron Microscopy

X-ray Diffraction and Topographic Techniques

TEM Analysis of Crack Wake Dislocation Morphologies

Insitu Auger Cracking and Chemical Analysis

These methods have not been widely applied to corrosion fatigue.

As an example, Davidson and Lankford employed stereoimaging to show that environment affects crack tip plasticity and crack growth mode [162-164]. For constant applied ΔK, near crack tip opening strain decreased for embrittling compared to inert environments. These studies were conducted with 1020 steel and 7075-T651 aluminum specimens which were loaded cyclically and observed in the SEM vacuum after prior fatigue cracking in either moist air or dry N_2. Additional work involved SEM analysis of crack wake subboundaries formed by prior fatigue in moist air or dry N_2. Insitu environmental cracking was not attempted. The mechanistic implications of this work are discussed in Section VII.2.b.

Wei and coworkers employed Auger spectroscopy to measure rates of water vapor and H_2S reactions with both polished and <u>in situ</u> fractured alloy surfaces [37,66,129]. These chemical kinetics were employed to model rates of corrosion fatigue crack propagation.

Since the early work of Brown [165], researchers have employed electrochemical probes to define the crack environment. Corrosion fatigue of a carbon-manganese steel in seawater has been extensively investigated by this approach [166-168]. Near crack tip pH, potential and chloride ion concentration were measured for comparisons with mass transport and reaction model predictions. Detailed reviews of these experimental measurements are presented elsewhere [138,169].

V. EFFECTS OF CRITICAL VARIABLES

V.1. Conclusion

A plethora of interactive variables influences the corrosion fatigue crack growth rate-stress intensity relationship. The effects of chemical, metallurgical and mechanical variables are well characterized and reasonably explained by qualitative arguments. Growth rates are affected by environment chemistry variables (viz: temperature; gas pressure and impurity content; electrolyte pH, potential, conductivity, and halogen or sulfide ion content); by mechanical variables such as ΔK, mean stress, frequency, waveform and overloads; and by metallurgical variables including impurity composition, microstructure and cyclic deformation mode. Time, or loading frequency, is critical; complicating long-life component performance predictions based on shorter term laboratory data. Limited studies show that yield strength is not a critical variable in cycle-time dependent corrosion fatigue. Fractographic analyses of microscopic crack paths provide a basis for failure analyses and input to mechanistic studies.

V.2. Introduction

Alloy development and life prediction approaches to control corrosion fatigue are confounded by the many interactive variables which affect crack propagation, beyond that expected based on benign environment fatigue. Table 1 lists these variables for steels in marine environments. The goal in corrosion fatigue is to develop $da/dN-\Delta K$ relationships which include the effects of all such variables.

The variables in Table 1 influence fatigue crack propagation in most alloy systems. Detailed analysis of each effect is not possible. Rather, the following discussion illustrates typical effects of the more important variables for ferrous, aluminum and titanium alloys. Qualitative explanations for the experimental trends are provided. Quantitative models of fatigue crack growth rate response are outlined in Section VI.

TABLE 1 -- MECHANICAL, ENVIRONMENT CHEMISTRY AND METALLURGICAL VARIABLES AFFECTING CORROSION FATIGUE IN MARINE ENVIRONMENTS

STRESS INTENSITY RANGE	MEAN STRESS
CRACK SIZE AND GEOMETRY	RESIDUAL STRESS
LOADING WAVEFORM AND SEQUENCE	LOADING FREQUENCY
SOLUTION Cl^-, H^+, O_2, Mg^{++}, Ca^{++}	ELECTRODE POTENTIAL
HYDROGEN UPTAKE PROMOTERS, $S^=$	SOLUTION FLOW
CALCAREOUS DEPOSIT FORMATION	EXPOSURE TIME
STEEL YIELD STRENGTH	SPECIMEN THICKNESS
STEEL COMPOSITION AND MICROSTRUCTURE	

V.3. Mechanical Loading Variables

V.3.a. **Stress Intensity Factor Range.** That applied stress intensity range affects rates of corrosion fatigue crack propagation in a complex fashion compared to inert environments is illustrated in Fig. 1. Specific data are presented in Figs. 3, 6, 9, 11, 13, 15 and 19.

While a simple powerlaw response is typical for a limited range of ΔK (Figs. 3, 6 and 11), the more general behavior is indicated in Fig. 19 for Ti-6Al-4V, X-65 controlled rolled microalloyed ferritic steel, and precipitation hardened aluminum alloy 7017-T651, each in aqueous chloride (see also Figs. 9, 13 and 15) [34,64,141,170]. Such results are expected because inert environment fatigue is driven by crack tip plasticity, which is simply related to ΔK and compared to the conjoint plastic strain and chemical processes involved in corrosion fatigue.

At present, there are only limited analytical predictions of the stress intensity dependence of corrosion fatigue crack propagation rates. Micromechanical-chemical models exist, as discussed in Section VI, however, most are based on simplifying assumptions. It is useful to consider that three regimes of corrosion fatigue crack growth are possible, as represented schematically in Fig. 1 for Type A cycle-time-dependent behavior.

Near-threshold ($da/dN < 10^{-6}$ mm/cycle), environmental effects may reduce ΔK_{th} and increase da/dN paralleling benign environment behavior. In Fig. 19 rates for the titanium alloy are well above 10^{-6} mm/cycle, however, imaginative extrapolation suggests that the environment could lower ΔK_{th} and raise growth rates relative to moist air. For steels, indications of this effect were reported by Booth et al. [123] and by Bardal [119]; however; little difference is seen for near-threshold cracking in chloride versus moist air in Fig. 19. In fact near-threshold rates for the former are less than moist air kinetics and perhaps approach vacuum behavior. Near-threshold corrosion fatigue in aluminum alloys is largely unexplored; limited data are shown in Fig. 12 [126].

Measurements of crack growth in the near-threshold regime are prohibitively time consuming owing to the low loading

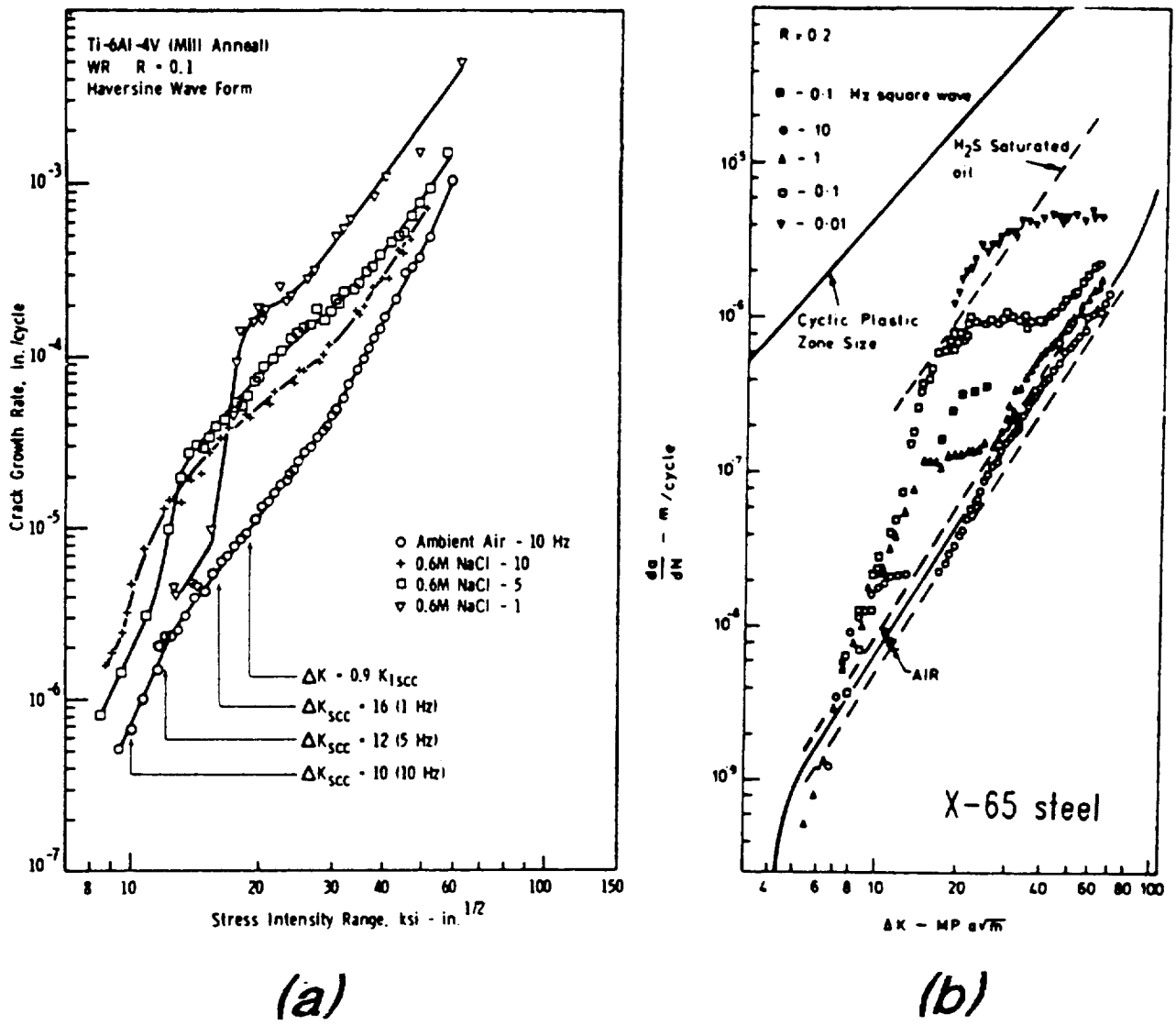

Fig. 19 Effect of ΔK on corrosion fatigue crack growth rate at several frequencies for: (a) Ti-6Al-4V in 0.6 M NaCl; after Dawson and Pelloux [141], (b) X-65 C-Mn steel in 3.5% NaCl with cathodic polarization; after Vosikovsky [34,170], and (c) 7071-T651 aluminum alloy in seawater; after Holroyd and Hardie [65]. (1 in/cycle = 25.4 mm/cycle, 1 ksi $\sqrt{in}$ = 1.098 MPa $\sqrt{m}$)

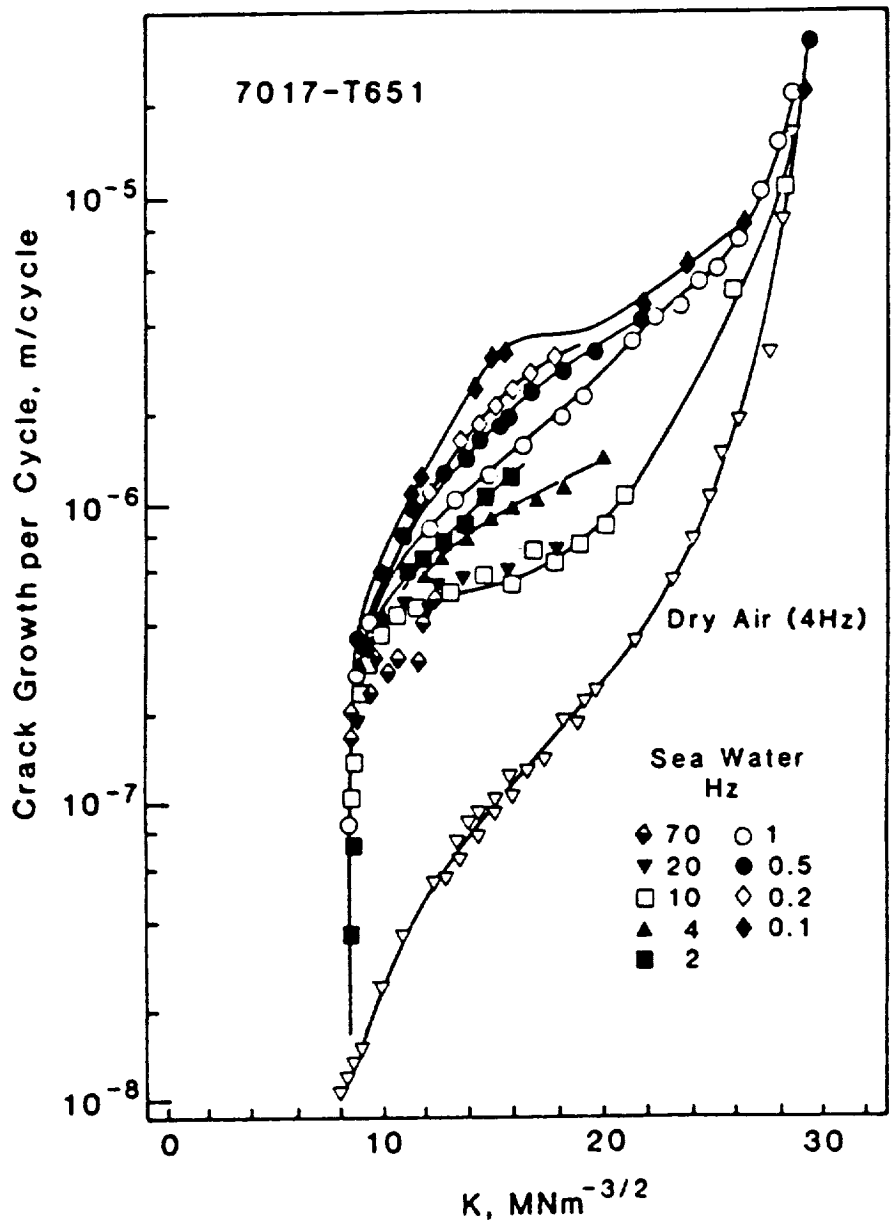
7017-T651
Crack Growth per Cycle, m/cycle
10^{-5}
10^{-6}
10^{-7}
10^{-8}
0
10
20
30
K, $MNm^{-3/2}$
Dry Air (4Hz)
Sea Water
Hz
70
20
10
4
2
1
0.5
0.2
0.1

(c)

frequencies relevant to corrosion fatigue [120,171]. As such, environmental effects are poorly understood, as illustrated by models which predict that hydrogen embrittlement may reduce ΔK_{th}, while corrosion blunting of the crack tip may increase the threshold relative to an inert reference environment [39,172]. The experimental procedure outlined in Fig. 18 provides a means of characterizing low growth rate corrosion fatigue.

A second regime of corrosion fatigue crack propagation is often observed for stress intensity levels above the fatigue threshold. Here corrosion fatigue da/dN values increase rapidly relative to the reference environment and with a significantly stronger power-law dependence. This behavior is shown for each alloy in Fig. 19 and may be interpreted as the intervention of cyclic deformation stimulated "stress corrosion cracking" [34,59,141]. The steep slope is interpreted as evidence of mechanically rate limited crack propagation in the presence of fast and sufficiently completed chemical reactions and mass transport.

A third regime of corrosion fatigue response at higher ΔK is typified by so called "plateau" nearly K-independent behavior, or more generally, by a reduction in the slope of the da/dN-ΔK dependence. This former behavior is indicated for the steel-NaCl system in Figs. 11 and 19, while a reduced power-law relationship is observed for the titanium and aluminum alloys. The reduced dependence on ΔK is interpreted as due to a constant, K-independent, transport limited "cyclic SCC" rate superimposed on a ΔK dependent mechanical fatigue process. Stated equivalently, plateau behavior may be due to chemically rate limited environmental cracking which cannot respond to increasing mechanical driving force.

Corrosion fatigue crack growth rates intersect and equal benign environment values at very high ΔK approaching K_{IC}. This regime is of little significance owing to the high levels of ΔK and fast crack growth rates involved.

The stress intensity dependence of corrosion fatigue is typically characterized by a simple constant load, increasing ΔK experiment. The data in Fig. 19 were determined by this method.

To date there have been no extensive studies of the load and crack length history dependence of the da/dN-ΔK relationship for corrosion fatigue. That the results in Fig. 19 are true material property laws which are independent of loading and geometry factors remains to be proven. This issue is particularly important when small crack and crack closure processes occur, as discussed in Section VII.

When characterizing the effects of variables on corrosion fatigue crack propagation and when developing models, it is important to recognize the various ΔK regimes.

V.3.b. **Mean Stress.** Increasing mean stress intensity, as characterized by the "stress ratio" ($R = K_{min}/K_{max}$), generally increases rates of fatigue crack propagation, particularly for low growth rates ($< 10^{-5}$ mm/cycle), and inert or aggressive environments. For the former case and at temperatures where time dependent plastic deformation is minimal, the casual mechanism is universally crack closure (Section VII.2) [153]. Effects of increasing K_{max}, the monotonic plastic zone size and crack tip mean strain on the da/dN-$\Delta K_{applied}$ relationship are not well defined for intrinsic mechanical fatigue crack propagation.

For cycle-time-dependent corrosion fatigue, closure certainly contributes to the R value effect, however, the magnitude of the maximum stress intensity could influence the cracking mechanism, as for example in hydrogen embrittlement. The relative contributions of crack closure and intrinsic mean stress effects have not been modeled. Dramatic stress ratio effects on corrosion fatigue above K_{ISCC} are well described by linear superposition modeling [50].

Vosikovsky and coworkers demonstrated the deleterious effect of stress ratio on corrosion fatigue in carbon and heat treated alloy steels exposed to NaCl [173,174]. For a specific frequency, single crack growth rate laws of the type shown in Fig. 19, were produced for air and for NaCl when ΔK was replaced by a function including the stress ratio; viz. ($\Delta K + 4R$) for X70 C-Mn steel and ($\Delta K + 3R$) for HY130 steel. The relative contributions of crack closure and R-sensitive environmental

cracking were not defined. Given that the ($\Delta K + R$) function equally correlates da/dN data for air and aqueous chloride, and based on the relatively small effect of R on corrosion fatigue, it is likely that mean stress predominantly affected crack closure for this system. Indeed Ewalds argued that these fatigue data are equally well correlated with an "effective ΔK" equal to $(0.6 + 0.3R)\Delta K$ and based on Elber's physical notion of plasticity induced crack closure [175].

The need in this area is to define the effect of stress ratio on intrinsic corrosion fatigue crack propagation, independent of crack closure. This aim is hindered by the complexity of measuring displacement in aggressive environments and by the lack of understanding of the relationship between such measurements, physical load transfer and the relevant stress intensity range.

V.3.c. **Loading Waveform and Loading Sequence.** Two factors, constant amplitude loading wave shape and loading spectra, can influence corrosion fatigue crack propagation. The data presented in this review were obtained for constant amplitude, sinusoidal loading. Results on waveform and load interaction effects in corrosion fatigue are limited.

Rates of corrosion fatigue crack propagation are well correlated by the root-mean-square of the applied stress intensity distribution for the steel-NaCl system under narrow band random loading [110,172,176,177]. Complex overload and associated delay retardation effects in corrosion fatigue are beginning to be examined, for example Reference 131. Hertzberg outlines a basis for such studies in benign environments [89].

Several studies show that cycle-time-dependent corrosion fatigue crack growth rates are increased by waveforms which involve slow rising load compared to fast rising-slow falling or fast rise-prolonged K_{max} hold periods for constant cyclic frequency. This trend was demonstrated by Pelloux and Selines for a 7075 aluminum alloy [128], by Barsom [51] for high strength steel, and by Vosikovsky [170] for low strength C-Mn steel, all exposed to aqueous NaCl. A typical example is presented in Fig.

3 [51,52]. Scott et al. observed a modest reduction in da/dN for the low strength carbon steel-seawater system when subjected to a fast rise sawtooth waveform and compared to equal corrosion fatigue for sinusoidal, triangular and slow rise sawtooth loadings at constant frequency [58]. In contrast Wei and Hudak reported that varying rise time had no effect on corrosion fatigue of 7075-T651 in distilled water [in Ref. 51].

It is reasonable to expect that environmental effects are stimulated by slow strain and surface creation rates during rising loading. None-the-less, the effect of waveform depends on the rate controlling mechanism and will be material-environment specific. Changing rate of loading may have little effect on corrosion fatigue governed by fast surface reactions, but a large effect on systems where hydrogen diffusion in the crack tip plastic zone is rate limiting. The microscopic processes of surface creation on loading and of crack tip shape change on unloading and varying convective mixing may also affect the waveform dependence.

Loading waveform effects on corrosion fatigue crack propagation above K_{ISCC} are well described by the integrated load-time history for each cycle [50]. Results suggest that crack growth only occurs on the loading portion of the cycle [26].

V.4. Cyclic Loading Frequency

The time dependence of corrosion fatigue is arguably the most important aspect of this fracture mode. The general notion is that corrosion fatigue crack growth rates increase with decreasing cyclic loading frequency (f) because of increasing time per cycle available for increased chemical reaction and mass transport. This trend may be altered for cases where increased frequency increases the rate of environmental cracking due to: (1) enhanced mass transport by convective mixing, (2) enhanced crack tip strain and surface creation rates, and (3) reduced crack tip blunting by dissolution. The frequency dependence of time-cycle-dependent corrosion fatigue is accordingly complex.

To understand frequency effects, it is of paramount

importance to identify the rate limiting step in the transport, chemical reaction and fracture sequence for corrosion fatigue crack growth [30,33,37,98]. Additionally, the effect of stress intensity must be considered; the frequency dependence may be specific to each of the three ΔK regimes.

V.4.a. **ΔK_{th} and Near-threshold Regimes.** Two unique frequency dependencies are reported for near-threshold corrosion fatigue crack propagation; da/dN is constant with increasing f, or alternately, da/dN increases with increasing f. No data are available which show increasing near-threshold corrosion fatigue crack growth rates with decreasing frequency. More research is required, particularly at slow loading frequencies where test times are prolonged.

Frequency independent corrosion fatigue crack growth was reported by Speidel for steels and nickel based alloys [26]. This "true" or cycle-dependent corrosion fatigue behavior is illustrated by the horizontal dashed lines in Fig.4 for both moist air and NaOH. A similar frequency independence of near-threshold da/dN was reported by Meyn for Ti-8Al-1Mo-1V in 3.5% NaCl [65], and by Piascik and Gangloff for an aluminum-lithium-copper alloy exposed to 1% NaCl with anodic polarization [126].

Frequency independent near-threshold cracking is well established for the steel-aqueous chloride system. Vosikovsky reported da/dN independent of f for X-65 and HY130 steels at low ΔK levels [170,174]; Fig. 19. This effect was also observed by Gangloff for carbon and heat treated alloy steels in 3% NaCl with cathodic polarization [178]. Specific data in Fig. 20 were obtained for constant ΔK, at a level within the steeply rising portion of the da/dN-ΔK dependence for each frequency. Note that crack growth rates in NaCl are independent of loading frequency, are about 3 to 4-fold greater than the value for moist air and are 20 times the da/dN for vacuum. At very low ΔK, frequency independent crack growth rates in aqueous chloride and moist air merge, as suggested in Fig. 19.

In selected instances low ΔK corrosion fatigue crack growth rates increase with increasing frequency. Specific examples were

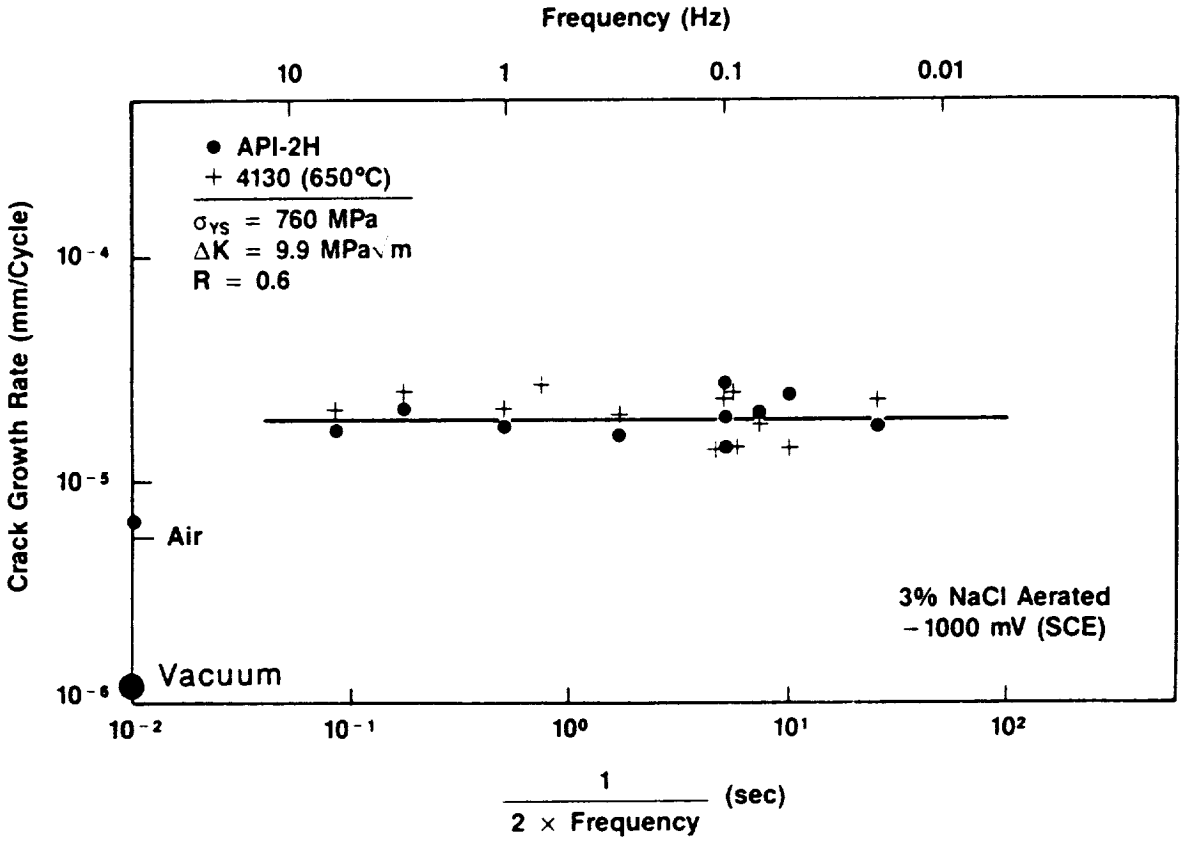

1285-37C-255

Fig. 20 Effect of frequency on low growth rate corrosion fatigue crack propagation in the steel-aqueous chloride system; after Gangloff [178].

reported by Dawson and Pelloux for Ti-6Al-4V in NaCl, Fig. 19 [141], and by Ford for an Al-7% Mg alloy loaded cyclically in 1 N Na_2SO_4 with cathodic polarization [72]. In the later case crack growth rates increased by an order of magnitude as f increased from 3 to 33 Hz; all rates were significantly faster than reference values for dry argon. This behavior was explained based on the film rupture/repassivation model and the idea that environmental crack extension per unit time increases strongly with increasing crack tip strain rate, equivalently increasing f, as discussed in Section VI.7 [72].

V.4.b. **Moderate ΔK "Plateau" Regime.** For ΔK levels where the power-law dependence of da/dN is reduced and approaching plateau behavior, sub-K_{ISCC} corrosion fatigue growth rates generally increase with decreasing frequency. A saturation crack growth rate is often observed for low frequencies. Extensive data supporting these trends were reported by Vosikovsky [170,174 and Fig. 19], Scott et al. [58,121], Gallagher [179], Gangloff [37,99,180] and Hinton and Procter [181] for steels in aqueous chloride; by Wei and Shim [37,182] for steels in distilled water and water vapor; by Brazill et al. [151] for an alloy steel in gaseous H_2S; by Holroyd and Hardie [64] for 7000 series aluminum alloys in seawater; by Wei and coworkers [61,129,183], and Dicus [184] for 2000 and 7000 series aluminum alloys in purified water vapor; by Chiou and Wei [185], and Dawson and Pelloux [141 and Fig. 19] for Ti-6Al-4V in aqueous NaCl; and by Ford and Andresen [39,137 and Fig. 14] for austenitic stainless steels in high temperature purified water. Three cases are discussed: steel in aqueous chloride, aluminum alloys in water vapor, and stainless/ferritic C-Mn steels in high temperature water.

V.4.b.(1). **Steels in Aqueous Chloride.** The frequency dependence of the corrosion fatigue crack propagation rate in API-2H C-Mn steel exposed to 3% NaCl with cathodic polarization is shown in Fig. 21 [180]. These results were obtained by constant stress intensity experimentation, with the specific ΔK level of 23 MPa$\sqrt{m}$ selected to be within the "plateau" region of corrosion fatigue

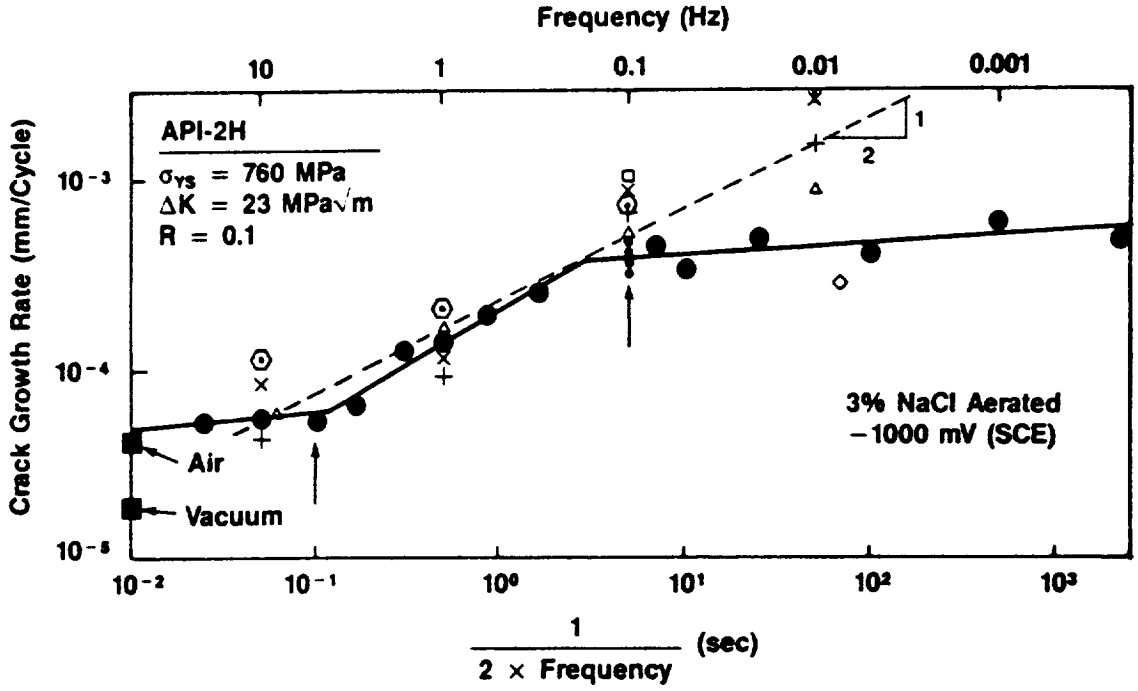

Fig. 21 Effect of frequency on corrosion fatigue crack propagation in the "plateau" regime of ΔK for API-2H steel in 3% NaCl with cathodic polarization; after Gangloff [180]. Literature data: +, ×, ⊡ X-65, △, ◇HY-130, ⬡ BS4360:50D [58,170,174,181,186].

cracking for this steel (see Fig. 32). The logarithmic plot of environmental crack growth rate versus reciprocal frequency is suggested by mechanistic modeling discussed in an ensuing section.

At frequencies above about 20 Hz, equal rates of fatigue crack propagation are observed for aqueous chloride and moist air; this value is about three times faster than crack growth in vacuum. Three regimes of behavior are observed with decreasing frequency. Initially, da/dN increases mildly, followed by a strong acceleration of corrosion fatigue for frequencies between 4 and 0.1 Hz, and leading to a third regime where da/dN is constant or mildly increasing as frequency declines to very small values.[2]

The trend shown in Fig. 21 is general, as indicated by the behavior of a variety of additional steels of varying yield strength, but similar ΔK, R and electrochemical conditions [37,58,121,170,174,179-182,186]. Results indicate similar behavior for the first two stages of the frequency response. Interestingly, the saturation behavior seems to be observed for the high strength quenched and tempered steels (viz, API-2H and HY-130 with σ_{ys} = 760 and 900 MPa, respectively), but not for lower strength ferrite-pearlite BS4360 and X-65 steels (σ_{ys} = 450 MPa). Additional experiments are required to explore this point.

The frequency dependence in Fig. 21 is explained by hydrogen embrittlement modeling reviewed in Section VI.6. The slope of the second regime is suggestive of the mechanism which controls corrosion fatigue, be it 1/2 indicating hydrogen diffusion control or some other value indicating hydrogen production (by surface reaction) rate control. The saturation behavior observed for the higher strength steels at the lower frequencies is also mechanistically significant. Similar results were reported for an aluminum alloy in seawater as indicated in Fig. 19c [64].

[2]For perspective, the data point at a cyclic loading frequency of 0.0002 Hz required 12 days to produce a crack length interval of 0.10 mm during 250 load cycles.

V.4.b.(2). **Aluminum Alloys in Water Vapor.** While no one study has examined the frequency dependence of corrosion fatigue crack propagation in the high strength aluminum alloy-pure water vapor system, in toto several investigations indicate that growth rates depend uniquely on environmental exposure, which is given by the product of load cycle period and water vapor pressure (P_{H2O}) (viz, P_{H2O}/loading frequency) [37,61,129]. Data are presented in Figs. 22 and 23 for two aluminum alloys, 2219-T851 and 7075-T651, in terms of environmental crack growth rate versus $P_{H2O}/2f$ or P_{H2O} at a single frequency. Several constant stress intensity range levels are represented for a single frequency of 5 Hz and variable P_{H2O}.[3]

The effect of frequency (water vapor pressure) on corrosion fatigue crack growth rates in the aluminum-water vapor system is similar to that exhibited by steel in aqueous chloride. Rates at high frequencies with water vapor are equal to values for inert environments. As frequency declines (or P_{H2O} increases), da/dN values increase sharply to a saturation level. Some alloys such as 7075-T651 exhibit a second rate increase and saturation level.

Since frequency was not varied, the data in Figs. 22 and 23 do not unequivocally establish the interchangeable influences of P_{H2O} and frequency. The role of exposure to describe both frequency and water vapor pressure effects on crack propagation is better established when several studies are considered. Bradshaw and Wheeler examined an Al-Cu-Mg alloy (DTA 5070A) in water vapor at two frequencies (1 and 100 Hz) and a range of P_{H2O} [187]. The pressure dependence at each frequency was equivalent to that shown in Figs. 22 and 23; the levels of P_{H2O} required to produce a given crack growth rate scaled with inverse frequency. Dicus concluded that frequencies between 1 and 10 Hz had no

[3]Environmental crack growth rate data are plotted for several constant stress intensity ranges in Figs. 22 and 23, however, experiments were conducted under constant load-increasing ΔK with several specimens cracked at a variety of frequencies or water vapor pressures. Data were cross-plotted from complete da/dN-ΔK relations. Constant ΔK was generally not maintained over an interval of crack extension in contrast to the results presented in Figs. 20 and 21.

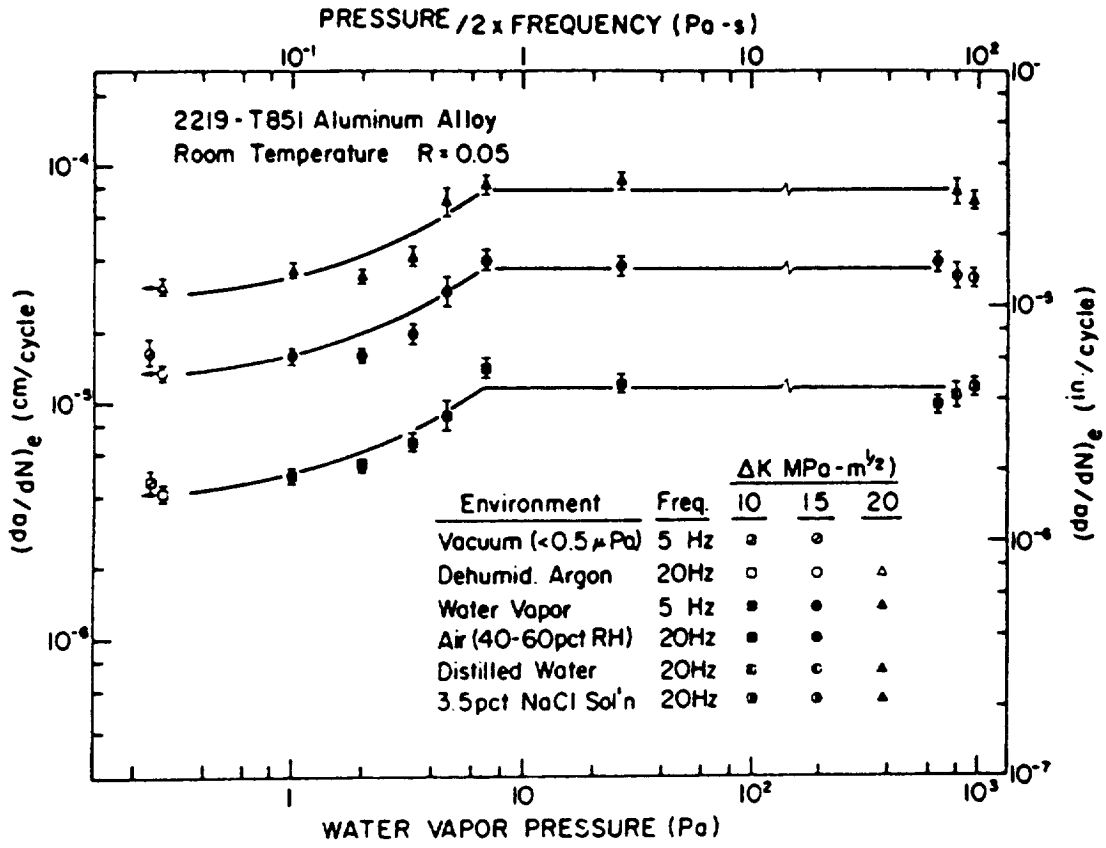

Fig. 22 Effect of environmental exposure, water vapor partial pressure/frequency, on corrosion fatigue crack propagation in a precipitation hardened aluminum alloy; after Wei et al. [129].

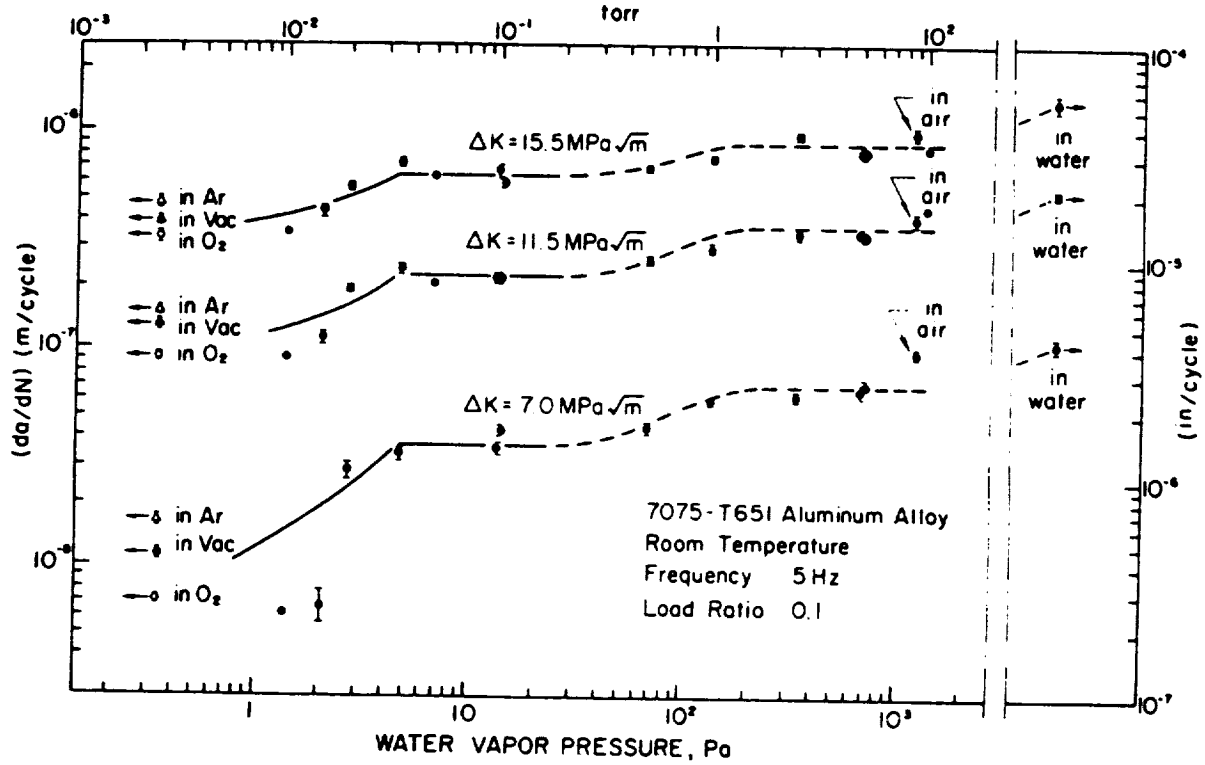

Fig. 23 Effect of water vapor pressure on corrosion fatigue crack propagation in high strength 7075-T651 at constant frequency; after Gao et al. [61].

influence on corrosion fatigue rates for 7475-T651; only water vapor pressure controlled da/dN [184]. These results are consistent with the saturation behavior in Figs. 22 and 23, at least for water vapor pressures up to the point of the second rise. Dicus found that this second rate transition occurred at a constant pressure for the two frequencies.

Theoretical modeling described in Sections VI.5.a and VI.6.b. supports the governing influence of the exposure parameter. None-the-less, a complete characterization of the frequency dependence for selected constant P_{H2O} levels would confirm this relationship.

The frequency dependence of corrosion fatigue in the aluminum-water vapor system has not been determined for near-threshold crack growth. Recent results for an Al-Li alloy suggest that the trends presented in Figs. 22 and 23 are obeyed near ΔK_{th} [125]. Limited data by Niegel and coworkers show that ΔK_{th} for the onset of environmental fatigue cracking along high angle grain boundaries in an Al-Zn-Mg alloy is reduced from the level for inert environment Stage II transgranular crack growth according to the reciprocal square root of P_{H2O} [132]. Presumably, the exposure parameter would describe the effect of pressure and frequency.

V.4.b.(3). Mass Transport and Reaction Rate Modeling: Hydrogen Embrittlement.

The essence of the mechanistic explanations for the aqueous and gaseous environment results contained in Figs. 21 to 23 is equivalent. Crack growth per cycle is assumed to be proportional to the amount of hydrogen generated at the crack tip by chemical or electrochemical reactions. The frequency dependence is determined by the slow rate limiting transport or reaction process, coupled with other fast steps in the corrosion fatigue sequence. This subject has been extensively investigated by Wei and coworkers [37]. For steel in aqueous chloride, hydrogen is produced by electrochemical reaction at the straining crack tip and in an amount proportional to the total charge passed per cycle. Electrochemical reaction on the clean crack surface is rate limiting. Measurements of the kinetics of these reactions

demonstrate that the rise in the frequency response in Fig. 21 is controlled by this slow surface reaction step; lower frequencies result in longer exposure time per cycle and increased charge passed and hydrogen produced [37,182,188]. At sufficiently low frequencies, the surface reaction per cycle is complete, with little additional hydrogen produced with further decreases in time; da/dN is constant. An alternate explanation based on hydrogen diffusion is described in Section VI.6.

For the aluminum-water vapor system, hydrogen is produced by water vapor oxidation of aluminum. This reaction is fast and not rate limiting. Rather, the first rise to saturation in Figs. 22 and 23 is due to slow water molecule transport along the crack, the rate limiting process, and as influenced by crack wall-molecule interactions or impeded Knudsen flow. Da/dN increases with decreasing frequency because the amount of fast reaction at the crack tip is increased by increased transport supply and crack tip pressure [61,129]. Above a specific exposure, rates are insensitive to frequency (and pressure) because mass transport is sufficient for the surface reaction to reach maximum completion; da/dN is constant. The second rise in Fig. 23 is ascribed to slow chemical reaction between water vapor and magnesium which is segregated to grain boundaries in aluminum alloys [183].

For both systems the transport and reaction processes have been modeled as discussed in Section VI. [37,61,129,182,188]. If the saturation growth rate is taken as an adjustable parameter, then the frequency dependencies shown in Fig. 21, 22 and 23 are predicted. A specific example is shown by the solid lines in Figs. 22 and 23; these are model predictions [61,129].

V.4.b.(4). **Steels in High Temperature Water: Film Rupture Modeling.** The strong effect of frequency on corrosion fatigue crack growth in "film rupture" systems is illustrated by the behavior of stainless and ferritic C-Mn steels in elevated temperature water [39,71,136]. Specific data and modeling predictions are shown in Figs. 14 and 24. Here, moderate ΔK corrosion fatigue crack growth rates increase with decreasing frequency. Notably,

(a)

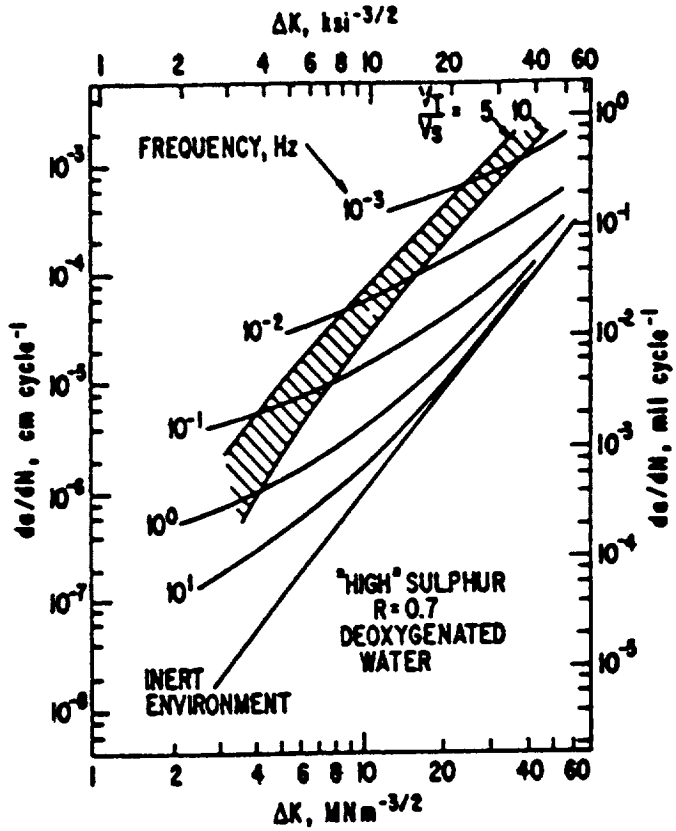

(b)

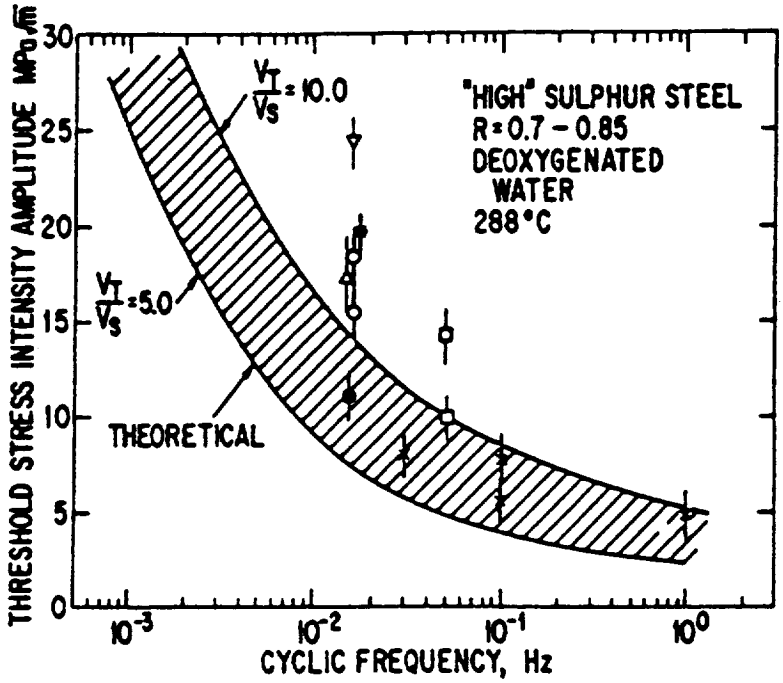

Fig. 24 Effect of frequency on corrosion fatigue crack propagation in ASTM A508/A533 type steels in deoxygenated water at 288° C. (a) Predictions of the film rupture model; (b) Predicted and measured threshold stress intensity values; after Ford [39].

however, ΔK_{th} decreases with increasing frequency as seen in Fig. 24b. Film rupture modeling, summarized in Section VI.7, predicts that da/dN increases with decreasing frequency, as indicated by the predicted sets of power-law lines in Figs. 14 and 24a.

For a given crack tip strain rate (equivalently, ΔK), a frequency exists below which brittle crack growth is replaced by crack tip blunting by corrosion. This behavior is approximated by the shaded band in Fig. 24a. Crack growth rates cannot be sustained above this band; a threshold stress intensity range is defined by the intersection of the blunting line and the film rupture crack growth rate prediction. As shown in Fig. 24b, ΔK_{th}, defined in this manner, is predicted to decrease with increasing frequency; that is, with decreasing time for blunting.

V.5. Environment Chemical Activity

Environment chemistry variables including temperature; gas pressure and purity; and electrolyte pH, potential, flow rate and halogen or sulfur ion content strongly affect rates of corrosion fatigue crack propagation. Understanding of these effects requires that a specific chemical variable be considered: (1) within each of the regimes of stress intensity behavior; (2) as a function of loading frequency; (3) and uniquely for cyclic deformation, crack initiation, microcrack propagation and long crack growth. This task is formidable.

Three environment chemistry variables have been extensively investigated: (1) water vapor pressure for aluminum alloys, as discussed in Section V.4.b.(2), (2) solution composition for stainless or carbon-manganese steels in high temperature water, and (3) electrode potential for steels and aluminum alloys in aqueous chloride environments. A fourth case, gaseous hydrogen pressure and temperature effects on corrosion fatigue in steels, is not well understood.

V.5.a. Stainless and C-Mn Ferritic Steels in High Temperature Water. Ford and Andresen broadly investigated the effects of electrolyte composition, oxygen concentration, solution flow and electrode potential on stress corrosion and corrosion fatigue crack

propagation in stainless and C-Mn ferritic steels exposed to high temperature water environments typical of nuclear reactor and piping applications [39,70,71,136,137]. Many of these effects are explained by mass transport and electrochemical analyses of crack chemistry and transient repassivation reactions, coupled with the film rupture model, as reviewed by Ford [138].

V.5.b. **Steels and Aluminum in Aqueous Chloride: Effect of Electrode Potential.** Studies have been conducted on the effect of electrode potential on aqueous chloride corrosion fatigue crack initiation and propagation in low strength C-Mn and heat treated alloy steels, and to a lesser extent in precipitation hardened aluminum alloys.

V.5.b.(1). **C-Mn Ferritic Steels.** For steels of yield strength below about 1000 MPa, fracture mechanics crack propagation experiments have emphasized the moderate ΔK "plateau" regime (> 18 MPa$\sqrt{m}$, Fig. 11), and frequencies generally within the saturation range (< 0.2 Hz, Fig. 21). Corrosion fatigue in this ΔK-f regime is cycle-time-dependent below K_{ISCC}.

Results from several laboratories demonstrate that corrosion fatigue crack growth rates generally increase with increasing cathodic polarization [58,115,122,170,173,174,178,189]. Specific data in Fig. 25 illustrate this trend for two carbon-manganese steels. Note, however, that "plateau ΔK" crack growth rates exhibit a minimum at about 200 mV cathodic to the free corrosion potential.

The behavior shown in Fig. 25 is explained based on hydrogen embrittlement and analytical modeling of crack chemistry. The notion is that da/dN increases with increasing crack tip hydrogen production, as discussed in Sections VI.5 and 6. The minima is explained because crack tip hydrogen is produced by both proton and water reduction; the former decreases with increasing cathodic polarization, while the later increases in importance for potentials below about -800 mV (SCE) [190,191].

The correlation of corrosion fatigue crack growth rate with the amount of hydrogen produced at the crack tip, and on surfaces exposed to bulk electrolyte, is suggested by static load hydrogen

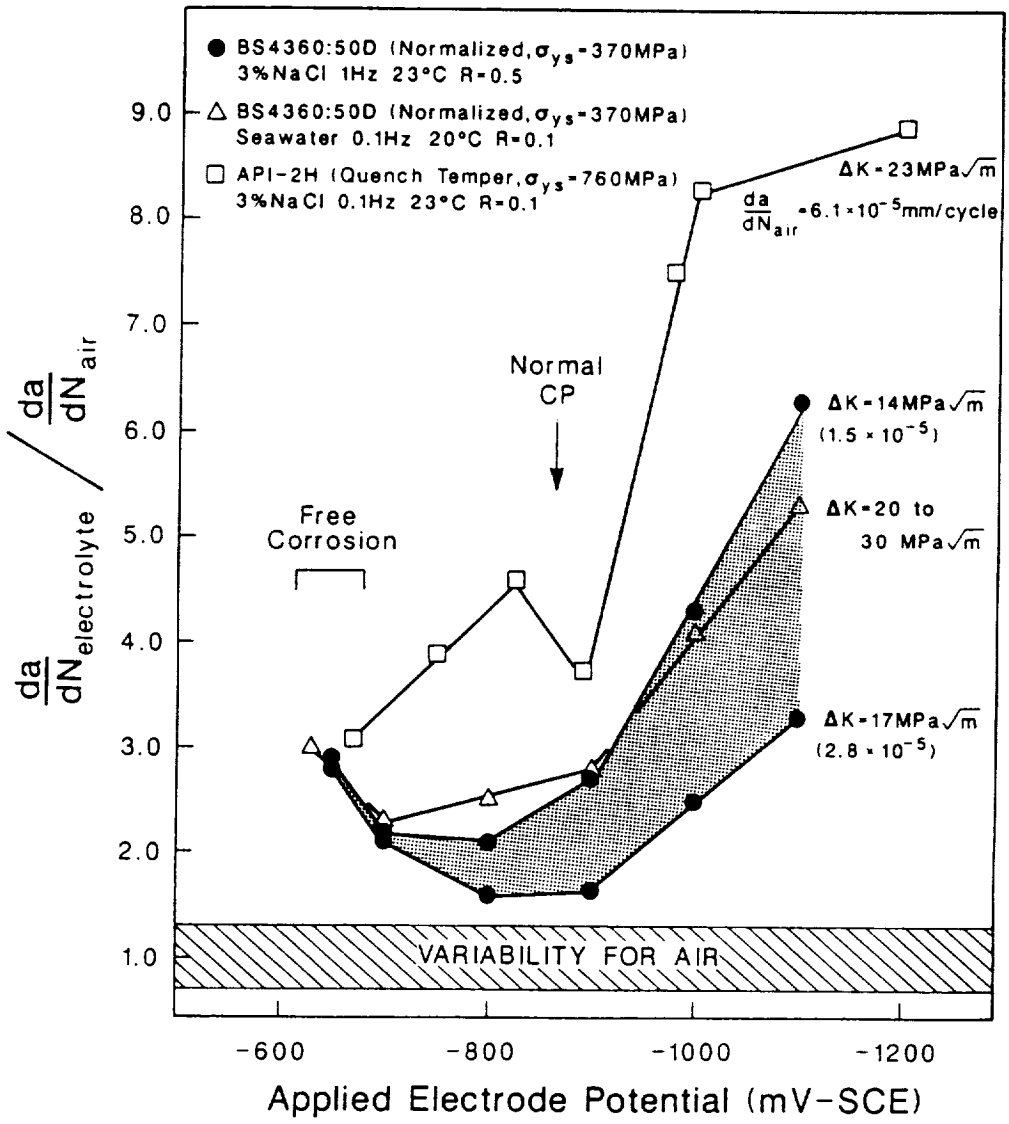

Fig. 25 Effect of applied cathodic potential on corrosion fatigue crack propagation in C-Mn steel/aqueous chloride system [115]. BS4360:50D in 3% NaCl [122], in seawater [58]; API-2H in 3% NaCl [178].

embrittlement models [192]. Turnbull developed analytical predictions of specimen surface and crack tip hydrogen production as a function of bulk solution pH and applied electrode potential [190,191,193]. Gangloff correlated K_{ISCC} with hydrogen uptake from electrolytes and gases for static load cracking of high strength steels [194,195]. Such information, coupled with in situ permeation measurements of hydrogen uptake in a component, provide a meaningful approach to control of cracking [57,113]. Yamakawa and coworkers, and DeLuccia and Berman developed hydrogen permeation sensors [113,114]. Unfortunately, this integrated sensor, crack chemistry and micromechanical cracking analysis has not been applied to corrosion fatigue.

Studies of the effect of electrode potential on corrosion fatigue illustrate an important distinction between crack initiation and propagation. Uhlig and coworkers reported that corrosion fatigue of polished specimens of 1020 and 4140 steels, exposed to NaCl during high frequency rotating bending "S-N" conditions, only occurred if a critical anodic corrosion current was exceeded [84-86]. Typical data are presented in Fig. 26 for 4140 steel in 3% NaCl at varying electrode potentials and loaded at stress levels above and below the moist air endurance limit of 379 MPa (55 ksi) [86]. Mild cathodic polarization restores this air endurance limit and the number of cycles (4×10^5 for dry air) for fatigue failure at 448 MPa. Polarization noble to a critical value degrades both of these fatigue properties. A similar beneficial effect of cathodic polarization was reported by Rajpathak and Hartt based on measurements of corrosion fatigue crack initiation and early growth to a 1 mm depth at the root of a notch (see Fig. 54) [196].

The opposite effects of cathodic polarization on smooth specimen life and crack propagation are readily understood. Presumably, anodic corrosion leading to either enhanced plastic deformation or localized pitting is required for corrosion fatigue crack initiation [1,29,36,87]. Here, hydrogen plays a secondary role, particularly for the moderate potentials, fast loading frequencies and near-threshold stress intensities typical of the smooth specimen studies. Anodic dissolution should

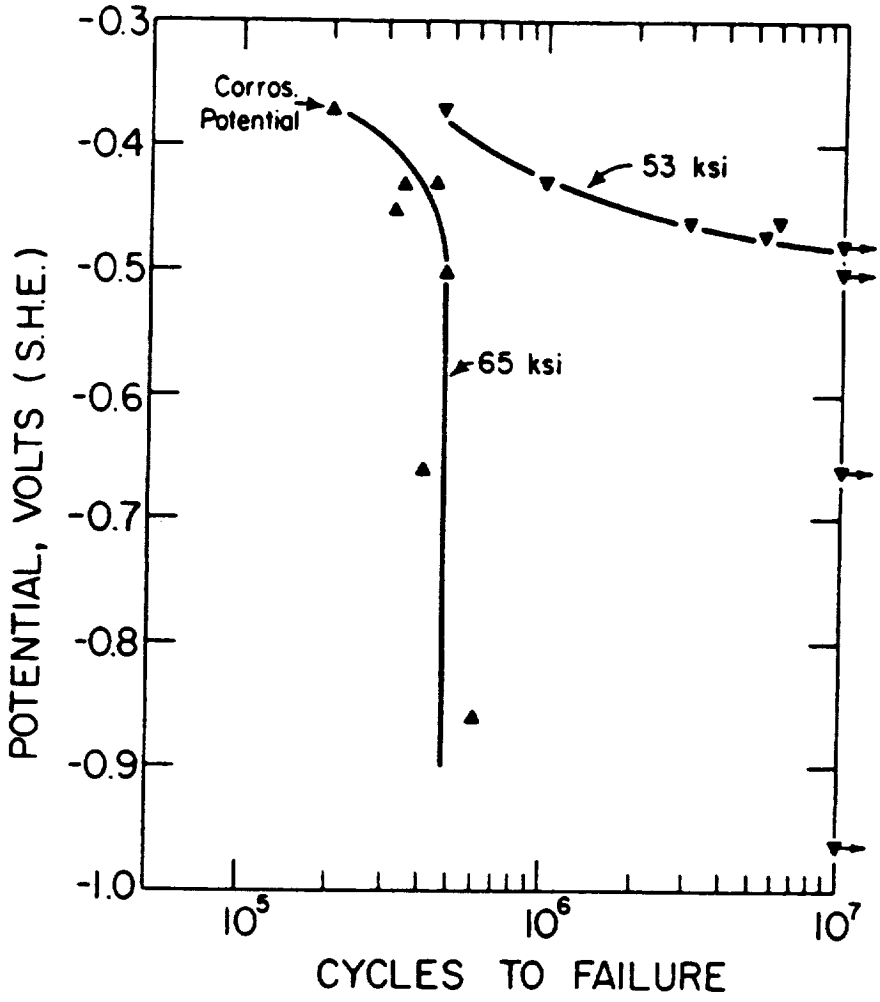

Fig. 26 Effect of applied electrode potential on corrosion fatigue of smooth, rotating bend specimens of 4140 steel (hardness = R_c 20) in 3% NaCl (free corrosion potential = -610 mV,SCE). The dry air endurance limit is 55 ksi and cycles to failure in moist air at 65 ksi equal 4 x 10^5. (1 ksi = 6.89 MPa); after Lee and Uhlig [86].

similarly affect near-threshold crack propagation in steels, however, evidence in this regard is lacking. Cathodic polarization enhances moderate ΔK rates of corrosion fatigue crack propagation by the hydrogen embrittlement mechanism. Slow loading frequencies, significant plastic straining and concentrated hydrogen production within the occluded crack provide the basis for hydrogen embrittlement as dissolution becomes less important.

Electrode potential effects on corrosion fatigue of steels in marine environments are critical because of the requirement to cathodically protect structures against general corrosion. Designers have debated the effects of cathodic potential on fatigue cracking [104-107]. From the above discussion, and based on experiments with large scale structural components, it is concluded that cathodic polarization can be either beneficial or deleterious to the corrosion fatigue resistance of a component [99,100,110]. The specific effect depends on the level of applied cathodic current and the regime of fatigue which dominates component life, be it initiation or propagation.

V.5.b.(2). **Precipitation Hardened Aluminum Alloys.** Applied electrode potential significantly affects corrosion fatigue crack propagation in precipitation hardened aluminum alloys in aqueous chloride. In general corrosion fatigue cracking occurs at the free corrosion potential, is exacerbated by either anodic polarization or large cathodic polarization, and is mitigated by mild cathodic polarization. Mechanistic explanations are lacking.

As reviewed by Speidel and later Holroyd and Scamans, fracture mechanics stress corrosion crack growth rates and slow strain rate tensile ductility both indicate a maximum resistance to cracking at potentials which are mildly cathodic to the free corrosion potential for 7000 series aluminum alloys in halogen bearing solutions [66,197]. Data are limited for 2000 series alloys, however, anodic polarization appears to enhance stress corrosion cracking [197]. A similar trend could be expected for corrosion fatigue crack propagation above K_{ISCC}; data in Fig. 5

for alloy 7079-T651 confirm this result [5].

Two studies of cycle-time-dependent corrosion fatigue crack propagation indicate the detrimental effect of anodic polarization and the beneficial effect of mildly cathodic potentials [77,126]. Specific data are presented in Fig. 27 for an advanced Al-Li-Cu alloy (2090) [126]. Here, corrosion fatigue crack propagation is enhanced by loading in 1% NaCl with anodic polarization compared to growth rates for either moist air or high purity helium. Cathodic polarization reduces crack growth rates to levels typical of moist air or lower. Similar results were reported for AA 7075 by Stoltz and Pelloux [77]. For the Al-Li alloy, the environmental effect is pronounced near ΔK_{th}; here, cracks growing at constant ΔK and R under anodic polarization were arrested by application of a cathodic potential. Prolonged cycling was required to reinitiate crack propagation upon a second application of the anodic potential [126].

Duquette and coworkers reported that the fatigue lives of smooth specimens of Al-4Mg-2Li and 7075 aluminum alloys in NaCl were maximum at potentials mildly cathodic relative to free corrosion [62,198]. Anodic and high cathodic polarizations degraded corrosion fatigue life, much like the behavior of 4140 steel [86].

The mechanism for the effect of electrode potential on corrosion fatigue in the aluminum alloy-chloride system is complex and unclear. Results can be speculatively interpreted in terms of anodic dissolution, hydrogen embrittlement, crack tip blunting by corrosion, surface film/dislocation interactions and surface film/reaction kinetics [62,77,126,197,198]. The problem in identifying the dominant mechanism is that both dissolution and hydrogen evolution occur on aluminum over a broad range of electrode potentials. Furthermore, the localized crack chemistry (viz. pH, potential and ionic composition) changes with varying applied potential. These effects have not been separated and quantified; as such, imaginative arguments can be constructed from each of the above perspectives. There is a strong likelihood that hydrogen embrittlement contributes to the

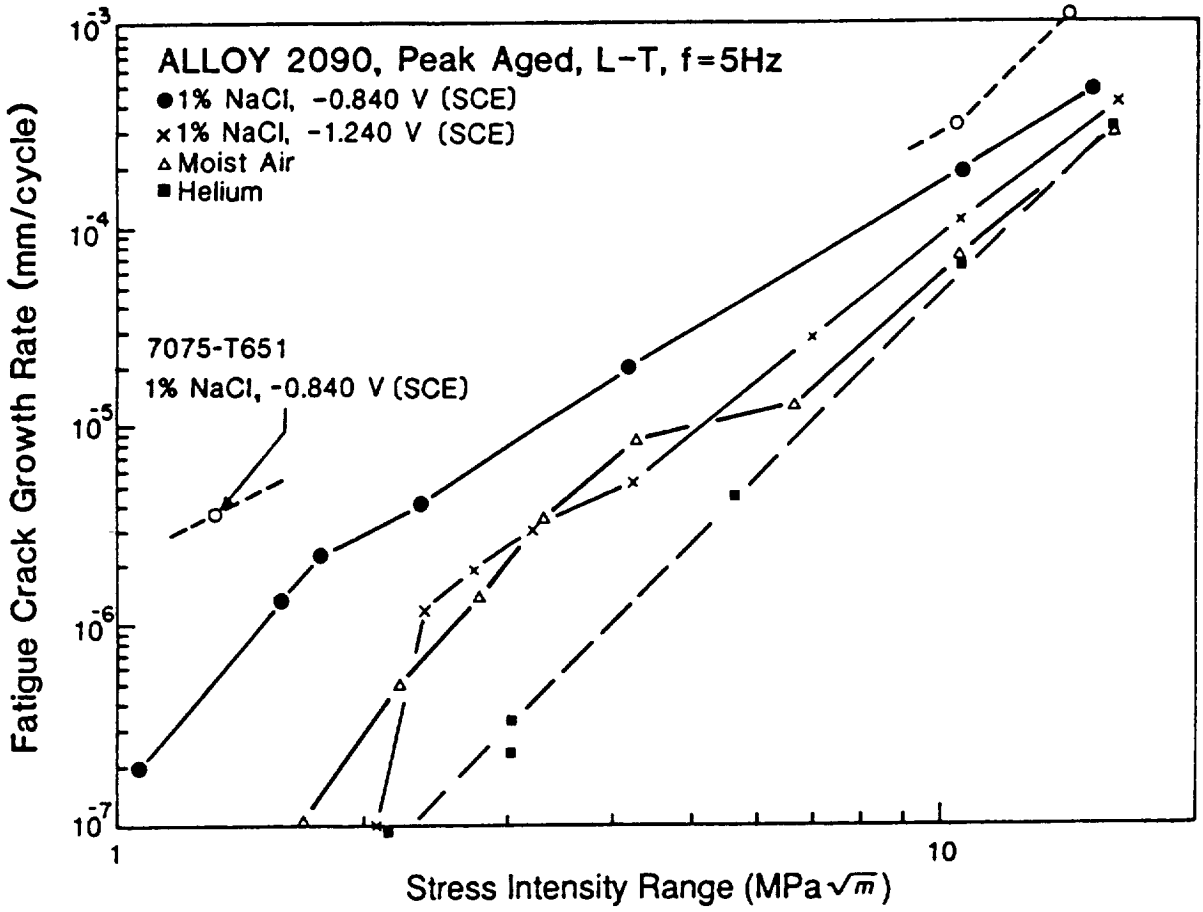

Fig. 27 Effect of electrode potential on corrosion fatigue crack propagation in Al-Li alloy 2090 in aqueous chloride at constant ΔK and high mean stress; after Piascik and Gangloff [126].

behavior shown in Fig. 27 [126].

V.5.c. **Corrosion Fatigue of Steels in Gaseous Hydrogen.** Nelson and others demonstrated that purified gaseous hydrogen produces cycle-time-dependent corrosion fatigue crack propagation in low to moderate strength steels well below K_{ISCC} [117,118,199]. Typical data are shown in Fig. 11. Ritchie and coworkers demonstrated H_2 accelerated fatigue crack propagation in moderate strength 2 1/4Cr-1Mo and in high strength 300M steels for stress intensity ranges within the Paris regime [200-202]. While generally below K_{ISCC}, corrosion fatigue crack growth rates in this regime increased with decreasing loading frequency and with increasing R. A typical example is reproduced in Fig. 28 [201].

Extensive data were reported for gaseous hydrogen effects on near-threshold corrosion fatigue crack propagation in steels [200-207]. As illustrated in Fig. 28, ΔK_{th} is decreased and growth rates are increased by hydrogen, relative to cracking in moist air, for low to moderate strength steels, particularly 2 1/4Cr-1Mo [200,202,204,205]. Similar crack growth rates were reported for hydrogen and helium, and the environmental effect diminished for high mean stress loading; leading Ritchie et al. to conclude that oxide induced crack closure dominated fatigue (see Section VII.2.a). In these experiments H_2 pressure was low and loading frequency was high; the possibility for hydrogen embrittlement apart from reduced closure was not explored.

An opposite hydrogen environment effect on ΔK_{th} was observed for high strength steels; near-threshold growth rates in H_2 were decreased and ΔK_{th} was increased relative to moist air [200,203,206, 207]. Hydrogen caused moderate embrittlement relative to inert environments. The mechanism for this effect is unclear, but may involve embrittlement in moist air due to a crack surface oxide film (see Section VI.8) or high activity hydrogen production by oxidation and perhaps capillary condensation of water in moist air. Alternately, hydrogen could produce enhanced crack tip plasticity and surface roughness, leading to a beneficial effect of crack closure which dominates a chemical embrittlement effect.

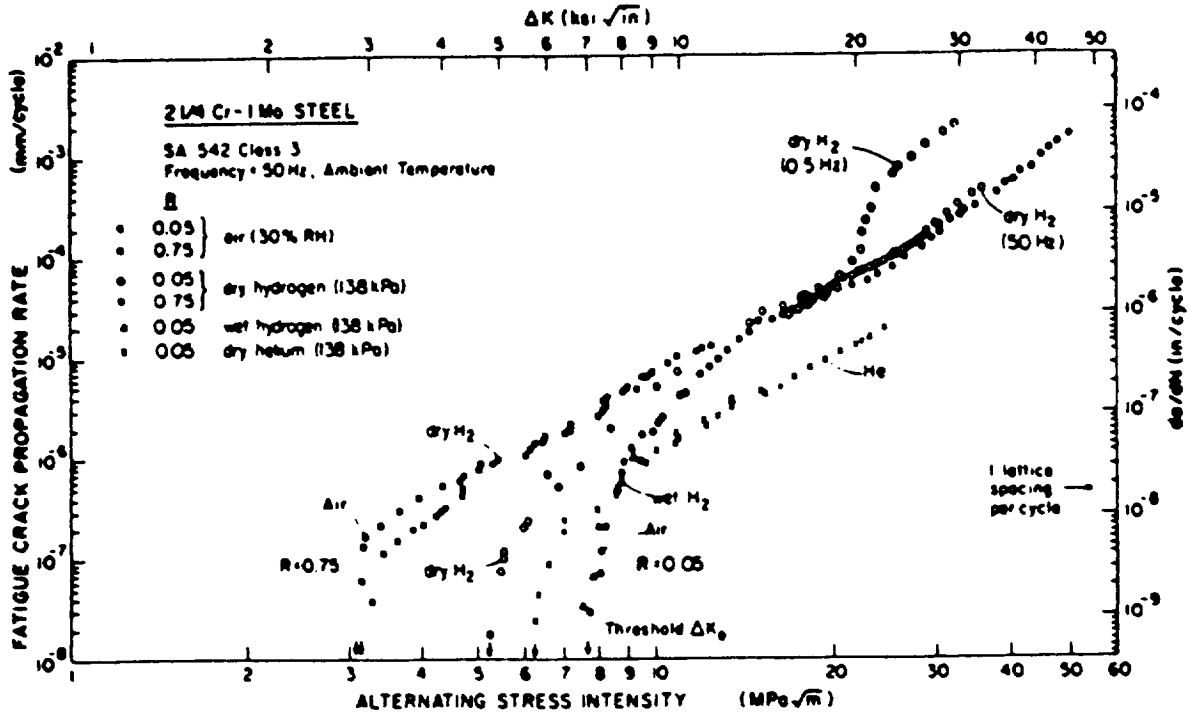

Fig. 28 Corrosion fatigue crack propagation in 2 1/4Cr-1Mo steel in low pressure gaseous hydrogen at room temperature; after Suresh and Ritchie [201,203].

There is a notable lack of data for moderate strength steels below K_{ISCC} and which emphasize the effects of H_2 pressure, temperature and environment impurities on corrosion fatigue. Such experiments and associated comparisons with surface reaction kinetics could lead to better understanding of the mechanisms for hydrogen effects in corrosion fatigue [37].

Brazill and coworkers characterized the effect of hydrogen sulfide pressure (P_{H2S}) on corrosion fatigue crack propagation in 2 1/4Cr-1Mo steel at room temperature for several relatively high stress intensity range levels [151]. Growth rates increased with increasing P_{H2S} and reached a saturation plateau, analogous to that illustrated in Fig. 23 for high strength aluminum alloys in water vapor. The relationship between da/dN and pressure was predicted quantitatively based on a model of fast surface reaction-gas transport control at low P_{H2S} and of fast transport-slow "second step" surface reaction control at high pressures of hydrogen sulfide [151].

Several studies have shown that hydrogen environment composition critically affects rates of corrosion fatigue crack propagation in steels. Molecules such as CO or O_2 preferentially adsorb on clean crack surfaces, block or "poison" dissociative chemisorption of H_2, and accordingly reduce rates of corrosion fatigue crack propagation. This effect was demonstrated by the pioneering work of Johnson on 4340 steel (see Fig. 6 [54]), and later by Nelson [118] and Cialone et al. [117,199] for carbon-manganese steels.

Gangloff established that certain hydrocarbon molecules mitigate corrosion fatigue crack propagation in steels exposed to otherwise pure H_2 [208]. Data are shown in Fig. 29. Relative to helium, low pressure gaseous hydrogen accelerates fatigue crack propagation in moderate strength (σ_{ys} = 1030 MPa, R_c 36) 4340 steel at constant ΔK and 1 Hz. The addition of equal partial pressures of saturated hydrocarbons such as methane (CH_4) and ethane (C_2H_6) had no effect on hydrogen enhanced fatigue cracking rates. In contrast ethylene (C_2H_4) with unsaturated double carbon bonding inhibited H_2 enhanced crack growth, albeit not completely relative to pure helium. Frandsen and Marcus reported

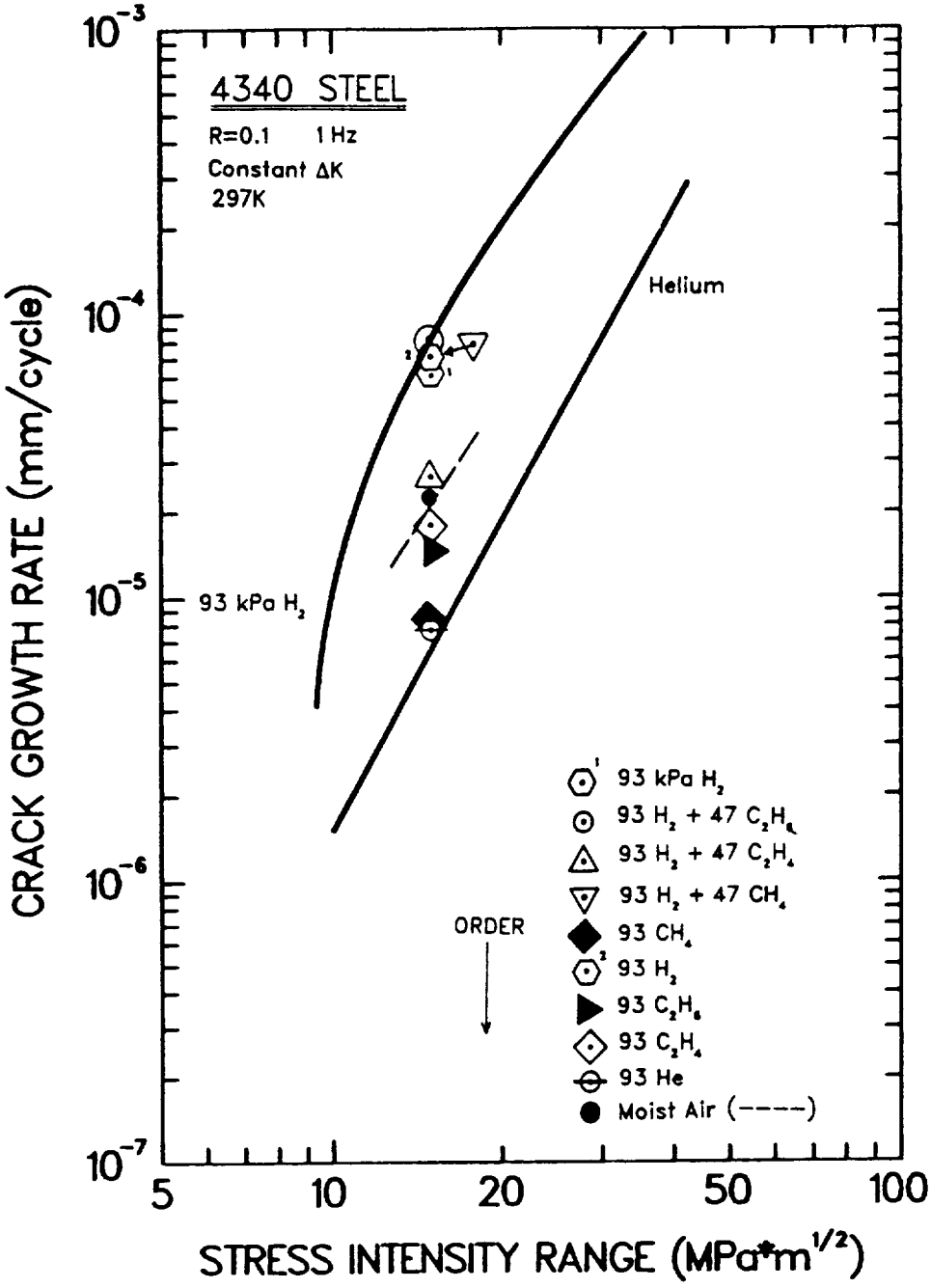

Fig. 29 Fatigue crack propagation rate data for high strength 4340 steel (R_c 36) in hydrogen-hydrocarbon gases at constant ΔK and frequency; after Gangloff [208].

a beneficial effect of acetylene (C_2H_2) on hydrogen enhanced fatigue of a high strength steel [209].

The mechanism for the beneficial effect of hydrocarbons on hydrogen cracking involves surface reaction between ethylene or acetylene and adsorbed hydrogen, where the concentration of the latter is reduced by the formation of inert methane. The prerequisite for "reactive gettering" of otherwise embrittling hydrogen is double or triple carbon-carbon bonds in the hydrocarbon which are catalytically split to combine with adsorbed hydrogen; a process likely for ethylene and acetylene at 300 K. Molecules such as methane or ethane have single (or saturated) carbon bonding and do not react with atomic hydrogen. Hydrocarbon molecules could also competitively chemisorb and reduce hydrogen uptake by a blocking mechanism.

Data in Fig. 29 show that pure environments embrittle steel according to the declining order of effect on da/dN:

$$H_2 > C_2H_4 > C_2H_6 > CH_4 = He$$

The embrittling potency of these gases is understood qualitatively based on the ease with which the molecule will dissociatively chemisorb to produce embrittling atomic hydrogen on the clean crack surface.

V.6. Yield Strength

To date, no systematic fracture mechanics data have been reported to demonstrate an effect of yield strength, either monotonic or cyclic, on corrosion fatigue crack propagation below K_{ISCC}. This variable is not well understood.

For benign environmental conditions including moist air, experimental measurements indicate that yield strength has little effect on rates of fatigue crack propagation within the Paris regime. Threshold stress intensity is either constant, or mildly decreases with increasing yield strength for high mean stress intensity loading where crack closure effects are minimal [200,202]. At low R, ΔK_{th} decreases strongly with increasing strength, largely due to strength effects on crack closure [201].

Micromechanical modeling (see Section VI.4.) indicates that the process zone size and the cyclic plastic strain distribution within the crack tip plastic zone decrease with increasing yield strength; fatigue crack extension by damage accumulation accordingly decreases and ΔK_{th} increases with increasing strength [210,211]. These effects are predicted to be small, and may be dominated by microstructural changes (eg. grain size) which are employed to vary strength.

Yield strength is a primary variable which influences environmental cracking for monotonic loading. For many material-environment systems, for example ferritic steels in hydrogen-producing gases and electrolytes, K_{ISCC} decreases and da/dt values increase with increasing strength [195]. Corrosion fatigue crack propagation above K_{ISCC} will be accordingly exacerbated by increasing yield strength, as predicted by linear superposition.

A striking example of the lack of a strong yield strength effect on cycle-time-dependent corrosion fatigue crack propagation is shown in Figs. 30 and 31 for ferritic steels in aqueous chloride with applied cathodic polarization and at low loading frequency. (The effects of these parameters are shown in Figs. 21 and 25.) Since corrosion fatigue is attributed to hydrogen embrittlement, a yield strength effect could be expected. Rather, data in Fig. 30 show an essentially constant environmental effect for steels which vary in monotonic yield strength from 390 MPa (BS4360:50D) to 1080 MPa (Ni-Cr-Mo) [115]. Crack growth rates at a "plateau" stress intensity range of 23 MPa m are plotted in Fig. 31 for each steel in Fig. 30. Corrosion fatigue crack growth rates are five to eight times faster than the yield strength independent value for moist air, however, no trend is observed for cyclic yield strengths from 190 to 870 MPa. The data in Figs. 30 and 31 were collected from the results of eight laboratories; differences in da/dN are reasonably attributed to interlaboratory variability. (Note the cross hatched region for API-2H, which shows the range of corrosion fatigue crack growth rates determined by a single laboratory on five separate specimens. Similar replicate data

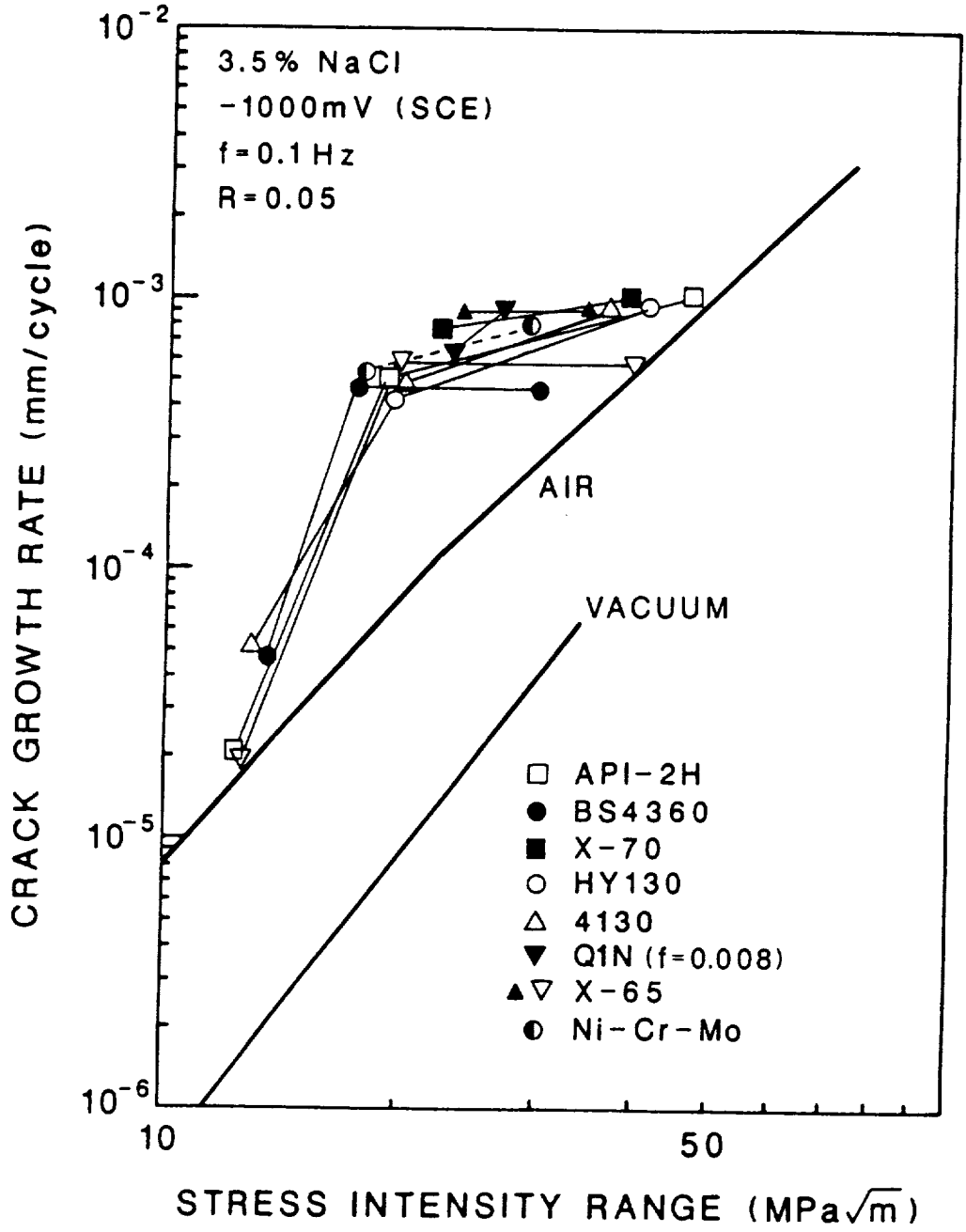

Fig. 30 Corrosion fatigue crack propagation in steels of varying yield strength and microstructure in 3.5% NaCl at constant cathodic potential and low loading frequency; after Krishnamurth et al. [115].

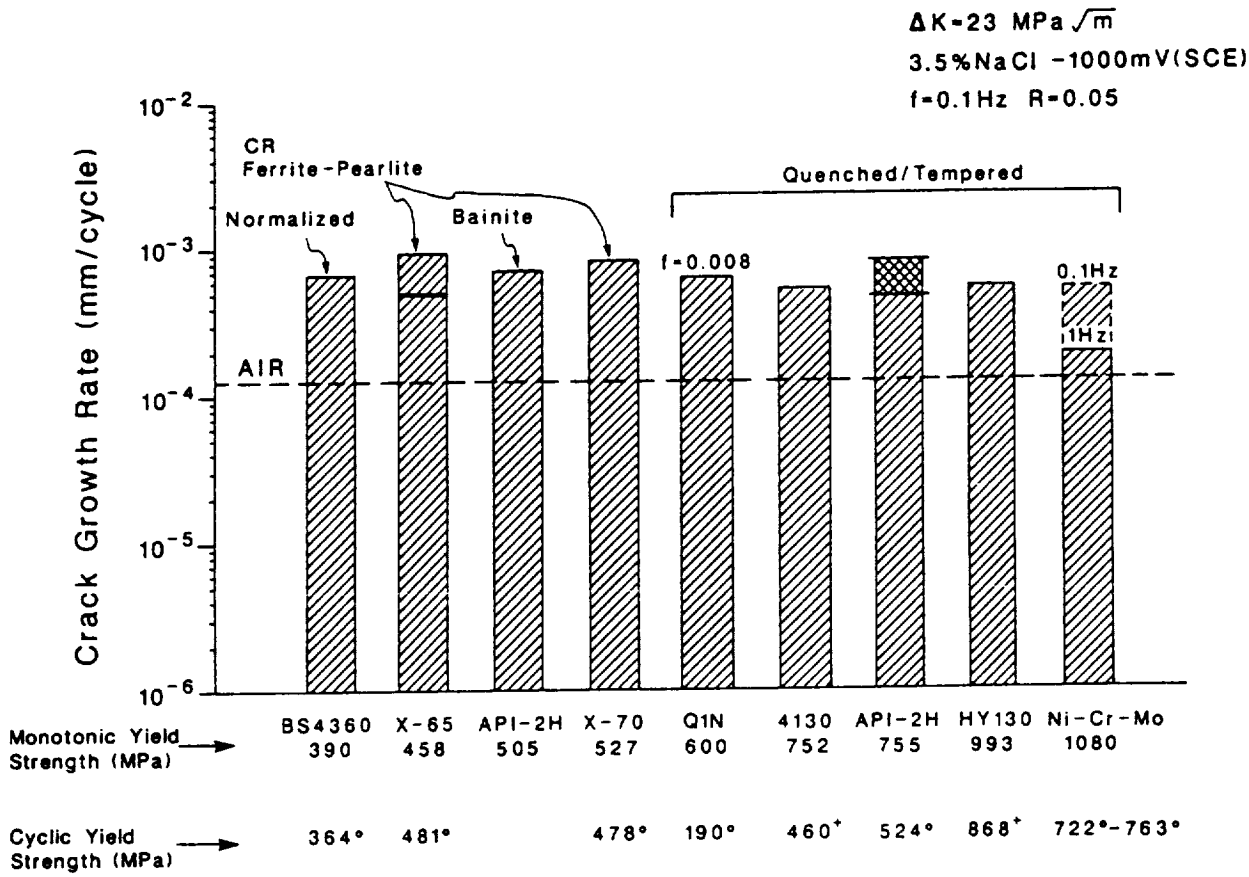

Fig. 31 Effect of steel yield strength and microstructure on corrosion fatigue crack propagation rate at constant cathodic potential, ΔK and frequency, from Fig. 30; after Krishnamurthy et al. [115].

are shown for X-65. This variability is of the same order as the strength effect in Fig. 31.)

While the data in Figs. 30 and 31 suggest that yield strength is not a critical variable in corrosion fatigue, much work remains. For steels in chloride, no single study has been reported where yield strength is systematically varied and corrosion fatigue characterized for constant chemical and loading conditions within the threshold and "plateau" ΔK regions, and as a function of frequency. Other alloy-environment systems must be investigated to examine strength effects for dissolution and film rupture based corrosion fatigue. A micromechanical damage model must be developed to predict the effect of yield strength and work hardening behavior on corrosion fatigue crack growth rate. Finally, studies of yield strength effects must cope with concomitant variations in microstructure. For the steels in Fig. 31, significant microstructural variations were necessary to develop the yield strength differences. Yield strength and microstructure effects on corrosion fatigue must be separated, to the extent possible.

V.7. Microstructure

Similar to yield strength, microstructural effects on corrosion fatigue crack propagation have received limited attention. Several examples are discussed; including steels in aqueous chloride and H_2, aluminum alloys in aqueous chloride, and stainless and carbon steels in high temperature water.

V.7.a. Ferritic Steels in Aqueous Chloride and Gaseous Hydrogen. For ferritic C-Mn and heat treated alloy steels in aqueous chloride with cathodic polarization, data in Fig. 31 indicate no systematic effect of microstructure on corrosion fatigue crack propagation. This conclusion is confirmed by an investigation summarized in Fig. 32 [178]. A C-Mn steel was heat treated to produce; in order of heat treatment on the figure; tempered martensite of two prior austenite grain sizes, upper and lower bainite, and dual phase ferrite + martensite with two martensite volume fractions. These heat treatments produced a constant

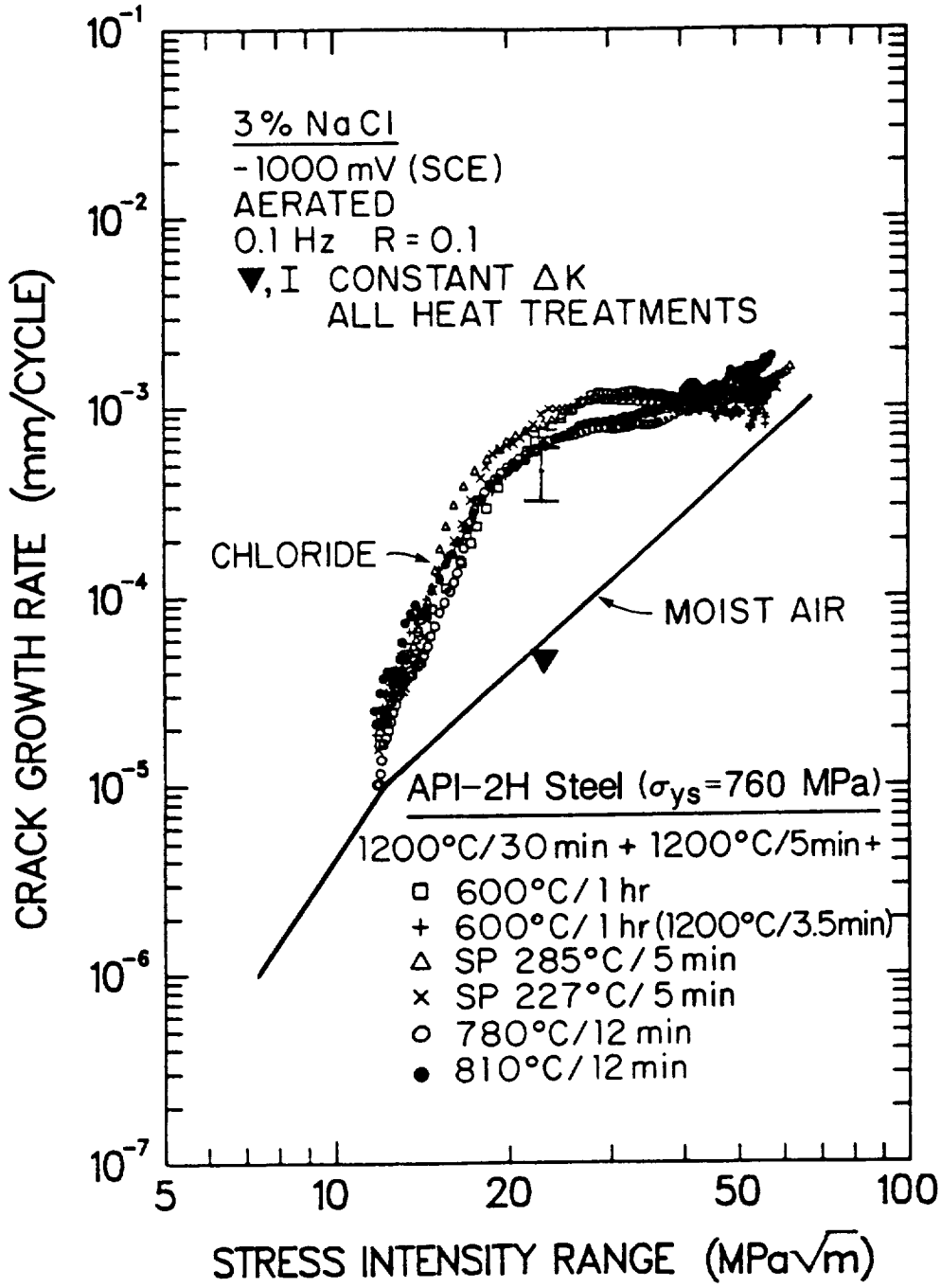

Fig. 32 Effect of microstructure on corrosion fatigue in C-Mn steel heat treated for constant yield strength (760 MPa), and stressed at either constant ΔK or constant load in aqueous 3% NaCl with cathodic polarization; after Gangloff, Koo and Marzinsky [178].

monotonic yield strength of 760 MPa based on measured hardness of R_C 27±2. These variations in microstructure have no effect on corrosion fatigue crack propagation for constant applied cathodic potential and low loading frequency. Corrosion fatigue crack growth rates for these API-2H microstructures are in good agreement with the behavior of normalized BS4360:50D C-Mn steel of ferrite-pearlite microstructure. (The shaded band in Fig. 32 represents corrosion fatigue in BS4360:50D reproduced from Fig. 11).

Jones reported that two quenched and tempered steels exhibit reduced corrosion fatigue crack growth rates compared to lower strength normalized microstructures for seawater at the free corrosion potential of -650 mV (SCE) [186]. Literature results support this conclusion as shown in Fig. 33 [115,186]. Here, quenched and tempered HY130, EN5 and Q1N show corrosion fatigue at reduced rates compared to normalized or controlled rolled (ferrite-pearlite) EN5 and X65. Since the yield strengths of the ferrite-pearlite steels vary between 300 and 450 MPa, while the tempered martensitic steels are of strengths between 600 and 950 MPa, the contributions of yield strength and microstructure in Fig. 33 are not understood.

Similar to aqueous chloride, only limited studies have been conducted on fatigue crack propagation in carbon or alloy steels exposed to gaseous hydrogen. Wachob and Nelson observed that ΔK_{th} increases with increasing yield strength and grain size for A516 steel in both moist air and high pressure hydrogen [212]. These results may be explained based on extrinsic crack closure effects (see section VII.2) and do not clearly indicate an effect of strength or microstructure on intrinsic hydrogen embrittlement. Cialone et al. showed that corrosion fatigue da/dN in gaseous hydrogen decreases dramatically for high carbon steels which contain pearlitic carbide and compared to pure iron or low carbon steel [199]. The authors speculated that carbide hinders hydrogen uptake, similar to the poisoning effect of CO discussed in Section V.5.c.

Temper embrittlement in steels, involving metalloid impurities segregated at prior austenite grain boundaries, is a

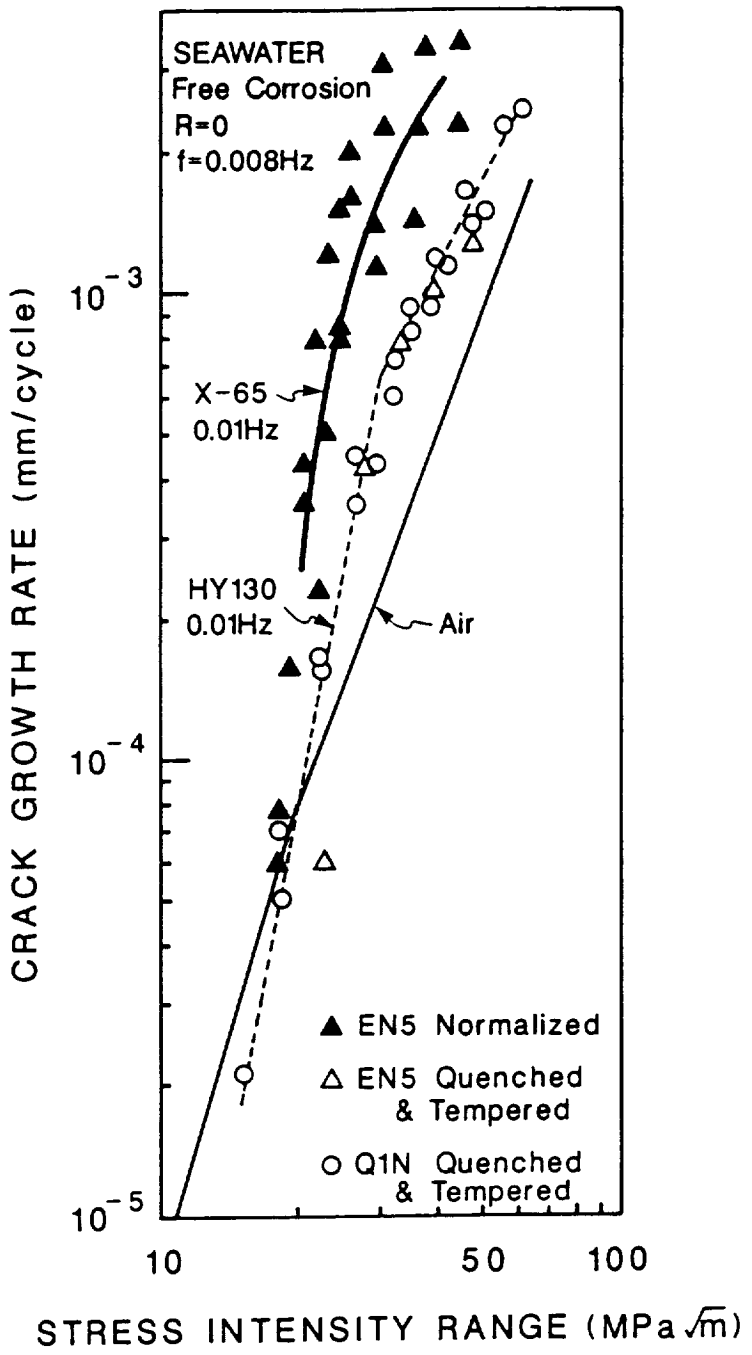

Fig. 33 Effect of microstructure and yield strength on corrosion fatigue crack propagation in C-Mn and alloy steels in seawater, freely corroding at -675 mV, SCE; after Jones [186].

well known promoter of gaseous and aqueous environment hydrogen embrittlement for static loading [213]. Hippsley demonstrated a similar deleterious effect of this metallurgical variable for cyclic loading of 2 1/4Cr-1Mo steel in gaseous hydrogen [214]. Results in Fig. 34 show that quenched and tempered steel with little or no impurity segregation (material L; austenitized at 960°C, quenched, tempered at 600°C; monotonic yield strength of 510 MPa) exhibits a hydrogen environment effect compared to vacuum, particularly at higher ΔK. Corrosion fatigue crack growth was along prior austenite grain boundaries. Notably, so called reversible temper embrittlement due to 1000 hour heating at 500°C of material L (material LE; monotonic yield strength of 530 MPa) caused a further increase in corrosion fatigue crack propagation rates, particularly near ΔK_{th} and for moderate Paris Regime stress intensities. Temper embrittlement also affects fatigue crack propagation in moist air; with equivalent growth rates observed for each heat treatment stressed cyclically in vacuum. The magnitude of the hydrogen effect in corrosion fatigue was correlated with increased percentages of intergranular fracture and increased phosphorus segregation to prior austenite grain boundaries.

Hippsley also reported a strong deleterious effect of so-called one step temper embrittlement, caused by low temperature tempering at 300 to 500°C of material which was austenitized at 960°C and quenched [214]. H_2 increased rates of corrosion fatigue for as-quenched steel (yield strength of 960 MPa), but substantially higher rates of crack propagation were reported for the tempered steel (yield strength of 890 to 1000 MPa). Crack growth was transgranular and associated with precipitate effects on crack tip plasticity and fracture.

This study of the H_2-temper embrittlement interaction during fatigue was limited to a single loading frequency (10 Hz), hydrogen pressure and mean stress. Additional work is required to explore this metallurgical effect for slower frequencies which allow increased time for chemical effects, for higher hydrogen environment activities, and for higher stress ratios which eliminate the complicating effect of crack closure.

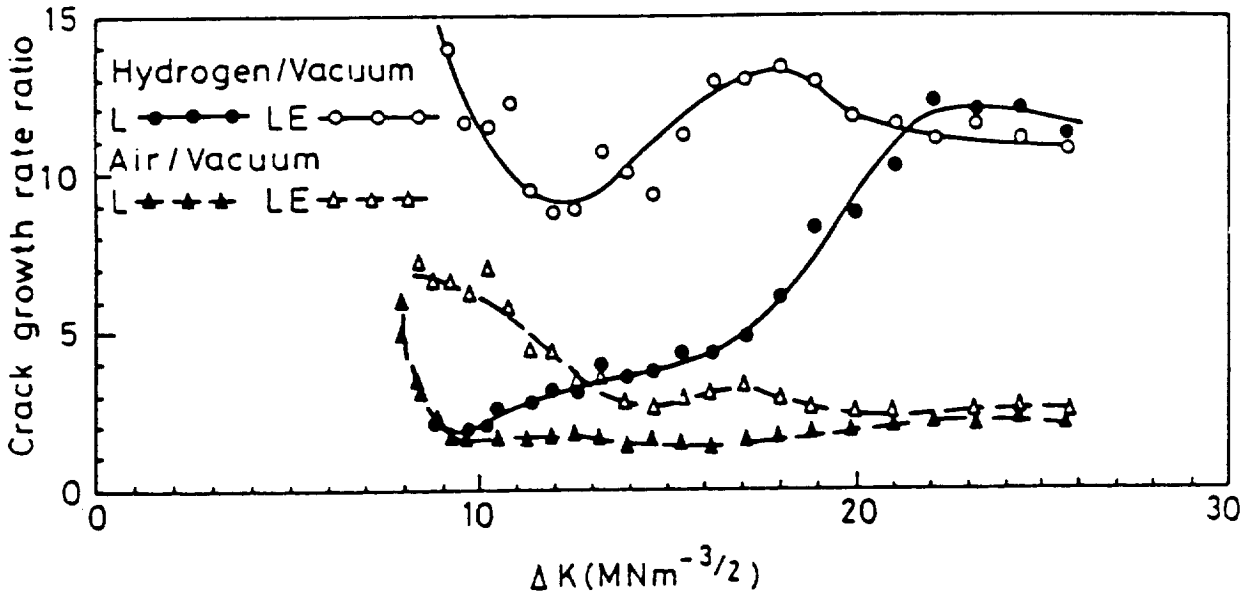

Fig. 34 Effect of temper embrittlement on H_2 enhanced fatigue crack propagation in 2 1/4Cr-1Mo steel. Material L is not temper embrittled, while LE was heat treated for reversible temper embrittlement (10 Hz, R = 0.30); after Hippsley [214].

V.7.b. **Aluminum Alloys in Aqueous Chloride.** Despite extensive work on microstructural effects on stress corrosion cracking in precipitation hardened aluminum alloys [66], corrosion fatigue-microstructure properties relations have received limited attention.

Lin and Starke demonstrated the effect of alloy copper content on corrosion fatigue crack propagation in four Al-6Zn-2Mg-Cu alloys, heat treated to either peak yield strength (T651 - 480 to 550 MPa) or over aged (T7351 - 400 to 460 MPa) [215]. Corrosion fatigue experiments were conducted in distilled water at a frequency of 10 Hz and R = 0.10. As shown in Figure 35, normalized corrosion fatigue growth rate decreased with increasing copper content, predominantly for the peak age condition and intermediate ΔK. These results were explained based on the damaging interaction between absorbed hydrogen and localized planar slip within the crack tip cyclic plastic zone. Planar slip is eliminated by increased copper and by overaging; factors which both reduce precipitate coherency and increase precipitate looping by dislocations to homogenize plastic deformation. These authors did not consider the effects of copper and precipitate/PFZ sizes on the electrochemical activity of precipitates (presuming that distilled water is sufficiently impure to be an electrolyte), on crack chemistry, and on hydrogen uptake. None-the-less, this work provides a hypothesis for the superior corrosion fatigue resistance of copper bearing 2000 aluminum alloys compared to 7000 series materials, see Fig. 12.

V.7.c. **Steels in High Temperature Water.** Two metallurgical variables are pertinent to corrosion fatigue crack propagation in ferrous alloys exposed to elevated temperature, pressurized water. Sensitization, that is near grain boundary chromium depletion due to carbide precipitation, induces intergranular stress corrosion cracking in austenitic stainless steels. Sulfide inclusions affect environmental cracking of C-Mn ferritic steels.

For AISI 304-type stainless steels, data and modeling show that corrosion fatigue crack growth rates are increased by

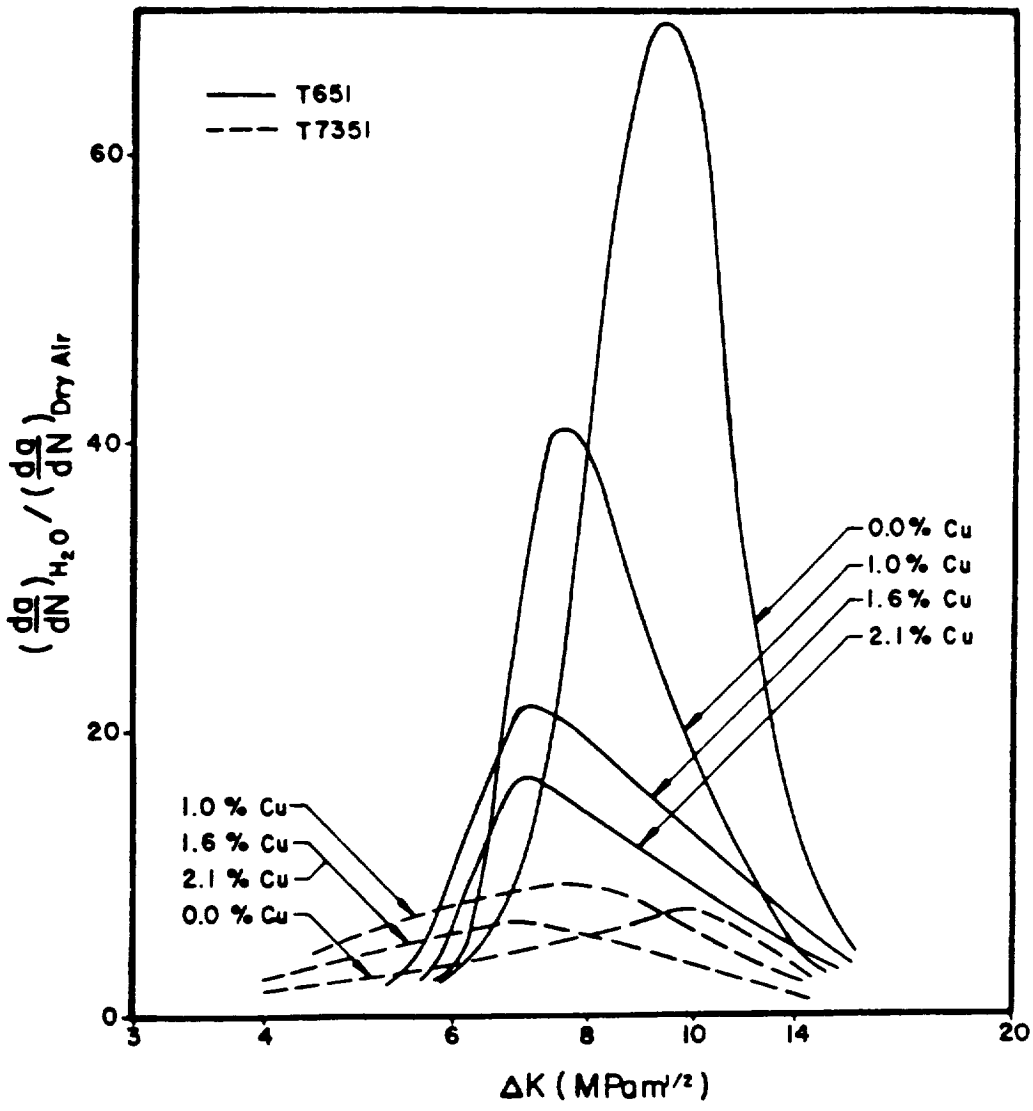

Fig. 35 Effect of copper content and aging treatment on corrosion fatigue crack propagation in Al-6Zn-2Mg exposed to distilled water (10 Hz, R = 0.10); after Lin and Starke [215].

sensitization. The da/dN-ΔK relationships in Fig. 14 are reduced by up to a factor of five for annealed and quenched (EPR $\leq$ 1 $C \cdot cm^{-2}$) compared to sensitized (EPR = 15 $C \cdot cm^{-2}$) stainless steel [137]. Other results show that sensitization enhances crack growth kinetics by up to 20 to 30 times for lower strain rates and more aggressive environmental conditions [216].

High da/dN levels due to sensitization and aggressive environmental or mechanical conditions correlate with intergranular corrosion fatigue crack propagation. Slower growth rates for nonsensitized stainless steel correlate with transgranular cracking. If the environment is mildly embrittling, transgranular crack growth occurs independent of the degree of sensitization. Andresen and coworkers argue that these differences are predictable based on the decreased rates of transient repassivation and enhanced anodic dissolution for chromium depleted regions of sensitized steels.

The sulfur content of ferritic pressure vessel steels is a critical metallurgical variable which influences corrosion fatigue crack initiation and propagation [39]. Data presented in Fig. 36 demonstrate that high sulfur content A533B or A508 steels crack in corrosion fatigue at over an order of magnitude faster rates than low sulfur heats for stagnant, low oxygen, pressurized water at 288°C. The mechanism for the deleterious effect of sulfur is based on dissolution of MnS inclusions intersected by the growing corrosion fatigue crack. Sulfur ions are introduced into the occluded crack solution and increase the amount of anodic current passed during repassivation of crack tip surfaces. By the film rupture concept, this chemical action increases rates of corrosion fatigue cracking [39].

The deleterious effect of MnS inclusions is only observed for certain bulk environment chemistries which favor high levels of dissolved S^{-2} at the crack tip [139]. Ford argues that such conditions include either turbulent high dissolved oxygen water (BWR), or stagnant solutions of any O_2 level [39]. Sulfur ions are also concentrated at crack tips in low sulfur steels exposed to stagnant, high O_2 water, but not to stagnant low O_2 water. These relationships illustrate the complexities associated with

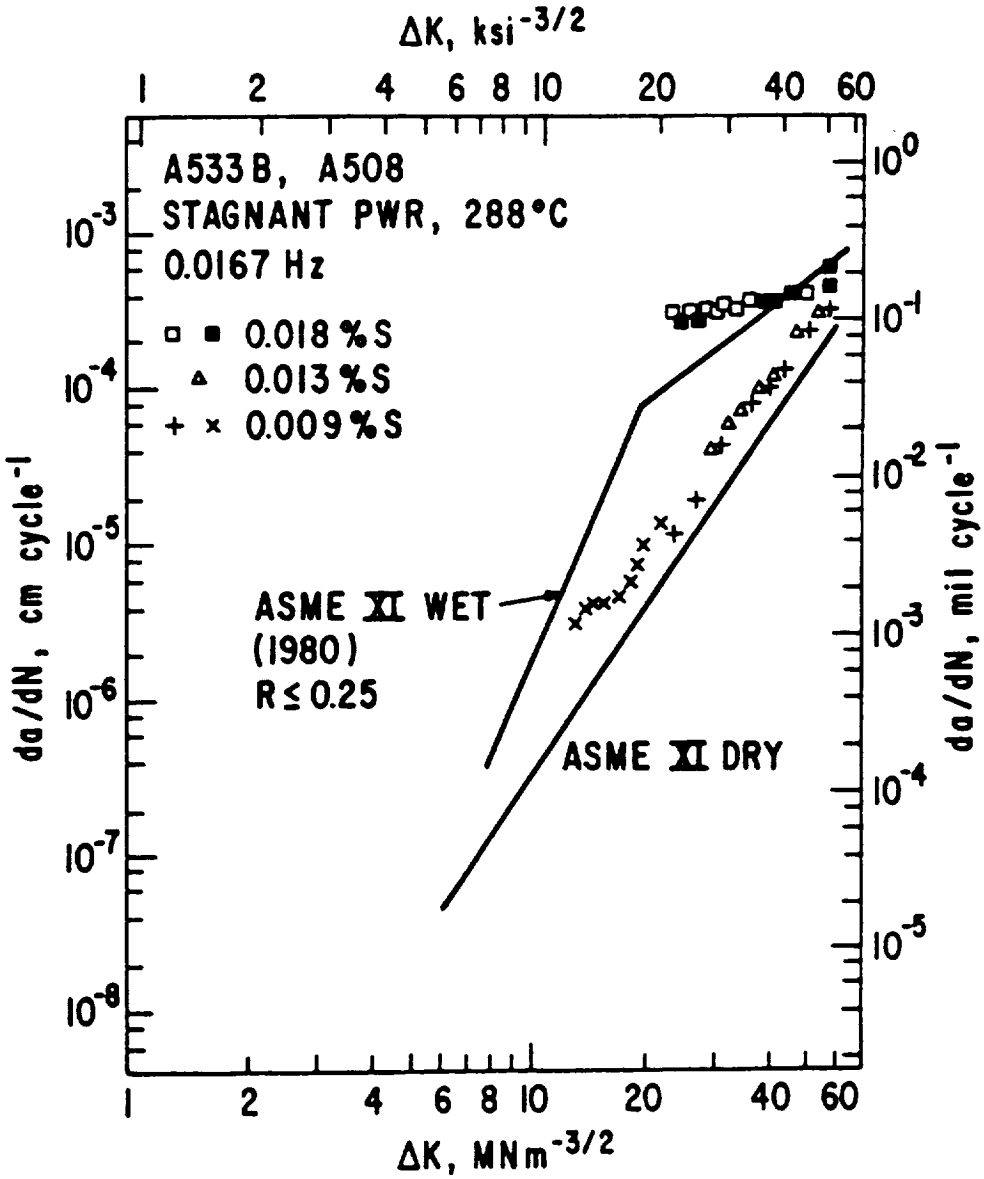

Fig. 36 Effect of steel sulfur content on corrosion fatigue crack propagation in A533B and A508 in high temperature, pressurized stagnant water with low dissolved oxygen (R = 0.20); after Ford [39].

C-2

unambiguous definitions of metallurgical effects on corrosion fatigue crack propagation.

V.7.d. **Microscopic Corrosion Fatigue Crack Path.** Determinations of corrosion fatigue crack paths through microstructures and associated surface features are critical to understanding cracking mechanisms and metallurgical effects. An example of this approach for the steel-moist air system was provided by Roven [210]. Such detailed study has not been applied to the corrosion fatigue problem. None-the-less, two corrosion fatigue cases have been investigated; aluminum alloys in chloride or water vapor, and ferritic steels in aqueous chloride.

V.7.d.(1). **Aluminum Alloys in Water Vapor and Aqueous Chloride.** Fatigue-environment interactions produce a variety of complex fracture surface morphologies in aluminum alloys. Gudladt and coworkers demonstrated that hydrogen from water vapor-aluminum reaction causes intergranular cracking and promotes rates of Stage I fatigue crack growth along persistent slip bands and transgranular Stage II crack growth [217-219]. Since these studies were conducted on single and bicrystals of high purity Al-Zn-Mg, the proportions and absolute rates of each fracture process were determined and demonstrated to depend on applied ΔK, water vapor pressure, grain boundary orientation and slip mode controlled by the extent of aging.

For sub-K_{ISCC} transgranular fatigue cracking in 7000 series aluminum alloys, Stoltz and Pelloux demonstrated the occurrence of "ductile" striations typical of crack propagation in inert dry air and certain benign aqueous environments; and "brittle" striations for fatigue in NaCl with anodic polarization as first reported by Forsyth [77,220]. Ductile striations are attributed to crack advance by multiple shear and tip blunting, particularly in microstructures where planar slip was not localized. Brittle striations are attributed to environment induced cleavage along {100} planes in the fcc aluminum lattice. Similar results were reported by Feeney et al. for 7075-T6; intergranular corrosion fatigue cracking in 2024-T3 was also reported [95].

Gao, Pao and Wei reported crystallographic corrosion fatigue cracking parallel to {100} planes in 7075-T651 aluminum exposed to water vapor [61]. Brittle crack facets contained fine striations which were parallel to either <100> or <110> directions. This finding was correlated with the rate limited and saturation regimes of the exposure parameter, Fig. 23. At lower pressures of H_2O or for crack growth in gaseous oxygen, the fracture surface features were not crystallographic, but rather were flat and featureless with evidence of ductile tearing.

Corrosion fatigue crack propagation in advanced Al-Li alloys (eg. Fig. 27) proceeds by a variety of microscopic mechanisms as outlined by Piascik [221]. Crack growth in vacuum, helium and oxygen occurs entirely by slip plane cracking producing large facets parallel to {111} planes. For moist air, pure water vapor and aqueous chloride, corrosion fatigue at moderate ΔK involves slip band cracking and intersubgrain boundary fracture. At low ΔK near threshold, corrosion fatigue is predominantly by cleavage along {100} planes. The change in environmental fracture mechanism with decreasing ΔK is attributed to reduced cyclic plastic zone size; cleavage is promoted when plasticity is contained within a single subgrain, while sub-boundary fracture occurs when deformation is distributed over several grains.

V.7.d.(2). **Ferritic Steels in Aqueous Chloride.** Procter and coworkers conducted quantitative fractographic analyses of corrosion fatigue in X-65 steel exposed to 3.5% NaCl with cathodic polarization [59]. Crack growth rate data for this steel are equivalent to the results for API-2H steel in Fig. 32 and BS4360:50D in Fig. 11. Environmental cracking is characterized by a variety of microscopic processes, including: intergranular separation, transgranular cleavage, brittle and ductile striation formation, and ductile tearing. The proportions of these features depend on ΔK and frequency, Fig. 37.

Intergranular cracking along ferrite grains dominates corrosion fatigue in the low ΔK, steeply rising portion of the da/dN-ΔK relationship. Fatigue crack propagation in moist air

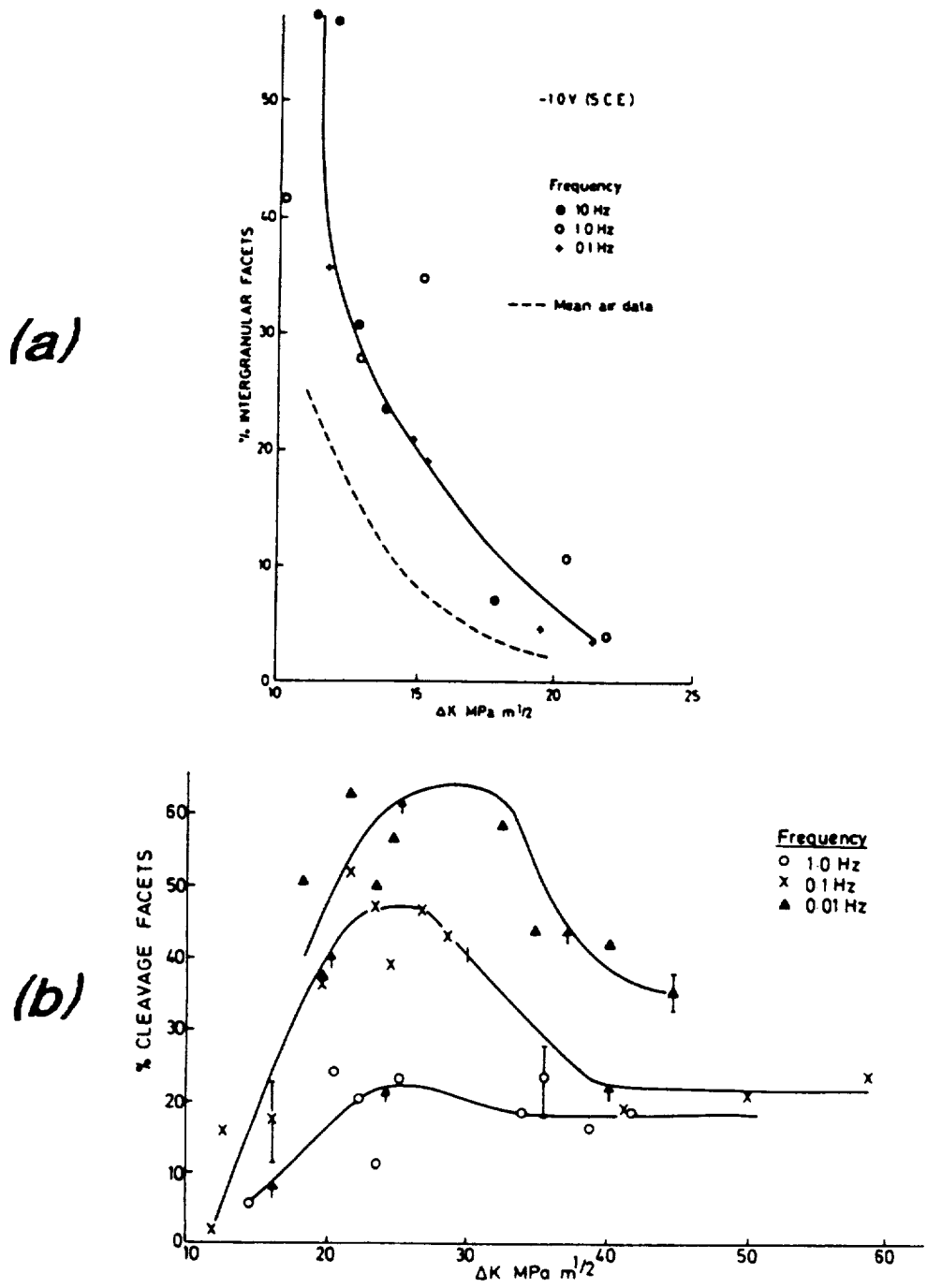

Fig. 37 Quantitative fractographic results for corrosion fatigue in controlled rolled X-65 steel in 3% NaCl (-1000 mV, SCE; R = 0.15). (a) Intergranular cracking along ferrite grain boundaries; air and chloride and (b) Transgranular cleavage with brittle striations; after Hinton and Procter [59].

produces a reduced amount of intergranular separation at low ΔK. Crack growth in the plateau regime is largely by cleavage of uncertain crystallography, but producing a facet about equal to the ferrite grain size. The proportion of cleavage increases with decreasing frequency and parallels increases in corrosion fatigue crack growth rate. Brittle striations are present on cleavage facets, indicating discontinuous crack propagation. Fatigue in air at plateau ΔK levels produces ductile transgranular striated fracture surfaces. Ductile fracture processes dominate at high ΔK levels.

Apart from usage in failure analyses, fractographic results of the type shown in Fig. 37 provide important indications on the mechanisms for corrosion fatigue. For the steel-aqueous chloride system, intergranular and cleavage cracking were interpreted as due to the entry of cathodically evolved hydrogen [59]. The ΔK induced transition from intergranular to cleavage cracking may depend on increasing plastic zone size beyond the ferrite grain size and on increasing deformation based hydrogen production and transport. Alternately, intergranular cracking appears to dominate when sufficient hydrogen is available at the crack tip, while transgranular cleavage occurs for those ΔK and frequency conditions where da/dN is limited by the electrochemical production and mass transport of atomic hydrogen.

V.8. Miscellaneous

Additional variables often unexpectedly affect corrosion fatigue crack propagation. As suggested by Staehle, a material-environment system should be assumed prone to environmental fracture until proven otherwise [222].

V.8.a. **Temperature.** Elevated temperature environments are likely to promote rates of fatigue crack propagation by various oxidation and hot corrosion processes, and by time-dependent plastic deformation. This important class of corrosion fatigue problems is reviewed by Pineau [4]. Moderate temperature effects on aqueous or gaseous corrosion fatigue are considered here. Temperature should influence corrosion fatigue crack propagation

through effects on mass transport and electrochemical or chemical reaction kinetics. It is surprising that the effect of temperature has received limited attention.

Marcus and coworkers demonstrated that fatigue crack growth rates in a high strength steel and Nickel-200 exposed to low pressure gaseous hydrogen increase with increasing temperature, exhibit a maximum near 300 K and then decline at higher temperatures [74,209]. Specific data for steel are shown in Fig. 38. This behavior is consistent with temperature-hydrogen pressure effects on monotonic load crack growth rates for high strength steels in H_2 [223], and with the general maximum in a variety of hydrogen environment embrittlement phenomena near ambient temperature [195].

The results in Fig. 38 indicate that hydrogen uptake and transport through the plastic zone are maximized at a specific temperature. At very low temperatures, dissociative chemical adsorption to produce hydrogen atoms is rate limiting and is thermally activated. At higher temperatures, hydrogen entry may be reduced by enhanced recombination of hydrogen atoms to form desorbed H_2, by elimination of an adsorbed precursor to chemisorption of H, by a surface phase transformation, or by thermal detrapping of dissolved hydrogen [223]. While these processes are debated for monotonic loading, no substantial studies of the gaseous hydrogen fatigue crack propagation case have been reported.

Vosikovsky and coworkers reported that reduced temperature between 300 K and 273 K resulted in up to a four-fold increase in corrosion fatigue crack growth rates for the ferritic steel-seawater system illustrated in Fig. 11 [224]. Nakai et al. showed that corrosion fatigue crack growth rates for the NiCrMoV steel-0.3 N Na_2SO_4 system increased with increasing temperature [188]. This effect was explained based on temperature enhanced rates of electrochemical reaction on clean crack surfaces to produce embrittling hydrogen.

V.8.b. **Biologically Induced Corrosion.** Biologically generated sulfur ions promote corrosion fatigue of steels in aqueous electrolytes.

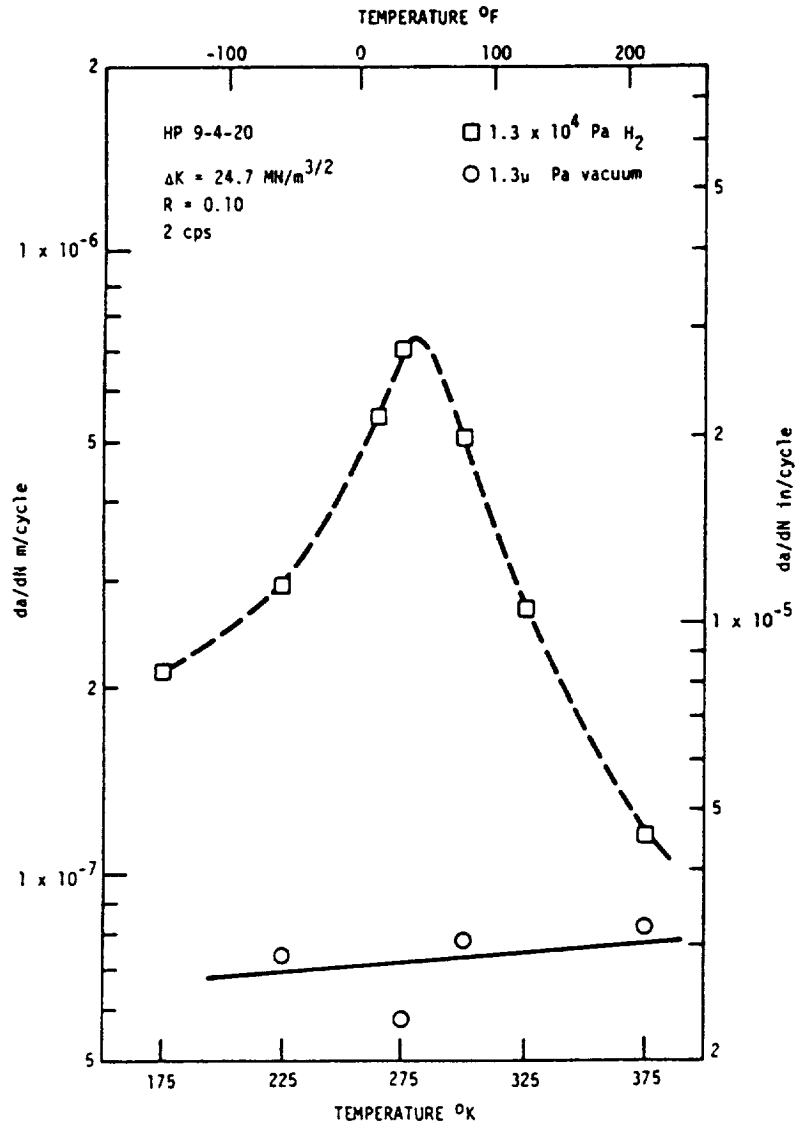

Fig. 38 Temperature dependence of H_2 assisted fatigue crack propagation in high strength HP-9-4-20 steel at constant ΔK and frequency; after Frandsen and Marcus [209].

This result is consistent with a large body of literature which demonstrates the deleterious effect of sulfur bearing environments on hydrogen embrittlement systems.

Sulfur specie enhance hydrogen uptake from electrolytes by adsorbing on metal surfaces to retard the recombination of hydrogen atoms to form molecules which would otherwise leave the surface. As a result, the proportion of cathodically produced hydrogen atoms which enters the metal increases. Stress corrosion cracking of steels is exacerbated by sulfur ions in electrolytes and by H_2S additions to gaseous environments [195]. H_2S dissolved in seawater enhances corrosion fatigue crack propagation in steel, as shown in Fig. 11 [116]. A similar effect was demonstrated for H_2S dissolved in crude oil [103,225]. H_2S gas is a potent embrittler of low strength alloy steels for fatigue loading [151].

Biologically enhanced corrosion fatigue of C-Mn steels in seawater was recently demonstrated by Thomas and coworkers and by Cowling and Appleton [122,226,227]. Typical data are presented in Fig. 39. The steel, RQT 501 (σ_{ys} = 470 MPa; Fe-0.18C-1.5Mn), exhibits enhanced rates of fatigue crack propagation in seawater containing between 75 and 450 weight ppm of H_2S formed by bacterially stimulated decomposition of marine algae [226]. These results are indicated by the data points for fatigue loading at R = 0.7 and 0.167 Hz. The solid line represents crack growth in natural seawater, while the dashed line gives da/dN-ΔK for H_2S gas saturated (520 wt ppm) seawater; see Fig. 11. Cowling and Appleton reported similarly high levels of corrosion fatigue crack growth for BS4360:50D C-Mn steel in anaerobic artificial seawater containing a culture of sulphate reducing bacteria harvested from the Lower Clyde Estuary in England [122].

The effect of biologically generated H_2S should be quantitatively modeled based on hydrogen uptake characterized by permeation experiments. Dissolved hydrogen should be related to corrosion fatigue crack propagation rate and independent of the chemical or electrode potential stimulation of atomic hydrogen production. This approach will be complicated by crack chemistry effects of the type discussed in Section VI.5.b, and by

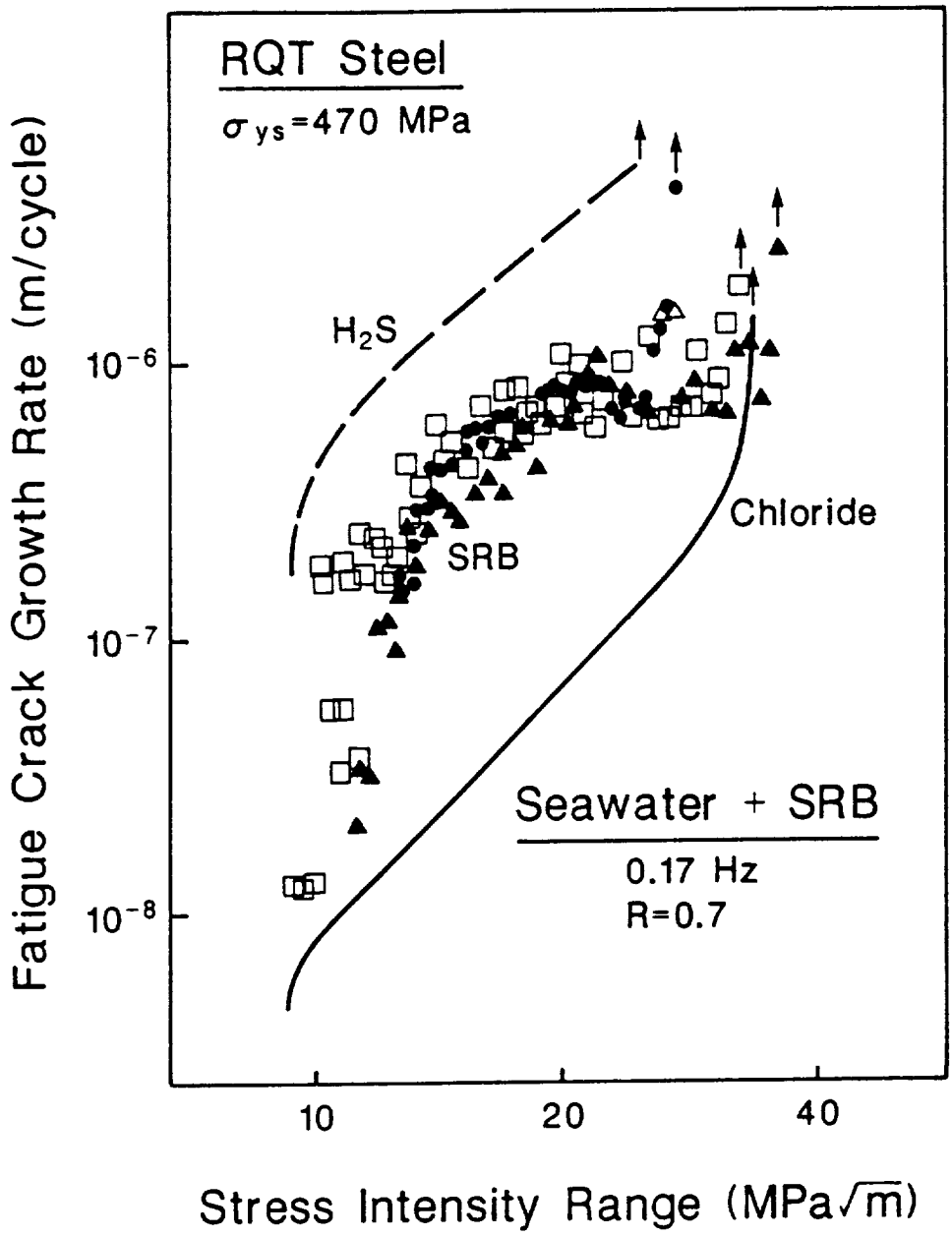

Fig. 39 Biologically stimulated corrosion fatigue in a low strength C-Mn steel, RQT 501, cycled at 0.167 Hz and R = 0.70. Solid line: cracking in pure seawater; data points: seawater with 75 to 450 wt ppm H_2S from decomposition of algae; and dashed line: gaseous H_2S saturated seawater (520 wt ppm); after Thomas et al. [226].

biological effects on crack tip anodic dissolution and hydrogen recombination reactions. This possibility is indicated by the fact that higher crack growth rates are observed for H_2S gas saturated chloride compared to biologically active solution at the same dissolved sulfide ion concentration [122,226].

Biologically enhanced corrosion fatigue is an infant field. The rapid crack growth rates indicated in Fig. 39 and the possibilities for organic species to be present in marine and industrial environments suggest that this problem will be more intensely researched in the future.

VI. QUANTITATIVE MODELS OF CORROSION FATIGUE CRACK PROPAGATION

VI.1. Conclusion

Micromechanical-chemical models of crack tip driving forces and process zone corrosion fatigue damage provide a sensible means to predict and extrapolate the effects of variables, and to modify the fracture mechanics approach to account for compromises in similitude. Models have been formulated based on hydrogen embrittlement and film rupture/transient dissolution/repassivation. Fatigue damage due to crack surface films has not been considered quantitatively. Models successfully predict the time (frequency) dependence of corrosion fatigue and the effects of electrode potential, solution composition and gas activity. All are, however, hindered by uncertainties associated with crack tip processes and the fundamental mechanisms of environmental embrittlement. A process zone model has not been developed for corrosion fatigue; as such, stress intensity, yield strength and microstructure effects are not predictable. Furthermore, absolute rates of hydrogen assisted crack growth are not predictable and the film rupture formulation is being debated. Successes to date indicate that a new level of mechanistic understanding is achievable.

VI.2. Introduction

Explanations for the effects of important variables on corrosion fatigue crack propagation, Section V, were qualitative.

Predictive models of crack tip damage must be developed to expand limited data bases. Recent conferences have focused on this theme for environmental fracture [20,24].

A quantitative model of corrosion fatigue crack propagation, developed within the fracture mechanics framework, must contain the following elements:

- oo The rate of environmental fatigue crack propagation must be partitioned into mechanical and chemical-mechanical components. The former may be zero (environment dominant), or finite and described by slip-based or cumulative damage models. This issue is discussed in Section VI.3.

- oo The mechanical contribution to environmental cracking is described by relating applied stress intensity factor to continuum crack tip stress, strain and strain rate fields; and to microscopic deformation. The location of the fracture process zone is critical. (Section VI.4.)

- oo The chemical contribution requires modeling of the local crack environment which develops based on mass transport limitations within the occluded crack. (Section VI.5.)

- oo The chemical contribution requires modeling of transient reaction kinetics for anodic dissolution, repassivation and cathodic hydrogen production on straining clean crack tip surfaces perhaps coupled to passivated flanks. (Section VI.5.)

- oo The rate limiting process must be defined. Either mass transport or chemical reaction will control corrosion fatigue crack propagation rates. (Section VI.5.)
- oo The fracture process zone, a specific crack tip damage process, and a failure criterion must be defined. (Sections VI.6 and 7.)

Each element of corrosion fatigue crack growth rate modeling is assessed in the following sections, within the frameworks of hydrogen embrittlement and film rupture. Substantial advances have been recorded in each area, however, no analysis has integrated the necessary chemical, mechanical and microstructural components into a broadly predictive model of corrosion fatigue crack propagation.

VI.3. Interaction of Mechanical and Environmental Fatigue

Early attempts to model corrosion fatigue crack propagation linearly summed the contributions from inert environment fatigue and stress corrosion cracking, with the time rate of the latter integrated over a single loading cycle [50]. This model is, of course, not applicable to corrosion fatigue below K_{ISCC}. Here several models have been proposed to combine mechanical fatigue and the chemical environment effect. An equation developed by Wei and coworkers provides a reasonable basis for modeling.

VI.3.a. **Superposition:** Cycle-time-dependent rates of corrosion fatigue crack propagation were first described by a superposition concept championed by Wei and coworkers [30,50,221]. Considering da/dN-ΔK data for an alloy in inert and aggressive environments:

$$\frac{da}{dN_e} = \frac{da}{dN_m} + \frac{da}{dN_{cf}} \qquad (1)$$

where: da/dN_e is the total measured crack growth rate for the aggressive environment

da/dN_m is the rate of plasticity driven fatigue crack propagation for an inert environment

da/dN_{cf} is the incremental difference on the crack growth rate plot, and represents the effect of interacting cyclic plastic deformation and chemical reaction.

This formulation follows directly from linear superposition of stress corrosion and inert environment fatigue cracking, and is associated with the incremental environmental effect on a da/dN-ΔK plot. The question, however, is: Why should inert environment fatigue crack propagation influence da/dN_e for the case where damage is entirely chemical-mechanical in origin? That is, cracking in an environment may progress by a unique microscopic mechanism with no relationship to inert environment fatigue processes. It is important to recognize that unique fracture processes are involved in corrosion fatigue.

A more physically reasonable formulation states that the rate of fatigue crack propagation in an environment is produced by concurrent parallel processes. For two processes, the superposition concept is then given by [228]:

$$\frac{da}{dN_e} = \frac{da}{dN_m}(\Theta) + \frac{da}{dN_c}(\Phi) \qquad (2)$$

where: da/dN_c is the rate of "pure" corrosion fatigue crack propagation.

θ is the fraction of the crack surface formed by mechanical fatigue.

Φ is the fraction of the crack surface formed by corrosion fatigue.

Da/dN_c represents the rate of crack advance along those portions of the crack front which are solely environmentally affected. θ and Φ are measured by fractographic analysis. For two parallel processes, θ equals $(1-\Phi)$.

Comparing equations 1 and 2 demonstrates that:

$$\frac{da}{dN_{cf}} = \left(\frac{da}{dN_c} - \frac{da}{dN_m}\right)\Phi \qquad (3)$$

That is, the phenomenological difference between inert and aggressive environment fatigue rates from the da/dN-ΔK relationship is equivalent to the difference between the rates of microscopic process driven chemical-mechanical and mechanical fatigue times the fractional occurrence of the former. This comparison relates the phenomenological difference in crack growth rates, da/dN_{cf}, and the underlying causes.

The rigorous basis for corrosion fatigue modeling is a derivation of da/dN_c and Φ as a function of chemical and metallurgical variables, as discussed in Sections VI.6 and 7. Only simplifications of this approach have been reported. For example, da/dN_{cf} is often assumed to be proportional to the

amount of hydrogen produced at the crack tip, or to the total electrochemical charge passed during multiple rupture events, per load cycle. Alternately from equation 3 and for a specific material and environment, (da/dN_c - da/dN_m) is assumed to be a constant which equals the maximum environmental enhancement (viz, $da/dN_c = da/dN_e$) due to complete chemical reaction where Φ equals 1.0. Here Φ, but not da/dN_c, is equated to the extent of varying environmental reaction for either mass transport or reaction rate control. For values of Φ less than one, the fatigue surface will be composed of fractions of mechanical and chemical-mechanical damage, with da/dN_{cf} given by equation 3 or da/dN_e given by equation 2.

VI.3.b. **Competition.** Austin and Walker argue that corrosion fatigue crack propagation is modeled as a competition, rather than a superposition, of independent mechanical and chemical processes [229]. They assume that the measured environmental crack growth rate, da/dN_e, is determined by the dominant (faster) of two processes including mechanical fatigue or cycle-time-dependent corrosion fatigue.

The competition model is a special case of equation 2. Considering environment dominant fatigue cracking, $\Phi = 1$ and $da/dN_m << da/dN_c$ in equation 2; therefore $da/dN_e = da/dN_c$. Here the superposition and competition models are equivalent. If crack growth involves a significant amount of mechanical fatigue at comparable rates to corrosion fatigue, then the competition model is not adequate. Rather, analyses of θ, Φ and the growth rate components in the superposition model (equation 2) provide an appropriate approach.

VI.3.c. **Other.** Several models of corrosion fatigue crack propagation begin with the assumption that [39,138]:

$$\frac{da}{dN_{cf}} = \frac{da}{dt}\left(\frac{1}{f}\right) \qquad (4)$$

where f is the cyclic loading frequency and da/dt is the average time based crack growth rate per loading cycle.

Austin and coworkers hypothesized that the corrosion fatigue crack propagation rate is given by the inert environment rate times a multiplicative factor which accounts for the aggressive environmental contribution [230,231]. This factor includes the accelerating effect of embrittling hydrogen and the mitigating effect of crack tip blunting by anodic dissolution.

VI.4. Models of Crack Tip Mechanics: Relationships Between ΔK and Local Plastic Strain, Strain Rate and Stress.

Crack tip stress and strain, not stress intensity, control fracture processes including corrosion fatigue. As such, quantitative models of corrosion fatigue crack propagation require a description of crack tip stress and strain fields, and microdeformation processes, explicitly defined as a function of the applied stress intensity factor.

Regarding the success of the fracture mechanics approach to describe fatigue and environmental cracking, four points are critical. Firstly, all analyses reported to date show that crack tip mechanical quantities depend uniquely on applied ΔK. As such, it is reasonable to expect that stress intensity will uniquely characterize the growth kinetics of corrosion fatigue cracks. Secondly, precise analyses of crack tip fields have not been conducted for growing fatigue cracks under cyclic loading, particularly for the region within several microns of the crack tip. Thirdly, ΔK is derived based on continuum mechanics without consideration of microscopic deformation processes. This limitation does not mean that stress intensity is impotent to correlate processes such as slip density or morphology and grain boundary strain localization. Rather, ΔK is analogous to "P/A" applied stress. The challenge is to experimentally or analytically develop the effect of stress intensity on noncontinuum deformation behavior. Finally, environment may modify crack tip plasticity and thus alter the relationship between ΔK and local stress or strain. This complication does not void the fracture mechanics approach. Rather, it requires

that time and environment dependent constitutive laws be determined for analyses of crack tip fields.

The state-of-the-art in crack tip fields is summarized here, and is reviewed in detail by Gerberich and by Sieradski in this volume [82,160], by Rice and McClintock at the Firminy conference [7], and by Lidbury [232], Ford [39] and Knott [233]. While elastic-plastic analyses have been rigorously developed to within microns of the crack tip for monotonic loading and strain hardening materials, the cyclic loading problem has received limited attention; only approximations have been developed.

One or more of the following quantities are necessary for corrosion fatigue crack propagation models. All results are for small scale yielding and plane strain crack tip deformation.

Monotonic plastic zone diameter, r_p

$$r_p = \frac{1}{3\pi}\left(\frac{K}{\sigma_{ys}}\right)^2 \tag{5}$$

Cyclic plastic zone diameter, r_{pc}

$$r_{pc} = \frac{1}{12\pi}\left(\frac{\Delta K}{\sigma_{ys}}\right)^2 \tag{6}$$

Maximum blunted crack tip opening displacement in fatigue, δ_{max}

$$\delta_{max} = \frac{0.5\Delta K^2}{(1-R)^2(2\sigma_{ys})E} \tag{7}$$

Cyclic blunted crack tip opening displacement, δ_c

$$\delta_c = \left(\frac{1+R}{1-R}\right)\frac{\Delta K^2}{4\sigma_{ys}E} \tag{8}$$

To approximate cyclic hardening or softening, the cyclic yield strength (σ_{ysc}) should be employed in equations 6 through 8 in place of monotonic yield strength (σ_{ys}).

For monotonic loading of a stationary crack, the maximum opening (normal) stress equals between 3 and 5 time σ_{ys}, depending on work hardening behavior, and independent of applied K. This maximum occurs at two crack tip opening displacements ahead of the crack tip; stresses then decay within the plastic zone to merge with the well known elastic stress distribution near the plastic zone boundary.

Cyclic plastic strain, and perhaps mean strain, govern mechanical fatigue damage.

Crack tip plastic opening strain (Monotonic load, stationary crack), ϵ_p

$$\varepsilon_p = \frac{\sigma_{ys}}{E}\left(\left(\frac{r_p}{X}\right)^{\frac{1}{n+1}} - 1\right) \tag{9}$$

The parameter, n, describes work hardening according to the Ramberg-Osgood formulation, with an elastic-perfectly plastic material characterized by n equal to zero. X is distance ahead of the crack tip.

Crack tip plastic opening strain (Monotonic load, moving crack), ϵ_{pm}

$$\varepsilon_{pm} = 5.5\frac{\sigma_{ys}}{E}\left(\ln\left(\frac{r_p}{X}\right)\right)^{\frac{1}{1-n}} \tag{10}$$

The total monotonic strain includes an elastic component (σ_{YS}/E) added to equations 9 and 10.

The cyclic plastic strain range, $\Delta\epsilon_p$ is estimated by substituting the cyclic plastic zone size (equation 6), and cyclic yield strength and work hardening parameters into equations 9 and 10. As an example:

Crack tip cyclic plastic strain range (n = 0, stationary crack), $\Delta\epsilon_p$

$$\Delta\varepsilon_p = \frac{1}{12\pi}\left(\frac{\Delta K^2}{\sigma_{ysc} E}\right)\frac{1}{x} - \left(\frac{\sigma_{ysc}}{E}\right) \tag{11}$$

Crack tip cyclic total strain range, $\Delta\epsilon_T$, may be measured experimentally by stereoimaging techniques (Section IV.4). An example was reported by Hudak for corrosion fatigue cracks in AISI 304 stainless steel exposed to either moist air or an electrolyte at 363 K [234,235].

$$\Delta\varepsilon_T = \varepsilon_0 \Delta K^{\gamma}\left(\Delta\varepsilon_1 - m\ln(x + A)\right) \tag{12}$$

Here, γ, ϵ_o, $\Delta\epsilon_1$, m and A, are empirical parameters defined by curve fitting, with γ equal to between 2 and 5.5. This result is similar to equation 11 based on cyclic plastic zone. Note, however, that the strain singularity is not observed experimentally.

Crack tip total strain rate $(d\epsilon/dt)_c$ is a critical element of film rupture models of corrosion fatigue [39,234]. While this parameter varies during a stress intensity cycle and with crack growth ($d\epsilon/dt = (d\epsilon/dK \cdot dK/dt) + (d\epsilon/da \cdot da/dt)$), a per cycle average strain rate, $(d\epsilon/dt)_c$, is estimated by:

$$\left(\overline{\frac{d\varepsilon}{dt}}\right)_c = \frac{\Delta\varepsilon_{T@x=0}}{t_{eff}} \tag{13}$$

for the case where strain rate is dominated by the rate of change of crack tip strain with respect to K. That is, where the rate of change of strain with crack growth is small. t_{eff} is given by reciprocal loading frequency times the fraction of the cycle where load is rising times the fraction of the rising load portion where the crack is opening above closure (Section VII.2). Several forms for the crack tip strain rate have been published:

Empirical from Eqns. 12 and 13 (Hudak et al. [234,235])

$$\dot{\varepsilon}_c = \alpha\varepsilon_0 f\left(\frac{(\Delta K - \Delta K_{th})^{\gamma}}{1-\left(\frac{\Delta K_{th}(1-R)}{\Delta K}\right)}\right) \tag{14}$$

Approximate analytical from Eqns. 11 and 13

$$\dot{\varepsilon}_c = \beta\frac{\Delta K^2}{\sigma_{ys}E} f \tag{15}$$

Analytical from time derivative of δ_c, Eqn. 8
(Atkinson [39])

$$\dot{\varepsilon}_c \propto \frac{d\delta_c}{dt} = \Phi\frac{\Delta K^2}{\sigma_{ys}E} f \tag{16}$$

Analytical based on crack tip shear band strain
(Cole [39])

$$\dot{\varepsilon}_c = \Theta \frac{\Delta K^2}{\sigma_{ys} E} f \tag{17}$$

Analytical based on crack tip shear within r_{pc}
(Lidbury [232])

$$\dot{\varepsilon}_c = \lambda \frac{\sigma_{ys}}{E} \left(\frac{\Delta K}{\Delta K_{th}} \right)^2 f \tag{18}$$

Analytical based on da/dt dominated strain rate
(Shoji [39])

$$\varepsilon_c = (10 \text{ to } 100) \frac{da}{dt} = (10 \text{ to } 100) f n \Delta K^{2 \text{ to } 6} \tag{19}$$

In these strain rate equations $\beta, \Phi, \theta, \lambda$ and n are unknown constants. In equation 19 the ΔK and R dependencies are derived from inert environment fatigue crack growth rates stated in terms of time based crack growth rates according to equation 5.

Crack tip strain rate measurements and predictions are shown in Fig. 40 [39]. Stereoimaging data (equation 14) are in reasonable agreement with the analytical predictions of equations 17 and 18. Only the forms of the equations are supported because the constants in these models were adjusted to give best fits. The prediction based on growth rate dominated strain, equation 19 and the lower solid line in Fig. 40, is in poor agreement with the data [234].

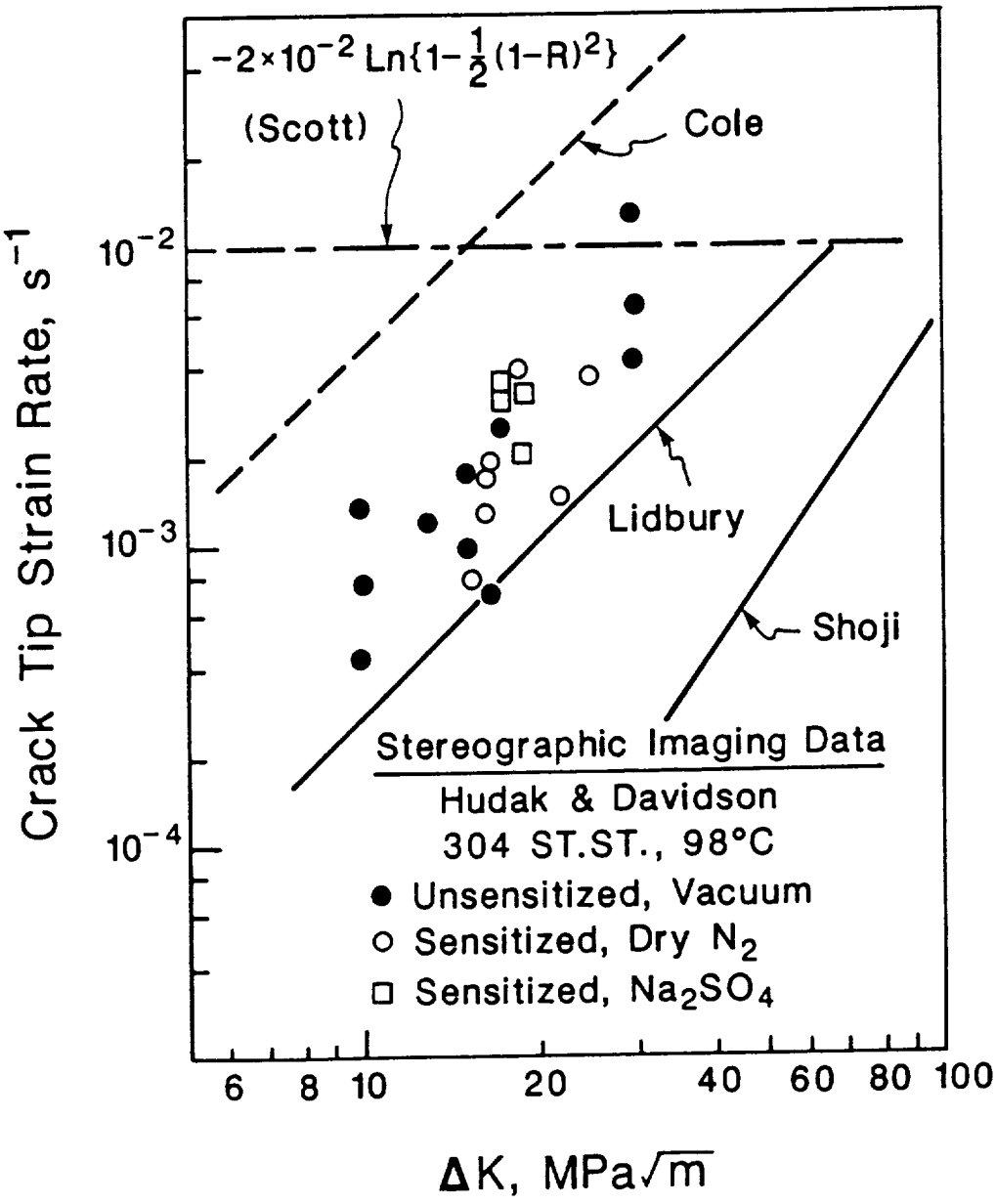

Fig. 40 Measured and analytically predicted average crack tip strain rate as a function of applied ΔK for R = 0.1 and f = 0.01 Hz. Data are described by equations 12 and 14, and the predictions by equations 17, 18 and 19; after Ford [39].

For corrosion fatigue modeling, it is reasonable to assume that crack tip strain rate varies as:

$$\dot{\varepsilon}_c \propto \left(\frac{1}{\sigma_{ys}}\right) f\Delta K^{\gamma} \qquad (20)$$

with γ equal to 2.

These analyses demonstrate that crack tip parameters which control corrosion fatigue crack propagation depend uniquely on stress intensity range. Similitude is expected, at least from the mechanical perspective. Crack tip field equations of the sort presented here have been successfully incorporated into micromechanical models for monotonic load fracture due to cleavage, hydrogen embrittlement and ductile rupture [57,160,192]. Benign environment fatigue crack propagation kinetics have been similarly modeled based on crack tip plastic strain coupled with a cumulative damage failure criterion [210,211]. Successes for corrosion fatigue crack propagation have been limited; additional work is required.

VI.5. Models of Occluded Crack Chemistry and Transient Reaction

A model of corrosion fatigue crack propagation must recognize that significant differences can exist in the crack tip environment compared to the bulk gas or electrolyte; and that rates of reaction on strained, transiently active surfaces are different compared to steady state kinetics. Crack chemistry can be either more benign or more aggressive than the nominal environment. Mass transport and reaction modeling are required to define the specific conditions which drive crack propagation. While dissolution and film rupture are clearly crack tip processes, embrittling hydrogen may be contributed from the crack tip and specimen surfaces in contact with the bulk environment. The relative importance of these hydrogen sources must considered.

Detailed discussions of localized crack chemistry and

reactions are beyond the scope of this review. Three international conferences were recently held to examine this topic [17,19,236]. Here, the conclusions of this work are assessed to provide a basis for discussions of corrosion fatigue crack propagation models in Sections VI.6 and 7.

VI.5.a. **Gaseous Environments.** For fatigue crack propagation in gases, the important consideration is that crack tip gas pressure may be attenuated compared to the surrounding environment due to impeded molecular, or Knudsen, flow [237]. Here, gas transport within the crack is controlled by molecule collisions with crack walls, rather than by intermolecular collisions. Da/dN is reduced by this pressure reduction if crack surface reactions are rapid, or on the same order as transport; as such, reaction is limited by gas supply.

The extent of the pressure decrease due to Knudsen flow depends on crack length and opening shape, molecular mean free path, and time determined by cyclic loading frequency and crack advance rate. As a generalization, impeded flow occurs when some multiple (about 10 to 100) of the mean free molecular path exceeds the crack opening displacement [238]. Since the mean free path for low pressure gases (water vapor, H_2, or O_2) is about 500 μm at 300 K and 20 Pa[4], and since a typical blunted crack tip opening displacement (equation 7) is about 4 μm with the crack mouth opening equalling 75 μm, impeded molecular flow is clearly important. The extent of the pressure attenuation must be calculated as a function of crack geometry. The approach to this problem follows from early treatments of simple slot geometries [237], with the challenge being to account for the complex opening shape of cracks as a function of stress intensity, and to define the crack length over which molecule-wall collisions dominate gas transport.

[4]Mean free path is directly proportional to temperature, inversely proportional to gas pressure, and inversely proportional to the square of the molecular diameter [237]. As such, the mean free path of these molecules at atmospheric pressure (100 kPa) is about 0.1μm.

Impeded molecular flow effects in corrosion fatigue have been investigated, predominantly for the aluminum-water vapor system. Lawn demonstrated the important interaction of mass transport and reaction for environmental cracking under monotonic load [238]. He derived an approximate solution for the stress intensity dependence of the gas "impedance factor" and related this term to static load crack growth rate. The first considerations of Knudsen flow control in fatigue crack growth were by Snowden and Bradshaw [239-241]. Snowden argued that the pressure below which moist air ceased to reduce the smooth specimen fatigue life of lead was consistent with the onset of substantially impeded molecular flow of deleterious oxygen [241]. Bradshaw recognized the possibility of mass transport impedance for Al-Cu-Mg in water vapor, but concluded that surface reaction kinetics are equally or more important [239]. Gangloff and Ritchie pointed out that crack geometry dependent gas pressure attenuation could lead to breakdowns in similitude if the local environment is controlled by stress and crack length, apart from a simple stress intensity description [203].

Bradshaw and Wheeler demonstrated that corrosion fatigue crack growth rates in the aluminum alloy-water vapor system decreased when a substantial pressure of inert gas was added to the low partial pressure water environment [187]. Here, the inert gas decreased molecular mean free path and caused a transition from impeded molecular transport to slower viscous flow governed by gas molecule-molecule collisions. This experimental observation is inconsistent with estimates of the gas mean free path for impedance by viscous flow, emphasizing the fact that Knudsen flow calculations, and the criteria for molecule-wall versus molecule-molecule interactions are rudimentary.

Wei and coworkers coupled crack tip gas-metal reaction kinetics with mass transport, controlled by molecule-wall interactions, to derive predictive relationships for corrosion fatigue crack growth rate [129,242]. This modeling was described qualitatively in Section V.4.b.(3) and quantitative relationships are presented in Section VI.6. Experimental observations (eg.

Figs. 22 and 23) supported model predictions of fatigue crack growth rate versus bulk environment gas pressure/loading frequency for aluminum alloys in water vapor and steel in gaseous H_2S [61,129,151,242-244]. This model predicts the bulk environment saturation pressure, P_o, below which gas transport limitations will reduce da/dN for the case where surface reactions are fast [61]:

$$P_0 = \left\{ 436\left(\frac{\beta}{\alpha}\right) f(R) \left[\frac{\sigma_{ys}^2 \ell}{N_0 kTE}\right]\left[\frac{T}{T_m}\right]^{1/2} \right\}^{-1} \qquad (21)$$

$$f(R) = 0.25\left\{\left(\frac{1+R}{1-R}\right)^2 + 0.5\right\}$$

T is temperature, M is the molecular weight of the gas, k is Boltzmann's constant, N_o is the number density of surface reaction sites, f is frequency, E is elastic modulus, σ_{ys} is yield strength, R is stress ratio, and l, β and α are parameters which describe that portion of the crack geometry over which impeded flow occurs. These parameters largely relate to molecular mean free path and crack geometry.

Experimental results plotted in Fig. 41 are in excellent agreement with the predicted stress ratio dependence of the saturation pressure, equation 21, for several aluminum alloys fatigued in pure water vapor [221].[5] This result and model emphasize the importance of the mean cyclic crack opening, rather than the maximum value, to gas transport and fatigue crack growth. Fig. 41 explains why extremely small levels of water vapor are capable of enhancing rates of near-threshold fatigue crack propagation in aluminum alloys [60,132,217,221].

[5]The regression line is calculated only for the data on alloy 2219. If all results are included, an excellent linear fit is achieved, as described by the equation: y = 0.8488 x - 0.5789. In either case saturation pressure is nearly directly proportional to the reciprocal stress ratio function.

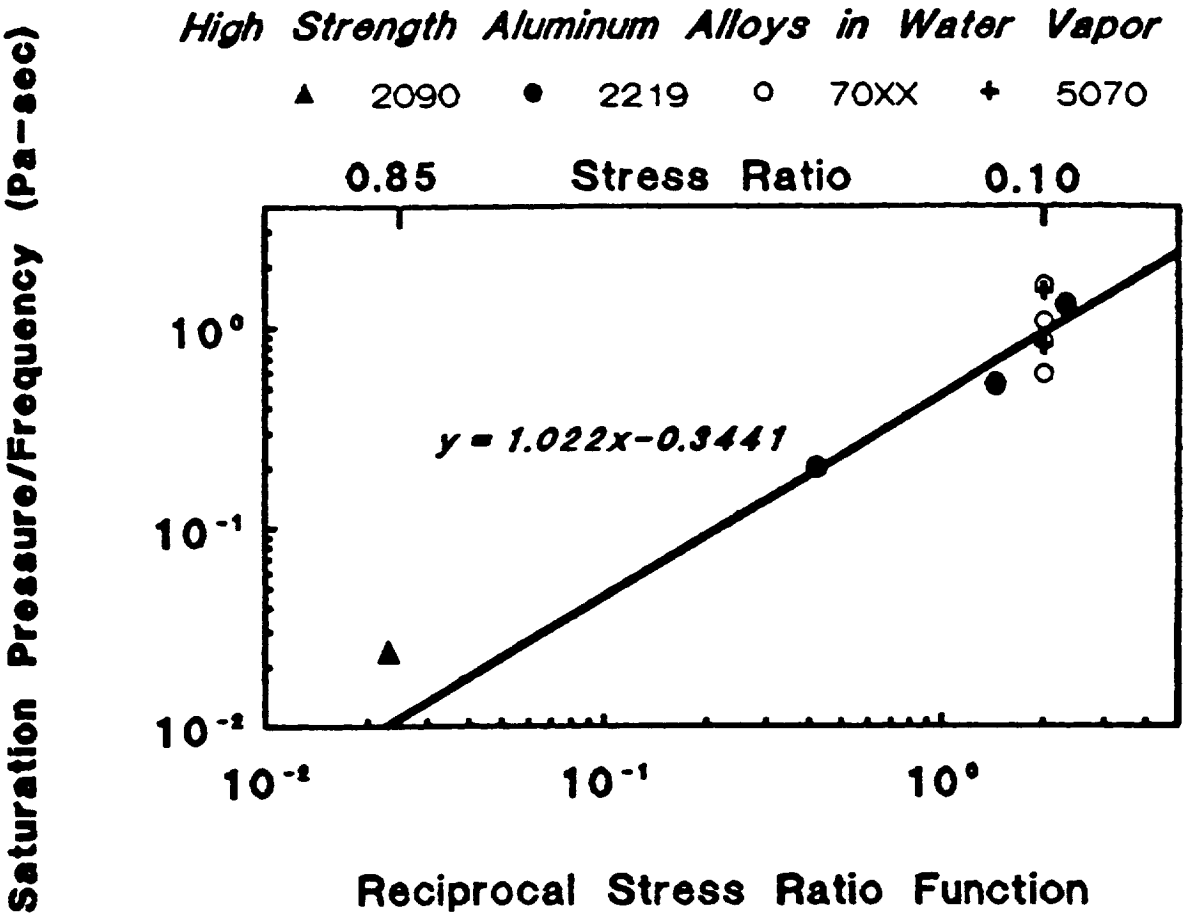

Fig. 41 Effect of mean crack opening shape, described by a function of R, on the saturation exposure (pressure/frequency) for corrosion fatigue crack propagation in aluminum alloys 2090 [125], 2219 [243], 70XX [61,244] and 5070 [184,187] in water vapor.

Specifically, the saturation pressure decreases strongly with increasing R value. Near-threshold cracking is often conducted at high R, either by design or due to the effects of crack closure as described in Section VII.2.

The main challenge to gas transport models is the uncertainty with the description of crack geometry, in fracture mechanics terms, and the crack length over which impeded flow occurs. As a result of this problem, the constants in equation 21 are determined from crack growth rate data. Crack closure effects on Knudsen flow have not been investigated. Gas transport models are insufficient to predict absolute rates of corrosion fatigue crack propagation. Transport, surface reaction and a crack damage criterion must be coupled as discussed in Section VI.6.

VI.5.b. Aqueous Electrolytes: Active Steels in Chloride-Crack Chemistry Modeling.

From the pioneering work of Brown in the late 1960s, it is well recognized that impeded mass transport and localized reactions render the electrochemical conditions within occluded cracks unique compared to bulk solution composition, electrode potential, and pH [165]. A quantitative approach to this problem requires solutions to the differential equations which describe coupled electrolyte transport and crack surface electrochemical and chemical reactions. Ideally, the kinetics of reactions on filmed crack flanks and the straining clean crack tip should be considered.

To date, localized crack chemistry has been modeled and probed experimentally for two systems; passive stainless and ferritic steels in high temperature water, and active C-Mn and alloy steels in aqueous chloride solutions. The former topic is discussed extensively by Ford and Andresen elsewhere [39,136,138], and provides important input to film rupture models of corrosion fatigue. Crack electrochemistry is reviewed here for steels in chloride, and as a basis for a hydrogen embrittlement model.

For steels in aqueous chloride, crack growth is accelerated by adsorbed hydrogen produced electrochemically at the crack tip.

As such, crack solution pH and electrode potential have been emphasized to calculate rates of crack tip hydrogen production. It is critical to determine hydrogen production rate as a function of external electrode potential, and to identify the contributions from the crack tip, the crack flanks and specimen surfaces. Brown experimentally demonstrated that acidic conditions develop within cracks in steels exposed to neutral seawater for anodic polarization and free corrosion [165]. As the bulk potential was made more cathodic, the crack solution became more alkaline. Understanding of these trends has emerged from a series of papers by Turnbull and coworkers [166,167,169,190,191,193,194,245-252].

The model of crack electrochemistry for corrosion fatigue in the steel-aqueous chloride system includes the following reactions [165,190,249,252]:

(1) Anodic dissolution of iron and major alloying elements, particularly chromium.

(2) Cation hydrolysis to produce hydrogen ions within the crack.

(3) Cathodic reduction of oxygen, both within the crack until depletion occurs, and on external specimen surfaces.

(4) Cathodic reduction of hydrogen ions and of water, both within the crack and on external specimen surfaces.

Hydrolysis is rapid, while rates of the electrochemical reactions are determined by polarization methods, and depend on pH and electrode potential in the standard way. The effect of straining on clean surface transient reactions was recently described by straining electrode measurements [191]. Reaction rates are coupled with descriptions of reactant supply and product removal through mass conservation. Mass transport by concentration gradient diffusion, ion migration and convective mixing is modeled essentially one dimensionally in the direction of crack propagation. The differential equation which describes these terms is solved for the steady state case. Appropriate boundary conditions and fracture mechanics descriptions of crack opening

shape complete the elements of the analysis.

The outputs of crack chemistry modeling include crack solution oxygen concentration, crack tip pH and electrode potential as a function of distance from the crack mouth to the crack tip. From pH and potential, it is possible to calculate the total rate of atomic hydrogen production, and from this, the concentration of adsorbed hydrogen on crack tip and external surfaces in equilibrium with the appropriate solutions. Each of these quantities is predicted as a function of applied potential, temperature, chloride composition (viz, seawater or NaCl), loading frequency, ΔK, R, crack length and load waveform. These mechanical variables influence crack shape and hence mass transport.

Since the detail of this work is extensive, only those conclusions relative to corrosion fatigue crack propagation models are discussed.

(1) The concentrations of reactants and products in a pulsating fatigue crack depend on crack depth, mouth opening, loading frequency, ΔK, R, σ_{ys} and specimen geometry. The interplay between diffusion and convection results in a minimum of reactant concentration and a maximum of products at a critical crack depth. Transport within cracks of varying length is controlled by different proportions of convection and diffusion. An example of specific calculations for crack tip reactant oxygen concentration is shown in Fig. 42 [248,252].

(2) Corrosion fatigue cracks in bulk aerated chloride are deoxygenated for most solution and loading parameters, owing to the rapid rate of oxygen reduction within the crack compared to diffusive and convective supply [246-249]. Without competition from oxygen, cathodic reactions solely produce adsorbed hydrogen. This result is controversial in the sense that crack surface contact will produce turbulent mixing and enhanced oxygen supply to the crack tip. In this case Gangloff proposed that corrosion fatigue crack growth rates are reduced by oxygen reduction which dominates cathodic reactions that otherwise produce embrittling hydrogen [253]. This hypothesis has not been proven by critical experimentation [189,208]

(3) For electrolytes such as NaCl or seawater, potential differences between the crack tip and bulk surfaces are less than 50 mV, with more cathodic values predicted for near-free corrosion and more noble values typical

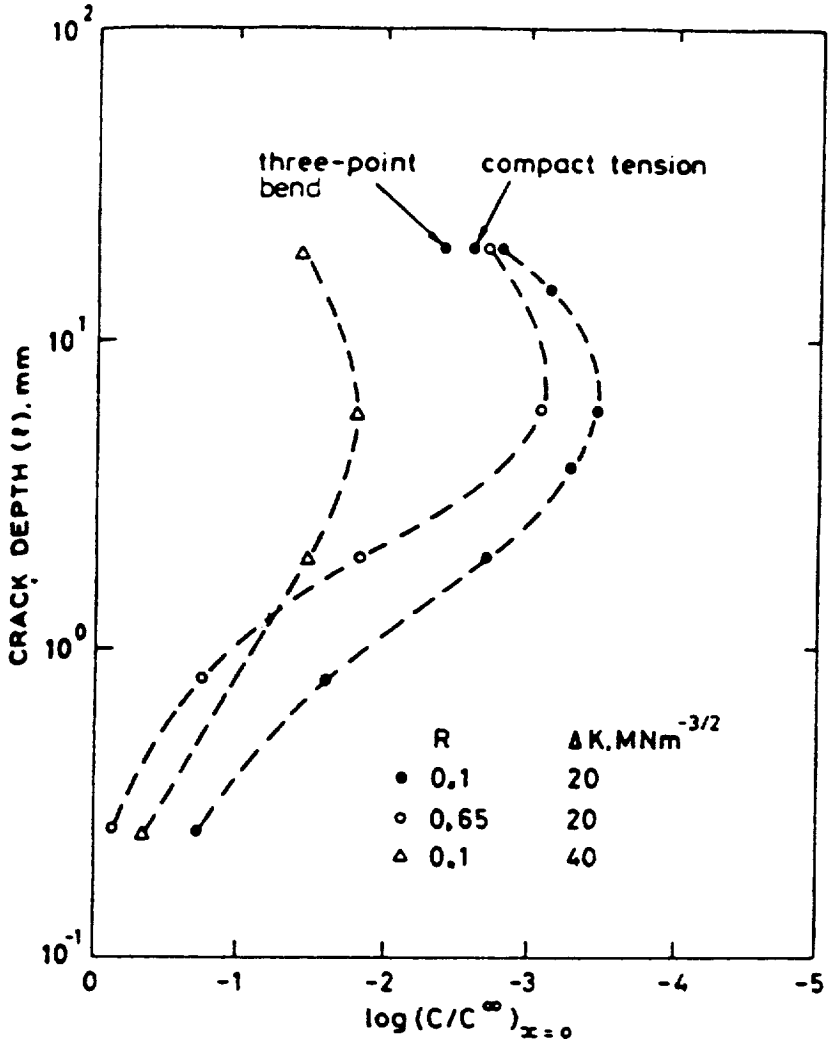

Fig. 42 Model predictions of the effect of crack depth on dissolved oxygen concentration at the crack tip normalized to the bulk solution level for several specimen geometries, stress ratios and ΔK levels; SEN, C-Mn steel, NaCl at -800 mV (SCE); after Turnbull [248].

of cathodic polarization. Hydrogen bubbles, a tortuous crack path or corrosion debris will increase "IR drops" along the crack [190,249].

(4) For neutral electrolytes, crack tip pH is mildly acidic (pH 6) for free corrosion potentials and basic for cathodic polarization. Crack acidification to pH 3-5 is only likely for applied anodic potentials, for cases where ferrous ions are oxidized to ferric, for short crack depths, or for steels containing strongly hydrolyzable specie such as chromium [249].

(5) Near free corrosion or for anodic polarization, crack tip dissolution, cation hydrolysis leading to acidification and H^+ reduction dominate crack chemistry. Cathodic polarization promotes an alkaline crack with pH approaching 10; hydrogen production is predominantly through water reduction. Total crack tip hydrogen production rate and the adsorbed H concentration are substantial and are predicted to generally increase with increasingly cathodic polarization as shown in Fig. 43. Effects of frequency, R, ΔK and waveform are of secondary importance [191,250].

(7) For specimens cathodically polarized below about -900 mV (SCE), water and proton reduction on external surfaces are the dominant sources of hydrogen for crack growth; see Fig. 43. Surface hydrogen supply is also dominant for acidic and H_2S bearing solutions [191,193,250].

(8) Model predictions of crack tip pH and electrode potential are in good agreement with measurements of local crack chemistry [141,167,249].

(9) The effects of crack tip straining, clean surface creation and the associated reaction kinetics have not been broadly incorporated in crack chemistry models; additional work is required [250].

These conclusions are important to interpretations of corrosion fatigue behavior in the steel-chloride system, however, modeling has been limited to predictions of crack electrochemistry and hydrogen production. No integrated model has been developed to relate crack chemistry calculations to da/dN by hydrogen embrittlement, as discussed in Section VI.6. Two initial results are noteworthy in this regard. Gangloff and Turnbull coupled crack chemistry modeling with an empirical hydrogen embrittlement failure criterion to predict K_{ISCC} as a

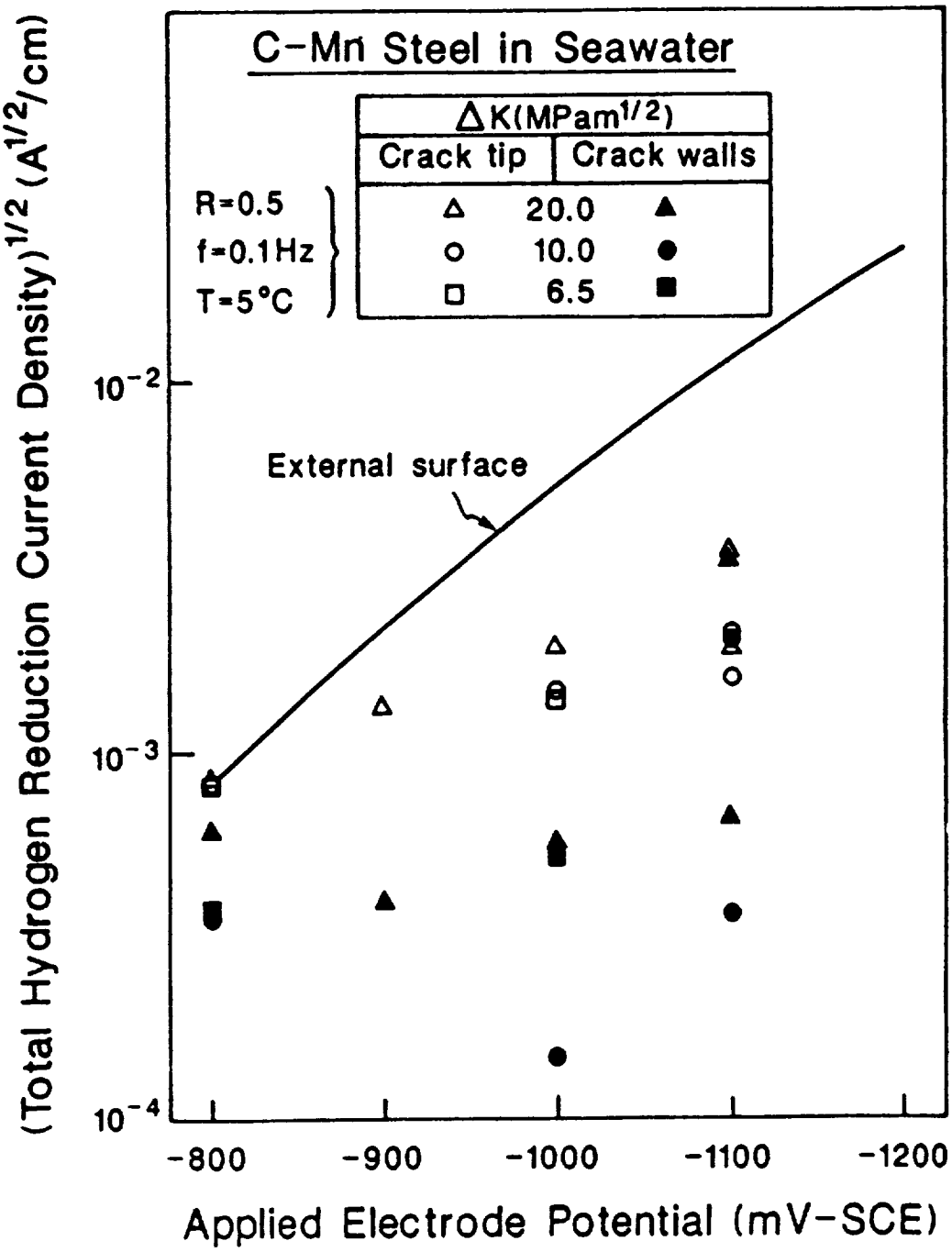

Fig. 43 Model predictions of the effect of applied electrode potential on total atomic hydrogen production rate for various locations on a fatigue cracked specimen of C-Mn steel; after Turnbull and de Santa Maria [191,250].

function of crack geometry [194]. Such predictions were confirmed by experiment.

Following this simplified approach, it is reasonable to assume that corrosion fatigue crack growth rate is proportional to the amount of hydrogen produced at the crack tip. Hydrogen concentration, and therefore da/dN_e, should be proportional to the square root of the total reduction rate, particularly for the chemically limited plateau regime. Data on the effect of electrode potential on da/dN_e for API-2H steel in NaCl (Fig. 25) were coupled with the calculated crack tip hydrogen production rates shown in Fig. 43 to yield the correlation in Fig. 44. (The crack chemistry calculations and corrosion fatigue measurements were for identical material, ΔK, R, frequency and electrolyte composition.)

Results in Fig. 44 show that crack growth rate correlates reasonably with crack tip hydrogen uptake, but the expected square root dependence is not observed. Rather, da/dN_e increases with hydrogen production to the 1/4 power. If the dominant hydrogen concentration, either crack tip or external surface, is used, then least squares analysis shows a similar good correlation. In this case da/dN_e is proportional to total hydrogen production to the 0.14 power ($y = 0.1393 \cdot x + 1.8682$). Since no micromechanical model exists to relate hydrogen concentration to crack growth, the result in Fig. 44 cannot be further explained. Additional work is required to pursue this approach; comparisons between electrolytes and gaseous H_2 would be particularly informative, as demonstrated for monotonic loading [194].

Predictions of those conditions where specimen surfaces are the dominant source of hydrogen compared to the crack tip, and vice-versa, are particularly amenable to evaluation with coated specimens and with electrode potential/frequency transient experiments. Despite arguments to the contrary by Turnbull [249], such existing evidence is weak.

The approach to crack chemistry modeling in steels should be applied to other systems where corrosion fatigue is governed by hydrogen embrittlement. A notable example is high strength

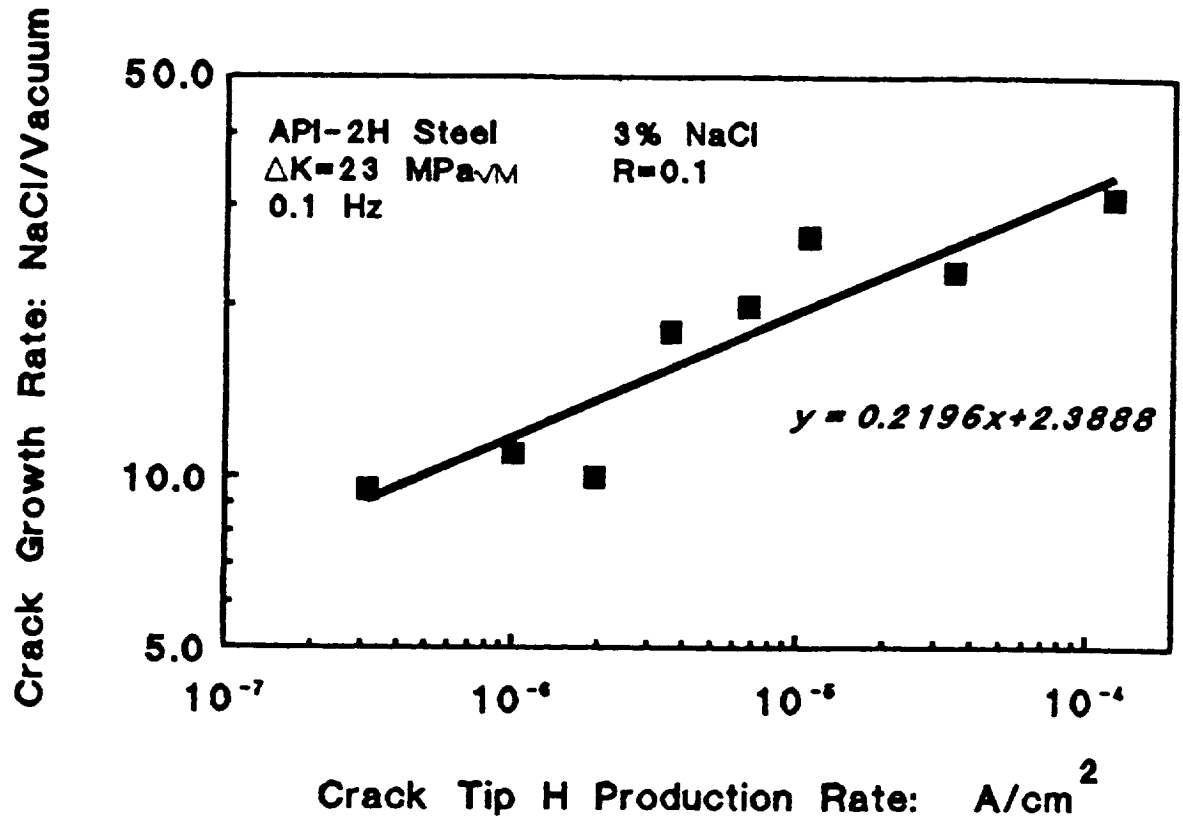

Fig. 44 Corrosion fatigue crack propagation rates for API-2H in 3% NaCl from Fig. 25, correlated with the crack tip hydrogen atom production rate (Fig. 43) to the 0.2 power.

aluminum alloys in distilled water and chloride, Fig. 12, where limited crack chemistry measurement and modeling results have been reported to date. Hydrogen production by hydrolysis is likely, however, the system is complicated because both anodic dissolution of aluminum and hydrogen reduction occur simultaneously over a broad range of potentials [254-256]. Additionally, a variety of surface films are likely to form and complicate reaction kinetics.

VI.5.c. **Aqueous Electrolytes: Active Steels in Chloride-Transient Crack Tip Reaction Kinetics.** The incorporation of transient reaction kinetics in crack chemistry and embrittlement modeling is controversial. Turnbull and coworkers replaced steady state, filmed surface polarization kinetics with similar results obtained with the straining electrode method [191,250]. Wei and coworkers have taken a different approach based on the idea that coupled and transient electrochemical reactions, which occur during each fatigue load cycle and as a cleaned surface refilms, control hydrogen production [33,182,188,257,258]. This work was recently reviewed [37,259].

The essence of Wei's approach is that hydrogen embrittlement causes an increment of crack growth at maximum load. The resultant clean surface reacts anodically during the time to the next load maximum and produces an amount of cathodically generated adsorbed hydrogen near the crack tip. The novel notion here is that rates of dissolution at the crack tip are controlled by the continuously changing (passivating) character of the reacting surface and as polarized by coupled, fully filmed crack flanks. The amount of hydrogen is assumed to be proportional to the integrated amount of current which passes during a load cycle; the environmental contribution to crack growth, da/dN_{cf}, is proportional to this quantity of hydrogen. The next increment of crack extension per load cycle is thusly produced. For steel in aqueous electrolytes, it is hypothesized that electrochemical reaction rate limits fatigue crack propagation. These ideas follow from work on mass transport and reaction rate limited fatigue crack propagation in gaseous environments [129,243].

From Section VI.4, crack tip reaction rate controlled corrosion fatigue is described by:

$$\frac{da}{dN_{cf}} = \left(\frac{da}{dN_c} - \frac{da}{dN_m}\right)\left(\frac{q}{q_s}\right) \qquad (22)$$

where q is the charge transferred per loading cycle and q_s is the amount of charge required for completed reaction on the clean surface. q may be expressed as $[1 - \exp(-\tau/f)]$, where τ is an empirically determined reaction rate constant.

A new method was devised to measure the transient charge relevant to corrosion fatigue [260-262]. A notched specimen, coupled electrically to oxidized electrodes of the same steel, is fractured and the current passed between the bare surface and the oxidized electrodes is measured as a function of time. This ensemble electrode is polarized to a fixed external potential by a counter electrode and with respect to a reference electrode, both contained in a separate solution coupled to the crack simulation by a salt bridge. In this way the current transient can be measured for a constant applied potential, which will differ from the potential of the notch surface due to the IR difference across the salt bridge. In principle the notch/oxidized electrode could be placed in an electrolyte which simulates crack solution pH and ionic concentration, however, such experiments have not been conducted.

Measurements of q/q_s, coupled with equation 22, were employed to predict the frequency dependence of corrosion fatigue crack propagation for ferritic steels in carbonate-bicarbonate, sulfate, buffered acetate and NaCl solutions [182,188,259,263]. These predictions were in good agreement with crack growth rate measurements, supporting this approach. Several points are notable. Firstly, the charge transfer model predicts a frequency response which is qualitatively similar to that shown in Fig. 21 for steel in chloride. Extensive charge measurements have not,

however, been reported for this important system [263]. Secondly, the charge transfer model has not incorporated crack environment changes into the analysis. Thirdly, the charge transfer model does not predict absolute values of crack growth rate because no micromechanical damage criterion has been included. Rather, charge transfer and crack growth kinetics are compared by multiplicative scaling factors. Finally, it is not clear how the charge transfer model will deal with cathodic polarization. Here, crack growth rates increase (Fig. 44) for applied potentials where crack tip dissolution is not likely. While one can argue that polarization of the crack tip will allow transient dissolution for applied cathodic potentials, no evidence exists to support this reasoning. Crack chemistry modeling, albeit steady state, suggests only small IR differences along cracks in conductive electrolytes.

Advances in our understanding of crack tip stress/strain fields, crack chemistry and crack tip transient reaction kinetics are outstanding. The challenge remains, however, to integrate these results into predictive models of corrosion fatigue crack propagation rate by either hydrogen embrittlement or film rupture.

VI.6. Corrosion Fatigue by Hydrogen Embrittlement

VI.6.a. **Justification for Hydrogen Embrittlement.** That hydrogen embrittlement is the dominant mechanism for corrosion fatigue has been effectively argued for several systems; notably ferritic/martensitic steels in gases and electrolytes near 300 K [34,37,51,57-59,116,122,170,174,189,194], and precipitation hardened aluminum alloys in water vapor and halogen bearing solutions [37,60,62-64,125,126,132,133,217-219,264]. This view is supported by extensive, but circumstantial evidence:

- Pure gaseous hydrogen embrittles ferrous alloys under cyclic loading below K_{ISCC} [54,117,118].
- Water vapor embrittles aluminum alloys under cyclic loading, but gases such as O_2 which produce surface films without releasing hydrogen are inert; see Figs. 12 and 27, and Section VI.8 [61,125,221].

- Water vapor embrittles aluminum alloys for stress intensity, frequency and pressure conditions where crack tip condensation and formation of an electrolyte are unlikely [221].

- Hydrogen, introduced by chemical exposure prior to fatigue loading, increases inert environment rates of fatigue crack propagation in steels and aluminum alloys [62,265,266].

- Plastic zone damage, produced by fatigue deformation during crack growth in a hydrogen producing environment, is evidenced by continued rapid fatigue crack propagation during loading in an inert environment. Damage is eliminated by heat treatment, albeit at high temperatures when atomic hydrogen is deeply trapped [132,217-219].

- Crack growth rates vary with changes in frequency, stress intensity and applied electrode potential in a manner consistent with hydrogen embrittlement of the cyclic plastic zone [58,267]. This point is controversial because of limited experimentation and because the fracture process zone may be within microns of the crack tip-environment interface.

- Similar fatigue fracture surface features (viz, transgranular cleavage, intergranular separation and interface cracking; Section V.7.d.) are observed for pure H_2, water vapor and electrolytes [59,221].

- Chemical measurements and modeling elucidate the reaction sequence for environmental hydrogen production from water vapor and correlate corrosion fatigue crack growth rate data (viz, Figs. 22, 23 and 41), including the deleterious effects of increasing P_{H2O} and decreasing frequency [61,98,129,221].

- Electrochemical measurements and modeling demonstrate environmental hydrogen production from electrolytes, and correlate da/dN data (viz, Figs. 21, 25, 43 and 44), including the deleterious effects of increasing cathodic potential and decreasing frequency. Corrosion fatigue in steels under cathodic potentials is only explainable by hydrogen embrittlement [190,191,249,253,258,259].

The role of hydrogen has not been directly revealed. The difficulty is the lack of probes of crack tip chemistry, surface reactions and process zone damage.

VI.6.b. **Quantitative Hydrogen Embrittlement Models.** Models of corrosion fatigue crack propagation rate are based on equation 2. The pure corrosion fatigue crack growth rate and the proportion of

corrosion fatigue depend on the rate and amount of hydrogen production by the reaction sequence for gases or electrolytes; and combined with the local crack tip field, most probably the cyclic plastic strain and hydrostatic normal stress distributions. Microstructure determines the diffusion kinetics and distribution of segregated hydrogen through trapping processes. Local fracture will be determined by a damage criteria. The elements of these relations are shown schematically in Fig. 45.[6]

The challenge in modeling is to derive equations which incorporate the processes shown in Fig. 45 (Sections VI.3 to 5) to predict da/dN_e as a function of ΔK, R, f, microstructural and environmental variables. Quantitative hydrogen embrittlement models for corrosion fatigue are summarized in Fig. 46 [57], and are classed as either hydrogen production-based (Scott, Gangloff, Wei et al.) or hydrogen diffusion-based (Holroyd and Hardie, Austin and Walker, Kim et al.). Each model was developed from considerations of crack chemistry and in order to explain specific data; some successes have been reported in this regard, however, generally predictive models are lacking.

The model by Scott assumes that the "plateau" corrosion fatigue crack growth rate, specifically for steels in aqueous chloride, is limited by hydrogen supply to the process zone [58]. Here, $da/dN_{eplateau} = da/dt \cdot 1/f$ and the time based crack growth rate is assumed to be proportional to the rate of crack tip electrochemical hydrogen production. Scott's original correlation with data was primitive. In fact crack growth rates correlate with crack tip hydrogen production current (Fig. 44), however, the function is not the predicted linear dependence. This model is an extension of crack chemistry and is not based on a specific damage criterion.

Gangloff assumed that the increment in growth rate for environmental cracking, da/dN_{cf}, is proportional to the amount of

[6]The crack tip stress and strain fields shown here are for the monotonically loaded, stationary crack. Less well established results are available for cyclic deformation; see Section VI.4.

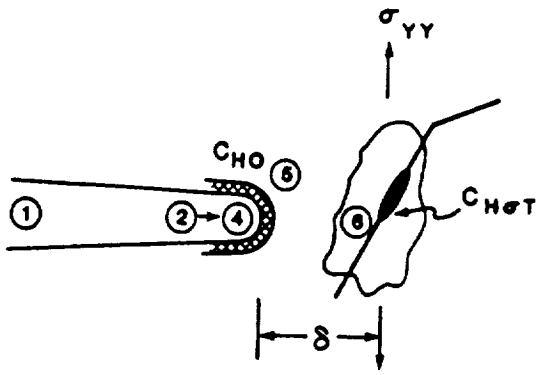

GASEOUS HYDROGEN		ELECTROLYTE
MOLECULAR TRANSPORT	(1)	OXYGEN DEPLETION
PHYSICAL ADSORPTION H_2	(2)	CATION DISSOLUTION, HYDROLYSIS
H_2 MIGRATION, DISSOCIATION TO ATOMIC H	(3)	H^+ REDUCTION TO H
CHEMICAL ADSORPTION	(4)	WATER REDUCTION TO H
	(5)	SOLUTION TO LATTICE, TRAP SITES (5)
	(6)	BULK DIFFUSION TO FPZ (6)

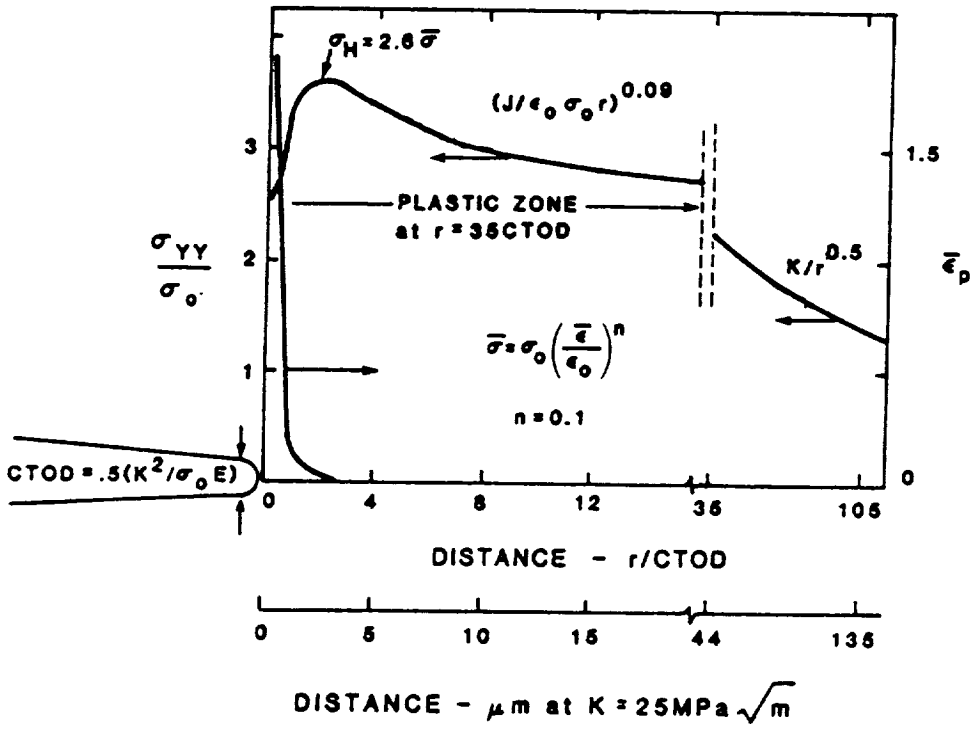

Fig. 45 Transport and reaction sequences which produce adsorbed hydrogen for interaction with the crack tip stress field and process zone microstructure; after Gangloff [57].

	CONTROL PROCESS	da/dN ASSUMPTION	GROWTH RATE PREDICTION
Scott	Crack Tip Cathodic Hydrogen Production	$\frac{da}{dN_{e,\,PLATEAU}} \alpha\ i_H$	$A(1/f)\ (\exp(-E/RT))$
Gangloff	Competition Between O_2 and H^+ Reduction	$\frac{da}{dN_{cf}} \alpha\ C_H$	$A'(V_{max})^{1/2} \exp(\alpha a_o / f V_{max})$
Wei et al.	Molecular Flow Gas Transport	$\frac{da}{dN_{cf}} \alpha\ C_H \alpha\ \theta$	$\frac{da}{dN_{cf,SAT}} \left(\frac{P_o}{f}\right) \Big/ \left(\frac{P_o}{f}\right)_{SAT}$
	Gas-Metal Reaction	$\frac{da}{dN_{cf}} \alpha\ C_H \alpha\ \theta$	$\frac{da}{dN_{cf,SAT}} (1-\exp(-kP_o/f))$
	Charge Transfer by Transient Reaction	$\frac{da}{dN_{cf}} \alpha\ C_H \alpha\ q$	$\frac{da}{dN_{cf,SAT}} (1-\exp(-\tau/f))$
Holroyd and Hardie	Hydrogen Diffusion in Plastic Zone	$\frac{da}{dN_e} \alpha\ \frac{\Delta x}{cycle}$	$4(\sqrt{D_H/f})$
Kim et al.	Hydrogen Diffusion in Plastic Zone	$\frac{da}{dN_{cf}} \alpha\ \frac{\Delta x}{cycle}$	$A'' (\sqrt{P_o D_H / f}) (\exp(-\Delta H/RT)) \Delta K^2$
Austin and Walker	Hydrogen Diffusion in Plastic Zone	$\frac{da}{dN_e} = \frac{da}{dN_m} X$	$\frac{(\Delta x - s)}{(r_p - s)} (\delta_{max} - s)$
			$\frac{da}{dN_{e,\,PLATEAU}} = 37.7 \frac{\sigma_{ys}}{E} (\sqrt{D_H/f})$

E-Modulus
Δx-Hydrogen penetration distance = $4\sqrt{D_H/f}$
C_H-Hydrogen concentration
C_{H^+}-Hydrogen ion concentration
T-Temperature
θ-Fractional surface coverage
X-Environmental factor

q-Electrochemical charge
σ_{ys}-Yield strength
f-Frequency
i_H-H production rate
a_o, A, A', A'', R-Constants
ΔH-Binding energy of hydrogen to dislocation
s-Striation spacing

τ-Clean surface reaction rate constant
α-Oxygen reduction rate constant
V-Crack mouth opening
P_o-Nominal gas pressure
D_H-Hydrogen diffusivity
E'-Crack tip electrode potential
k-Reaction rate constant

Fig. 46 Models for cycle-time-dependent corrosion fatigue crack propagation by hydrogen embrittlement. Scott et al. [58], Gangloff [253], Wei et al. [61,182,258,259], Holroyd and Hardie [65], Austin and Walker [230,231], Kim et al. [258].

hydrogen produced per loading cycle by H^+ reduction at the crack tip for steel in aqueous chloride [208,253]. Acidification was caused by the hydrolysis reaction sequence. Dissolved oxygen, supplied by convective mixing, is reduced within the occluded crack solution and competes to decrease the amount of cathodic hydrogen. The dependence of da/dN_{cf} on crack opening displacement and oxygen reduction kinetics follows from an expression for perfect convective mixing and reaction. This da/dN dependence was confirmed by experiment, however, the beneficial effect of oxygen reduction at constant electrode potential was not demonstrated. The weaknesses of this model are similar to those discussed for the Scott model.

Wei and coworkers relate corrosion fatigue crack growth rate to the amount of hydrogen which is produced per loading cycle and proportionate to the extent of transient crack tip surface reaction [61,129,182,258,259]. Quantitative relationships are derived for the cases of mass transport and surface reaction limited crack growth with the aim of predicting the time dependence of corrosion fatigue, as discussed for aluminum alloys in water vapor (Section V.4.b.) and steels in aqueous chloride (Section VI.5.c.). For gases at low pressures and with fast surface reactions, crack growth is limited by impeded molecular flow; the saturation exposure (P_o/f) is given by equation 21. For gases at high exposures or with slow reaction kinetics, surface reaction is growth rate limiting. The expression for electrochemical reaction rate control by charge transfer was presented in equation 22. The successes of these models in correlating corrosion fatigue crack growth rate data are significant (see Figs. 22, 23 and 41, and References 61,129,182,258 and 259).

Several crack growth models are based on the assumption that da/dN_e is determined by the extent of hydrogen diffusion, Δx, within the plastic zone and during the time of a single loading cycle. Holroyd and Hardie [64] argue that cycle-time-dependent crack growth in the aluminum-seawater system occurs by this process and at rates which are much greater than those of mechanical fatigue. The mechanical contribution to fatigue is

ignored and:

$$\frac{da}{dN_e} = \frac{\Delta x}{1\ cycle} = 4\sqrt{D_H t} = 4\sqrt{\frac{D_H}{f}} \qquad (23)$$

with D_H the diffusivity of hydrogen in steel and t the time per load cycle, 1/f. For an aluminum alloy in seawater, this relationship describes the frequency dependence of the maximum crack growth rate where environmental intergranular cracking was replaced by environmental transgranular cracking. A similar result was obtained for the environmental transgranular to mechanical transgranular fracture surface transition. Measured da/dN_e depend on the reciprocal of the square root of frequency; reasonable values of hydrogen diffusivity were calculated from the growth rate data.

Holroyd and Hardie present no direct evidence to support the hypothesis that the growth kinetics are controlled by hydrogen diffusion. They further argue that the diffusion model reasonably describes the frequency dependence for corrosion fatigue in the steel-water vapor and steel aqueous chloride systems which have been alternately described by crack environment mass transport and surface reaction rate models.

Austin and Walker postulate that corrosion fatigue crack growth rates are given by an enhancement of the mechanical propagation rate due to hydrogen diffusion within the plastic zone and countered by a reduction due to crack tip blunting by corrosion [116,230,231]. This model incorporates a rudimentary micromechanical description of fatigue based on the crack tip opening displacement approach after Tompkins [233]. Physically, da/dN_e is equated to the mechanical fatigue rate when the extent of hydrogen diffusion is less than one striation spacing (s). For diffusion distances which exceed the monotonic plastic zone size (equation 5), da/dN_e equals the maximum fatigue crack tip opening displacement per cycle, equation 7. For intermediate Δx,

corrosion fatigue crack growth rate is governed by the following equations:

$$\frac{da}{dN_e} = \left(\frac{\Delta x - s}{r_p - s}\right)(\delta_{max} - s) \tag{24}$$

$$s = C\Delta K^m \tag{25}$$

with the striation spacing described by the standard Paris expression with C and m as material constants.

The Austin and Walker model predicts ΔK dependent plateau crack growth rates:

$$\left(\frac{da}{dN_e}\right)_{plateau} = 37.7\frac{\sigma_{ys}}{E}\sqrt{\frac{D_H}{f}} \tag{26}$$

for the case when ΔK, σ_{ys} and f are small and R is large. The coefficient in equation 26 was changed from the original value of 3.2 to be consistent with the best estimate for crack tip opening displacement, equation 7, and the fact that hydrogen diffusion occurs throughout the entire loading cycle, equation 23. With this change in coefficient, equation 26 provides a reasonable prediction of absolute plateau velocities for the steel-seawater system. For X-65 steel (ΔK = 21 MPa$\sqrt{m}$, R = 0.2, σ_{ys} = 450 MPa, f = 0.1 Hz) with a trap affected D_H value of 4 x 10^{-7} cm^2/sec, a plateau velocity of 1.7 x 10^{-6} m/cycle is predicted from equation 26 (and S = 8.0 x 10^{-5} mm, Δx = 8 x 10^{-2} mm, r_p = 0.09 mm, δ_{max} = 2 x 10^{-3} mm). The measured da/dN in Fig. 19 is 9 x 10^{-7} m/cycle. Data in Fig. 25 suggest that the plateau crack growth rate for

steel in chloride varies by two to three-fold depending on applied electrode potential. This factor is not predicted by the Austin and Walker model which relates da/dN to hydrogen penetration, without a concentration based failure criterion and ignoring the level of crack surface hydrogen.

The Austin and Walker model describes the frequency dependence of corrosion fatigue similar to the Holroyd and Hardie model, and at odds with the electrochemical surface reaction rate model of Wei and coworkers. The predicted inverse square root dependence of da/dN_e on f from diffusion is in good agreement with the measured frequency dependence of plateau crack growth rates for API-2H steel in 3% NaCl with cathodic polarization, Fig. 21. Crack growth rates become independent of frequency below 0.1 Hz. At this point, Δx equals 0.08 mm compared to a maximum plastic zone size of 0.09 mm. For a diffusivity of 5.1 x 10^{-7} cm^2/sec, the penetration distance equals the plastic zone size and growth rate is predicted to be constant at one δ_{max} per cycle, or 2 x 10^{-3} mm/cycle. The higher frequency portion of the data is presumably described by that time where the penetration distance becomes less than the striation spacing of 8 x 10^{-5} mm. The calculated frequency is 10^5 Hz; clearly this prediction is not consistent with the data in Fig. 21.

Austin and Walker described the beneficial effect of corrosion blunting of the crack tip by scaling the applied stress intensity according to:

$$\Delta K_{blunt} = \Delta K\left(\frac{\rho_s}{\rho_c}\right)^{1/2} \qquad (27)$$

where ρ_s is the radius of a sharp fatigue crack and ρ_c is the enlarged radius due to corrosion. This reduced value of ΔK_B is used in equation 24 for those cases where anodic dissolution occurs.

While the Austin and Walker model reasonably predicts some experimental observations of corrosion fatigue for steels in

aqueous chloride, the approach is not firmly established. The basis for equation 24 is speculative, particularly the assumption that the environmental crack growth rate equals, or may be no faster than, the maximum crack tip opening displacement scaled by that proportion of the plastic zone which is penetrated by hydrogen [58]. No evidence is provided that hydrogen diffusion occurs over a substantial portion of the plastic zone to cause discontinuous crack propagation which rate limits corrosion fatigue. Regarding blunting, while the assumption that crack tip stresses scale with the square root of radius is reasonable for notches with tip radii greater than about 0.05 mm [89,158,231], it is not clear that such a relationship applies for radii on the size scale of a corroded crack tip. The extent of corrosion blunting and the associated effect on the crack tip stress field remain to be established quantitatively.

While reasonable first steps, the models listed in Fig. 46 are of limited use because none provide broad and absolute predictions of crack growth rate. Specifically note that da/dN is apriori assumed to depend on hydrogen production or diffusion; no process zone failure criteria are employed. Without a damage criterion, models are unable to predict the stress intensity dependence of corrosion fatigue.

The chemical and mechanical elements have been sufficiently developed to permit a next generation of corrosion fatigue crack growth rate models based on hydrogen embrittlement. For steels, aluminum and titanium alloys in electrolytes such as aqueous chloride, what is needed is to:

-- build on the basis provided by damage accumulation models for mechanical fatigue [210];

-- establish crack tip pH and electrode potential [191];

-- determine rates of clean surface dissolution and hydrogen production [259];

-- develop a hydrogen fracture criterion within an identified process zone;

-- partition the chemical-mechanical and mechanical

components to crack growth [228].

VI.7. Corrosion Fatigue by Film Rupture and Transient Dissolution

Over several decades, models of environmental fracture have been developed for both monotonic and cyclic loading based on a sequence of passive film rupture at the crack tip, oxidation and progressive repassivation of the exposed metal, and a new rupture of the freshly formed film. The elements of this approach include crack tip strain rate, transient metal dissolution and film formation kinetics, and film ductility. This model was extensively applied to ferritic and stainless steels in high purity water over a temperature range from 300 to 600 K. Quantitative expressions for crack growth rate reasonably predict the effects of ΔK, frequency, metallurgical variables and environment chemistry. This work was reviewed by Ford and coworkers [39,70,71,138] and is briefly discussed here for comparison with hydrogen embrittlement formulations.

For corrosion fatigue crack propagation, film rupture models are based on two equivalent relationships for per cycle crack advance [39,70,234]:

$$\frac{da}{dN_{cf}} = \frac{da}{dr} \cdot \frac{dr}{dN} = \frac{1}{f}\frac{da}{dt} \qquad (28)$$

Da/dr is the crack advance per film rupture plus dissolution event and dr/dN is the number of rupture events per load cycle, N. Both da/dr and da/dt are related by Faraday's Law to the amount of charge (Q_f) which passes during dissolution between rupture events. The time between rupture events (t_f) is given by the film fracture strain (ϵ_f) to crack tip strain rate ($(d\epsilon/dt)_c = \epsilon_c$) ratio. The crack tip strain range ($\Delta\epsilon_{CT}$) is given by the average crack tip strain rate divided by loading frequency. Dr/dN is given by the crack tip strain range to ϵ_f ratio. Combining these terms with equation 28 leads to:

$$\frac{da}{dN_{cf}} = \frac{M}{\rho Z F}\left(\frac{\Delta\varepsilon_{cT}}{\varepsilon_f}\right)Q_f = \frac{1}{f}\left(\frac{M}{\rho Z F}\right)Q_f\left(\frac{\dot{\varepsilon}_c}{\varepsilon_f}\right) \tag{29}$$

where M and ρ are the atomic weight and density of the dissolving metal, Z is the number of electrons involved in oxidation and F is Faraday's constant. Charge passed per rupture event is given by:

$$Q_f = \int_0^{t_f=\varepsilon_f/\dot{\varepsilon}_c} i(t)dt \tag{30}$$

where i(t) is the transient current associated with dissolution during reformation of the ruptured film. This treatment of film rupture is equivalent for static and cyclic loading, as described in equations 28 to 30; only the crack tip strain rate differs.

Hudak [234] and Ford and Andresen [71] have further derived the film rupture model for 304 stainless steel in sodium sulfate and high temperature water, respectively. Hudak determined i(t) for a straining electrode in simulated crack tip solution; calculation of Q_f for substitution into equation 29 yielded:

$$\frac{da}{dN_{cf}} = \left(\frac{2Mi_0}{\rho Z F}\right)\frac{1}{f}\left(\frac{t_0}{\varepsilon_f}\right)^{1/2}\dot{\varepsilon}_c^{1/2} \tag{31}$$

where i_o is the bare surface current density at the instant of film rupture, t_o is the time for the initial decrease in the

transient current. Equation 31 is based on the current decreasing according to the reciprocal square root of time between ruptures; more generally, current depends on time to the $-\beta$ power. Hudak determined the ΔK dependence of crack tip strain rate for 304 stainless steel; equations 12 and 14 in Section VI.4. The total environmental crack growth rate was obtained by summing equation 31 with an empirical result for inert environment mechanical fatigue:

$$\frac{da}{dN_e} = C\left(\Delta K - \Delta K_{th}\right)^n + \left(\frac{2Mi_0}{\rho ZF}\right)\left(\frac{t_0\varepsilon_0}{\varepsilon_f}\right)^{1/2} \Delta K \frac{1}{\sqrt{f}} \qquad (32)$$

C and n are material constants from the inert environment fatigue law, and ϵ_o is a constant from the measured $(d\epsilon/dt)_c$-ΔK relationship. This summation of rates is consistent with the superposition model, equation 3 in Section VI.3.

Ford and Andresen previously derived an analogous expression for da/dN_e [70,71]:

$$\begin{aligned} \frac{da}{dN_e} &= \frac{da}{dN_m} + \frac{1}{2f}\left(g(\beta)\dot{\varepsilon}_c^{\beta}\right) \\ &= \frac{da}{dN_m} + \eta g(\beta)\Delta K^{\gamma\beta} f^{(\beta-1)} \end{aligned} \qquad (33)$$

Here, $g(\beta)$ is stated generally to describe environment chemistry and metallurgical effects on corrosion fatigue crack growth kinetics. $\dot{\epsilon}_c$ is taken from equation 20, with η as a constant.

Environmental effects on near-threshold cracking are modeled in terms of crack tip blunting by corrosion [39,234]. The predictions of equations 32 and 33 are extended to low growth rates and are truncated by the intersection with a blunting prediction. An example of this analysis is shown in Fig. 24a by the intersection of the shaded band for blunting and the predictions from equation 33. Blunting by dissolution of the

crack flanks is not well described. As discussed in Section VII, environment sensitive crack closure near ΔK_{th} introduces additional uncertainties.

The terms contained in equations 32 and 33 are either known or are determined experimentally; modern film rupture models are capable of predicting corrosion fatigue crack growth rates. Ford and Andresen report significant successes in predicting the effects of pertinent electrochemical variables (viz, temperature, solution conductivity, dissolved oxygen, electrode potential, bulk flow, radiation) and the effects of sensitization in 304 stainless steels and dissolvable sulfide bearing inclusions in ferritic pressure vessel steels in nuclear reactor environments [39,70,71,99,138]. Excellent agreement between predictions and measurements of time based crack growth rates, for either monotonic or cyclic loading indicate the potency of this approach; for example, see Fig.47.

On balance, however, controversy surrounds determinations of crack chemistry, crack tip strain rate, the fracture behavior of a film of uncertain structure and adherence, and transient electrochemical reactions. Currently, judgement is employed with reliance on adjustable parameters; a situation which has been improving rapidly.

Film rupture predictions of the stress intensity and frequency dependencies of da/dN_e are pertinent to this review. Crack tip strain rate increases with increasing ΔK for fixed frequency, resulting in a linear dependence of da/dN_{cf} on ΔK. This dependence is weaker than the typical power law relationship for mechanical fatigue, and contributes little to total crack growth rates at very high ΔK where rates of mechanical cracking are substantial. This prediction is in good agreement with crack growth rate data, as indicated in Fig. 14.

The film rupture model predicts a variety of frequency effects on corrosion fatigue. Physically, increasing frequency results in increasing crack tip strain rate; and thus in decreased time between ruptures, in increased charge passed per film rupture and in increased crack advance per event. Crack growth per unit time, da/dt, is predicted to increase with

increasing f, as indicated in Fig. 47 and confirmed by extensive data for both monotonic and cyclic loading [71].

For corrosion fatigue, the effect of frequency on da/dt is countered by the inverse effect of 1/f on time per load cycle; equation 28. The net effect of f on da/dN_{cf} depends on alloy repassivation kinetics, particularly the β exponent. Typically, β equals 1/2 and da/dN_{cf} is predicted to increase with decreasing frequency as indicated by the reciprocal square root relationship in equation 32. In the more general case, equation 33 and Fig. 24a, da/dN_{cf} is predicted to increase with decreasing f provided that β is less than 1.0. This behavior is confirmed by the experimental results in Figs. 14 and 47. In principle the film rupture model predicts that da/dN_{cf} could be independent of frequency ($\beta = 1.0$), or could increase with increasing frequency ($\beta > 1.0$). This behavior, while not typically observed, was recently reported for an Al-Li alloy in aqueous NaCl [221]. The predictions in equations 32 and 33 are based on the assumption that mass transport is rapid and does not rate limit crack propagation.

Hudak recently demonstrated substantial differences in the predicted and measured frequency dependencies of corrosion fatigue for 304 stainless steel in high temperature water and in NaCl solution [234]. This comparison provides an important critique of quantitative film rupture and hydrogen embrittlement models. Specifically in conjunction with equation 32, Hudak employed reaction kinetics for 304 stainless steel in dilute sulfate to simulate crack solution for pure water, and measured transient reaction kinetics for the chloride. Predicted and measured frequency dependencies of da/dN_{cf} are given in Fig. 48. For the water environment, the agreement is of the same order of magnitude, however, a stronger (inverse square root) frequency response is predicted than is measured for several applied electrode potentials typical of the crack tip.

A dramatic underprediction of crack growth rates, by one to two orders of magnitude, is seen for ambient temperature chloride. Hudak argues that these differences persist for wide ranges of values of the parameters employed in equation 32. The

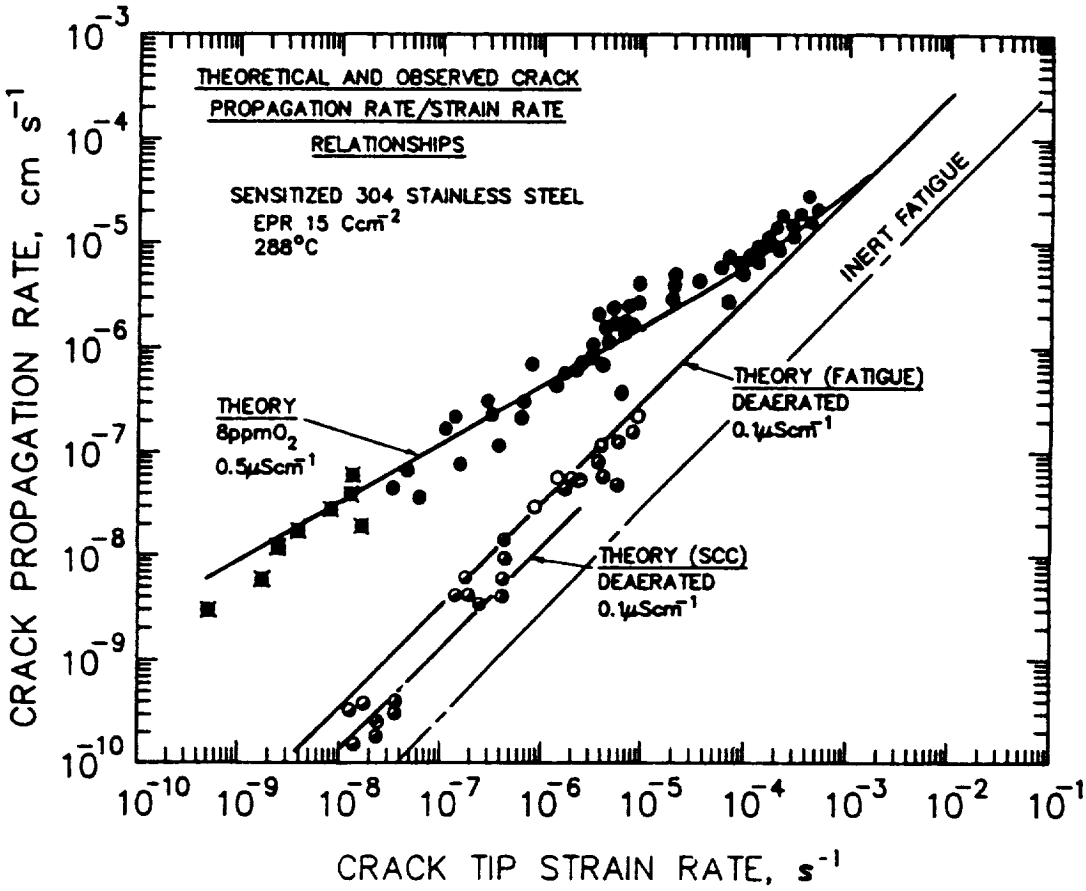

Fig. 47 Film rupture model predictions and measurements of time based crack growth rates versus crack tip strain rate for monotonic and cyclic loading of AISI 304 stainless steel in high temperature water; after Ford and Andresen [71].

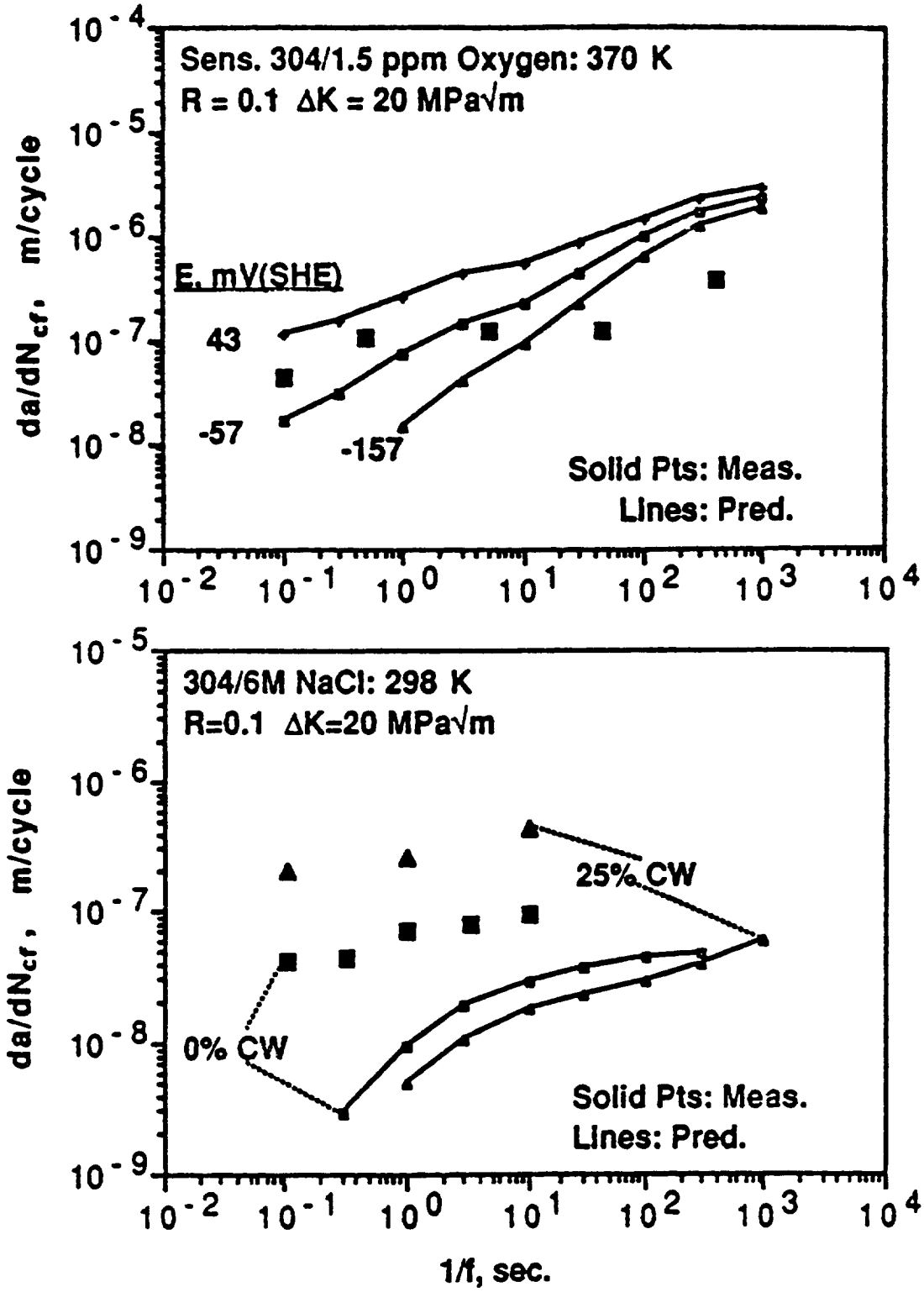

Fig. 48 Film rupture predictions and measurements of the frequency dependence of corrosion fatigue crack growth rate for AISI 340 stainless steel in two electrolytes; after Hudak [234].

poor agreement is ascribed to a dominant hydrogen embrittlement contribution to corrosion fatigue. The data in Fig. 48 were better described by the charge transfer-based hydrogen embrittlement model described in Section VI.5.c.[7]

As transient reaction models for hydrogen embrittlement and film rupture are further developed and simultaneously applied to predict the frequency dependence of corrosion fatigue in model systems, mechanistic understanding will improve dramatically. Advances to date, and the likelihood for future refinements, suggest that in-depth mechanistic understanding of corrosion fatigue crack propagation is at hand. Predictive models will play a critical role in fracture mechanics based life prediction procedures.

VI.8. Corrosion Fatigue by Surface Film Effects

While environmentally produced thin surface films could accelerate fatigue crack growth rates by the plasticity mechanisms outlined in Section II.3.c, such effects have been neither demonstrated by systematic experiment nor predicted analytically. This issue is important because crack tip and flank films are produced by gaseous and electrolytic environments which are claimed to promote hydrogen embrittlement and film rupture. As an example for most metals, moist air is an aggressive environment relative to vacuum or helium. While atomic hydrogen production by water vapor oxidation is often cited as the mechanism for enhanced crack growth in moist air, the lack of a defined frequency dependence and the uncertain role of surface films on deformation preclude a clear statement of mechanism.

The first question to address is the extent to which crack

[7]The observed effect of cold work indicated in Fig. 48 cannot be explained by the film rupture model, but may be rationalized in terms of hydrogen. Cold work, while not affecting electrochemical reactions, produces martensite which reduces the amount of hydrogen required for a given crack extension. Unfortunately, the hydrogen model does not predict absolute rates of crack advance, but scales a frequency response to the saturation rate, da/dN_c.

growth rate data demonstrate effects of surface films, apart from hydrogen and dissolution mechanisms. Gaseous oxygen provides an excellent environment in this regard. Data obtained in the author's laboratory are presented in Fig. 49. For an Al-Li alloy, equal crack growth rates are observed for vacuum, highly purified helium and oxygen; while cracking is enhanced for water vapor and moist air [125,221]. In contrast for a C-Mn steel, crack growth in oxygen is strongly accelerated compared to vacuum or helium and similar to that observed for gaseous hydrogen, moist air and water vapor [159]. These data indicate that surface films produced by fatigue in oxygen lead to crack tip damage for steel, but not aluminum. As such, the hydrogen mechanism is the sole cause of corrosion fatigue for the latter material in water vapor. For steel in moist air, the contributions of hydrogen and film formation cannot be separated.

The results contained in Fig. 49 are consistent with literature data, however, some controversy exists. Oxygen has no effect on fatigue crack propagation in 7075-T651 and 2219-T87 alloys compared to vacuum [61,268,269]. Swanson and Marcus [268] and Piascik [221] employed Auger spectroscopy and SIMS to show that substantial amounts of surface oxide were formed and that oxygen penetrated into the crack tip plastic zone during fatigue. None-the-less, crack growth rates were not affected. For three alloy and C-Mn steels, Frandsen and Marcus reported that crack growth rates were increased by up to a factor of two by loading in oxygen compared to vacuum [209]. In one of three cases, crack growth in O_2 was as rapid as that likely for moist air. Auger spectroscopy indicated that oxygen penetrated the steel during exposure to O_2.

A detailed study by Bradshaw and Wheeler demonstrated a strong corrosion fatigue action of O_2 on a 7000 aluminum alloy [187]. While oxygen either had no effect, or slightly retarded crack growth rates compared to vacuum for ΔK levels above 6 to 8 MPa m, this gas enhanced crack growth rates within the near-threshold regime; da/dN_e values exceeded vacuum levels by over an order of magnitude and ΔK_{th} was reduced. A similar trend was observed for near-threshold cracking in alloy 5070, however,

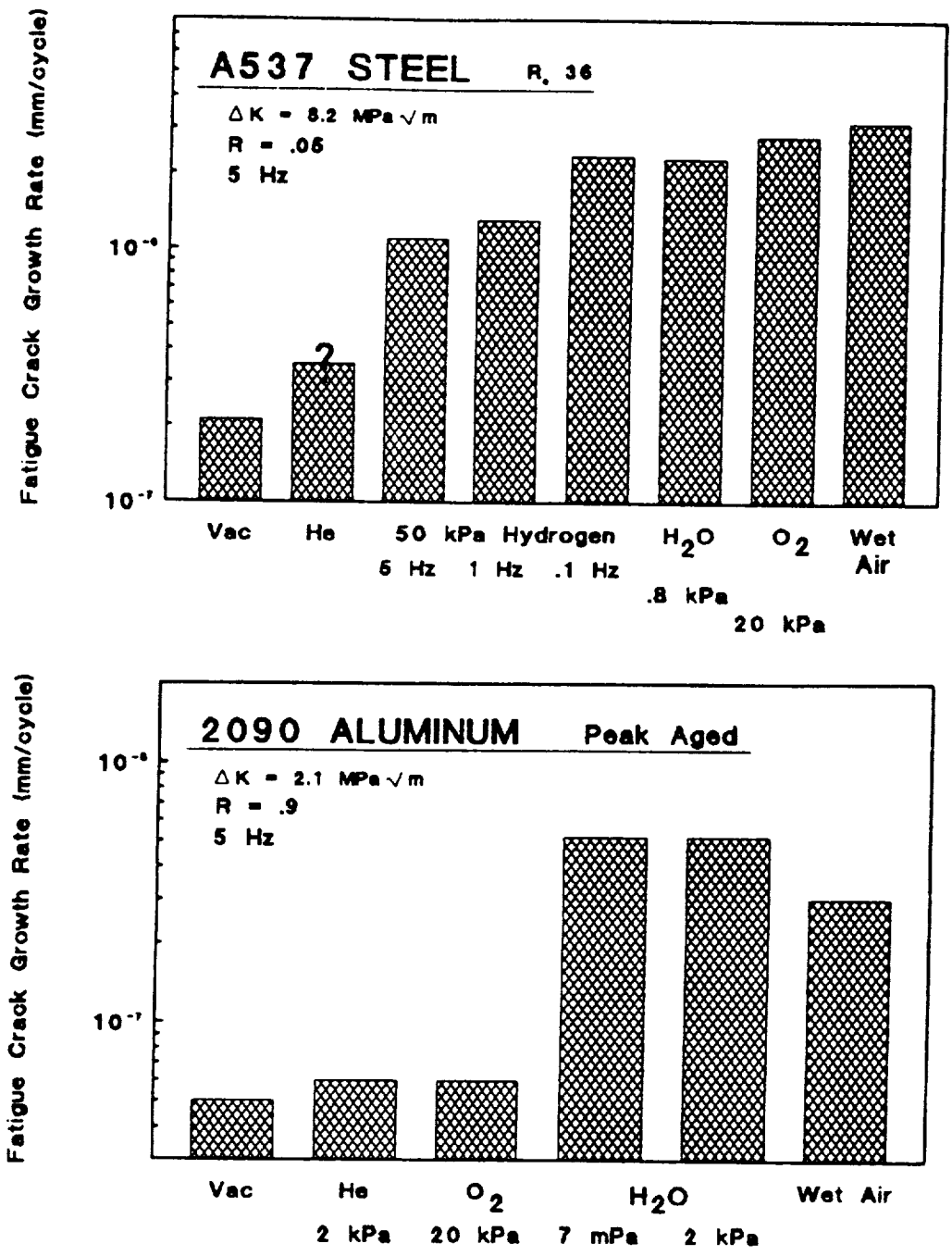

Fig. 49 Fatigue crack propagation in a C-Mn steel and an Al-Li alloy as a function of the surrounding gas for constant ΔK and frequency. [125,159,221].

growth in O_2 was only two-fold faster than that in vacuum. Extensive experiments with the 7000 series alloy further demonstrated that da/dN_e decreased with decreasing oxygen partial pressure at fixed frequency, analogous to the water vapor exposure effect illustrated in Figs. 22 and 23. Oxygen affected a fatigue crack path transition. Growth in vacuum was faceted along slip bands for vacuum, while a flat "tensile" mode of unspecified morphology was observed for O_2. Piascik recently reported a similar result of O_2 accelerated near-threshold crack growth in 7075 [221].

Frandsen and Marcus reported four to five-fold increases in crack growth rates for Monel 404 and commercially pure titanium cycled in oxygen compared to vacuum [209]. Clearly, additional work is required to characterize the effects of oxygen and other film forming environments on fatigue crack propagation. It is particularly important to characterize the effects of ΔK, loading frequency, environment activity and temperature.

Given an effect of film forming environments, it is important to question the causal mechanism. Those listed in Section II.3.c., and the ideas on film induced cleavage described by Sieradzki in this volume [82], provide the basis for quantitative film-based models of corrosion fatigue. Bradshaw and Wheeler concluded that the results on cracking in O_2 give support for damage mechanisms based on surface films, however, no quantitative relationships have been derived to date. Surface film effects on crack tip plasticity and dislocation morphologies must be considered [75]. A problem here will be to separate surface film effects from the influences of dissociated and dissolved solute.

Studies of surface film effects in corrosion fatigue are hindered by two problems. The rough crack surface typical of fatigue in vacuum, and oxidation debris of thickness on the order of 0.1 to 1 μm, can cause crack closure which complicates analysis of intrinsic chemical damage mechanisms as discussed in the next section. Indeed, the Bradshaw and Wheeler study can be interpreted based on oxide induced closure for O_2 at moderate ΔK and roughness induced closure for vacuum at low ΔK. Near-

threshold, faceted cracking and surface roughness could decrease, and da/dN_e could increase, with increasing oxygen pressure. Piascik provided a means to eliminate crack closure [221]. Secondly, the demonstration of an O_2 effect is only broadly established for alloy 7075, and perhaps steels, which are sensitive to hydrogen embrittlement. Recent data suggest that extremely small amounts of water vapor in O_2 affect crack propagation [221]. The purity of the oxygen environment must be carefully controlled.

VII. COMPLICATIONS AND COMPROMISES OF FRACTURE MECHANICS

VII.1. Conclusion

Fracture mechanics descriptions of corrosion fatigue and the similitude concept are complicated by the inability of stress intensity to describe the controlling crack tip mechanical and chemical driving forces. The so-called "closure", "small crack" and "high strain" problems in mechanical fatigue are relevant to corrosion fatigue. Data and analyses demonstrate that the unique relationship between da/dN and ΔK is compromised by mechanisms including (1) premature crack wake surface contact, (2) deflected, branched and multiple cracking, and (3) time and geometry dependent occluded crack chemistry. Stress intensity descriptions of elastic-plastic stresses, strains and strain rates in the crack tip plastic zone are uncertain within about 5 μm of the crack tip, within single grains which are not well described by the constitutive behavior of the polycrystal and when deformation is time or environment sensitive. These limitations do not preclude the only quantitative approach developed to date to characterize subcritical crack propagation. Rather, they indicate the need for crack tip modeling.

VII.2. Crack Mechanics

The fracture mechanics approach to fatigue crack propagation, and the associated similitude concept, are unambiguous if the applied stress intensity accurately describes local crack tip stress and strain fields. Extensive work over

the past 20 years on benign environment fatigue has demonstrated four situations where the basic linear elastic formulation of applied ΔK must be modified to better define the governing driving force. These areas; crack closure, small crack size, large scale yielding, and deflected cracks; are relevant to corrosion fatigue crack propagation. The environmental aspects of these issues have not been extensively investigated.

The fracture mechanics approach discussed in this review is based on the assumption that cracked specimens and components are loaded within the small scale yielding regime [88]. Dowling conducted extensive studies on "high strain" crack propagation and correlated growth rates with a nonlinear field parameter, the J-contour integral [157]. Unique geometry independent crack growth rate laws are observed and a variety of J solutions are available for various specimen and component geometries. This work has not been extended to crack growth in aggressive environments; but it is likely that many of the principles established for corrosion fatigue under small scale yielding will be relevant.

Most stress intensity analyses are derived for a single crack perpendicular to the applied load and growing in a nominally Mode I fashion. In corrosion fatigue, or with anisotropic microstructures, cracks may branch or deflect from this idealized geometry. In this case growth proceeds under mixed Modes I and II. The governing stress intensity factor must be calculated to include a summation of the Mode I and II K levels for the deflected crack. Suresh has analyzed this problem and provided branched crack stress intensity factors [270]. This analysis has not been broadly applied in corrosion fatigue; often the effect of deflection on ΔK is secondary, particularly within the Paris regime. Deflection effects on near-threshold environmental cracking, and the associated closure phenomena, are important and further study is warranted.

VII.2.a. **Crack Closure.** Premature crack wake surface contact during the unloading portion of a fatigue cycle (viz, "crack closure") reduces the applied stress intensity range to an

effective value defined as $\Delta K_{eff} = K_{max} - f(K_{cl})$. Concurrently, the effective stress ratio increases to K_{cl}/K_{max}. When considered based on applied $\Delta K = (K_{max} - K_{min})$, fatigue crack growth rates decline as closure effects increase. Crack growth rate data which are closure affected are often referred to as extrinsic. Da/dN values which are obtained in the absence of closure, or which are based on a closure compensated ΔK level, are referred to as intrinsic. The topic of crack closure has been extensively reviewed for fatigue crack propagation in benign environments, particularly by Ritchie, McEvily and their students [41-43,47,202,271].

VII.2.a.(1). **Overview for Benign Environments.** Several mechanisms cause fatigue crack closure, including:

- oo Crack wake plasticity [272,273],
- oo Crack surface roughness or deflections with Mode II sliding displacements [274],
- oo Crack corrosion debris [205,275],
- oo Crack fluid pressure [276].

Quantitative models which estimate the degree of closure are provided in the indicated references.

Models and measurements of crack closure loads by crack mouth compliance or back face strain gauge techniques demonstrate that closure effects are exacerbated by: (1) near-threshold loading, (2) low stress ratio loading, (3) tension dominated loading spectra or single overloads, (4) environments which produce corrosion debris within the crack, (5) anisotropic or planar slip materials which cause deflected and microscopically rough fatigue crack surfaces, and (6) environments which produce tortuous crack surfaces.

While the effects of closure on da/dN are clear, controversy exists as to the proper stress intensity range which governs crack growth. The majority of studies have employed an effective ΔK value ($\Delta K_{eff} = K_{max} - K_{cl}$), with K_{cl} determined from compliance measurements. Recent data indicate, however, that fatigue damage

continues over a distributed range of loads below K_{cl}; ΔK_{eff} is too small [277]. A constant maximum stress intensity procedure offers an alternate means of characterizing crack growth independent of closure as discussed in Section IV.4 [156].

When corrosion fatigue crack propagation data are obtained under the above conditions, it is likely that they are affected by crack closure. Such behavior has several implications for this review. It is necessary to assume that most of the results described here reflect closure influences. Given the complexities of making displacement measurements in aggressive environments, only limited work has been carried out to define closure in corrosion fatigue. An alternate approach is to design corrosion fatigue experiments which yield growth rates that are closure free; this approach with constant K_{max} and high R methods was taken by Piascik and Gangloff [125,126,221].

In terms of crack growth mechanisms, it is reasonable to develop and evaluate models of the sort described in Section VI in terms of intrinsic crack growth rates. As a separate problem, it is necessary to develop environmental mechanisms for crack closure. As an example, Hudak considered crack closure contributions in film rupture modeling of da/dN_e for stainless steels [234]. It is reasonable to question those studies which claim to have proved a specific corrosion fatigue model by crack growth rate measurements, if crack closure has not been accounted for.

In terms of life prediction under complex loading spectra, the crack growth rate law which describes the proper degree of closure for the component and loading history of interest is unclear. This problem has not been adequately dealt with for benign environment fatigue.

VII.2.a.(2). **Crack Closure in Aggressive Environments.** Several mechanisms for closure are pertinent to corrosion fatigue [35,60,196]. For steel in aqueous chloride, Todd and coworkers demonstrated that grains, displaced or detached by environment induced intergranular fatigue, act as wedges to hinder crack displacement [152]. Viscous fluids can exert closure forces on fatigue crack

flanks [276]. Gangloff and Ritchie speculated that hydrogen may enhance plasticity and the extent of crack wake induced closure [203]. Environment induced crack deflection is often encountered, but detailed closure analyses have not been applied to corrosion fatigue studies. Additional research is required to examine these environment sensitive closure mechanisms.

Studies of closure have emphasized reductions in stress intensity factor and hence crack tip cyclic strain. It is also reasonable to suggest that crack closure will affect crack chemistry by influencing mass transport. Certainly the opening shape of the crack, varying with loading time, is an important factor in diffusion and convective mixing; Section VI.5.b. As an example, Gangloff suggested that crack surface contact will transform an otherwise orderly mass flow situation into transport by turbulent mixing [253]. For this case a perfect mixing model may be more accurate than detailed calculations based on slow laminar flow. Crack closure effects on local environment chemistry have not been considered in detail.

Corrosion debris, the so-called oxide induced closure mechanism, has a potent effect on fatigue crack growth rates. This process has been extensively investigated for low strength alloy steels in moist gases and for C-Mn steels in seawater. Oxide induced crack closure was broadly recognized by Ritchie for steels in various gas environments; for an example, see the data in Fig. 28 [200-205]. These and other results show that near-threshold crack growth rates are increased for all gases which prevent the formation of crack surface oxide, including pure H_2, He and vacuum. For water vapor, wet H_2 and moist air, oxides of thicknesses on the order of the cyclic crack tip opening displacement and enhanced by a fretting mechanism, cause reduced crack growth rates. This effect is observed for low stress ratios; equal crack growth rates are reported for all gases at R values above about 0.6, typical of closure.

Oxide induced closure is not significant at higher stress intensities or for high strength steels and precipitation hardened aluminum alloys. For these materials in moist gases, oxide thicknesses are small, presumably because fretting is not

an effective mechanism for accelerated oxidation [278]. More corrosive environments may, of course, cause debris induced closure in these materials.

Crack closure of the sort illustrated in Fig. 28 complicates mechanistic understanding of near-threshold cracking. The effect of closure must be eliminated or measured and growth rates adjusted in order to determine the extent of intrinsic environmental embrittlement. Since this is rarely done, data and models on near-threshold corrosion fatigue are lacking.

Suresh and Ritchie modeled oxide induced closure in terms of the effect of a rigid wedge on the crack tip stress intensity at the point of closure contact [202,274]:

$$K_{cl} = \frac{dE}{4\sqrt{\pi \ell}(1-\nu^2)} \tag{34}$$

where d is the maximum thickness of oxide film and on the order of 0.01 to 0.1 μm, l is the distance behind the crack tip to the location of maximum oxide thickness and on the order of several μm, E is the elastic modulus and ν is Poisson's ratio. This analysis predicts K_{cl} levels on the order of 1.5 to 2 MPa$\sqrt{m}$ for steels.

Corrosion debris may promote crack closure for steels in aqueous chloride environments, as studied by Hartt, Scott, Bardal, van der Velden and coworkers [34,58,119,121,279-281]. This phenomenon results in extremely low near-threshold growth rates and high levels of ΔK_{th} for environmental conditions which would otherwise promote hydrogen embrittlement; Section VI.6. A typical example is shown in Fig. 11. ΔK_{th} is increased markedly by seawater with cathodic polarization at low R (curve 5) and compared to moist air, seawater with free corrosion (curve 4) or seawater with cathodic polarization at high R (curve 3). Closure during cathodic polarization is often sufficiently potent to cause crack arrest.

Corrosion product induced closure depends sensitively on the

electrochemistry of the chloride environment because this governs the precipitation of calcium and magnesium bearing salts, the offending corrosion debris [279,280]. These reactants are found in seawater, but not in pure 3% NaCl solution; as such, corrosion product induced closure only occurs in the former solution. As shown in Fig. 44, cathodic polarization promotes corrosion fatigue crack growth in NaCl, but greatly retards cracking in seawater. Here, precipitation of magnesium and calcium salts only occurs at electrode potentials below about -850 mV (SCE) where the solubility product is sufficiently reduced. As such, calcareous deposit induced closure is likely for cathodic polarization, but not for anodic potentials. This trend is clearly evident for crack growth in seawater in Fig. 11. (Van der Velden reported that iron hydroxide can form on crack surfaces of steel in oxygenated 3% NaCl near free corrosion and cause crack closure [281]. This observation is not general, as no evidence of crack closure has been reported in extensive studies of such steels in this environment [115,170,173, 174,180,189,253].)

It is likely that corrosion product deposition and crack closure are possible for other material-environment systems. The occurrence of this phenomenon is evidenced by time-dependent reductions in crack growth rates at constant applied stress intensity, by crack arrest at very high threshold stress intensities, and by compliance or back face strain gauge measurements of closure contact upon unloading. Crack chemistry modeling of the sort described in Section VI.5.b. predicts the occurrence of precipitation from occluded crack solution [190,249,279].

The benefits of corrosion product induced closure to component life are unclear. The degree of product precipitation and the resulting effect on crack growth kinetics are possibly geometry and loading spectra dependent. For example, large compressive underloads may obliterate the corrosion product and reduce the closure effect compared to that expected from laboratory experiments with small specimens and simple tension loading. Application of the similitude concept in such cases is

unclear [100,101]; additional work is required.

VII.2.b. **Environment Sensitive Microscopic Deformation.** From the continuum perspective, crack tip stresses and strains depend on the shape of the blunted crack tip and on material constitutive behavior through stress intensity [Section VI.4 and Ref. 160]. Environment may influence these properties in a time dependent fashion during corrosion fatigue crack propagation, and thus influence the magnitude of the crack tip fields. Crack tip dissolution may affect blunting, and intergranular or transgranular fracture modes could produce unique crack tip shapes compared to deformation blunting models. Hydrogen, dissolved in the plastic zone, could influence deformation mode and material flow properties. For these cases, stress intensity will describe crack tip deformation, however, the appropriate crack shape and flow properties must be used in finite element models of the crack tip. No work has been reported in these regards.

The influence of hydrogen on metal plasticity is controversial and has not been broadly demonstrated for materials subjected to the boundary conditions typical of a crack tip plastic zone. No data have been presented to demonstrate alloy stress-strain behavior which is altered by dissolved hydrogen. None-the-less, the possibility for such effects is strong based on: (1) extensive evidence for hydrogen induced plasticity in thin foils strained in the electron microscope [68], (2) interpretations of fracture surface features [69], and (3) electron microscope evidence for hydrogen induced changes in the dislocation morphology within the crack wake [282].

Information on environment sensitive deformation at growing crack tips is provided by <u>in situ</u> fatigue loading in the scanning electron microscope coupled with stereoimaging analysis (see Section IV.4.). Lankford and Davidson [162-164] and Hudak [234] report that crack tip opening strain ranges are lower for aggressive compared to inert environments for any constant applied ΔK. These studies were conducted with 1005 steel and 7075-T651 aluminum in moist air or dry N_2, and with AISI 304

stainless steel in aqueous Na_2SO_4; an example of data for the latter material is presented in Fig. 50 [232].[8] Here strain ranges are decreased by between a factor of four and eight for the sulfate; corresponding crack growth rates increased by between four and twenty-fold due to the environmental effect. Lankford and Davidson concluded that water vapor similarly lowered the crack tip strain range for 7075, however, this point was obscured by substantial variability [162].

The mechanism for the effect of environment on crack tip strain is related to embrittlement of a fracture process zone on the order of 1 to 10 μm [162,234]. For the alloys examined, hydrogen is held to lower the "load bearing" or "accumulated strain" capacity of the process zone; the crack extends at a lower strain and after fewer cycles for any ΔK. Fatigue crack propagation progresses discontinuously, governed by a damage accumulation model for each environment [162,210]. For cyclic loading at constant ΔK, plastic strains build to a critical level causing an increment of crack growth. The process zone failure strain, and measured crack tip strains, are reduced by environmental exposure consistent with Fig. 50.

While crack tip strains within the process zone differ with environment at constant ΔK, and are therefore not well described by a continuum model, stress intensity provides the boundary condition which scales the magnitude of process zone loading. Crack tip strains, along with the near crack tip opening shape, correlate with applied stress intensity as indicated in Fig. 50. Stress intensity is not, however, capable of describing the cyclic evolution of the process zone strain. A dislocation hardening theory may be relevant.

Apart from the concept of a reduction in strain accumulation capacity, other factors could contribute to environment sensitive crack tip deformation. Varying process zone strain, either hardening or softening, with cycling at constant ΔK is a critical

[8]Note that the line indicated with a slope of 2:1 is incorrectly labeled. The data for Na_2SO_4 are not described by a ΔK squared dependence; rather, the slope of the data is somewhat lower.

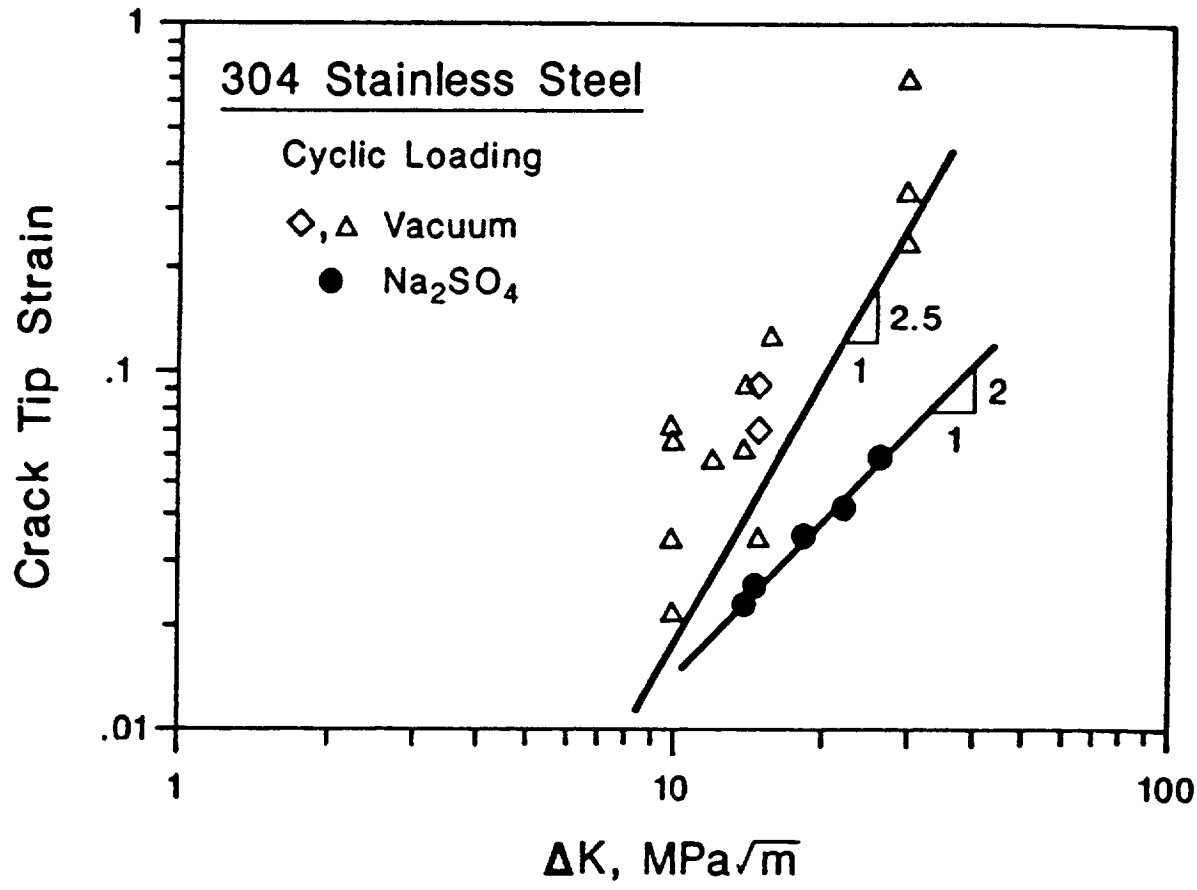

Fig. 50 Measured fatigue crack tip cyclic strain range as a function of applied ΔK for AISI 304 stainless steel cycled at 300 K in aqueous 0.1 M Na_2SO_4 or vacuum, and then characterized by <u>in situ</u> SEM loading and stereoimaging analysis; after Hudak [234].

assumption. Alternately local plastic strain ranges may saturate at equal strains, independent of environment, for the same applied ΔK and at numbers of cycles well below the failure "life". An environmental reduction in a strain-life failure limit would then mean that fewer load cycles are required to cause an increment of crack extension and an increased growth rate, but measured crack tip strains should be equal for aggressive and inert environments. The mechanism for the effect of environment on crack tip strain may be more complex than indicated above. For example if dissolved hydrogen homogeneously enhances plasticity, then crack tip strains are expected to increase for environmental exposure at constant ΔK. Crack tip strains will decrease, on average, if hydrogen promotes slip localization. Hydrogen effects on crack tip shape, through an environmental fracture mechanism transition, could also alter the crack tip strain distribution.

Experimental measurements of crack tip shape, deformation and dislocation configurations are critically needed as a function of applied ΔK and environment.

VII.2.c. **Small Crack Problem.** The essence of the "small crack problem" is that stress corrosion, mechanical fatigue and corrosion fatigue cracks propagate at unpredictably high rates when sized below a critical level and compared to the growth rates of long cracks. Small fatigue cracks propagate at stress intensity ranges well below long crack thresholds. The similitude principle breaks down; crack size and applied stress effects on growth kinetics are not uniquely described by a single parameter, ΔK. Extensive measurements and modeling indicate that crack size effects are important for crack depths below about 1 to 5 mm. The definition of a "small" or "short" crack depends on the mechanism for the rapid growth rates.

Small cracks are technologically important because the early growth of cracks between 0.05 and 5 mm often dominates the fatigue life of components. An example is provided by corrosion fatigue crack growth in the weld of a pipe carrying H_2S contaminated oil [103]. Here, 80% of the predicted life was

involved with crack growth form 0.5 to 1.0 mm; cracking to failure required only 20% of life. Errors in the growth rates of small cracks have a large adverse effect on life prediction.

Small fatigue crack growth behavior has been extensively reviewed for benign environments by Ritchie, Lankford, Davidson, McEvily, Tanaka, Morris and Hudak [45,153,283,284]. Gangloff, Wei and Petit considered the behavior of small cracks in aggressive environments [36,60,180,203,285].

VII.2.c.(1). **Overview for Benign Environments.** Several mechanisms have been established to explain small fatigue crack behavior, as summarized in Fig. 51. Cracks are classified as short if they intersect many grains along the crack front and have a cyclic plastic zone which is much larger than the grain size, but are of limited length dimension. A small crack, and associated plastic zone, are wholly contained within 1 to 5 grains. The absolute size of the small crack is microstructure dependent and may be quite large for a single crystal.

From the mechanical perspective, short cracks are poorly described by ΔK when small scale yielding is violated by high net section stress, or when the crack size is less than 1 to 5 times the monotonic plastic zone size. The J-integral approach may correlate cracking as discussed in Section VII.2. Microstructurally small cracks grow rapidly when the cyclic plastic zone is encased within a single grain because of abnormally large crack tip opening strains compared to that expected based on applied ΔK. This effect appears to be related to single crystal and localized deformation mode effects on the crack tip strain field.

Short and small cracks grow at accelerated rates because of a physical mechanism. Such cracks have reduced wakes and, as such, reduced levels of shielding crack closure. As the small crack propagates from the embryonic stage at constant applied ΔK; the crack wake develops, closure stress intensity rises and crack growth rates decrease. Crack length independent cracking is achieved when closure reaches saturation or steady state above a specific crack size. Physical short/small crack behavior is

MECHANISMS FOR SMALL FATIGUE CRACK BEHAVIOR

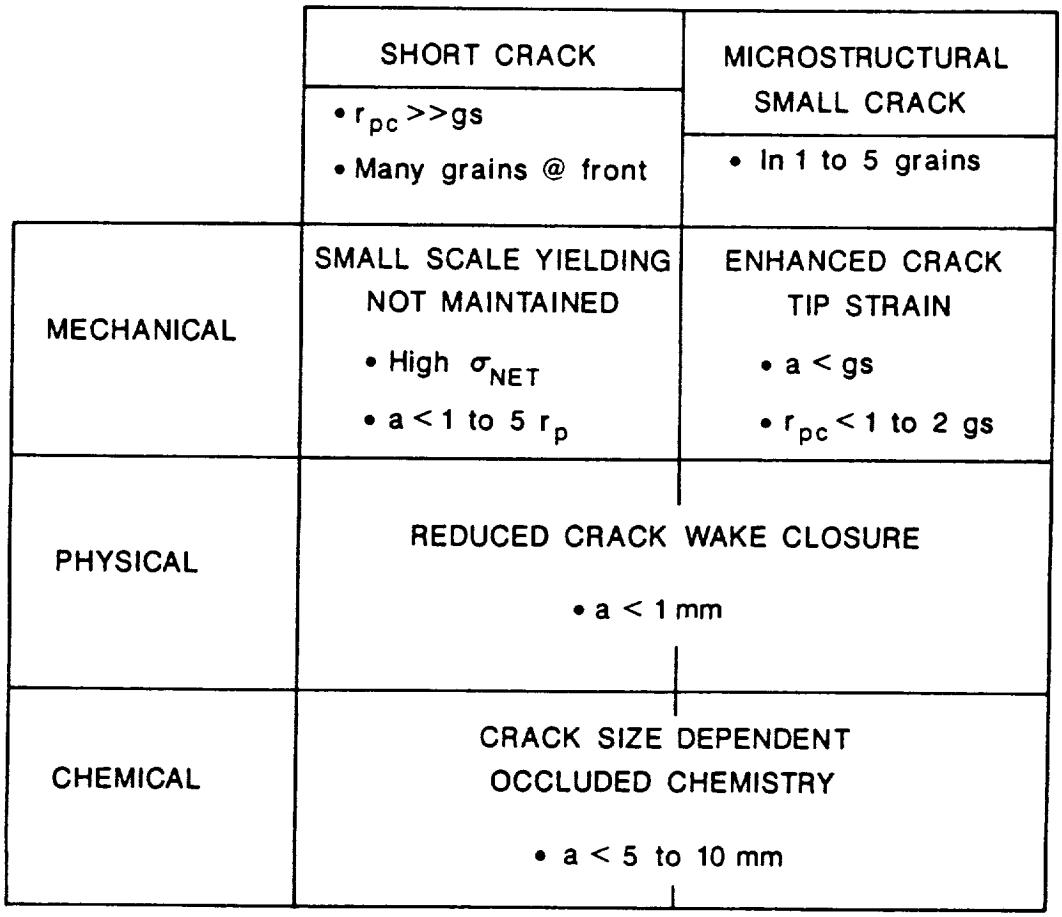

Fig. 51 **Mechanisms for the unique behavior of small fatigue cracks.**

correlated by stress intensity approaches which account for closure; that is, either ΔK_{eff} or high stress ratio constant K_{max} [156,277]. Similitude is observed if rates are compared on a closure free basis.

The mechanisms represented Fig. 51 are important because they enable definitions of what constitutes a small crack; a question that has been posed for the past 20 years and which can now be reasonably answered for fatigue in benign environments [283].

VII.2.c.(2). **Aggressive Environments.** Chemical effects unique to the small crack geometry are an important aspect of corrosion fatigue behavior. The growth rates of small fatigue cracks (< 5 mm) may be significantly faster than expected from longer crack da/dN-ΔK data for gases and liquids, while being predictable for benign environments. Aggressive environments play a role in mechanical and closure based short/small crack mechanisms. Additionally, the chemistry within such cracks may be uniquely embrittling (or benign), thus providing the basis for a chemical mechanism. These views are supported, albeit to a limited extent, by modeling and experiment as reviewed in detail by Gangloff and coworkers [180,203].

Undoubtedly, experimental difficulties have hindered studies of small corrosion fatigue cracks. Surface replication techniques have been applied to fatigue in moist air, however, this tedious method with the necessity for test interruptions is not suited for aggressive environments. The electrical potential method (Section IV.3) was successfully applied to continuously monitor short cracks of length greater than 0.1 mm for a variety of materials and aggressive environments and under programmed applied ΔK [158,159,221]. Microstructurally small cracks have been monitored, provided that the grain size is enlarged above about 500 μm [159]. As developed, this method is not suited for naturally initiated corrosion fatigue cracks because the location of cracking must be precisely known for probe attachment. No measurements have been obtained on the closure behavior of small cracks in environments other than moist air [159].

The mechanical and closure mechanisms for crack size effects in corrosion fatigue have not been extensively investigated. Presumably, the ideas and results on closure in benign environments, Section VII.2.a, are relevant to corrosion fatigue cracks with limited wakes. As discussed by Piascik and Gangloff [125,126,221], this situation provides for severe near-threshold corrosion fatigue crack growth effects and is worthy of additional study.

Enhanced crack opening strain for microstructurally small cracks should play an important role in corrosion fatigue by either film rupture or hydrogen embrittlement. No measurements exist to support this speculation, however, Hudak and Ford demonstrated the potency of this mechanism based on film rupture model calculations, equations 31 to 33 [286]. The prediction contained in Fig. 52 indicates that enhanced crack tip strain and strain rate for the small fatigue crack enable propagation at high rates and well below the long crack threshold for the stainless steel-high temperature water system. This potential mechanism must be evaluated.

Experimental and analytical support for novel corrosion fatigue effects in the small crack regime exists for steels in aqueous chloride, a likely hydrogen embrittlement system [180]. A systematic study of short corrosion fatigue cracks was reported by Gangloff for a high strength martensitic steel in 3% NaCl [96,97]. Typical data are presented in Fig. 9. Note the one to two order of magnitude increases in the growth rates of short cracks (0.1 to 2 mm long, through thickness and elliptical surface cracks in a steel with 20 μm grain size) at any applied ΔK for the chloride and compared to compact tension results. In contrast crack growth in air and vacuum was uniquely correlated by applied stress intensity, independent of stress and crack size. This result demonstrates that crack closure and plasticity mechanisms do not explain the rapid growth of the short corrosion fatigue cracks.

A chemical mechanism must explain the short crack effect in Fig. 9, as detailed in Section VII.3. This point was reinforced by short crack corrosion fatigue data which show that da/dN_e

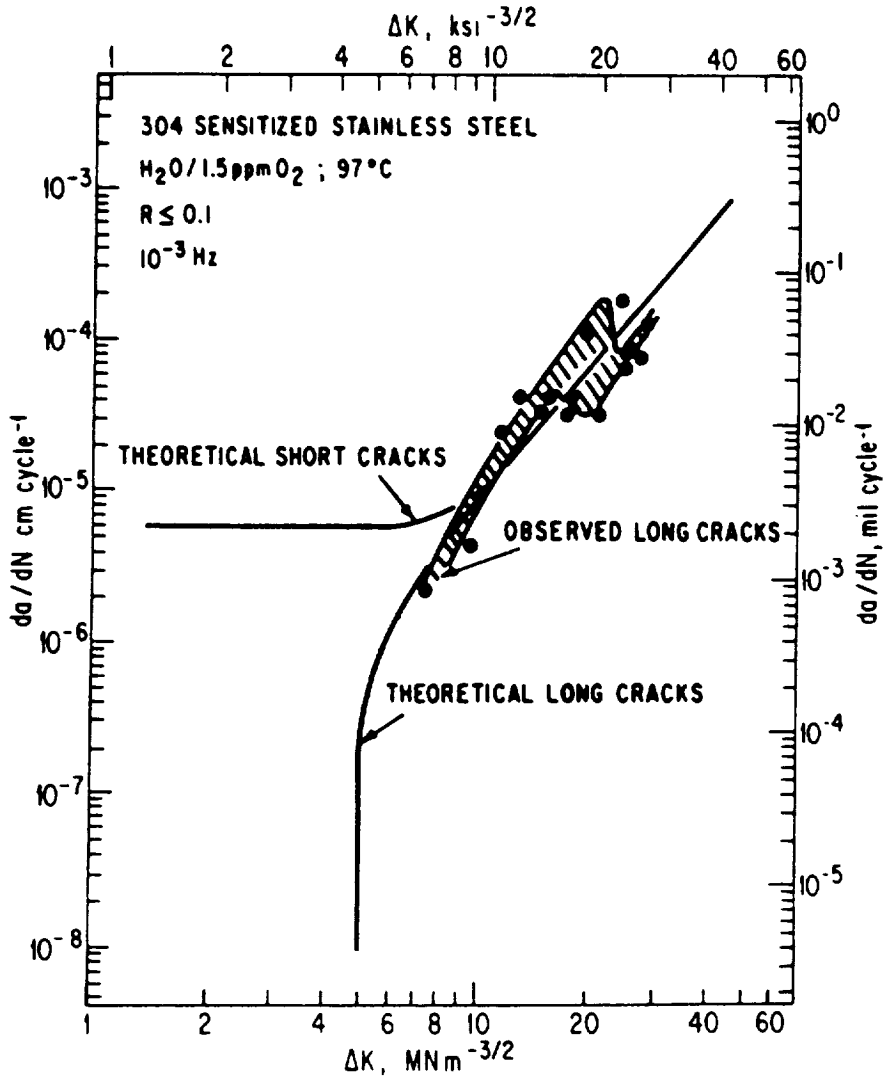

Fig. 52 The predicted effect of small crack depth on corrosion fatigue crack propagation by film rupture for stainless steel in high temperature water; after Hudak and Ford [286].

decreases with increasing initial applied stress range at constant R and with increasing R at constant ΔK [97]. A rapidly growing crack in NaCl was slowed by a stress range increase; in air or vacuum increased stress caused increased crack growth rates as expected from increasing ΔK. These crack growth rate data correlated with the reciprocal of the maximum crack mouth opening displacement (V_{max}) at constant ΔK according to [253]:

$$\log\left(\frac{da}{dN_{cf}}\right) = \left(\frac{\alpha\tau a^*}{V_{max}}\right) + \Phi \qquad (35)$$

Φ, α, τ and a^* are constants which characterize the chemical reactions which control corrosion fatigue, as discussed in the next Section. $(V_{max})^{-1}$ decreases with increasing crack length and increasing K_{max}; particularly for crack lengths between 0.1 and 1 mm. For long cracks, changing crack length has only a small effect on V_{max}, indicating that ΔK would reasonably correlate crack growth rates.

Several points are relevant to the short crack results represented in Fig. 9 and equation 35. As the magnitude of the crack size effect increases, the fracture mechanism changes from brittle transgranular cracking associated with the martensitic microstructure to intergranular crack growth along prior austenite boundaries [97]. Secondly, K_{ISCC} equals between 24 and 30 MPa$\sqrt{m}$ for long cracks, but declines to about 8 MPa$\sqrt{m}$ for the smallest cracks represented in Fig. 9 [194]. As such, it is likely that the result in Fig. 9 is for time-dominant corrosion fatigue. A simple superposition model will not describe short crack growth because of the effect of crack shape on local chemistry; for example as indicated by the observation that da/dN_e decreases with increasing R. Finally, the "small" crack regime for this case extends to sizes on the order of several millimeters.

Cycle-time-dependent corrosion fatigue in the steel-chloride

system is generally enhanced by reduced crack size, however, the magnitude of the effect decreases substantially with decreasing steel yield strength [180]. While systematic studies are limited, the data represented in Fig. 53 show that da/dN_e is increased by between 1.5 to 2-fold for low strength steels, comparing small crack kinetics to standard compact tension data.[9] This result is further illustrated in Fig. 17. As yield strength increases, short crack size becomes more important; for moderate strength steels such as HY130, small cracks grow up to 4 times faster than long cracks [180,287]. This interaction between crack size and strength is consistent with the moderate effect of hydrogen for this class of steels. For high strength steels, small corrosion fatigue cracks grow at unpredictably high rates, varying from long crack data by one to two orders of magnitude.

Small crack effects in corrosion fatigue have not been reported for nonferrous alloy and environment systems. A likely hydrogen embrittlement system, high strength aluminum alloys in aqueous chloride, was examined by Piascik and Gangloff [126,221]. Similar corrosion fatigue crack growth rates were observed for through thickness edge cracks sized between 0.2 and 5 mm and for 25 mm long cracks in compact tension specimens. While the high angle grain size was large, no microstructure-environment interaction was observed. Corrosion fatigue crack growth rates were consistent with the broad base of data presented in Fig. 12.

VII.3. Crack Geometry Dependent Occluded Environment Chemistry

If occluded crack chemistry changes as a function of crack size, time, specimen geometry or loading; then corrosion fatigue crack growth rates will not be steady state and will not be meaningfully described by applied ΔK. Crack chemistry effects

[9]Subtle small crack effects are best characterized by constant ΔK experimentation with electrical potential monitoring. For example in Fig. 17, da/dN is constant with increasing crack length from 0.3 to 2.7 mm for moist air. Da/dN, while higher than the air rate, decreases with increasing crack length for the chloride [178]. Surface replication methods would not indicate the behavior shown in Fig. 17.

Material	σ_{YS} (MPa)	Environment	Crack Size Type (mm)	da/dN Defined by ΔK_T	$\frac{da/dN_{SMALL}}{da/dN_{LONG}}$	Limiting Small Crack Size (mm)	Comments	Reference	
AISI 4130 (.3C-.9Cr-.2Ni)	1330	3% NaCl	.1–40 Long 1.9 Wide Edge, Elliptical	Yes - Air, Vacuum No - NaCl	1.2 to 500	>2.5	Growth Retarded by Increased K_{max}, R; ΔK_{max} Describes da/dN. 15 μm Grain Size.	13, 21	High Strength
ASTM A289-B (18.2Mn-4.8Cr-.6C)	1120	655 kPa H_2 Sat. H_2O 88°C	.1–40 Long 25 Wide Edge .8 Notch	Yes - Air 23°C Yes - 10 Hz H_2 No - .02 Hz H_2	1.0 to 100	.8	Small Crack Growth Enhanced by Increased Initial ΔK and Loading Time. 100 μm Grain Size.	26	
HY130 (.1C-.5Cr-5Ni)	930	3% NaCl	.1–40 Long 1.9 Wide Edge	Yes - Air No - NaCl	4	>1.0	Initial ΔK Not Important.	22	Medium Strength
	972	3% NaCl	.4–40 Long 7.6 Wide Edge	Yes - Air No - NaCl	2	1.1	Limiting Crack Size Unaffected by $\Delta\sigma$, R.	18, 27	
	972	3% NaCl	.4–40 Long 7.6 Wide Edge	Yes - Air No - NaCl	1.0–1.8 Free Corrosion 0.8–1.3 Cathodic	0.8–1.4 5	Limiting Crack Sizes Up to 10 mm at Constant ΔK. No Significant Crack Closure Measured.	28	
	950	Seawater	>.5 Long 12.7 Wide Edge	Yes	1.0	<.5	Limited Data.	29	
13 Cr (.03C-12.8Cr-5Ni)	770	Water	?	No	4	?	High Frequency, Near Threshold Data. Magnitude of Small Crack Effect Enhanced at High R.	25	
Q1N (.17C-1.2Cr-2.4Ni)	625	Seawater	.5–8 Long 12.7 Wide Edge	Yes - Air No - NaCl	4	2.0	No Crack Size Effect at R = 0.5 or $\Delta K > 30$ MPa$\sqrt{m}$. Limited Data for Air.	29, 30	Low Strength
BS4360:50D (.18C-1.2Mn)	370	Seawater	1–7 Long 23.5 Wide Edge	Yes - Air No - NaCl	3	1.0–3.0	Crack Size Effect Eliminated by Cathodic Polarization: da/dN Small to Large < 1.0.	31	
EN5 (.3C-.7Mn)	300	Seawater	.5–6 Long 12.7 Wide Edge	? - Air No - NaCl	2	2.0	Limited Data.	29	

1285-37C-259

Fig. 53 Literature results on the effect of crack size on corrosion fatigue in the steel/aqueous chloride system. Reference numbers refer to the original paper; after Gangloff and Wei [180].

are particularly important within the short and small crack regimes.

Mathematical modeling provides a means to assess varying crack tip electrolyte pH, potential, ionic composition, dissolution and hydrogen production rates, as discussed in Section VI.5.b. Such work for ferritic steels in aqueous chloride provides predictions of crack size and loading effects on local chemistry. Generally, reactant and product concentrations in a fatigue crack depend on crack depth and mouth opening, and thus on ΔK, R, load waveform and specimen geometry [248,252].

An example of crack tip reactant oxygen concentration is provided in Fig. 42; this specie is normally consumed by a reduction reaction within the crack, and which competes with hydrogen ion and water reduction. As crack length initially increases to 1 mm, the concentration of crack tip oxygen declines because the diffusional supply of reactant O_2 from aerated bulk solution becomes increasingly difficult. This effect is offset by convective mixing supply which becomes increasingly effective as crack length increases; a minimum in the oxygen level is predicted for a specific crack length. The relationship in Fig. 42 depends on the rate of oxygen reduction, loading frequency and crack surface area to occluded solution volume ratio.

The crack chemistry predictions in Fig. 42 suggest that da/dN_e could either increase though a maximum or decrease through a minimum with increasing crack length at constant ΔK; the specific dependence would depend on the embrittlement mechanism. Only limited experimental evidence support this prediction. For the steel-chloride system, Gangloff demonstrated the former trend, as expected from an inhibiting effect of dissolved oxygen on hydrogen embrittlement [189]. Experiments with variable O_2, but constant electrode potential and ΔK, failed to confirm this chemical model.

Crack geometry dependent local chemistry is an important explanation for the small crack effect in the steel-chloride system. Initial modeling of the data in Fig. 9 was based on a perfect mixing description of convection to supply oxygen to the

crack tip [253]. Those crack shape and loading conditions which reduce oxygen concentration (slow loading frequency, large crack surface area to solution volume given by large $(V_{max})^{-1}$, and fast oxygen reduction kinetics) promote hydrogen production by cathodic reduction and hence crack propagation by hydrogen embrittlement. Equation 35 resulted from this modeling, and explained how small crack size and low stress ratio enhanced da/dN_e.

Detailed modeling of crack chemistry further indicated that unexpectedly large and geometry dependent adsorbed hydrogen concentrations develop at the tips of small corrosion fatigue cracks for steels in chloride. For monotonic loading, Gangloff and Turnbull demonstrated that crack tip pH decreases with decreasing crack size due to enhanced hydrolysis. Here, cations are eliminated by diffusion from the tip of the short crack; dissolution is not transport limited [194]. Decreased pH dominated a slightly less cathodic crack tip to produce increased amounts of adsorbed hydrogen for the short crack. Turnbull and Ferriss extended this work to cyclic loading with convective mixing and demonstrated a similar enhancement of hydrogen production for the short crack [249]. For this case, crack potential variation played a more important role than reduced acidification.

These calculations suggest an important effect of steel composition [249]. Chromium, typical of alloy steels such as AISI 4130, hydrolizes to produce acidic crack tip conditions for electrode potentials near free corrosion. Cracks in C-Mn steels are less acidified, water reduction is an important source of embrittling hydrogen and crack geometry appears to play a secondary role in local chemistry.

Crack chemistry modeling sensitizes the user of corrosion fatigue crack propagation data to possible problems with similitude. The use of laboratory specimens to predict the behavior of components can be questioned when crack chemistries differ due to geometry. This complex situation discourages the fracture mechanics approach to life prediction.

On balance, however, fracture mechanics studies of corrosion

fatigue crack propagation demonstrate substantial steady state and orderly material behavior. Applied stress intensity control of da/dN_e is supported, perhaps because crack chemistry generally reaches constant conditions for most cracking situations, as suggested by modeling. The influences of specimen geometry, ΔK, R, waveform and crack size above 1 to 5 mm are secondary. Note that time and specimen geometry effects on corrosion fatigue have not been examined systematically. Exceptions in this regard are the small crack issue [97,180], predictions of surface crack corrosion fatigue behavior from compact tension data [121], and work on transient crack propagation preceding steady state growth rates [154].

Rapid progress over the past 5 years suggests that crack chemistry modeling will intensify, and that similitude will be broadly tested for corrosion fatigue. There is no doubt that corrosion fatigue crack growth rate laws will be strengthened when necessary, and applied to life predictions; despite the complexity of this endeavor.

VII.4. Whole Life

While the fracture mechanics approach emphasizes crack propagation, one must ultimately predict the whole life of components. A rational means to this end is to couple fracture mechanics studies of single small, short and long corrosion fatigue cracks with work on environment sensitive cyclic deformation and crack nucleation in homogeneous microstructures and near defects [1,36]. This can only be accomplished if each stage of fatigue deformation and fracture is isolated and characterized.

Fatigue crack initiation is correctly characterized by cyclic plastic strain amplitude, as reviewed by Dowling [289]. A fracture mechanics parameter (viz, applied ΔK divided by the square root of the notch tip radius, ρ) equals an elastic pseudo-stress range which is a unique function of local plastic strain amplitude at the root of a notch; specifically for slender notches. This parameter is easily calculated for a variety of notched specimens and correlates notch initiation data, as

demonstrated for a variety of materials in benign air [290]. This approach has been successfully applied to corrosion fatigue crack initiation.

Corrosion fatigue crack initiation in carbon and high strength low alloy steels is exacerbated by exposure to aqueous chloride electrolytes. An example is shown in Fig. 54. Here, the load cycles required to produce a 1 mm deep fatigue crack at the root of a notch are plotted versus $\Delta K/\rho$ for the keyhole-notched compact tension specimen [290-293]. A variety of modern steels; strengthened by microalloying, thermomechanical processing including controlled rolling, quench/tempering and precipitation; were stressed in seawater and air. Classic endurance limit behavior is observed for fatigue in moist air, with the limiting stress range increasing with increasing steel yield strength [290]. In sharp contrast exposure to either natural seawater or 3.5 wt% NaCl at free corrosion potentials produced a dramatic reduction in initiation life. The endurance limit is eliminated by environmental exposure for each steel. Cathodic polarization up to about -1000 mV (SCE) restores the majority of the air fatigue performance; more cathodic polarization reduced initiation life.

Two points are notable in Fig. 54 and are consistent with previous discussions of corrosion fatigue. Firstly, notch crack initiation in the ferritic steel-chloride system is mitigated by mild cathodic polarization, despite the likelihood of hydrogen embrittlement. This behavior is analogous to that of smooth specimens, but is in contrast to crack growth in precracked specimens, as indicated in Figs. 25 and 26. An explanation for the effects of cathodic polarization on the initiation and growth stages of corrosion fatigue is given in V.5.b.(1).

Secondly, steel composition, microstructure and strength have no resolvable effect on corrosion fatigue crack initiation and early growth, as indicated by the results for eight steels reported by Rajpathak and Hartt and for four steels by Novak, Fig. 54. Apart from a variety of microstructures, monotonic yield strength varied from 275 MPa for normalized A36 steel to 1070 MPa for quenched and tempered V150. This conclusion is

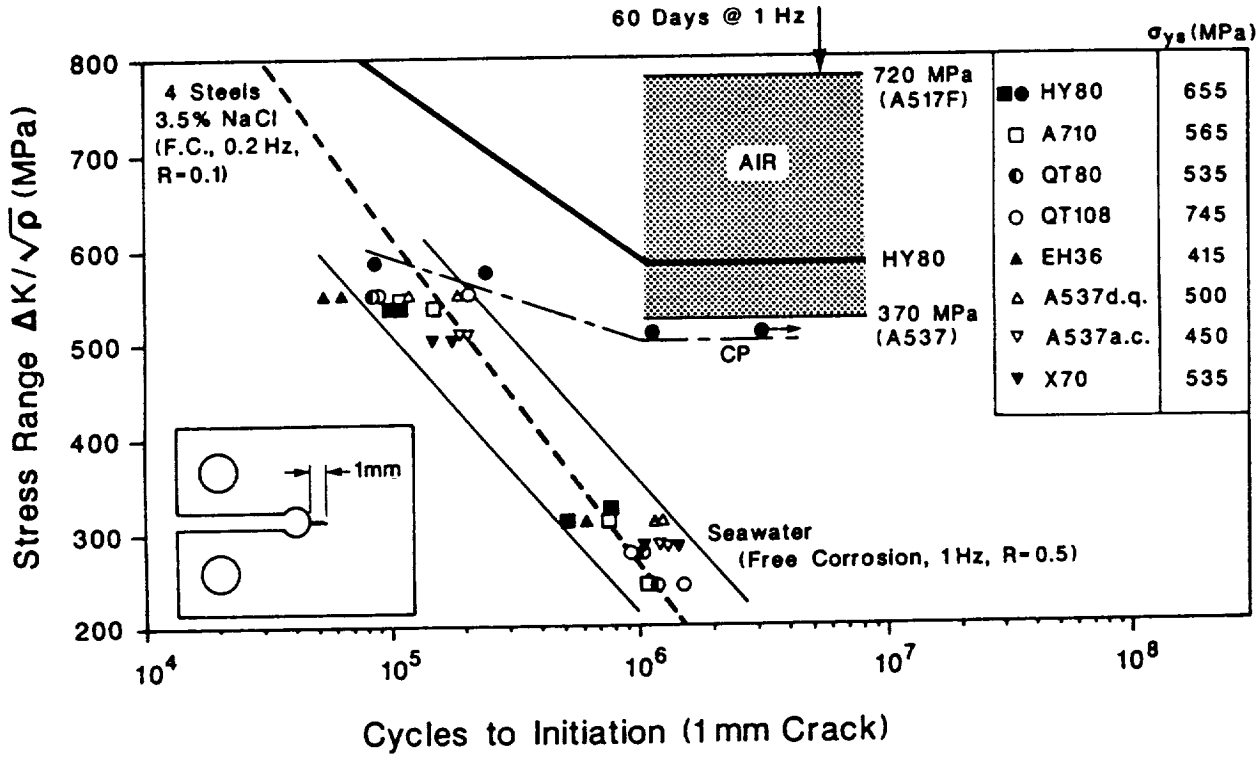

Fig. 54 Corrosion fatigue crack initiation (Δa = 1 mm) at blunt notches in HSLA steels in seawater or NaCl. Local strain is approximated by elastic pseudo-stress from applied ΔK divided by the square root of the notch radius; after Hartt et al. [196,292,293], Novak [291], and Rolfe and Barsom [290].

consistent with the lack of microstructure and yield strength effects on corrosion fatigue crack propagation in this system, Sections V.6 and V.7 and Figs. 30 and 31.

The local strain approach to corrosion fatigue crack initiation, enabled by fracture mechanics solutions for stress intensity, provides an important complement to fatigue crack propagation studies. Additional work in this direction is warranted. Needs in this regard are for additional materials and environments, for improved in situ measurements of notch root crack initiation, and for the study of small notches typical of material and corrosion produced defects. The results in Fig. 54 were obtained by optical monitoring of large machined notches. The electrical potential method is well suited for high resolution, continuous measurement of crack initiation in complex environments [158]. The method was successfully applied to mechanically or spark eroded defects as small as 75 μm semicircles. Crack initiation at preexposure corrosion pitting damage could be monitored by this approach.

VIII. NECESSARY RESEARCH

VIII.1. Conclusion

Opportunities exist for research on corrosion fatigue to: (a) broaden phenomenological understanding, particularly near-threshold, (b) develop integrated and quantitative micromechanical-chemical models, (c) develop experimental methods to probe crack tip damage, and to measure near-threshold time-cycle-dependent crack growth, (d) characterize the behavior of advanced monolithic and composite alloys, and (e) develop damage tolerant life prediction methods and in situ sensors for environment chemistry and crack growth.

VIII.2. Future Research

The data and modeling studies presented in previous sections establish that the fracture mechanics approach can be exploited and extended to control corrosion fatigue crack propagation. Unresolved issues are listed for each of the main areas of this

review.

VIII.2.a. **Crack Growth Rate Data Bases.** Experiments must be conducted to determine:

(1) Environmental effects on near-threshold crack propagation, particularly as a function of cyclic loading frequency. Extrinsic closure and intrinsic environmental embrittlement must be separated.

(2) Yield strength and microstructural effects on corrosion fatigue crack propagation, with developments of reliable cracking resistant alloys for extreme environments.

(3) Correlations between crack growth rates and environmental hydrogen uptake.

(4) Corrosion fatigue crack propagation behavior of advanced alloys and composites. For the latter, the extent to which corrosion fatigue damage is distributed, and hence not described by continuum fracture mechanics, must be defined.

(5) Corrosion fatigue crack propagation under complex spectrum loading, including the effects of single and multiple over/under-loads and load history.

VIII.2.b. **Experimental Methods.** New experimental methods are required for:

(6) Measurement of low growth rate corrosion fatigue crack propagation at low cyclic loading frequencies.

(7) In situ measurement of the early growth of microstructurally small corrosion fatigue cracks, without loading interruptions.

(8) Probes for crack tip chemistry, surface reaction kinetics and process zone fatigue damage.

VIII.2.c. **Fracture Mechanics Similitude.** Work in this area is required for:

(10) Measurement and analysis of crack closure in aggressive environments.

(11) Determinations of the growth kinetics of short/small cracks, with associated chemical and mechanical mechanisms to extend similitude.

VIII.2.d. **Micromechanical-Chemical Mechanism Modeling.** Modeling work must be expanded to include:

(12) Fractographic interpretations of the micromechanisms of corrosion fatigue crack propagation.

(13) Integrated occluded crack mass transport and transient straining surface reaction kinetics models.

(14) Integrated hydrogen production or film rupture and microscopic process zone fatigue damage models.

(15) Understanding of the effects of crack surface films on cyclic plasticity and corrosion fatigue damage.

(16) Determinations of microscopic deformation and dislocation processes within the crack tip process zone and relations with stress intensity.

(17) Environmental effects on material flow properties, incorporated into time dependent crack tip field models.

(18) Quantitative modeling of corrosion fatigue in aluminum, titanium and nickel based superalloys.

VIII.2.e. **Life Prediction.** Applications of the fracture mechanics approach must include:

(19) Life prediction codes which incorporate environmental effects on crack growth, extrapolated from short term laboratory data and confirmed by component tests.

(20) Developments of sensors to monitor environmental conditions, hydrogen uptake, and fatigue crack propagation during component service.

ACKNOWLEDGEMENTS

Financial support for research on corrosion fatigue in light metals and for the preparation of this review was provided by the NASA-Langley Research Center under Grant NAG-1-745. Mr. D. L. Dicus of the Metallic Materials Branch is the Program Monitor. Dr. Robert S. Piascik conducted much of the research on advanced Al-Li alloys. The University of Virginia Center for

Electrochemical Sciences and Engineering provided additional financial and facilities support. These contributions are gratefully acknowledged.

IX. REFERENCES

1. Duquette, D.J., Environment Induced Cracking of Metals, R. P. Gangloff and M. B. Ives, eds., (Houston, TX: NACE, 1990), pp. 45-54.

2. Parkins, R.N., Environment Induced Cracking of Metals, R. P. Gangloff and M. B. Ives, eds., (Houston, TX: NACE, 1990), pp. 1-20.

3. Spahn, H., Environment Induced Cracking of Metals, R. P. Gangloff and M. B. Ives, eds., (Houston, TX: NACE, 1990), pp. 449-488.

4. Pineau, A., Environment Induced Cracking of Metals, R. P. Gangloff and M. B. Ives, eds., (Houston, TX: NACE, 1990), pp. 111-122.

5. Speidel, M.O., Blackburn, M.J., Beck, T.R. and Feeney, J.A., Corrosion Fatigue, Chemistry, Mechanics and Microstructure, O. Devereux, A.J. McEvily and R.W. Staehle, eds., (Houston, TX: NACE, 1972), pp. 324-345.

6. Corrosion Fatigue, Chemistry, Mechanics and Microstructure, O. Devereux, A.J. McEvily and R.W. Staehle, eds., (Houston, TX: NACE, 1972).

7. Stress Corrosion Cracking and Hydrogen Embrittlement of Iron Based Alloys, J. Hochmann, J. Slater, R.D. McCright and R.W. Staehle, eds., (Houston, TX: NACE, 1977).

8. Hydrogen in Metals, I.M. Bernstein and A.W. Thompson, eds., (Metals Park, OH: ASM, 1974).

9. Effect of Hydrogen on the Behavior of Materials, A.W. Thompson and I.M. Bernstein, eds., (Warrendale, PA: TMS-AIME, 1976).

10. Corrosion Fatigue Technology, ASTM STP 642, H.L. Craig, Jr., T.W. Crooker, and D.W. Hoeppner, eds., (Philadelphia, PA: ASTM, 1978).

11. Proceedings, Conference on the Influence of Environment on Fatigue, (London, UK: Inst. Mech. Engr., 1978).

12. Environment Sensitive Fracture of Engineering Materials, Z.A. Foroulis, ed., (Warrendale, PA: TMS-AIME, 1979).

13. Hydrogen Effects in Metals, I.M. Bernstein and A.W. Thompson, eds., (Warrendale, PA: TMS-AIME, 1981).

14. Environmental Degradation of Engineering Materials in Hydrogen, M.R. Louthan, R.P. McNitt and R.D. Sisson, eds., (Blacksburg, VA: VPI Press, 1981).

15. Fatigue: Environment and Temperature Effects, J.J. Burke and V. Weiss, eds., (Watertown, MA: U.S. Army Materials Technology Laboratory, 1984).

16. Corrosion Fatigue: Mechanics, Metallurgy, Electrochemistry and Engineering, ASTM STP 801, T.W. Crooker and B.N. Leis, eds., (Philadelphia, PA: ASTM, 1984).

17. Embrittlement by the Localized Crack Environment, R.P. Gangloff, ed., (Warrendale, PA: TMS-AIME, 1984).

18. Hydrogen Degradation of Ferrous Alloys, R.A. Oriani, J.P. Hirth and M. Smialowski, eds., (Park Ridge, NJ: Noyes Publications, 1985).

19. Corrosion Chemistry Within Pits, Crevices and Cracks, A. Turnbull, ed., (London, UK: HMSO, 1987).

20. Modeling Environmental Effects on Crack Initiation and Propagation, R.H. Jones and W.W. Gerberich, eds., (Warrendale, PA: TMS-AIME, 1986).

21. Environmental Degradation of Engineering Materials-III, M.R. Louthan, R.P. McNitt and R.D. Sisson, eds., (University Park, PA: Pennsylvania State University, 1987).

22. Environment Sensitive Fracture of Metals and Alloys, (Arlington, VA: Office of Naval Research, 1987).

23. Environmentally Assisted Cracking: Science and Engineering, ASTM STP 1049, W.B. Lisagor, T.W. Crooker and B.N. Leis, eds, (Philadelphia, PA: ASTM, 1990).

24. Mechanics and Physics of Crack Growth:Application to Life Prediction, R.B. Thompson, R.O. Ritchie, J.L. Bassani and R.H. Jones, eds., (London, UK: Elsevier, 1988).

25. McEvily, A.J. and Wei, R.P., Corrosion Fatigue: Chemistry, Mechanics and Microstructure, O. Devereux, A.J. McEvily and R.W. Staehle, eds., (Houston, TX: NACE, 1972), pp. 381-395.

26. Speidel, M.O., Stress Corrosion Cracking and Hydrogen Embrittlement of Iron Based Alloys, J. Hochmann, J. Slater, R.D. McCright and R.W. Staehle, eds., (Houston, TX: NACE, 1977), pp. 1071-1094.

27. Moskovitz, J.A. and Pelloux, R.M., Corrosion Fatigue Technology, ASTM STP 642, H.L. Craig, Jr., T.W. Crooker and D.W. Hoeppner, eds., (Philadelphia, PA: ASTM, 1978), pp. 133-154.

28. Parkins, R.N., Metals Science, July (1979): pp. 381-386.

29. Duquette, D.J., Environment Sensitive Fracture of Engineering Materials, Z.A. Foroulis, ed., (Warrendale, PA: TMS-AIME, 1979), pp. 521-537.

30. Wei, R.P., Fatigue Mechanisms, ASTM STP 675, J.T. Fong, ed., (Philadelphia, PA: ASTM, 1979), pp. 816-840).

31. Marcus, H.L., Fatigue and Microstructure, M. Meshi, ed., (Metals Park, OH: ASM, 1979), pp. 365-383.

32. Jaske, C.E., Payer, J.H. and Balint, V.S., Corrosion Fatigue of Metals in Marine Environments, Metals and Ceramics Information Center, MCIC-81-42 (1981).

33. Wei, R.P. and Shim, G., Corrosion Fatigue: Mechanics, Metallurgy, Electrochemistry and Engineering, ASTM STP 801, T.W. Crooker and B.N. Leis, eds., (Philadelphia, PA: ASTM, 1983), pp. 5-25.

34. Scott, P.M., Corrosion Fatigue: Mechanics, Metallurgy, Electrochemistry and Engineering, ASTM STP 801, T.W. Crooker and B.N. Leis, eds., (Philadelphia, PA: ASTM, 1983), pp. 319-350.

35. Komai, K.,Current Research on Fatigue Cracks, T. Tanaka, M. Jono and K. Komai, eds., (Kyoto, Japan: Society of Materials Science, Japan, 1985), pp. 235-253.

36. Gangloff, R.P. and Duquette, D.J., Chemistry and Physics of Fracture, R.M. Latanision and R.H. Jones, eds., (Netherlands: Martinus Nijhoff Publishers BV, 1987), pp. 612-645.

37. Wei, R.P. and Gangloff, R.P., Fracture Mechanics: Perspectives and Directions, ASTM STP 1020, R.P. Wei and R.P. Gangloff, eds., (Philadelphia, PA: ASTM, 1989), pp. 233-264.

38. Sudarshan, T.S. and Louthan, Jr., M.R., Intl. Metall. Rev., Vol. 32, No. 3 (1987): pp. 121-151.

39. Ford, F.P., J. Press. Ves. Tech, Trans. ASME, Vol. 110, pp. 113-128 (1988).

40. Fatigue Mechanisms, ASTM STP 675, J.T. Fong, ed., (Philadelphia, PA: ASTM, 1979).

41. Fatigue Crack Growth Threshold Concepts, D.L. Davidson and S. Suresh, eds., (Warrendale, PA: TMS-AIME, 1984).

42. Current Research on Fatigue Cracks, T. Tanaka, M. Jono and K. Komai, eds., (Kyoto, Japan: Society of Materials Science, Japan, 1985).

43. Fatigue 84, C.J. Beevers, ed., (West Midlands, UK: EMAS, 1984).

44. Fatigue Crack Growth, 30 Years of Progress, R.A. Smith, ed., (Oxford, UK: Pergamon Press, 1986).

45. Small Fatigue Cracks, R.O. Ritchie and J. Lankford, eds., (Warrendale, PA: TMS-AIME, 1986).

46. Fatigue and Life Analysis and Prediction, V.S. Goel, ed., (Metals Park, OH: ASM, 1986).

47. Fatigue 87, R.O. Ritchie and E.A. Starke, Jr., eds., (West Midlands, UK: EMAS, 1987).

48. Basic Questions in Fatigue, ASTM STP 924, Vol. 2, R.P. Wei and R.P. Gangloff, eds., (Philadelphia, PA: ASTM, 1988).

49. Wei, R.P. and Simmons, G.W., Stress Corrosion Cracking and Hydrogen Embrittlement of Iron Based Alloys, J. Hochmann, J. Slater, R.D. McCright and R.W. Staehle, eds., (Houston, TX: NACE, 1977), pp. 751-765.

50. Wei, R.P. and Landes, J.D., Matls. Res. Stds., Vol. 9 (1969): pp. 25-28.

51. Barsom, J.M., Corrosion Fatigue, Chemistry, Mechanics and Microstructure, O. Devereux, A.J. McEvily and R.W. Staehle, eds., (Houston, TX: NACE, 1972), pp. 424-436.

52. Barsom, J.M., Intl. J. Frac. Mech., Vol. 7 (1971): pp. 163-182.

53. Speidel, M.O., Unpublished research (1975), reported in: J.C. Scully, Environment Sensitive Fracture of Engineering Materials, Z.A. Foroulis, ed., (Warrendale, PA: TMS-AIME, 1979), pp. 71-90.

54. Johnson, H.H., Stress Corrosion Cracking and Hydrogen Embrittlement of Iron Based Alloys, J. Hochmann, J. Slater, R.D. McCright and R.W. Staehle, eds., (Houston, TX: NACE, 1977), pp. 382-389.

55. Oriani, R.A., Corrosion, Vol. 43 (1987): pp. 390-397.

56. Oriani, R.A., Ann. Rev. Matl. Sci., Vol. 8 (1978): pp. 327-357.

57. Gangloff, R.P., Matls. Sci. Engr., Vol. A103 (1988): pp. 157-166.

58. Scott, P.M., Thorpe, T.W. and Silvester, D.R.V., Corrosion Science, Vol. 23 (1983): pp. 559-575.

59. Hinton, B.R.W. and Procter, R.P.M., Metals Forum, Vol. 5 (1982): pp. 80-91.

60. Petit, J. and Zeghloul, A., Environmentally Assisted Cracking: Science and Engineering, ASTM STP 1049, W.B. Lisagor, T.W. Crooker and B.N. Leis, eds., (Philadephia, PA: ASTM, (1990), pp. 334-346.

61. Gao, M., Pao, P.S. and Wei, R.P., Metall. Trans. A, Vol. 19A (1988): pp. 1739-1750.

62. Duquette, D. J., "Mechanisms of Corrosion Fatigue of Aluminum Alloys", AGARD Report No. AGARD-CP-316 (1981).

63. Gruhl, W., Z. Metallkde, Vol. 75 (1984): pp. 819-826.

64. Meyn, D.A., Met. Trans., Vol. 2 (1971): pp. 853-865.

65. Holroyd, N.J.H. and Hardie, D., Corrosion Science, Vol. 23 (1983): pp. 527-546.

66. Speidel, M. O., Metall. Trans. A, Vol. 6A (1975): pp. 631-651.

67. Oriani, R.A., Environment Induced Cracking of Metals, R.P. Gangloff and M.B. Ives, eds., (Houston, TX: NACE, 1990), pp. 439-448.

68. Birnbaum, H.K., Environment Induced Cracking of Metals, R.P. Gangloff and M.B. Ives, eds., (Houston, TX: NACE, 1990), pp. 21-30.

69. Lynch, S.P., Atomistics of Fracture, R.M. Latanision and J.R. Pickens, eds., (New York, NY: Plenum Press, 1983), pp. 955-963.

70. Ford, R.P., Embrittlement by the Localized Crack Environment, R.P. Gangloff, ed., (Warrendale, PA: TMS-AIME, 1984), pp. 117-147.

71. Ford, F.P. and Andresen, P.L., Advances in Fracture Research, K. Salema, K. Ravi-Chandor, D.M.R. Taplin and P. Ramo Rao, eds., (Oxford, UK: Pergamon Press, 1989), pp. 1571-1584.

72. Ford, F.P. Corrosion, Vol. 35 (1979): pp. 281-287.

73. Duquette, D.J., Fatigue and Microstructure, M. Meshi, ed., (Metals Park, OH: ASM, 1978), pp. 335-363.

74. Marcus, H.L, Williams, J.C. and Paton, N.E., Corrosion Fatigue, Chemistry, Mechanics and Microstructure, O. Devereux, A.J. McEvily and R.W. Staehle, eds., (Houston, TX: NACE, 1972), pp. 346-358.

75. Grinberg, N.M., Intl. J. Fatigue, April (1982): pp. 83-95.

76. Grosskreutz, J.C., Corrosion Fatigué, Chemistry, Mechanics and Microstructure, O. Devereux, A.J. McEvily and R.W. Staehle, eds., (Houston, TX: NACE, 1972), pp. 201-210.

77. Stoltz, R.E. and Pelloux, R.M., Met. Trans., Vol. 3 (1972): pp. 2433-2441.

78. Lindigkeit, J., Terlinde, G., Gysler, A. and Lutjering, G., Acta Metall., Vol. 27 (1979): pp. 1717-1726.

79. Jata, K. and Starke, Jr., E.A., Metall. Trans. A., Vol. 17A (1986): pp. 1011-1026.

80. Pelloux, R.M.N., Trans. ASM, Vol. 62 (1969): pp. 281-285.

81. Meyn, D.A., Trans. ASM, Vol. 61 (1968): pp. 52-61.

82. Sieradzki, K., Environment Induced Cracking of Metals, R.P. Gangloff and M.B. Ives, eds., (Houston, TX: NACE, 1990), pp. 125-138.

83. Lee, H.H. and Uhlig, H.H., J. Electrochem. Soc., Vol. 117 (1970): pp. 18-22.

84. Duquette, D.J. and Uhlig, H.H., Trans. ASM, Vol. 61 (1968): pp. 449-456.

85. Duquette, D.J., and Uhlig, H.H., Trans. ASM, Vol. 62 (1969): pp. 839-845.

86. Lee, H.H. and Uhlig, H.H., Met. Trans., Vol. 3 (1972): pp. 2949-2957.

87. Jones, D.A., Environment Induced Cracking of Metals, R.P. Gangloff and M.B. Ives, eds., (Houston, TX: NACE, 1990), pp. 265-270.

88. Paris, P.C., Gomez, M.P. and Anderson, W.E., The Trend in Engineering, Washington State Univ., Vol. 13, No. 1 (1961): pp. 9-14.

89. Hertzberg, R. W., Deformation and Fracture Mechanics of Engineering Materials, Ch. 13, 2nd Ed. (New York, NY: John Wiley and Sons, 1983).

90. Wei, R.P., Fundamental Aspects of SCC, R.W. Staehle, A.J. Forty and D. VanRooyen, eds., (Houston, TX: NACE, 1969), pp.104-112.

91. Brown, B.F., Met. Rev., No. 129 (1968): pp.171-183.

92. Bradshaw, F.J. and Wheeler, C. Applied Matls. Res., Vol. 5 (1966): pp. 112-120.

93. Hartman, A., Intl. J. Frac. Mech., Vol. 1 (1965), pp. 167-188.

94. Wei, R.P., Talda, P.M. and Li, Che-Yu, Fatigue Crack Propagation, ASTM STP 415, (Philadelphia, PA: ASTM, 1967), pp. 460-485.

95. Feeney, J.A., McMillan, J.C. and Wei, R.P. Met. Trans., Vol. 1 (1970): pp. 1741-1757.

96. Gangloff, R.P., Res. Mech. Let., Vol. 1 (1981): pp. 299-306.

97. Gangloff, R.P., Metall. Trans. A., Vol. 16A (1985): pp. 953-969.

98. Wei, R.P. and Simmons, G.W., Int. J. Fract., Vol. 17 (1981): pp. 235-247.

99. Andresen, P.L., Gangloff, R.P., Coffin, L.F. and Ford, F.P., Fatigue 87, R.O. Ritchie and E.A. Starke, Jr., eds., (West Midlands, England: EMAS, 1987), pp. 1723-1751.

100. Tompkins, B. and Scott, P.M., Metals Tech., Vol. 9 (1982): pp. 240-248.

101. Scott, P.M., Mem. Etudes Sci. Rev. Metall., (1983): pp. 651-660.

102. Barsom, J.M. and Novak, S.R., "Subcritical Crack Growth and Fracture of Bridge Steels", National Cooperative Highway Research Report 181, (Washington, DC: National Research Council, 1977).

103. Vosikovsky, O. and Cooke, R.J., Int. J. Pres. Ves. & Piping, Vol. 6 (1978): pp. 113-129.

104. Fatigue in Offshore Structural Steels, (London, UK: Thomas Telford, Ltd., 1981).

105. Proceedings of the International Conference on Steel in Marine Structures, (Paris, France: Comptoir des produits Siderurgiques, 1981).

106. Proceedings Institute of Mechanical Engineers Conference on Fatigue and Crack Growth in Offshore Structures, (London, UK: Inst. Mech. Engr., 1986).

107. Steel in Marine Structures, (Amsterdam: Elsevier, 1987).

108. "Guidance on the Design and Construction of Offshore Installations" (1977). "Background to Proposed New Fatigue Design Rules for Steel Welded Joints in Offshore Structures", (London, UK: United Kingdom Department of Energy, HMSO, 1983).

109. Dover, W.D., Int. J. Fatigue, Vol. 3 (1981), pp. 52-60.

110. Dover, W.D. and Dharmavasan, S., Fatigue 84, C.J. Beevers, ed., (West Midlands, England: EMAS, 1984), pp. 1417-1434.

111. Hudak, S.J., Burnside, O.H. and Chan, K.S., J. Energy Resources Tech., ASME Trans., Vol. 107 (1985): pp. 212-219.

112. Dover, W.D., Charlesworth, F.D.W., Taylor, K.A., Collins, R. and Michael, D.H., Eddy Current Characterization of Materials and Structures, ASTM STP 722, G. Birnbaum and G. Free, eds., (Philadelphia, PA: ASTM, 1985), pp. 401-427.

113. Yamakawa, K., Harushige, T. and Yoshizawa, S., Corrosion Monitoring in Industrial Plants Using Nondestructive Testing and Electrochemical Methods, ASTM STP 908, G.C. Moran and P. Labine, eds., (Philadelphia, PA: ASTM, 1986), pp. 221-236.

114. DeLuccia, J.J. and Berman, D.A. Electrochemical Corrosion Testing, ASTM STP 727, F. Mansfeld and U. Bertocci, eds., (Philadelphia, PA: ASTM, 1981), pp. 256-273.

115. Krishnamurthy, R., Marzinsky, C.N. and Gangloff, R.P., Effects of Hydrogen on Material Behavior, N. R. Moody and A. W. Thompson, eds., (Warrendale, PA: TMS-AIME, 1990), pp. 807-825.

116. Austen, I.M. and Walker, E.F., Fatigue 84, C.J. Beevers, ed., (West Midlands, England: EMAS, 1984), pp. 1457-1469.

117. Cialone, H.J. and Holbrook, J.H., Metall. Trans. A., Vol. 16A (1985): pp. 115-122.

118. Nelson, H. G., Effect of Hydrogen on the Behavior of Materials, A.W. Thompson and I.M. Bernstein, eds., (Warrendale, PA: TMS-AIME, 1976), pp. 602-611.

119. Bardal, E., Fatigue Handbook, A.A. Naess, ed., (Tapir, 1985), pp. 291-312.

120. Bardal, E., Haagensen, P.J., Grovlen, M. and Saether, F., Fatigue 84, C.J. Beevers, ed., (West Midlands, UK: EMAS, 1984), pp. 1541-1551.

121. Thorpe, T.W., Scott, P.M., Rance, A. and Silvester, D., Intl. J. Fatigue, Vol. 5 (1983): pp. 123-133.

122. Cowling, M.J. and Appleton, R.J., Proceedings Institute of Mechanical Engineers Conference on Fatigue and Crack Growth in Offshore Structures, (London, UK: Inst. Mech. Engr., 1986), pp. 77-92.

123. Booth, G.S., Wylde, J.G. and Iwasaki, T., Fatigue 84, C.J. Beevers, ed., (West Midlands, UK: EMAS, 1984), pp. 1471-1484.

124. Bertini, L., Managing Engineering Data: The Competivie Edge, (New York, NY: ASME, 1987), pp. 113-119.

125. Piascik, R.S. and Gangloff, R.P. Advances in Fracture Research, K. Salema, K. Ravi-Chandor, D.M.R. Taplin and P. Ramo Rao, eds., (London, UK: Pergamon Presss, 1989), pp. 907-918.

126. Piascik, R.S. and Gangloff, R.P., Environment Induced Cracking of Metals, R.P. Gangloff and M.B. Ives, eds., (Houston, TX: NACE, 1990), pp. 233-240.

127. Aliaga, D. and Budillon, E., "Corrosion Fatigue Behavior of Some Aluminum Alloys", AGARD Report No. AGARD-CP-316 (1981).

128. Selines, R.J. and Pelloux, R.M., Met. Trans., Vol. 3 (1972): pp. 2525-2531.

129. Wei, R.P., Pao, P.S., Hart, R.G., Weir, T.W. and Simmons, G.W., Metall. Trans. A, Vol. 11A (1980): pp. 151-158.

130. Pao, P.S., Imam, M.A., Cooley, L.A. and Yoder, G.R., Corrosion, Vol. 45 (1989): pp. 530-535.

131. Ranganathan, N., Quintard, M. and Petit, J., in Environmentally Assisted Cracking: Science and Engineering, ASTM STP, W.B. Lisagor, T.W. Crooker and B.N. Leis, eds., (Philadelphia, PA: ASTM, 1990), pp. 374-391.

132. Niegel, A., Gudladt, H.J. and Gerold, V., in Fatigue 87, R.O. Ritchie and E.A. Starke, Jr., eds., (West Midlands, UK: EMAS, 1987), pp. 1229-1238.

133. Holroyd, N.J.H., Environment Induced Cracking of Metals, R.P. Gangloff and M.B. Ives, eds., (Houston, TX: NACE, 1990), pp. 311-346.

134. Proceedings of the First International Atomic Energy Agency Specialists Meeting on Subcritical Crack Growth, Vol. I and II, US Nuclear Regulatory Commission Document, NUREG CP-0044 (1982).

135. Proceedings of the Second International Atomic Energy Agency Specialists Meeting on Subcritical Crack Growth, Vol. I and II, US Nuclear Regulatory Commission Document, NUREG CP-0067 (1986).

136. Andresen, P.L. and Ford, F.P., Matls. Sci. Engr., Vol. A103 (1988): pp. 167-184.

137. Ford, F.P., Taylor, D.F., Andresen, P.L. and Ballinger, R.G. "Environmentally Controlled Cracking of Stainless and Low-Alloy Steels in Light Water Reactor Environments", EPRI Report No. NP-5064M, (Palo Alto, CA: EPRI, 1987).

138. Ford, F.P., Environment Induced Cracking of Metals, R.P. Gangloff and M.B. Ives, eds., (Houston, TX: NACE, 1990), pp. 139-166.

139. Scott, P.M., Truswell, A.E. and Druce, S.G., Corrosion, Vol. 40 (1984): pp. 350-357.

140. Brown, B.F., Matls. Res. Stds., Vol. 6, No. 3 (1966): pp. 129-133.

141. Dawson, D.B. and Pelloux, R.M., Metall. Trans., Vol. 5 (1974): pp. 723-731.

142. Yoder, G.R., Cooley, L.A. and Crooker, T.W., Corrosion Fatigue: Mechanics, Metallurgy, Electrochemistry and Engineering, ASTM STP 801, T.W. Crooker and B.N. Leis, eds., (Philadelphia, PA: ASTM, 1984), pp. 159-174.

143. "Standard Test Method for Measurement of Fatigue Crack Growth Rates", ASTM Standard E647-88, ASTM Book of Standards, Vol. 03.01 (Philadelphia, PA: ASTM, 1988), pp. 899-926.

144. Utah, D.A., et al., Metals Handbook: Mechanical Testing, Vol. 8, 9th Ed. (Metals Park, OH: ASM International, 1985), pp. 376-402.

145. Fatigue Crack Growth Measurement and Data Analysis, ASTM STP 738, S.J. Hudak, Jr. and R.J. Bucci, eds., (Philadelphia, PA: ASTM, 1981).

146. Crooker, T.W., Gill, S.J., Yoder, G.R. and Bogar, F.D. Environment Sensitive Fracture: Evaluation and Comparison of Test Methods, ASTM STP 821, S.W. Dean, E.N. Pugh and G.M. Ugiansky, eds., (Philadelphia, PA: ASTM, 1984), pp. 415-425.

147. Gangloff, R.P., et al., in Metals Handbook: Mechanical Testing, Vol. 8, 9th Ed. (Metals Park, OH: ASM International, 1985), pp. 403-435.

148. Marsh, K.J. and Smith, R.A., Fatigue Crack Growth, 30 Years of Progress, R.A. Smith, ed., (Oxford, UK: Pergamon Press, 1986), pp. 17-30.

149. Measurement of Crack Length and Shape During Fracture and Fatigue, C.J. Beevers, ed., (West Midlands, UK: EMAS, 1980).

150. Advances in Crack Length Measurement, C.J. Beevers, ed., (West Midlands, UK: EMAS, 1982).

151. Brazill, R., Simmons, G.W. and Wei, R.P., J. Engr. Matls. Tech., Trans. ASME, Vol. 101 (1979): pp. 199-204.

152. Todd, J.A., Li, P., Liu, G. and Raman, V., Environmental Degradation of Engineering Materials, M.R. Louthan, R.P. McNitt and R.D. Sisson, Jr., eds., (University Park, PA: Pennsylvania State University, 1987), pp. 533-541.

153. Suresh, S. and Ritchie, R.O., Int. Metall. Rev., Vol. 29 (1984): pp. 445-476.

154. Hudak, Jr., S.J., and Wei, R.P., Intl. J. Pressure Vessels and Piping, Vol. 9 (1981): pp. 63-74.

155. Saxena, A., Hudak, Jr., S.J., Donald, J.K. and Schmidt, R.W., J. Test. Eval., Vol. 6 (1978): pp. 167-174.

156. Herman,W.A., Hertzberg, R.W. and Jaccard, R., J. Fat. and Frac. of Engr. Matls. and Struc., Vol. 11 (1988): pp. 303-320.

157. Dowling, N.E., Cyclic Stress-Strain and Plastic Deformation Aspects of Fatigue Crack Growth, ASTM STP 637, (Philadelphia, PA: ASTM 1977), pp. 97-121.

158. Gangloff, R.P., Advances in Crack Length Measurement, Ed., C.J. Beevers, (West Midlands, UK: EMAS, 1982), pp. 175-229.

159. Heubaum, F.H., "Propagation Kinetics of Short Fatigue Cracks in Low Alloy Steels", PhD Dissertation, (Evanston, IL: Northwestern Univeristy, 1986).

160. Gerberich, W.W. and Chen, S., Environment Induced Cracking of Metals, R.P. Gangloff and M.B. Ives, eds., (Houston, TX: NACE, 1990), pp. 167-188.

161. Fracture: Measurement of Localized Deformation by Novel Techniques, W.W. Gerberich and D.L. Davidson, eds., (Warrendale, PA: TMS-AIME, 1985).

162. Davidson, D.L. and Lankford, J., Fat. Engr. Matls. and Struc., Vol. 6 (1983): pp. 241-256.

163. Lankford, J., Fat. Engr. Matls. and Struc., Vol. 6 (1983): pp. 15-31.

164. Davidson, D.L. and Lankford, J., Intl. J. Frac., Vol. 17 (1981): pp. 257-275.

165. Brown, B.F., Stress Corrosion Cracking and Hydrogen Embrittlement of Iron Based Alloys, J. Hochmann, J. Slater, R.D. McCright and R.W. Staehle, eds., (Houston, TX: NACE, 1977), pp. 747-751.

166. Dolphin, A.S. and Turnbull, A.,Corrosion Chemistry Within Pits, Crevices and Cracks, A. Turnbull, ed., (Teddington, UK: National Physical Laboratory, 1985), pp. 397-412.

167. Turnbull, A., Dolphin, A.S. and Rackley, F.A., Corrosion, Vol. 44 (1988): pp. 55-61.

168. Hodgkiess, T. and Cannon, M.J., Proceedings Institute of Mechanical Engineers Conference on Fatigue and Crack Growth in Offshore Structures, (London, UK: Inst. Mech. Engr., 1986), pp. 69-76.

169. Turnbull, A., Embrittlement by the Localized Crack Environment, R.P. Gangloff, ed., (Warrendale, PA: TMS-AIME, 1984), pp. 3-48.

170. Vosikovsky, O., Trans. ASME, J. Engr. Matls. Tech., Vol. 97 (1975): pp. 298-304.

171. Bardal, E., Berge, T., Grovlen, M., Haagensen, P.J. and Forre, B.M., Advances in Crack Length Measurement, C.J. Beevers, ed., (West Midlands, UK: EMAS, 1982), pp. 139-158.

172. Austin, I.M. and Walker, E.F., Steel in Marine Structures, (Amsterdam: Elsevier: (1987), pp. 859-870.

173. Vosikovsky, O., J. Test. Eval., Vol. 8 (1980): pp. 68-73.

174. Vosikovsky, O., J. Test. Eval., Vol. 6 (1978): pp. 175-182.

175. Ewalds, H.L., J. Test. Eval., Vol. 9 (1981): pp. 158-161.

176. Barsom, J.M. and Novak, S.R., "Subcritical Crack Growth and Fracture of Bridge Steels", National Cooperative Highway Research Program Report 181, (Washington, DC: National Research Council, 1977).

177. Orjasaeter, O. and Dragen, A., Fatigue 84, C.J. Beevers, ed., (West Midlands, UK: EMAS, 1984), pp. 1553-1564.

178. Gangloff, R.P., "The Environmental Effect on Fatigue Crack Propagation", Report No. CR. 13BV.85, (Annandale, VA: Exxon Research and Engineering Company, 1985).

179. Gallagher, J.P., "Corrosion Fatigue Crack Growth Behavior Above and Below K_{ISCC}", Report No. NRL-7064, AD708377, (Washington, DC: Naval Research Laboratory, 1970).

180. Gangloff, R.P. and Wei, R.P., Small Fatigue Cracks, R.O. Ritchie and J. Lankford, eds., (Warrendale, PA: TMS-AIME, 1986), pp. 239-264.

181. Hinton, B.R.W. and Procter, R.P.M., Hydrogen Effects in Metals, I.M. Bernstein and A.W. Thompson, eds., (Warrendale, PA: TMS-AIME, 1981), pp. 1005-1015.

182. Shim, G., Nakai, Y. and Wei, R.P., Basic Questions in Fatigue, Vol.II, ASTM STP 924, R.P. Wei and R.P. Gangloff, eds., (Philadelphia, PA: ASTM, 1987), pp. 211-229.

183. Wei, R.P., Gao, M. and Pao, P.S., Scripta Metall., Vol. 18 (1984), pp. 1195-1198.

184. Dicus, D.L., Environment Sensitive Fracture: Evaluation and Comparison of Test Methods, ASTM STP 821, S.W. Dean, E.N. Pugh and G.M. Ugiansky, eds., (Philadelphia, PA: ASTM, 1984), pp. 513-533.

185. Chiou, S. and Wei, R.P., "Corrosion Fatigue Cracking Response of Beta-Annealed Ti-6Al-4V in 3.5% NaCl Solution", Report No. NADC-83126-60, (Warminster, PA: U.S. Naval Air Development Center, 1984).

186. Jones, B.F., Embrittlement by the Localized Crack Environment, R.P. Gangloff, ed., (Warrendale, PA: TMS-AIME, 1984), pp. 453-469.

187. Bradshaw, F.J. and Wheeler, C., Intl. J. Frac. Mech., Vol. 5 (1969): pp. 255-268.

188. Nakai, R., Alavi, A. and Wei, R.P., Metall. Trans. A., Vol. 19A (1988): pp. 543-548.

189. Gangloff, R.P., Critical Issues in Reducing the Corrosion of Steel, H. Leidheiser, Jr. and S. Haruyama, eds., (Tokyo, Japan: NSF/JSPS, 1985), pp. 28-50.

190. Turnbull, A. and Ferriss, D.H., Corrosion Science, Vol. 26 (1986): pp. 601-621.

191. Turnbull, A. and Saenz de Santa Maria, M., Metall. Trans. A., Vol. 19A (1988): pp. 1795-1806.

192. Akhurst, K.N. and Baker, T.J., Metall. Trans. A., Vol. 12A (1981): pp. 1059-1070.

193. Turnbull, A., Scripta Metall., Vol. 20 (1986): pp. 365-369.

194. Gangloff, R.P. and Turnbull, A., Modeling Environmental Effects on Crack Initiation and Propagation, R.H. Jones and W.W. Gerberich, eds., TMS-AIME, (Warrendale, PA: TMS-AIME, 1986), pp. 55-81.

195. Gangloff, R.P., Corrosion Prevention and Control, Proc. Sagamore Army Materials Research Conference, Vol. 33, M. Levy and S. Isserow, eds., (Watertown, MA: U.S. Army Materials Technology Laboratory, 1987), pp. 64-111.

196. Rajpathak, S.S. and Hartt, W.H., in Environmentally Assisted Cracking: Science and Engineering, ASTM STP, W.B. Lisagor, T.W. Crooker and B. N. Leis, eds., (Philadelphia, PA: ASTM, 1990), pp. 425-446.

197. Holroyd, N.J.H. and Scamans, G.M., Environment-Sensitive Fracture: Evaluation and Comparison of Test Methods, ASTM 821, S.W. Dean, E.N. Pugh and G.W. Ugiansky, eds., (Philadelphia, PA: ASTM, 1984), pp. 202-241.

198. Ricker, R.E. and Duquette, D.J., "The Use of Electrochemical Potential to Control and Monitor Fatigue of Aluminum Alloys", Paper No. 354, Corrosion 85, (Houston, TX: NACE, 1985).

199. Cialone, H.J., Holbrook, J.H. and Louthan, M.R., "Hydrogen-Enhanced Fatigue Crack Growth in Line Pipe Steels", presented at International Conference on Environmental Degradation of Engineering Materials III, (University Park, PA: Pennsylvania State University, 1987).

200. Ritchie, R.O., Suresh, S. and Liaw, P.K., Ultrasonic Fatigue, J.M. Wells, O. Buck, L.K. Roth and J.K. Tien, eds., (Warrendale, PA: TMS-AIME, 1982), pp. 443-460.

201. Suresh, S. and Ritchie, R.O., Metal Science, Vol. 16 (1982): pp. 529-538.

202. Suresh, S. and Ritchie, R.O., Fatigue Crack Growth Threshold Concepts, D. Davidson and S. Suresh, eds., (Warrendale, PA: TMS-AIME, 1984), pp. 227-261.

203. Gangloff, R.P. and Ritchie, R.O., Fundamentals of Deformation and Fracture, B.A. Bilby, K.J. Miller and J.R. Willis, eds., (Cambridge, UK: Cambridge University Press, 1985), pp. 529-558.

204. Ritchie, R.O., Suresh, S. and Moss, C.M., J. Engr. Matls. Tech., Trans. ASME, Vol. 102 (1980): pp. 293-299.

205. Suresh, S., Zaminski, G.F. and Ritchie, R.O., Metall. Trans. A., Vol. 12A (1981): pp. 1435-1443.

206. Toplosky, J. and Ritchie, R.O., Scripta Metall., Vol. 15 (1981): pp. 905-908.

207. Liaw, P.K., Hudak, Jr. S.J. and Donald, J.K., Fracture Mechanics: Fourteenth Symposium-Vol. II, ASTM STP 791, J.C. Lewis and G. Sines, eds., (Philadelphia, PA: ASTM, 1983), pp. 370-388.

208. Gangloff, R.P., Basic Questions in Fatigue, Vol. II, ASTM STP 924, R.P. Wei and R.P. Gangloff, eds., (Philadelphia, PA: ASTM, 1988), pp. 230-251.

209. Frandsen, J.D. and Marcus, H.L., Metall. Trans. A, Vol. 8A (1977): pp. 265-272.

210. Roven, H.J., "Cyclic Deformation and Fatigue Crack Propagation in a Low Alloyed Steel", Thesis for Doctor Technique, (Trondheim, Norway: Norwegian Institute of Technology, 1988).

211. Starke, Jr., E.A., Lin, F.S., Chen, R.T. and Heikkenen, H.C. Fatigue Crack Growth Threshold Concepts, D. Davidson and S. Suresh, eds., (Warrendale, PA: TMS-AIME, 1984), pp. 43-61.

212. Wachob, H.F. and Nelson, H.G., Hydrogen in Metals, I.M. Bernstein and A.W. Thompson, eds., (Warrendale, PA: TMS-AIME, 1980), pp. 703-711.

213. Bandyopadhay, N., Kameda, J. and McMahon, Jr., C.J., Metall. Trans. A., Vol. 14A (1983): pp. 881-888.

214. Hippsley, C.A., "Hydrogen and Temper Embrittlement Interactions in Fatigue of 2 1/4Cr-1Mo Steel", Harwell Laboratory Report AERE R 12322, (Oxon, England, 1986).

215. Lin, F.S. and Starke, Jr., E.A., Hydrogen Effects in Metals, I.M. Bernstein and A.W. Thompson, eds., (Warrendale, PA: TMS-AIME, 1981), pp. 485-492.

216. Ford, F.P., Taylor, D.F., Andresen, P.L. and Ballinger, R.G., "Corrosion Assisted Cracking of Stainless and Low Alloy Steels in LWR Environments", EPRI Contract RP-2006-6, Rpt. No. NP 5064M, (Palo Alto, CA: Electric Power Research Institute, 1987).

217. Niegel, A., Gudladt, H.-J. and Gerold, V., J. de Physique, Colloque C5, Vol. 49 (1988): pp. 659-663.

218. Gudladt, H.-J., Niegel, A. and Liang, P. Proc. Matls. Res. Soc., Vol. 122 (Boston, MA: MRS, 1988), pp. 405-409.

219. Liang, P., Gudladt, H.-J. and Gerold, V., Low Cycle Fatigue and Elastic Plastic Behavior of Materials, K.-T. Rie, ed., (London, UK: Elsvier Applied Science, 1987), pp. 687-692.

220. Forsyth, P.J.E., Stubbington, C.A. and Clark, D., J. Inst. Metals, Vol. 90 (1961-62): pp. 238-239.

221. Piascik, R.S., "Mechanisms of Intrinsic Damage Localization During Corrosion Fatigue: Al-Li-Cu System", PhD Dissertation, (Charlottesville, VA: University of Virginia, 1989).

222. Staehle, R.W., "Situation Dependent Strength", Environment Induced Cracking of Metals, R.P. Gangloff and M.B. Ives, eds., (Houston, TX: NACE, in press, 1989).

223. Gangloff, R.P. and Wei, R.P., Metall. Trans. A, Vol. 8A (1977): pp. 1043-1053.

224. Vosikovsky, O., Neill, W.R., Carlyle, D.A. and Rivard, A., Canadian Metall. Quart., Vol. 26 (1987): pp. 251-257.

225. Vosikovsky, O. and Rivard, A., Corrosion, Vol. 38 (1982): pp. 19-22.

226. Thomas, C.J., Edyvean, R.G.J. and Brook, R., Biofouling, Vol. 1 (1988): pp. 65-77.

227. Edyvean, R.G.J., Thomas, C.J., Brook, R. and Austen, I.M., Biologically Induced Corrosion, S.C. Dexter, ed., (Houston, TX: NACE, 1986), pp. 254-267.

228. Wei, R.P. and Gao, M., Scripta Met., Vol. 17 (1983): pp. 959-962.

229. Austin, I.M. and Walker, E.F., Proc. Intl. Conf. Influence of Environment on Fatigue, (London, UK: I. Mech. Engr., 1977), pp. 1-16.

230. Austin, I.M., Rudd, W.J. and Walker, E.F., Proceedings of the International Conference on Steel in Marine Structures, paper ST 5.4 (Paris, France: Comptoir des produits Siderurgiques, 1981),

231. Austin, I.M., "Quantitative Assessment of Corrosion Fatigue Crack Growth Under Variable Amplitude Loading", British Steel Company Report BSC FR S132-8/862, (Rotherham, England: Swinden Laboratories, 1987).

232. Lidbury, D.P.G., Embrittlement by the Localized Crack Environment, R.P. Gangloff, ed., (Warrendale, PA: TMS-AIME, 1984): pp. 149-172.

233. Knott, J.F., Fatigue Crack Growth, 30 Years of Progress, R.A. Smith, ed., (Oxford, UK: Pergamon Press, 1986), pp. 31-52.

234. Hudak, S.J., "Corrosion Fatigue Crack Growth: The Role of Crack-Tip Deformation and Film Formation Kinetics", PhD Dissertation, (Bethlehem, PA: Lehigh University, 1988).

235. Hudak, S.J., Davidson, D.L. and Page, R.A., Embrittlement by the Localized Crack Environment, R.P. Gangloff, ed., (Warrendale, PA: TMS-AIME, 1984), pp. 173-198.

236. Localized Corrosion, (Houston, TX: NACE, 1990).

237. Dushman, S., Scientific Foundations of Vacuum Technique, (New York, NY: John Wiley and Sons, 1962), Chapters 1-2.

238. Lawn, B.R., Matls. Sci. Engr., Vol. 13 (1974): pp. 277-283.

239. Bradshaw, F.J., Scripta. Metall., Vol. 1 (1967): pp. 41-43.

240. Snowden, K.U., J. Appl. Phys., Vol. 34 (1963): pp. 3150-3151.

241. Snowden, K.U., Acta Metall., Vol. 12 (1964): pp. 295-303.

242. Weir, T.W., Simmons, G.W., Hart, R.G. and Wei, R.P., Scripta Metall., Vol. 14 (1980): pp. 357-364.

243. Shih, True-Hwa, and Wei, R.P., Engr. Frac. Mech., Vol. 18 (1983): pp. 827-837.

244. Pao, P.S., Gao, Ming and Wei, R.P., Basic Questions in Fatigue, ASTM STP 924, Vol. 2, R.P. Wei and R.P. Gangloff, eds., (Philadelphia, PA: ASTM, 1988), pp. 182-195.

245. Turnbull, A. and Thomas, J.G.N., J. Electrochem. Soc., Vol. 129 (1982): pp. 1412-1422.

246. Turnbull, A.,Br. Corros. J., Vol. 15 (1980): pp. 162-171.

247. Turnbull, A., Corr. Sci., Vol. 22 (1982): pp. 877-893.

248. Turnbull, A., Matls. Sci. Tech., Vol. 1 (1985): pp. 700-710.

249. Turnbull, A. and Ferriss, D.H., Corr. Sci., Vol. 27 (1987): pp. 1323-1350.

250. Turnbull, A. and Saenz de Santa Maria, M., Environment Induced Cracking of Metals, R.P. Gangloff and M.B. Ives, eds., (Houston, TX: NACE, 1990), pp. 193-196.

251. Turnbull, A. and May, A.T., Brit. Corros. J., Vol. 22 (1987): pp. 176-181.

252. Turnbull, A. and Ferriss, D.H., Corrosion Chemistry Within Pits, Crevices and Cracks, A. Turnbull, ed., (London, UK: HMSO, 1987), pp. 397-412.

253. Gangloff, R.P., Embrittlement by the Localized Crack Environment, R.P. Gangloff, ed., (Warrendale, PA: TMS-AIME, 1984), pp. 265-290.

254. Holroyd, N.J.H., Scamans, G.M. and Hermann, R., Embrittlement by the Localized Crack Environment, R.P. Gangloff, ed., (Warrendale, PA: TMS-AIME, 1984), pp. 327-347.

255. Le, A.H. and Foley, R.T., Corrosion, Vol. 40 (1984): pp. 195-197.

256. Brown, B.F., Fujii, C.T. and Dahlberg, E.P., J. Electrochem. Soc., Vol. 116 (1969): pp. 218-219.

257. Wei, R.P., Shim, G. and Tanaka, K., Embrittlement by the Localized Crack Environment, R.P. Gangloff, ed., (Warrendale, PA: TMS-AIME, 1984), pp. 243-263.

258. Wei, R.P., Fatigue 87, R.O. Ritchie and E.A. Starke, Jr., eds., (West Midlands, UK: EMAS, 1987), pp. 1541-1560.

259. Wei, R.P., "Corrosion Fatigue Crack Growth and Reactions with Bare Steel Surfaces", Corrosion 89, Paper No. 569, (Houston, TX: NACE, 1989).

260. Alavi, A., Miller, C.D. and Wei, R.P., Corrosion, Vol. 43 (1987): pp. 204-207.

261. Shim, Gunchoo and Wei, R.P., Matls. Sci. and Engr., Vol. 87 (1986): pp. 121-135.

262. Wei, R.P. and Alavi, A., Scripta Metall., Vol. 22 (1988): pp. 969-974.

263. Thomas, J.P., Alavi, A. and Wei, R.P., Scripta Metall., Vol. 20 (1986): pp. 1015-1018.

264. Jacko, R.J. and Duquette, D.J., Metall. Trans. A., Vol. 8A (1977): pp. 1821-1827.

265. Esaklul, K.A., Wright, G.A. and Gerberich, W.W., Fatigue Crack Growth Threshold Concepts, D.L. Davidson and S. Suresh, eds., (Warrendale, PA: TMS-AIME, 1984), pp. 299-326.

266. Ricker, R.E. and Duquette, D.J., Metall. Trans. A, Vol. 19A (1988): pp. 1775-1783.

267. Pao, P.S., Wei, W. and Wei, R.P., Environment Sensitive Fracture of Engineering Materials, Z.A. Foroulis, ed., (Warrendale, PA: TMS-AIME, 1979), pp. 565-580.

268. Swanson, J. W. and Marcus, H.L., Metall. Trans. A., Vol. 9A (1978): pp. 291-293.

269. Wei, R.P., Intl. J. Frac. Mech., Vol. 4 (1968): pp. 159-170.

270. Suresh, S., Metall. Trans. A., Vol. 14A (1983): pp. 2375-2385.

271. Ritchie, R.O., Intl. Metall. Rev., Vol. 20 (1979): pp. 205-230.

272. Elber, W., Damage Tolerance in Aircraft Structures, ASTM STP 486, (Philadelphia, PA: ASTM, 1979), pp. 230-243.

273. Mechanics of Fatigue Crack Closure, ASTM STP 982, J.C. Newman and W. Elber, eds., (Philadelphia, PA: ASTM, 1988).

274. Suresh, S. and Ritchie, R.O., Metall. Trans. A., Vol. 13A (1982): pp. 1627-1631.

275. Suresh, S. and Ritchie, R.O., Scripta Metall., Vol. 17 (1983): pp. 575-580.

276. Tzou, J.-L., Hsueh, C.H., Evans, A.G. and Ritchie, R.O., Acta Metall., Vol. 33 (1985): pp. 117-127.

277. Venkateswara, K.T., Piascik, R.S., Gangloff, R.P. and Ritchie, R.O., in Proceedings, 5th International Aluminum-Lithium Conference, T.H. Sanders, Jr. and E.A. Starke, Jr., (Birmingham, UK: Materials and Component Engineering Publications, Ltd., 1989), pp. 955-971.

278. Suresh, S., Vasudevan, A.K. and Bretz, P.E., Metall. Trans. A., Vol. 15A (1984): pp. 369-379.

279. Hartt, W.H., Culberson, C.H. and Smith, S.W., Corrosion, Vol. 40 (1984): pp. 609-618.

280. Hartt, W.H. and Rajpathak, S.S., "Formation of Calcareous Deposits Within Simulated Fatigue Cracks in Seawater", Corrosion 83, Paper No. 62, (Houston, TX: NACE, 1983).

281. van der Velden, R., Ewalds, H.L., Schultze, W.A. and Punter, A., Corrosion Fatigue: Mechanics, Metallurgy, Electrochemistry and Engineering, ASTM STP 801, T.W. Crooker and B.N. Leis, eds., (Philadelphia, PA: ASTM, 1984), pp. 64-80.

282. Jani, S.C., Merek, M., Hochman, R.F. and Meletis, E.I., Environment Induced Cracking of Metals, R.P. Gangloff and M.B. Ives, eds., (Houston, TX: NACE, 1990), pp. 541-544.

283. Ritchie, R.O. and Lankford, J., Matls. Sci. Engr., Vol. 84 (1986): pp. 11-16.

284. Hudak, S.J., J. Engr. Matls. Tech., Vol. 103 (1981): pp. 26-35.

285. Zeghloul, A. and Petit, J., Small Fatigue Cracks, R.O. Ritchie and J. Lankford, eds., (Warrendale, PA: TMS-AIME, 1986), pp. 225-235.

286. Hudak, S.J. and Ford, F.P., Small Fatigue Cracks, R.O. Ritchie and J. Lankford, eds., (Warrendale, PA: TMS-AIME, 1986), pp. 289-310.

287. Tanaka, K. and Wei, R. P., Engr. Fract. Mech., Vol. 21 (1985): pp. 293-305.

288. Turnbull, A. and Newman, R.C., Small Fatigue Cracks, R.O. Ritchie and J. Lankford, eds., (Warrendale, PA: TMS-AIME, 1986), pp. 269-288.

289. Dowling, N.E., Fracture Mechanics, ASTM STP 677, C.W. Smith, ed., (Philadelphia, PA: ASTM, 1979), pp. 247-273.

290. Rolfe, S.T. and Barsom, J.M., Fracture and Fatigue Control in Structures, (Englewood Cliffs, NJ: Prentice-Hall, Inc., 1977), pp. 213-222.

291. Novak, S.R., Corrosion Fatigue Technology, ASTM STP 642, H.L. Craig, Jr., T.W. Crooker and D.W. Hoeppner, eds., (Philadelphia, PA: ASTM, 1978), pp. 26-63.

292. Badve, A.P., Hartt, W.H. and Rajpathak, S.S., "Effects of Cathodic Polarization Upon Fatigue of Selected High Strength Steels in Sea Water", Corrosion 89, Paper No. 570, (Houston, TX: NACE, 1989).

293. Rajpathak, S.S. and Hartt, W.H., Proc. Offshore Mech. and Arctic Engr., Vol. III (1988): pp. 323-337.

NASA
National Aeronautics and Space Administration

Report Documentation Page

1. Report No.	2. Government Accession No.	3. Recipient's Catalog No.
NASA CR-4301		

4. Title and Subtitle	5. Report Date
Corrosion Fatigue Crack Propagation in Metals	June 1990
	6. Performing Organization Code

7. Author(s)	8. Performing Organization Report No.
Richard P. Gangloff	
	10. Work Unit No. 505-63-01

9. Performing Organization Name and Address	11. Contract or Grant No.
Department of Materials Science University of Virginia Charlottesville, VA 22903-2442	NAG1-745
	13. Type of Report and Period Covered: Contractor Report

12. Sponsoring Agency Name and Address	14. Sponsoring Agency Code
NASA Langley Research Center Hampton, VA 23665-5225	

15. Supplementary Notes: Langley Technical Monitor: Dennis L. Dicus
Presented at the 1st International Conference on Environment Induced Cracking of Metals; Kohler, WI, September 1988.

Published in: Environment Induced Cracking of Metals, R. P. Gangloff and M. B. Ives, eds., NACE, Houston, TX (1990).

16. Abstract

This review assesses fracture mechanics data and mechanistic models for corrosion fatigue crack propagation in structural alloys exposed to ambient temperature gases and electrolytes. Extensive stress intensity-crack growth rate data exist for ferrous, aluminum and nickel based alloys in a variety of environments. Interactive variables (viz., stress intensity range, mean stress, alloy composition and microstructure, loading frequency, temperature, gas pressure and electrode potential) strongly affect crack growth kinetics and complicate fatigue control. Mechanistic models to predict crack growth rates have been formulated by coupling crack tip mechanics with occluded crack chemistry, and from both the hydrogen embrittlement and anodic dissolution/film rupture perspectives. Research is required to better define: a) environmental effects near threshold and on crack closure, b) damage tolerant life prediction codes and the validity of similitude, c) the behavior of microcracks, d) probes and improved models of crack tip damage, and e) the cracking performance of advanced alloys and composites.

17. Key Words (Suggested by Author(s))	18. Distribution Statement
Corrosion Fatigue Fracture Mechanics Hydrogen Embrittlement Steel Aluminum Alloy	Unclassified-Unlimited Subject Category 26

19. Security Classif. (of this report)	20. Security Classif. (of this page)	21. No. of pages	22. Price
Unclassified	Unclassified	204	A10

NASA FORM 1626 OCT 86

For sale by the National Technical Information Service, Springfield, Virginia 22161-2171

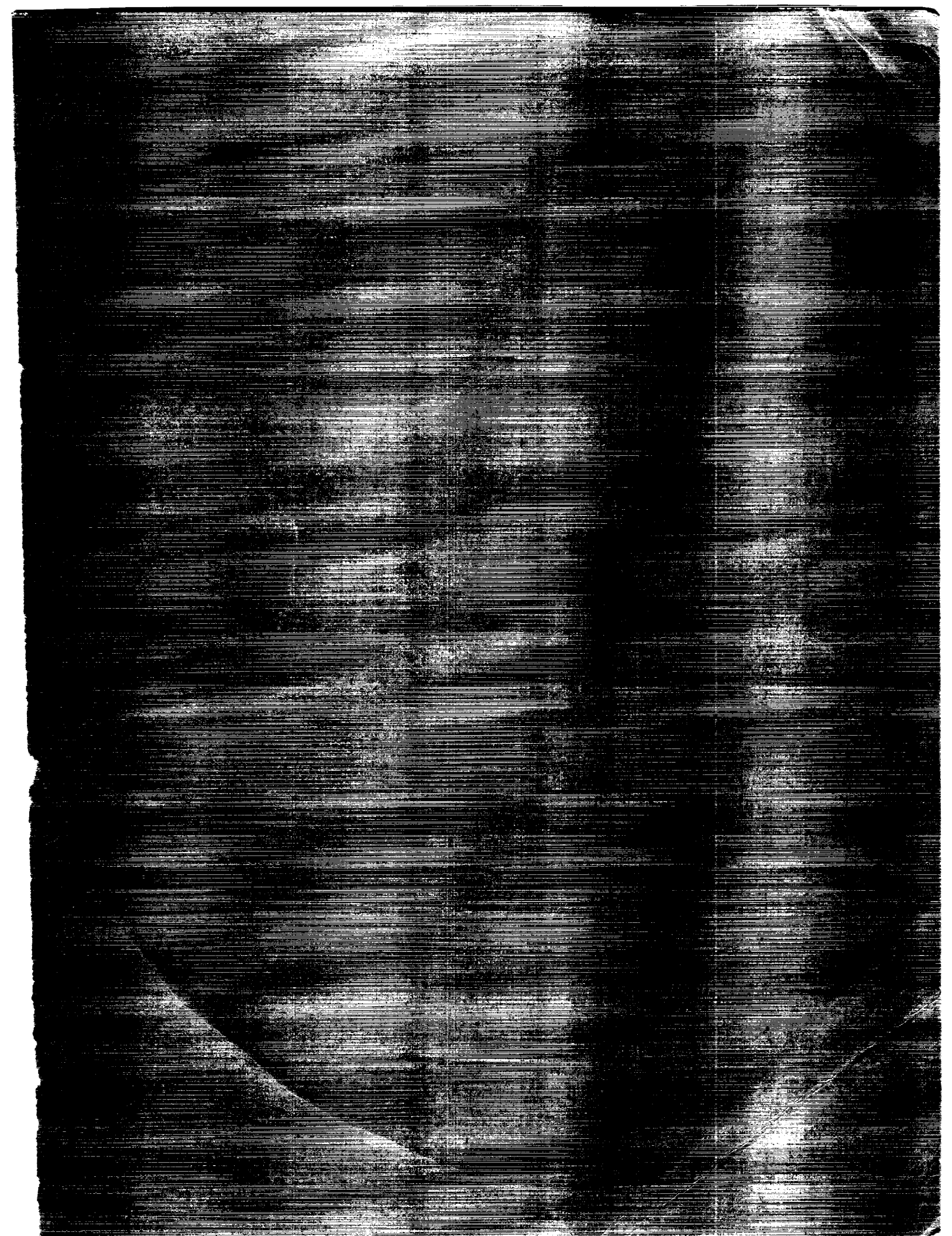

NASA

National Aeronautics and
Space Administration

Washington, D.C.
20546

SPECIAL FOURTH CLASS MAIL
BOOK

Postage and Fees Paid
National Aeronautics and
Space Administration
NASA-451

Official Business
Penalty for Private Use $300

U.S. MAIL

L2 001 CR-4301 900615S090569
NASA
SCIEN & TECH INFO FACILITY
ACCESSIONING DEPT
P O BOX 8757 BWI ARPRT
BALTIMORE MD 21240